Generation of tissue-specific vectors by *in vivo* selection of random peptide libraries displayed on the surface of adeno-associated virus type 2

Dissertation
Zur Erlangung der Würde des Doktors der Naturwissenschaften des Fachbereichs Biologie, der Fakultät für Mathematik, Informatik und Naturwissenschaften, der Universität Hamburg

vorgelegt von

Jakob Körbelin

aus

Henstedt-Ulzburg

Hamburg, 2013

Gutachter:
Prof. Dr. Thosten Burmester
Prof. Dr. Martin Trepel

Tag der Disputation: 15.11.2013

Vorsitz:
Prof. Dr. Susanne Dobler

Genehmigt vom Fachbereich Biologie
der Fakultät für Mathematik, Informatik und Naturwissenschaften
an der Universität Hamburg
auf Antrag von Professor Dr. M. TREPEL
Weiterer Gutachter der Dissertation:
Professor Dr. T. BURMESTER
Tag der Disputation: 15. November 2013

Hamburg, den 31. Oktober 2013

Professor Dr. C. Lohr
Vorsitzender des
Fach-Promotionsausschusses Biologie

Eidesstattliche Versicherung /*Declaration on Oath*

Hiermit versichere ich, dass ich die vorliegende Dissertationsschrift mit dem Titel „*Generation of tissue specific vectors by in vivo selection of random peptide libraries displayed on the surface of adeno-associated virus type 2*“ selbstständig verfasst, keine anderen als die angegebenen Quellen und Hilfsmittel benutzt und die den benutzen Werken wörtlich oder inhaltlich entnommenen Stellen als solche kenntlich gemacht habe. Ferner versichere ich, dass diese Arbeit noch nie in derselben oder einer ähnlichen Fassung, auch nicht in Teilen, in einem anderen Prüfungsverfahren eingereicht oder veröffentlicht wurde.

*I hereby declare, on oath, that I have written the presented dissertation with the title “*Generation of tissue specific vectors by in vivo selection of random peptide libraries displayed on the surface of adeno-associated virus type 2*” on my own, that I have not used other than the acknowledged sources or aids and that all passages adopted literally or with regard to their content are marked as such.*
I further declare that this work has never been published or submitted in a previous doctoral procedure, in this or any other form, not even partially.

Hamburg, 09.09.2013

Jakob Körbelin

“There is grandeur in this view of life, with its several powers, having been originally breathed into a few forms or into one; and that, whilst this planet has gone cycling on according to the fixed law of gravity, from so simple a beginning endless forms most beautiful and most wonderful have been, and are being, evolved”

- Charles Darwin (On the Origin of Species, 1859)

Contents

List of Figures

List of Tables

Abbreviations

A	adenosine
A	alanine
aa	amino acid
AAT	alpha-1-antitrypsin
AAV	adeno-associated virus
ACE	angiotensin-converting enzyme
Ad	adenovirus
ADA-SCID	severe combined immune deficiency due to adenosine deaminase deficiency
AMP	ampicillin
ANOVA	analysis of variance
AP	alkaline phosphatase
Arg	arginine (R)
BBB	blood brain barrier
BCIP	5-bromo-4-chloro-3'-indolyphosphate p-toluidine salt
BMPR2	bone morphogenetic protein receptor type II
bp	base pair(s)
BSA	bovine serum albumin ("Fraction V")
c	concentration
C	cytidine/cysteine
$CaCl_2$	calcium chloride
CAG	cytomegalovirus early enhancer + chicken ß-actin promoter
Cap	capsid protein
CCL2	CC-chemokine ligand 2
CCR2	CC-chemokine receptor 2
CD13	cluster of differentiation 13: Alanine aminopeptidase
CD31	cluster of differentiation 31: Platelet endothelial cell adhesion molecule (PECAM-1)
CF	cystic fibrosis
CMV	cytomegalovirus
CNS	central nervous system
Cy3	Cyanine dye, fluoresce yellow-green (~550 nm excitation, ~570 nm emission)
d	day(s)/dilution
$_{dd}H_2O$	ultra-pure double-destilled water
D	aspartic acid
d.p.i.	days post injection
DMEM	Dulbecco's modified Eagle's Minimal Essential Medium
DMF	dimethylformamide
DMSO	dimethyl sulfoxide
dNTP(s)	deoxyribonucleotide(s)
E	glutamic acid
E. coli	*Escherichia coli*
EDTA	ethylenediaminetetraacetic acid

eGFP	enhanced green fluorescent protein
ELISA	enzyme linked immunosorbent assay
eNOS	endothelial nitric oxide synthase
F	phenylalanine
FBS	fetal bovine serum
FGFR	fibroblast growth factor receptor
G	gauge (unit for the diameter of needles)/ guanosine/ glycine
GENT	gentamycin
GFP	green fluorescent protein, originated from Aequorea victoria (~395/475 nm excitation, ~509 nm emission)
gp	genomic particle(s)
H	histidine
HCl	hydrochloric acid
HEK 293T	human embryonic kidney 293 cells with the simian virus 40 large T antigen
HEPES	4-(2-hydroxyethyl)-1-piperazineethanesulfonic acid
HGFR	hepatocyte growth factor receptor
HSPG	heparan sulphate proteglycan
HSV	herpes simplex virus
I	isoleucine
i.p.	intraperitoneal
i.v.	intravenous
iNOS	inducible nitric oxide synthase
IPTG	isopropyl β-D-1-thiogalactopyranoside
ITR	inverted Terminal Repeat
IVC	individual ventilated cage(s)
K2HPO4	dipotassium phosphate
KAN	kanamycin
kb	kilobase(s)
KCl	potassium chloride
KH_2PO	potassium hydrogen phosphate
L	leucine/lysine
LB	lysogenic broth
M	molar (= mol/l)
m	mass
M	metheonine
$MgCl_2$	magnesium chloride
$MgCl_2$ $6H_2O$	magnesium chloride hexahydrate
min	minute(s)
miRNA	microRNA
MOI	multiplicity of infection
n	number
N	one of the nucleotides adenosine (A), cytidine (C), guanosine (G) or thymidine (T)/asparagine
Na_2HPO_4 $2H_2O$	disodium hydrogen phosphate dihydrate
NaCl	sodium chloride
NBT	nitro-blue tetrazolium chloride

o/n	over night
OD	optical density
ORF	open reading frame
P	proline
PAGE	polyacrylamide gel electrophoresis
PBS	phosphate buffered saline
PBS-MK	phosphate buffered saline with magnesium and potassium
PCR	polymerase chain reaction
PDGFR	platelet derived growth factor receptor
PEG	polyethylene glycol
PH	pulmonary hypertension
polh	polyhedrin
PVDF	polyvinylidene fluoride
Q	glutamine
qPCR	quantitative Polymerase Chain Reaction
R	arginine (Arg)
rAAV	recombinant adeno associated virus
RBE	Rep binding element
Rep	replication protein
rep U	replicative unit(s)
RLU	relative light unit(s)
rpm	rounds per minute
RT	room temperature
S	serine
SCID	severe combined immune deficiency
SD	standard deviation
SDS	sodium dodecyl sulfate
Sf9	ovarian Spodoptera frugiperda cell line
SOB	super optimal broth
SOC	super optimal broth with catabolite
SV40	simian virus 40
T	thymidine
T	threonine
TAE	tris(hydroxymethyl)aminomethane-acetate-ethylenediaminetetraacetic acid
TB	terrific broth
TBS-T	tris buffered saline with Tween
TE (Tris-EDTA)	tris(hydroxymethyl)aminomethane ethylenediaminetetraacetic acid
TEMED	tetramethylethylenediamine
TET	tetracycline
Tris	tris(hydroxymethyl)aminomethane
trs	terminal resolution site
U	enzyme unit(s)
UKE	Universitätsklinikum Hamburg-Eppendorf
UV	ultra violet
V	valine
v/v	volume per volume

vg	viral genome(s)
vol.	volume
VP	virion protein
W	tryptophan
w/v	weight per volume
x g	multitude of the gravitiy of Earth (g)
X-Gal	5-bromo-4-chloro-3-indolyl-β-D-galactopyranoside
Y	tyrosine

Further standard abbreviations, especially for measurement units as well as common prefixes have been used without being listed in this table

Zusammenfassung

Eines der größten Probleme im noch jungen Feld der Gentherapie stellt das Fehlen zielgerichteter Vektorsysteme dar, die den enormen Sicherheitsansprüchen genügen. Rekombinante Vektoren auf Basis des Adeno-assoziierten Virus (AAV) entwickleten sich im Laufe des letzten Jahrzehnts zu äußerst vielversprechenden Kandidaten zur Lösung dieses Problems. Um den unspezifischen Tropismus von AAV umzulenken, sind auf dem AAV-Kapsid präsentierte randomsierte Peptidbanken entwickelt worden, welche aus einer enorm großen Anzahl viraler Partikel mit unterschiedlichsten Eigenschaften bestehen. Ziel der vorliegenden Arbeit war die Isolierung und Charakterisierung von Kapsidvarianten aus randomisierten AAV-Peptidbanken, die nach systemischer Applikation *in vivo* einen effizienten und zielgerichteten Gentransfer in vordefiniertes Gewebe erlauben. Dafür wurden die Ergebnisse zweier methodisch geringfügig verschiedener *in vivo* Selektionen im Mausmodell in zwei therapeutisch relevanten Organen (Gehirn und Lunge) analysiert, von denen eine Selektion im Rahmen der vorliegenden Arbeit durchgeführt wurde. Die vielversprechendsten Klone mit den Peptiden NRGTEWD (selektiert für Gehirntropismus) und ESGHGYF (selektiert für Lungentropismus) wurden als Reportergen-vektoren (Luciferase) getestet und erlaubten erstmalig zielgerichtete Genexpression nach systemischer Applikation mit bisher unerreichter Spezifität. Mittels quantitativer PCR konnte verifiziert werden, dass die vektorvermittelte Genexpression tatsächlich auf organspezifischer Transduktion beruht. Die Effizienz der Transgenexpression im Zielgewebe konnte im Falle des Hirn-gerichteten Klons NRGTEWD durch den Einsatz des CAG-Promoters weiter erhöht werden. Getestet für den Lungen-gerichteten Klon ESGHGYF, zeigte die Analyse der Genexpression im Langzeitversuch eine sehr hohe Stabilität was auf das Ausbleiben eines immunassoziierten Vektor-Silencings schließen lässt und damit die potentielle Anwendbarkeit dieses Klons für therapeutische Zwecke bestätigt. Mittels immunhistologischer Untersuchungen wurde gezeigt, dass beide getesteten Vektoren extrem effizient das Endothel ihrer Zielorgane transduzieren, was sie zu äußerst interessanten Kandidaten für zukünftige gentherapeutische Interventionen in diesem klinisch hochgradig relevanten Gewebe macht. Weitere Informationen über Funktionalität der selektierten Peptide konnten mittels Alanin-Scan Mutagenese gewonnen werden. Hierbei zeigte sich im Falle von ESGHGYF ein potentiell negativer Einfluss einer einzelnen Aminosäure (E), was Raum für zukünftige Peptid-Optimierungen lässt, während im Falle des Peptids NRGTEWD jede einzelne Aminosäure funktionell wichtig zu sein scheint. Die Ergebnisse dieser Arbeit implizieren die Existenz eines gemeinsamen Zelloberflächenmoleküls auf Endothelzellen der Mikrovaskulatur des zentralen Nervensystems (ZNS) und der Lunge, welches diese vom Rest des Endothels abgrenzt. Damit bereitet der in dieser Arbeit beschriebene erfolgreiche *in vivo*- Einsatz von AAV-Peptidbibliotheken die Grundlage für zukünftige Gentherapievektoren des ZNS und der Lunge, von denen sich einige bereits in Entwicklung für präklinische Untersuchungen befinden.

Summary

After an initial period of enthusiasm, it was realized that major obstacles have to be overcome before the young discipline of gene therapy would fulfill its high expectations. The lack of highly efficient and target-specific vector systems with a superior safety profile was soon identified as the biggest hurdle. Recombinant vectors based on adeno-associated virus (AAV) have emerged as promising candidates to solve this problem. Peptide libraries displayed on the surface of the AAV capsid have been developed to generate viral particles with new tropism, thereby broadening the spectrum of potential host cells and increasing specificity.

This study aimed at identifying AAV variants that allow efficient and specific transduction of target tissues after systemic application by screening random AAV display peptide libraries *in vivo* and characterizing selected AAV variants. Choosing brain and lung as therapeutically highly relevant targets, the results of two methodically slightly different *in vivo* screenings in a mouse model were analyzed, one of which was performed as part of this study. The most promising library clones NRGTEWD (brain) and ESGHGYF (lung) were used to generate luciferase reporter gene vectors which for the first time enabled highly efficient transgene expression specifically in the organs of interest. The specific transgene expression was proven to be caused by specific vector homing on DNA level. Efficiency and specificity of transgene expression mediated by the brain-enriched peptide NRGTEWD could be further enhanced by utilization of the CAG promoter instead of the CMV promoter. Long-term analyses revealed durability of transgene expression mediated by the lung-selected clone ESGHYGF and the absence of immune-related vector silencing, proving the general applicability for therapeutic approaches. Both vectors (NRGTEWD and ESGHGYF) were shown to transduce the vascular endothelium of their respective target organs with high efficiency, thereby providing a promising tool for future gene therapy interventions in this clinically highly relevant tissue. Alanine scanning mutagenesis of the enriched peptides was performed to gain more information about their structural functionality and revealed the potential negative influence of a single amino acid (E) within the peptide ESGHGYF, thereby giving room for futher optimizations, whereas every single amino acid seemed to be functionally important in case of the peptide NRGTEWD.

The results of this study do not only indicate the existence of a common cell surface molecule in the endothelial cells of the microvasculature of the central nervous system (CNS) and the lung which allow to differentiate these cells from the rest of the endothelium, they also prove the general applicability of random AAV display peptide libraries *in vivo* by providing potential gene therapy vectors for the CNS and the pulmonary microvasculature, some of which are already under development. Thus, this study is likely to have broad implications on applied vectorology as well as on basic biomedical research.

1 Introduction

1.1 Gene therapy – limitations and prospects

1.1.1 The concept of gene therapy

The idea of curing genetically determined diseases by correcting the corresponding part of the patient's genome instead of relying solely on pharmaceutical agents was first articulated in the 1960s by Tatum[1] and was further specified in 1972 by Friedmann & Roblin[2]. However, the vision of gene therapy did not become reality until the emergence of sufficient biotechnological techniques in the 1980s and 1990s. Only 25 years passed by from the first mention of the concept of gene therapy to the first approved clinical trial on humans in 1990, which involved the treatment of severe combined immune deficiency due to adenosine deaminase deficiency (ADA-SCID)[3]. Gene therapy, as the replacement or correction of a mutated and non-functional gene by a functional therapeutic version, is theoretically applicable for all diseases that are linked to monogenetic defects. In addition, gene therapeutic targeted change of protein expression patterns is a promising approach for the treatment of complex diseases such as cancer, e.g. by the killing of malignant cells via the transfer of so called "suicide genes" which encode proteins with cytotoxic effects. Indeed many different diseases have been treated with gene therapy approaches within the last two decades. Additional to the first clinical trial involving SCID[3], cardiovascular disorders[4], pulmonary disorders like cystic fibrosis[5], neurological disorders like Parkinson's disease[6], and several forms of cancer[7] have been treated with gene therapy to a varying degree of success. An overview over more than 1900 clinical trials in the field of gene therapy can be found in the online database "Gene Therapy Clinical Trials Worldwide" by the Journal of Gene Medicine[8].

1.1.2 Ways of gene delivery

Basically, there are three different routes to deliver genes in patients, indicated for different therapeutic targets.

One way of gene delivery is the insertion of a therapeutic gene into the cells of interest after having them temporarily removed from the patient (*ex vivo gene delivery*). The cells can afterwards be screened for successful genetic modification and the modified cells can be re-administered to the patient. This approach benefits from the possibility to check the cells for unintended damages like insertional mutagenesis before their re-administration to the patient. It has been successfully used for treating different kinds of cells associated with several diseases in humans[9] like hepatocytes for treating familial hypercholesterolemia[10] or bone marrow cells for treating SCID[11]. Despite some impressive success in clinical trials, *ex vivo* gene therapy is time- and work- intensive, not always very

efficient and only suitable for a very limited number of indications since the relevant cells need to be easily accessible and amenable to transduction by available vectors.

Local administration of a therapeutic gene directly into the patient (*in vivo*) is another way of gene delivery. Depending on the target tissue, this procedure varies from being almost non-invasive and very easy to perform (e.g. intramuscular injection of vector; a clinical trial about the treatment of muscular dystrophy has recently been started[12]) to being significantly invasive (e.g., intracranial administration of vector in Parkinson's disease[13]). Like *ex vivo* gene therapy, local vector administration *in vivo* is only suitable for a limited number of diseases. This approach is not feasible for large or widely distributed target tissues. Compared to the *ex vivo* approach, there is no possibility to check genetically modified cells before administration to the patient as the genetic modification itself takes place within the patient's body. Therefore, the availability of a safe and efficient vector system is crucial for this approach.

A third way of performing gene therapy is the systemic administration of a therapeutic gene into the patient *in vivo*. This approach is easy to perform, almost non-invasive and therefore the most favourable way of gene therapy. Theoretically, it is applicable for the treatment of almost any disease that is generally suited for gene therapy. On the other hand, this approach strongly depends on an extremely safe and highly specific vector system to circumvent side-effects like unwanted gene transfer to non-target tissue.

1.1.3 Gene transfer vectors

Although more than 1900 clinical trials (phase 1-3) and countless preliminary studies *in vitro* and *in vivo* have been performed since 1990 [ref.8], there is still very limited availability of gene therapy vectors suitable for systemic administration. The need of a highly efficient vector system with a superior safety profile and low immunogenicity, which enables strong long-term expression of a therapeutic gene specifically in the tissue of interest, has not yet been met. However, despite several deficits, numerous vector systems have been proven to be more or less suitable for their use in gene therapy *in vivo*, especially for local administration. Most of them are virus-derived[14].

During their evolution, viruses have developed very efficient mechanisms of host cell infection and delivery of their packaged genome. Many viruses are able to mediate long-term gene expression at a high level in a broad range of cells, what makes them highly interesting for gene therapy approaches[14]. On the other hand, viruses often provoke immune responses, some bare the potential risk of insertional mutagenesis and many of them (as intact wild type viruses) can cause diseases, what restricts the number of potential candidates that can be used for therapeutic gene delivery. Modified recombinant adenovirus (Ad), adeno-associated virus (AAV), herpes simplex virus (HSV) and

several retroviruses are the most commonly used viral vectors for gene therapy as they appear to be sufficiently safe[15].

There also is a broad range of other , virus-independent methods to deliver DNA to different tissues *in vivo*[16]. Local administration of naked nucleic acid (e.g., by injection, electroporation or gene gun) and the use of cationic lipids or synthetic dendrimers coupled to nucleic acids are sometimes preferred methods of gene delivery as these methods show a superior safety profile compared to several viral vectors, they are comparably easy to perform in large scale and the size of the therapeutic gene is not limited by any viral packaging capacity[17]. Besides their mentioned benefits, most non-viral methods of gene delivery lack the ability to mediate transgene expression at a high level over prolonged time periods, leaving them insufficient for most therapeutic approaches. In addition, most of them are not suited for systemic administration.

As many of the discussed viral and non-viral vectors have been proven to be safe enough to be used in gene therapy, currently a substantial part of the research is focussed on the development of vector systems that enable improved – and even more favourably - specific transduction of therapeutic targets after systemic administration. Since local vector administration is not always feasible, especially when treating larger organs or widely distributed targets like muscle or metastatic cancer cells, the need for vectors with the ability to home to the desired therapeutic target after systemic administration is quite urgent. Several strategies have been developed to solve this problem[18]. Most of them include the incorporation of targeting peptides or antibodies and other high affinity ligands into the viral or non-viral vectors. Some of the most promising approaches are introduced in section **1.3.5** in more detail. After all, the choice of the best suitable vector system always depends on the specific therapeutic requirements and the desired way of application, as every vector system has its own unique properties. Among the potential gene therapy vectors, AAV has gained great importance over the last decade, mainly due to its superior safety profile compared to other viruses, its low immunogenicity and its high transduction efficiency[19].

1.2 Adeno-associated virus (AAV)

1.2.1 General biology

Adeno-associated virus (AAV) is a single-stranded DNA virus with a non-enveloped capsid of icosahedral symmetry which is approximately 22 nm in diameter. AAV infects dividing and non-dividing cells in primates, including humans. Interestingly, it has not been linked to any disease and its immunogenicity is very low[20] although the seroprevalence of AAV2, the type species and best described AAV-serotype, is about 70% in the human population[21]. Today,more than 100 different AAV isolates have been identified, including twelve human and non-human AAV serotypes[22].

The different AAV variants are members of the genus *Dependovirus*, belonging to the family *Parvoviridae.* As the name *Dependovirus* suggests, AAV does not only need a host cell for being replicated, its replication is also dependent on a helper virus, like Adenovirus (Ad), Herpes simplex virus (HSV) or Cytomegalovirus (CMV)[20]. In the absence of such a helper virus AAV persists in the host cell as episomal circular double-stranded DNA or it integrates into the host genome[23]. In most cases genome integration takes place at a specific position on the long arm of chromosome 19 [refs.24-26], designated "AAVS1" (19q13.4q).
Since the initial discovery of AAV as contaminant of adenovirus preparations[27] in 1965, there has been made a lot of progress in uncovering the genomic organisation and the capsid structure of AAV.

1.2.2 Genome organization

The single stranded AAV genome has a size of approximately 4.7 kb[28] and is flanked by 145 nts long inverted terminal repeats (ITRs) at each end of the DNA strand. The ITRs are GC-rich palindromic sequences which form T-shaped hairpins[29]. They are the starting point for self-primed second strand synthesis by a cellular DNA polymerase and thereby necessary for AAV replication[30]. The ITRs are also used as packaging signal for encapsidation of the genome into the capsid. Due to the limited size of its genome, AAV, like many other viruses, has developed a complex structure of genome organisation which includes the use of overlapping open reading frames (ORFs), nonconventional translation initiation codons and different splice variants.

The first viral gene, the *rep* gene, encodes non-structural proteins which are necessary for genome replication. By the use of two promoters (p5 and p19) and an internal splicing site, the *rep* gene is finally translated into four proteins with different lengths. Named after their molecular weight (78; 68; 52; 40 kDa), those proteins are called Rep78, Rep68, Rep52 and Rep40. All rep proteins share the same C-terminus but the bigger rep proteins Rep68 and Rep78 comprise additional amino acids (aa) at their N-termini. During the process of replication, the two bigger proteins Rep78 and Rep68 bind to a so called Rep Binding Element (RBE) within the ITR[31]. The Rep proteins show endonuclease activity and are believed to introduce a nick at the so called terminal resolution site (trs) within the ITR for providing a free 3' hydroxyl group for replication of the ITR itself after the self-primed AAV genome replication[32-34]. The two smaller Rep proteins Rep52 and Rep40 play a role at converting double-stranded DNA intermediates into the single-stranded AAV genome[35-37]. All Rep proteins share helicase and ATPase activity[32, 35, 36].

Transcription of the second AAV gene, the *cap* gene, is driven by one promoter (p40) but its translation finally results in the three virion proteins VP1, VP2 and VP3 [ref.38] as well as the recently discovered assembly-activating protein (AAP)[39]. By means of to two splice acceptor sites, the *cap* transcript is processed into two different mRNAs. Translation of the 87kDa VP1 starts from a conventional start codon (AUG) which is located only on the long and minor splice product. The shorter version is translated into three different proteins: The use of an alternative start codon (ACG) results in translation of the 72 kDa protein VP2 while the use of second conventional start codon (AUG) results in translation of the 62 kDa protein VP3. The complete viral capsid consists of 60 protein subunits at a ratio of VP1:VP2:VP3 = 1:1:10. It is thought that this molar ratio reflects the efficiency of translation of the three different virion proteins[20]. The N-termini of the VPs contain basic regions which constitute a nuclear localisation sequence (NLS), necessary for the nuclear transport[40, 41]. Additionally, VP1 contains a phospholipase 2 domain at its N-terminus which plays a role in the endosomal escape of the virions[36, 42].

The AAP is encoded in an alternative ORF within the *cap* gene. Its translation starts with the non-conventional start codon CUG and results in a protein with a molecular weight of approximately 23 kDa. It is believed to target newly synthesized capsid proteins to the nucleolus where it mediates their assembly, thereby playing a crucial role in the formation of functional AAV capsids[39]. A schematic overview of the AAV genome is displayed in **Figure 1**.

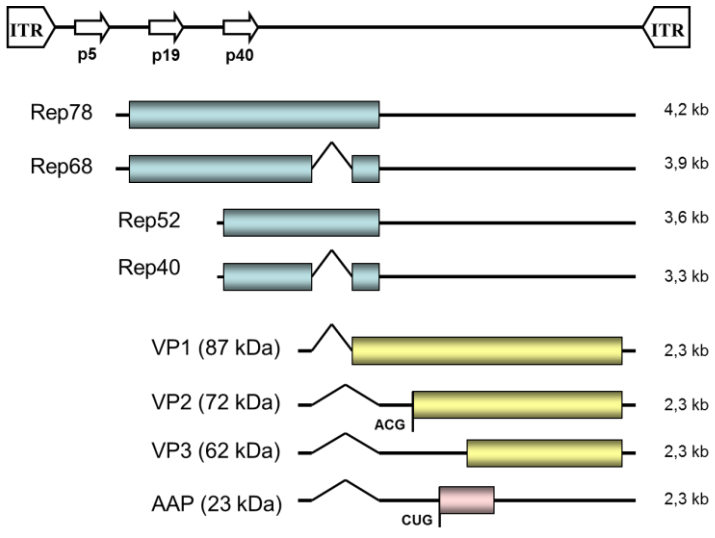

Figure 1. Genome organization of AAV
The pre-mRNAs of the different Rep proteins are transcribed from the promoters p5 and p19 and are spliced to four versions of mRNA which are translated into the four Rep proteins (Rep78/68/52/40). The pre-mRNA of the different virion proteins is transcribed from the p40 promoter and is alternatively spliced into two versions of mRNA. The usage of alternative translation initiation codons (ACG, CUG) results in translation of three versions of the virion protein (VP1; VP2; VP3) as well as the assembly-activating protein (AAP). Each Rep protein is named after its molecular mass, the molecular masses of VPs and AAP are indicated in parentheses. The lengths of the different mRNAs are indicated on the right.

1.2.3 Virion structure and host cell receptors

The crystal structure of AAV2 was first determined at a 3-Å resolution in 2002 [ref.43]. Each VP consists of eight antiparallel ß-sheets located in the core of the assembled capsid while large loops between those ß-sheets contribute to the formation of the capsid surface. The T=1 icosahedral AAV capsid displays characteristic protrusions on its surface, clustered around the three-fold axis of symmetry. These protrusions are formed by loops of three VP subunits and are called three-fold spikes. The virion structure of AAV2 is displayed in **Figure 2**.

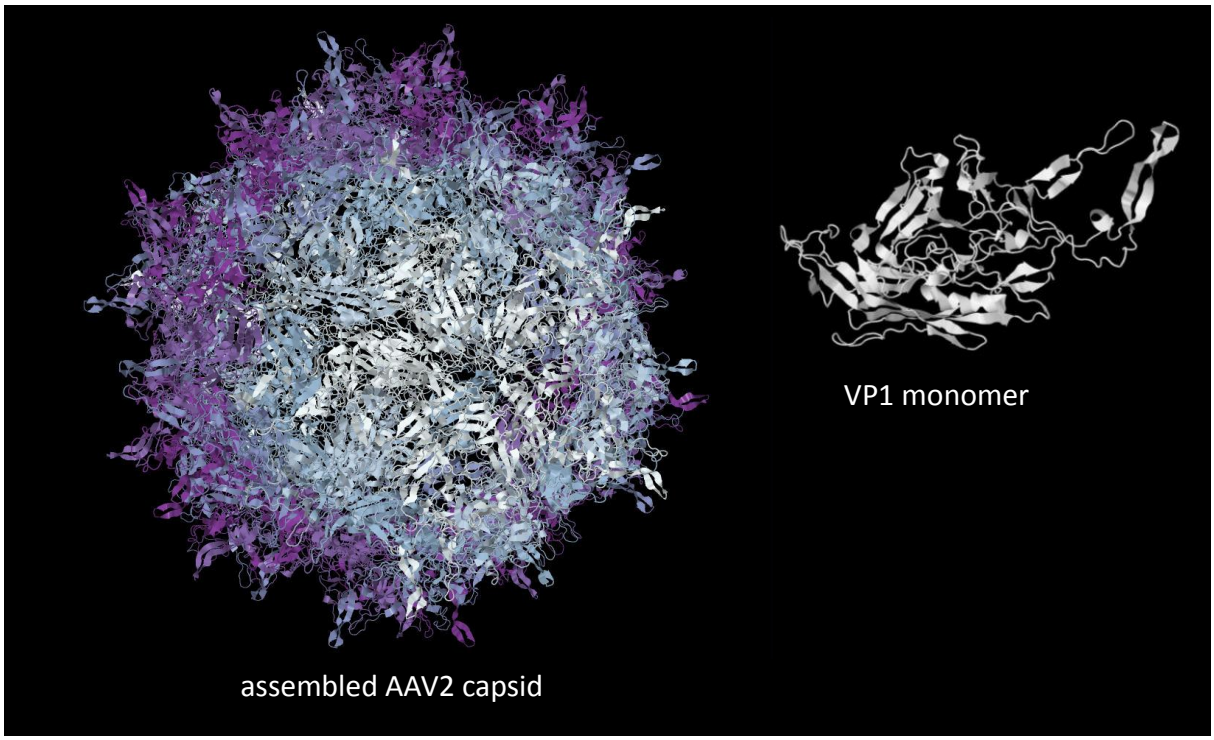

Figure 2. Molecular structure of AAV
The assembled AAV virion with T = 1 icosahedral symmetry consists of 60 virion protein subunits at a ratio 1:1:10 (VP1:VP2:VP3). Three subunits together form the so called three-fold spikes. The molecular structure of AAV2 in 3-Å resolution was visualized with the software Jmol 13.0 from the protein databank entry pdb:1LP3, obtained by Xie et al.[43].

The basic residues R484, R487, K532, R585 and R588 (VP1 numbering) in the three-fold spike region are necessary for binding heparan sulphate proteoglycan (HSPG) which is used as primary attachment receptors for AAV2 [refs.43-46]. Internalization of AAV2 is guided by one of the co-receptors αvß5 integrin[47], αvß1 integrin[48], fibroblast growth factor receptor 1 (FGFR-1)[49], hepatocyte growth factor receptor-1 (HGFR-1)[50] or the 37/67 kDa laminin receptor (LamR)[51]. Since 2002, additionally to AAV2, the structures of AAV3B[52], AAV4 [ref.53], AAV5 [ref.54], AAV6 [ref.55], AAV8 [ref.56] and AAV9 [ref.57] have been determined. The structural variety of the different AAV serotypes especially within their three-fold spike regions corresponds to the use of different receptors for host cell infection. Alternative attachment- and co-receptors of several AAV serotypes are listed in

Table 1. The broad tropism of AAV can be explained by the exploitation of ubiquitous cellular structures as attachment receptors.

Table 1. AAV receptors

	Attachment receptor(s)	Co-receptor(s)
AAV 1	Sialic acid	?
AAV 2	Heparan sulphate proteoglycan (HSPG)[44]	Integrin αV/β5 [ref.47] Integrin α5/β1 [ref.48] Fibroblast growth factor1 receptor (FGFR1)[49] Hepatocyte growth factor receptor (HGFR)[50] Laminin receptor[51]
AAV 3	Heparan sulphate proteoglycan (HSPG)[58]	Fibroblast growth factor1 receptor (FGFR1) Laminin receptor [51]
AAV 4	O-linked sialic acid[59]	?
AAV 5	N-linked sialic acid[59]	Platelet derived growth factor receptor-α (PDGFR)[60]
AAV 6	Sialic acid[61] Heparan sulphate proteoglycan (HSPG)[62]	Epidermal growth factor receptor (EGFR)[63]
AAV 7	Heparan sulphate proteoglycan (HSPG)	?
AAV 8	?	Laminin receptor[51]
AAV 9	Terminal N-linked galactose[64]	Laminin receptor[51]
AAV 10	?	?
AAV 11	?	?
AAV 12	?	?

1.2.4 Life cycle of AAV

The way of AAV host cell infection has not yet been understood in every detail. AAV seems to enter the cell by receptor-mediated endocytosis via the formation of clathrin-coated pits[65-67]. Sanlioglu et al.[68] proposed that binding of AAV to integrin triggers a kinase pathway via the activation of the G-protein rac1 that leads to intracellular traffic of the endosome along microtubules towards the nucleus. Recently this finding was confirmed by Xiao et al.[69] who showed that, once it has entered the cell, AAV is rapidly transported towards the nucleus by microtubules followed by pH-dependent endosomal escape of the virions.

Due to the unique feature of site-specific integration into the host's genome (AAVS1), the provirus is replicated with each cell cycle. The frequency of non-specific integration of AAV seems to be extremely low[26]. The viral proteins Rep78 and Rep68 as well as the ITRs and some short elements

within the AAVS1 site which resemble the RBE and the trs of the ITRs are believed to be crucial for the process of genome integration[70-72].

Co-infection with viruses like Ad, HSV or CMV results in AAV replication by a cellular DNA polymerase, starting self-primed at the ITRs as described above. Although a direct interaction of AAV with some of the adenoviral proteins E1a, E1b, E2a, E4 and VA has been determined in detail[73], they do not seem to be absolutely mandatory since replication of AAV has also been observed in cells after irradiation or the treatment of genotoxic agents[74, 75]. After replication and expression of the AAV genome, the capsid assembly takes place within the nucleoli before the assembled capsids are distributed to the nucleoplasm[76, 77]. Within the nucleoplasm, the rep proteins unwind the AAV DNA and transfer the single stranded genome into the capsid through pores at the fivefold axis of symmetry followed by cell lyses[36, 37].

1.3 AAV as gene therapy vector

1.3.1 Recombinant AAV vectors and their organization

As mentioned before, AAV has become one of the most commonly used vectors for gene therapy, mainly due to its superior safety profile and the possibility to choose capsids from several AAV serotypes for generating pseudotyped vectors with tropism towards different types of cells. Some well-established methods for large scale production of recombinant AAV vectors (rAAV) have been developed within the last decade. Almost all of them include the replacement of the viral *rep* and *cap* genes by a transgene expression cassette of choice which simply needs to be embedded within two AAV ITRs (**Figure 3**). The ITRs are the only structures which have to be provided *in cis* for functional replication of the AAV genome and its packaging into viral capsids, whereas the *rep* and *cap* genes can be provided *in trans*[78]. The most common way of rAAV production involves transient triple-transfection of producer cells (e.g. HEK 293T) with a plasmid containing the desired transgene expression cassette and the ITRs (“vector plasmid”), another plasmid containing *rep* and *cap* but no ITRs (“AAV helper plasmid”) and an adenoviral helper plasmid[79] which provides genes for adenoviral proteins that are necessary for AAV replication. Within the transfected cells, the transgene cassette is replicated by the translated viral proteins and the single-stranded DNA copies are packaged into the assembled viral capsids. Before the adenoviral helper plasmid[79] had been developed, the double-transfected cells needed to be incubated with functional adenoviruses which led to a high degree of adenoviral contamination in vector preparations. Other, more recent protocols for the production of rAAV vectors involve the co-infection of insect cells (Sf9) with baculoviruses encoding the AAV- and

adenoviral helper proteins and the transgene of choice, respectively[80, 81]. The vector titers obtained by this approaches exceed the titers which can be obtained by the triple-transfection protocol.

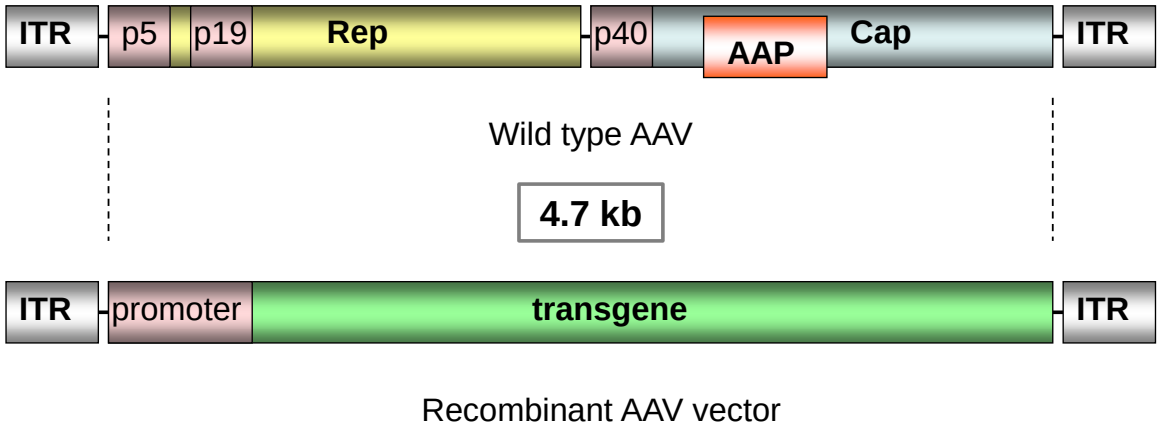

Figure 3. Genome organization of rAAV vectors
The ITRs are the only viral elements that are necessary in *cis* for encapsidation of the chosen transgene cassette into viral particles. All other structural elements can be provided in *trans*, allowing the complete exchange of the AAV genome's coding region and its promoters.

Since the ITRs are the only genomic elements derived from AAV that are encapsidated by these recombinant vectors, the risk of unwanted replication or insertional mutagenesis in patients is negligible[82] and genome integration of these vectors only takes place at a very low rate[23]. The reports of increased tumor formation in some mouse strains in context with the use of rAAV vectors[83, 84] were discussed controversially[78] and the observed effects seem more likely to be artefacts, maybe caused by the combination of the used transgenes, and mice. The safety of rAAV vectors, containing no viral elements beside the ITRs, has not only been proven in different animal models[85-87] but also in numerous clinical trials[8, 82] and not even the parental virus, natural AAV itself, has ever been linked to malignancies in humans or animals[23].

1.3.2 Packaging capacity of rAAV vectors

Being an extremely small virus (≈ 25 nm) with a short genome, AAV only provides limited packaging capacity. Most studies indicate that transgene cassettes up to the lengths of the natural AAV genome (≈ 4.7 kb) can efficiently be encapsidated without altering the vector's functionality whereas longer genomes either get truncated without being completely encapsidated or they get completely encapsidated but lead to decreased vector infectiousness[88-90]. This problem has been solved by the development of so-called trans-splicing or overlapping vectors which enable the usage of bigger transgenes by splitting and distributing them into different capsids and allowing them to reconstitute by concatamer formation or head-to-tail recombination after infection[91].

The second strand synthesis of transgenes delivered by rAAV within the nucleus of infected cells is a rate limiting step on the way to successful transgene expression[92]. In cases in which the packaging capacity of AAV is of minor importance since the chosen transgene is small enough, so called self-complementary AAVs (scAAVs) can be used to overcome this step[93-95]. Modified ITRs enable scAAV vectors to encapsidate dimeric self-complementary DNA which further reduces the compatible length of the transgene to approximately 2.5 kb. On the other hand, the transgene can directly be transcribed and translated into proteins after host cell infection without the rate limiting step of previous second strand synthesis.

1.3.3 Immunogenicity of AAV vectors

AAV is described as being mildly immunogenic and has long time been thought to only elicit humoral immune responses[96, 97]. Decreased transgene expression of rAAV vectors after repeated administration due to neutralizing antibodies has been thought to be the major immune-related problem when working with AAV[98]. Numerous preclinical and clinical studies confirm the general good tolerability of rAAV vectors (reviewed in ref.[99]). Still, cases of capsid-related cytotoxic T-cell immune responses have repeatedly been reported within the last few years[100-105]. The exploitation of new AAV serotypes and systematic modifications of the AAV capsid may help to circumvent this problem[105, 106].

1.3.4 AAV serotypes - exploiting differences in tropism

When considering the use of AAV as vector for gene therapy in a systemic *in vivo* approach, two major obstacles have to be taken into account. On the one hand, AAV is able to infect a broad range of different cells, since it utilizes wide-spread cellular structures as attachment receptors (e.g. polysaccharides like HSPG) which results in a low degree of specificity for any chosen target tissue. On the other hand there are many therapeutically relevant cell types which cannot be infected by AAV at all or just to a limited extent. Over the last years, numerous strategies have been developed to overcome these problems. Different AAV serotypes have been analyzed for their tropism and the generation of pseudotyped vectors has broaden the spectrum of infectable cell types and tissues[107]. Analyses revealed that the different AAV serotypes vary in their transduction profile after systemic application *in vivo* and therefore can be used in different therapeutic settings. To further extend the vector tropism to other targets, either capsid protein subunits or single protein domains of different serotypes have been mixed, resulting in so called mosaic- or chimeric rAAV vectors[108-118]. Additional capsid modifications e.g. by error-prone PCR could further enhance the capsid diversity[119, 120]. Indeed,

vectors with extended tropism to previously barely infectable cell types have been isolated by screening pools of such mosaic- or chimeric vectors and one of them even made its way into a clinical trial[121]. However, most of those vectors still only mediate moderate tissue specificity, since they lack a systematic disruption of the natural receptor binding sites.

1.3.5 AAV capsid engineering

The conjugation of specific antibodies or ligands to the AAV capsid seemed to be a more straight forward approach to re-direct AAV to alternative receptors than combining different serotypes[78]. Like vectors based on other viruses[18], AAV vectors have successfully been re-directed to new target tissues by coupling them to antibodies or other ligands[122-124]. Nevertheless, such vectors often are of limited use for *in vivo* applications since they are comparably large and unstable, they may increase immunogenicity, they do not necessarily mediate target cell infection and their large-scale production is expensive and time-consuming[125]. The genetic incorporation of targeting ligands into the AAV capsid protein was the next logical step to circumvent the problems mentioned above. Proteins up to a size of ≈ 15 kDa have successfully been fused to the N-termini of VP1 and VP2 without altering vector stability[126-130]. Other approaches aim to modify relevant regions of the most abundant AAV capsid protein VP3 and several sites have been proven to tolerate the insertion of peptides up to a length of 34 bp[78]. The first discovered and still most commonly used site[78] for the insertion of targeting peptides into the AAV2 capsid is located at amino acid positions N587 [ref.131] or R588 [ref.132] (VP1 numbering), a prominent region within the viral three-fold spikes. In contrast to the insertion of peptides at other positions that are generally suited (e.g. amino acids G520 and Q584)[128, 131, 133], peptide insertions at position 587/R588 very likely interfere with the HSPG binding motif (amino acids R484, R487, K532, R585 and R588)[43-46] and thereby enhance the chance to abrogate the endogenous tropism and re-direct AAV to a peptide targeted structure[78], at least if the peptide's nature does not restore the endogenous binding properties[134]. Particles modified by this means have also been shown to escape neutralizing antibodies[135], but choosing the right targeting peptide remains a challenging task. Numerous peptides, many of which had previously been identified by screening phage display peptide libraries, have successfully been integrated into the AAV capsid to extend the vector tropism *in vitro*[136] and *in vivo*[132, 137-140]. Nonetheless, the introduction of pre-selected targeting peptides into the AAV capsid with all its tight structural constraints is typically associated with a loss of specificity and efficacy, since the properties of peptides widely vary with the structural context in which they are embedded. This problem has been approached by the development of so-called random AAV display peptide libraries which for the first time enabled the

selection of targeting peptides directly within the structural constraint of the capsids of AAV2 [refs.141, 142] or AAV9 [ref.143].

1.3.6 Random AAV display peptide libraries

Taking into account the shortcomings of prior targeting approaches, Müller et al.[141] developed a system to generate peptide libraries displayed on the capsid surface of AAV2. These libraries consist of a large pool of diverse AAV virions (i.e. ≈ 1 x 10^8), differing from each other within their prominent three-fold spike regions by displaying random peptides at amino acid position R588 (VP1 numbering) of their 60 capsid subunits (**Figure 4**).

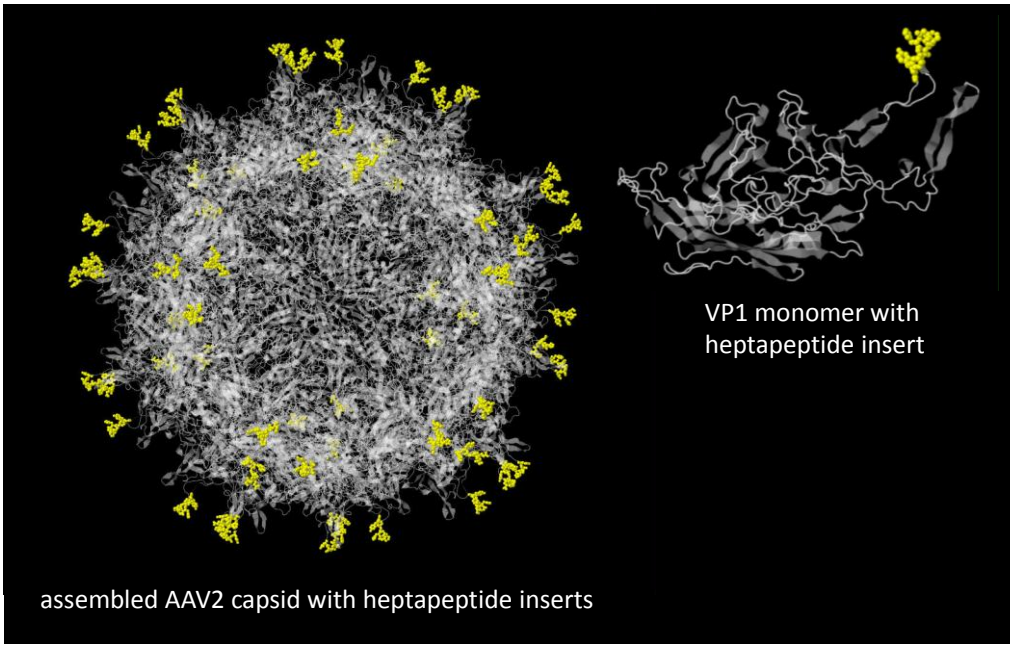

Figure 4. Schematic representation of a modified AAV2 capsid displaying random heptapeptides in its three-fold spikes
Each AAV2 library particle (grey) displays 60 copies of a random heptapeptide (yellow). The genetic information of the modified capsid with the peptide insertion at amino acid position R588 (VP1 numbering) is encoded in the encapsidated genome. A random AAV2 display peptide library contains up to 10^8 almost identical particles, only differing from each other in the sequence of the random peptide displayed within the three-fold spike region. This image was visualized with the software Jmol 13.0 from the protein databank entry pdb:1LP3 [ref.43] complemented with peptide insertion at R588

Random AAV display peptide libraries such as the one used in this study are produced in a three step protocol to ensure a high library titer, the absence of wild type AAV2 contamination and the genomic integritiy of the library. A plasmid library encoding the modified AAV capsids is generated in the first step of the three step protocol by cloning commercially purchased random oligonucleotides into the library plasmid backbone. Then, so called “AAV library transfer shuttles” are generated by triple-

transfection of HEK 293T cells with the plasmid library[141], a plasmid encoding the wild type AAV2 capsid (codon modified to prevent homologous recombination[144]) and an adenoviral helper plasmid[79] to enable replication within the producer cells. By assembling subunits of library proteins and wild type AAV2 proteins into functional capsids, the resulting transfer shuttles retain infectiousness for HSPG-positive cells like HEK 293T due to their wild type parts, while the library parts mediate new and at this step unpredictable binding properties. Although displaying mosaic capsids, these transfer shuttles only encapsidate the genetic information of the library plasmids, since solely these plasmids have been equipped with ITRs as packaging signals. In a third step, the transfer shuttles are used to produce the final random AAV display peptide library by infecting HEK 293T cells at a very low multiplicity of infection (MOI; ≤1), followed by superinfection with adenovirus, ensuring that each cell is just infected by one transfer shuttle and therefore restricted to the production of library particles corresponding to one single encapsidated genome. Finally, the AAV display peptide library can be harvested and purified and afterwards be screened for targeting peptides *in vitro* and *in vivo*. A schematic representation of the three step protocol for generation of random AAV2 display peptide libraries is displayed in **Figure 5**.

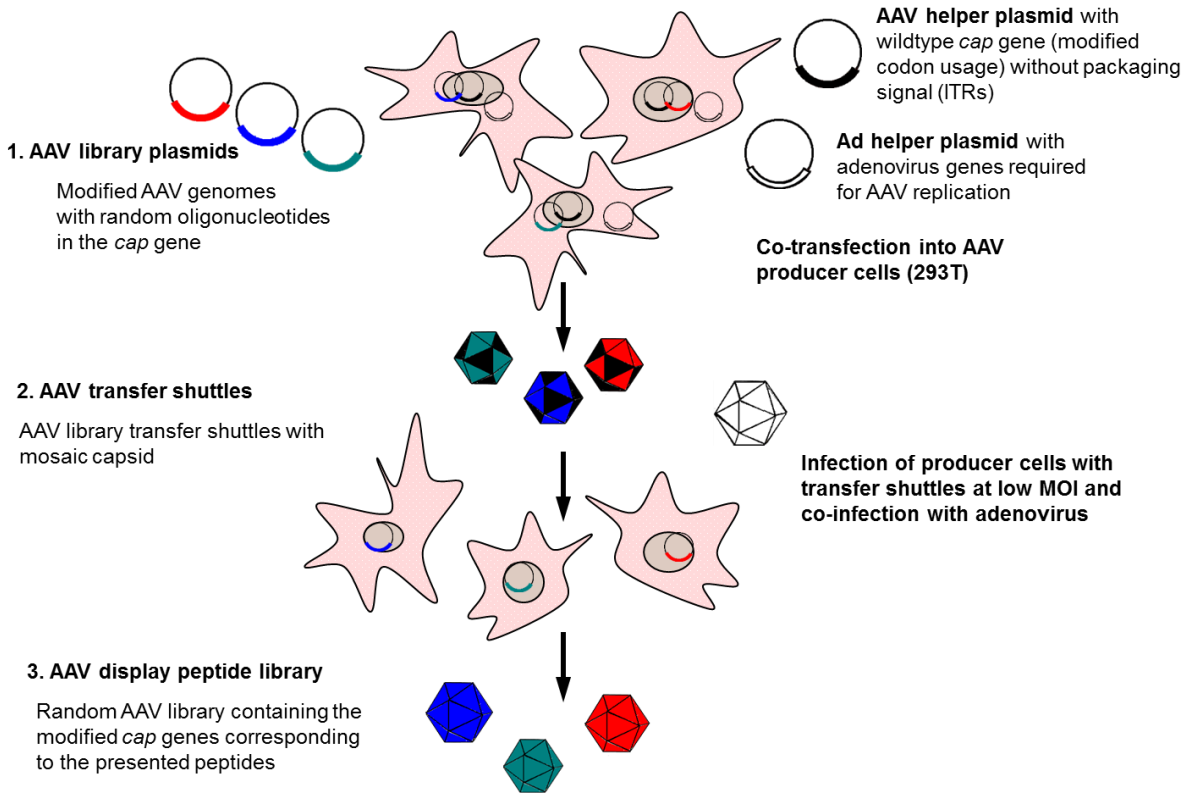

Figure 5. Three step protocol for generation of random AAV display peptide libraries
Adapted from Müller et al.[141] **Step 1**: Cloning of the AAV plasmid library by insertion of heptapeptide-encoding oligonucleotides at nucleotide position 3,967 (R588). **Step 2**: Transfection of HEK 293T producer cells with the AAV plasmid library, an adenoviral helper plasmid and an AAV helper plasmid encoding the wild type AAV2 cap gene for generation of AAV transfer shuttles. **Step 3**: Infection of HEK 293T producer cells with the library transfer shuttles at low MOI and superinfection with adenovirus for generation of the final random AAV display peptide library.

To benefit from the high transduction efficiency of AAV serotype 9, the library system has recently been adopted to this serotype, after suggesting that amino acid position A589 of the AAV9 capsid might be equally suited as peptide insertion site to AAV2 R588 [ref.143].

1.3.7 Screening AAV display peptide libraries

Based on their large diversity (≈ 1×10^8), random AAV display peptide libraries are extremely powerful tools to generate targeted vectors for virtually any cell type or tissue of interest. Since such libraries consist of so many different virions with unpredictable tropism, they need to be screened for suitable variants with desired tropism towards the tissues of interest. The screening process can be performed over several rounds of selection *in vitro* or *in vivo* and is also referred to as *directed evolution*.

Today, *in vitro* screening is a well-established procedure during which only infectious library viruses with the desired tropism are replicated in a cell type of interest by superinfection with adenovirus, whereas non-infectious particles are removed during subsequent rounds of selection. A lot of different library-derived virus capsids have successfully been enriched by this approach, showing strongly enhanced tropism for a diverse range of cells like human coronary artery endothelial cells[141], human chronic lymphatic leukemia cells[142], human acute myeloid leukemia cells[145], human peripheral blood hematopoietic progenitor cells[146], human umbilical vein endothelial cells[143] and murine Polyoma middle T antigen induced tumor cells[147]. Despite their success in specifically transducing diverse cell types *in vitro* and, coming along with that, their potential feasibility for therapeutic *ex vivo* trials or functional studies, these vectors are only of limited use for *in vivo* trials. Since the expression profile of many cells fundamentally changes when they are taken from the living organism into culture, in *vivo* screenings of random AAV peptide libraries are far more promising than *in vitro* based approaches[125]. Specific ligand-receptor interactions under circulating conditions, endothelial cell layers and the extracellular matrix acting as physical barriers as well as vector clearance from the circulation by the reticuloendothelial system can be taken into account when screening random AAV libraries *in vivo*. The protocol of *in vivo* screening is much more sophisticated than the *in vitro* approach and is still under development. In one of the most promising protocols, successfully homing library viruses within the tissue of interest are amplified by PCR after intravenous injection of the AAV library, instead of being replicated by superinfection with adenovirus[147]. The non-target tissues in the living organism provide efficient negative selection by competing for circulating library particles with the tissue of interest, which further increases vector specificity. The screening of AAV display peptide libraries is schematically depicted in **Figure 6**. Vectors obtained by *in vivo* screenings indeed have shown highly enhanced transduction capability for murine heart[148], lung[112, 147]or

Polyoma middle T antigen induced breast tumors in mice[147] after intravenous injection. Still, almost all of these vectors lack the high degree of tissue specificity which is needed for therapeutic approaches and most of them are of low efficacy. Thus, the high potential of the random AAV display peptide libraries has not been fully exploited yet.

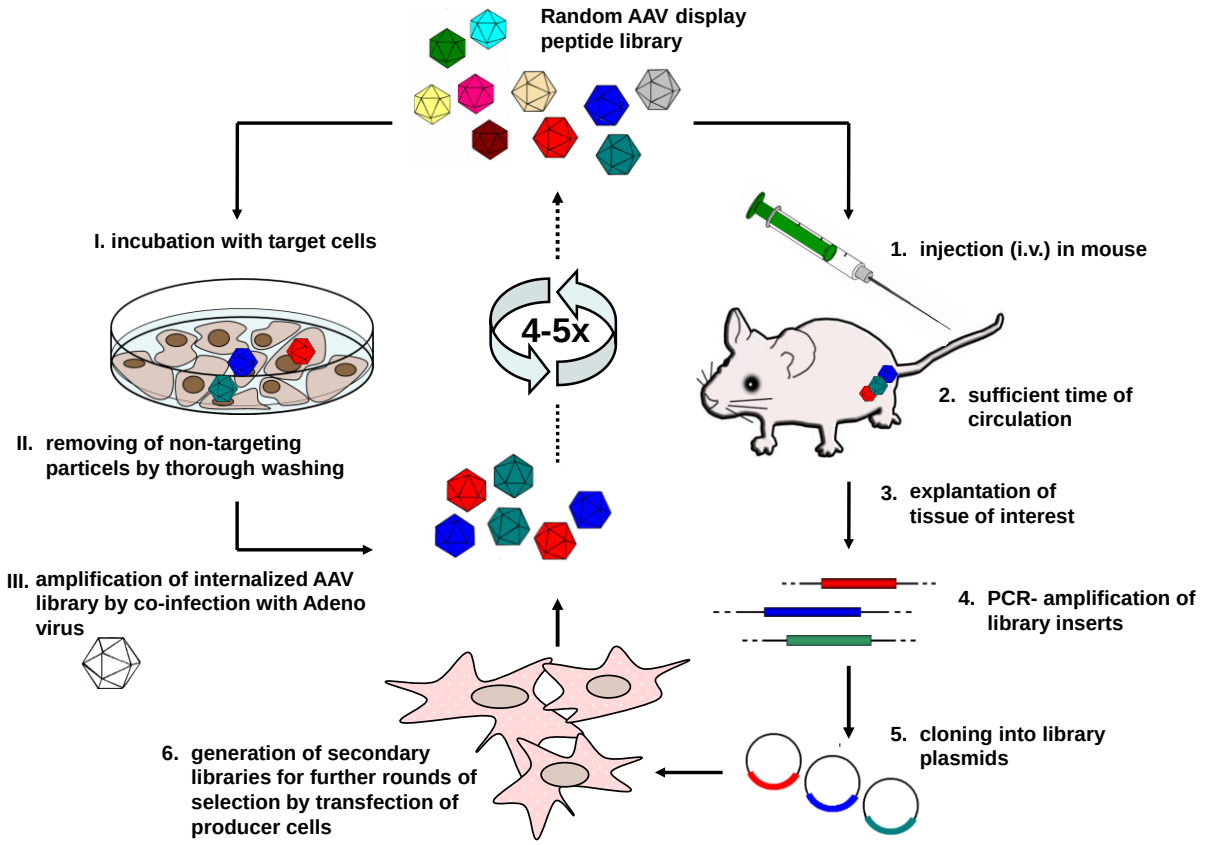

Figure 6. Screening of random AAV display peptide libraries
During the *in vitro* screening (left), the AAV library is incubated with the cells of interest (**I**), followed by removal of non-infectious particles by thorough washing (**II**) and adenoviral amplification of successfully internalized particles (**III**). Pre-selected and amplified particles are used for further rounds of selection. For the *in vivo* screening (right) the AAV library is injected i.v. into a mouse (**1**) where particles are given time to infect their target tissues during circulation (**2**). The tissue of interest is harvested (**3**) and viral DNA containing the library inserts is amplified by PCR (**4**). The insert-encoding fragments are used to generate a new, pre-selected plasmid library (**5**) which is used to produce a secondary AAV library for subsequent rounds of selection (**6**).

1.3.8 Improving vector specificity: transcriptional and post-transcriptional targeting

Expanding vector tropism to formerly insusceptible cell types or tissues is just the first step towards clinical use. Specificity for relevant target cells and absence of gene expression in non-target tissues seems to be at least equally important to vector efficacy. Since vector specificity is not easily achievable solely by re-targeting approaches based on manipulating viral capsids, it often needs to be improved e.g. by the use of tissue specific promoters (transcriptional targeting). A lot of different

promoters have been evaluated in preclinical or clinical settings to improve the specificity of AAV mediated transgene expression in the central nervous system[149-151], the eye[152], muscles[153], the heart[154]and the liver[102, 155]. Another option is the use of binding sites for tissue specific microRNAs (miRNAs) to suppress vector-mediated transgene expression in non-target tissues (post-transcriptional targeting). Expression, e.g. in the liver, heart, or hematopoietic cells could successfully be suppressed by the use of miRNA binding sites in vector systems based on AAV[156, 157]and other viruses[158-161]. Although transcriptional and post-transcriptional targeting are successful approaches to enhance tissue specificity of transgene expression, they do not prevent unspecific vectors from transducing non-target cells and, especially important in case of AAV, they further reduce space in the expression cassette due to the limited packaging capacity. Therefore, highly specific vector homing without the need of additional transcriptional or post-transcriptional targeting can still be considered the “holy grail” of vectorology.

1.4 Potential target tissues for gene therapeutic intervention

1.4.1 The brain as target for gene therapy

Numerous severe neurodegenerative and inherited metabolic diseases of the central nervous system (CNS) such as Huntington disease, amyotrophic lateral sclerosis, Parkinson’s disease and multiple sclerosis are still associated with a poor quality of live lead to an early death. Since they are at least partially caused by malfunctions of genetic components, these diseases have drawn attention on the brain as an organ which could strongly benefit from gene therapeutic interventions. Numerous animal studies and clinical trials[13, 162, 163] involving gene therapy for neurodegenerative disorders have been performed within the last two decades, utilizing AAV and other viral vectors[164]. The brain is separated from the circulating bloodstream by the blood brain barrier (BBB), which is a very tight physical barrier formed by the interaction of endothelial cells, pericytes, astrocytes and the extracellular matrix. The tight junctions of the endothelial cells selectively detain most circulating compounds from entering the central nervous system[165]. Delivery of vectors to the brain therefore requires direct intracranial injection which, despite all risks, today still is the administration route of choice also in clinical trials[164]. Most AAV serotypes have been analyzed for their transduction profile within the brain upon intracranial injection[166-172] and the serotypes AAV5 [refs.169, 170], AAV9 and AAV10Rh[171] have performed comparably well, most of them predominantly transducing neurons. Transient disruption of the BBB e.g. by chemical compounds[118] or ultrasound[173] is another way of delivering vectors to the brain without the need of direct injection. Also, the stroke-affected BBB is easily traversable by viral vectors [174]. On the downside, the disruption of the BBB bares the risk of

toxicity and unwanted immune response. To overcome the need of intracranial injection or transient BBB disruption, several investigators analyzed the capability of AAV to cross the intact BBB after intravenous injection, thereby setting focus on serotype AAV9 [ref.175]. In neonatal mice, AAV9 seems to be able to completely cross the BBB (as far it is developed at this stage) and to transduce different neurons[176], whereas in adult mice, AAV9 is at least able to transduce astrocytes[176] and motor neurons in the spinal cord[177]. Despite being the most efficient serotype for gene delivery into the brain after simple intravenous injection, AAV9 predominantly transduces the heart and therefore only is of limited clinical relevance for CNS diseases if applied systemically. Recently, it has been shown that vectors do not necessarily have to deliver genes through the BBB to mediate therapeutic effects[140]. Delivery of the β-glucuronidase gene to the brain vasculature endothelium by a modified AAV vector was sufficient to correct lysosomal storage disease in mice. Still, the vector utilized in this study was of poor specificity and efficacy. Thus, the need of vectors that mediate efficient and specific gene transfer through the BBB or at least to the brain vasculature endothelium is still unmet.

1.4.2 The lung as a target for gene therapy

Like the brain, the lung is an organ which could benefit from gene therapeutic approaches[178]. Severe lung diseases like cystic fibrosis (CF)[179] or α-1-antitrypsin (AAT) deficiency[180] are already being treated by gene therapy in clinical trials using AAV and other viral vectors. The airway epithelium, one of the target tissues for the treatment of CF, can be reached comparably easy by inhalation of aerosolized vectors, especially with adenoviral vectors[181, 182], while AAT deficiency can be treated by targeting the endogenous site of AAT production, the liver[183] or other ectopic sites like muscles[183-186], since AAT freely circulates through the body. Different AAV serotypes have been tested for their transduction profile within the lung after intranasal application. Concerning transduction of the airway- and alveolar epithelium, AAV9 [ref.187], AAV5 [refs.188, 189] and AAV6 [refs.62, 190] seem to be more effective than AAV2 [refs.188, 189], while chimeric vectors displaying capsid subunits from AAV1, AAV6 and AAV9 seem to be performing even better[115] than their parental serotypes. Another clinically very relevant tissue, the endothelium of the pulmonary vasculature, is poorly accessible by vectors after inhalative administration and requires intravenous vector injection. Although AAV4 seems to preferably home to the lung after intravenous injection[107], there is no available vector system which specifically and efficiently transduces the pulmonary vasculature.

Severe diseases of the pulmonary vasculature like pulmonary hypertension (PH) have been treated by gene therapeutic approaches in animal models[191-194] mostly with aerosolized adenoviral vectors, regardless of non-target transduction. Due to potentially inducible side-effects by these unspecific vectors, they are not suited for the treatment of human patients. Therefore, gene therapeutic

treatment of diseases like PH is mainly limited by the lack of vectors that specifically and efficiently transduce the pulmonary vasculature.

1.5 Aim of this study

As outlined in chapter **1.3.6**, random AAV display peptide libraries like the one developed by Müller et al.[141] seem to be extremely powerful tools to generate cell type-specific vectors, which are urgently needed in the field of gene therapy. Although they have already proven their utility *in vitro*, AAV libraries barely yielded vectors with convincing properties for *in vivo* applications, with one exception[148]. This study aimed at proving that efficient vectors with high tissue specificity can indeed be screened *in vivo* from random AAV display peptide libraries and that their huge potential has not been fully exploited yet. It was speculated that screening such libraries is a very error-prone process with many variables influencing the outcome. Therefore it was planned to analyze two slightly different protocols of *in vivo* selection, one of which was applied as part of this study. Choosing the brain and the lung as therapeutically highly relevant targets, AAV library clones potentially enriched in these organs were to be analyzed in detail regarding their desired qualities like efficacy and specificity for the target tissue. In the end, the goal of this study was not only to achieve a better understanding of the complex system of random AAV display peptide libraries but also to finally provide gene therapy vectors for the CNS and the lung that potentially meet all the high expectations regarding safety, efficacy and tissue specificity.

2 Material

2.1 Laboratory equipment

Laboratory equipment used in this study is listed in **Table 2.**

Table 2. Laboratory equipment

Equipment	Product name	Manufacturer/distributor
1D protein electrophoresis system	Mini-PROTEAN® Tetra Cell	Biorad
Absorbance reader	Sunrise	Tecan
Agarose gel electrophoresis systems	Sub-Cell® GT & Wide Mini Sub-Cell® GT	Biorad
Benchtop centrifuge (small)	centrifuge 5424	Eppendorf
Benchtop centrifuge (large)	centrifuge 5810	Eppendorf
Benchtop incubatated and refrigerated shaker	MaxQ 4000	Thermo Fisher Scientific
Benchtop mixer/shaker	Vortex Genie® 2	Thermo Fisher Scientific
Cell culture incubator	HERAcell 240	Thermo Fisher Scientific
Digital microscope camera	DP-25	Olympus
Electroporation system	Gene Pulser Xcell™ Microbial System	Biorad
Fluorescence microscopes	Axiovert 40 CFL/ BX-51/ DMI6000 B	Carl Zeiss/ Olympus/ Leica
Freezer (-20 °C)	Biomedical Freezer	Sanyo Biomedical
Freezer (-80 °C)	V.I.P.™ Series	Sanyo Biomedical
Gel documentation system	Gene Genius Bio Imaging System	Syngene
In vivo imaging system	IVIS 200	Caliper Lifescience
Laminar flow safety bench	HeraSafe HS 15	Heraeus Instruments
Light microscope	CK 2	Olympus
Luminometer	Mithras LB 940	Berthold Technologies
Microbiological incubator	Kelvitron® t	Heraeus Instruments
Microbiological incubator shaker	Model G25	New Brunswick Scientific/Eppendorf
Microtome	HM 355 S	Microm
pH meter	Microprocessor pH Meter	WTW
Power supply	PowerPac™ Basic	Biorad
Precision balance	Lab Style 3002	Mettler Toledo
Preparative ultracentrifuge	Optima™ LE-80K, Rotor: Type 70.1	Beckman Coulter
Real-time PCR cycler	LightCycler® Nano	Roche Diagnostics
Refrigerated benchtop centrifuge	centrifuge 5417 R	Eppendorf AG
Refrigerated centrifuge	Avanti® J-E, Rotors: JA-14, JA-25.5, JA-20.1	Beckman Coulter
Spectrophotometer	NanoDrop 2000c	Thermo Fisher Scientific
Spin tissue processor	Microm STP 120	Thermo Fisher Scientific
Steam sterilizer	Varioklav®	HP Medizintechnik
Thermal cycler	Mastercycler® personal	Eppendorf
Thermal gradient cycler	Mastercycler® gradient	Eppendorf
Thermo blocks	TB2/ Thermoblock	Biometra / Peqlab
Tube topper/sealer	Quick-Seal Cordless Tube Topper	Beckman Coulter
Vibratome	VT1200S	Leica
Water bath/circulator	Thermomix ME	B. Braun

2.2 Molecular biology kits & ready-to-use reagents

Ready-to-use reagents and kits used in this study are listed in **Table 3.**

Table 3. Molecular biology kits & ready-to-use reagents

Kit or reagent	Manufacturer/distributor
30% Acrylamide/Bis Solution	Biorad GmbH
DNeasy® Blood & Tissue Kit (250)	Qiagen
Gel Pilot Loading Dye (5x)	Qiagen
Luciferase Assay Reagent (LAR)	Promega
NucleoBond® PC 100	Macherey-Nagel
NucleoBond® Xtra Maxi	Macherey-Nagel
OptiPrep™ Density Gradient Medium (60% w/v iodixanol)	Axis-Shield
PeqGold Gel Extraction Kit	Peqlab
PeqGold Plasmid Mini Kit	Peqlab
Qiaquick® PCR Purification Kit (250)	Qiagen
Qiaquick® Nucleotide Removal Kit (250)	Qiagen
Roti® Nanoquant	Carl Roth
Sequenase Version 2.0 DNA Sequencing Kit	USB®/Affymetrix

2.3 Enzymes

Enzymes used in this study are listed in **Table 4.**

Table 4. Enzymes

Enzyme	Manufacturer/distributor
Antarctic Phosphatase (5,000 U/ml)	New England Biolabs
Benzonase® Nuclease (≥ 250 U/µl)	Sigma-Aldrich
DNA Polymerase I, Klenow Fragment (5,000 U/ml)	New England Biolabs
FastStart Essential Green Mastermix (SYBR Green)	Roche
GoTaq® DNA Polymerase (5 U/µl)	Promega
HotStar Taq® DNA Polymerase (5 U/µl)	Qiagen
Phusion High Fidelity DNA Polymerase (2,000 U/ml)	New England Biolabs
Proteinase K	Qiagen
Restriction Endonucleases (diverse)	Fermentas & New England Biolabs
RNase A (100 mg/ml)	Qiagen
T4 DNA Ligase (400,000 U/ml)	New England Biolabs
Trypsin/EDTA 10x Solution	PAA Laboratories

2.4 Antibodies

Antibodies used in this study are listed in **Table 5**.

Table 5. Antibodies

Denotation	Description	Source
A-11122	Polyclonal rabbit anti-GFP, IgG	Invitrogen
A-3563	Polyclonal sheep anti-mouse IgG, AP-conjugated F(ab'2)	Sigma- Aldrich
ab28364	Polyclonal rabbit anti-CD31, IgG	Abcam
ab6586	Polyconal rabbit anti-collagen IV, IgG	Abcam
AK76.3	Monoclonal mouse anti-AAV Rep [ref.195], supernatant from hybridoma cells	Prof. Dr. Jürgen Kleinschmidt (DKFZ, Heidelberg, Germany)
AP189C	Polyclonal donkey anti-rat IgG, Cy3-conjugated IgG	Merck Milipore
B1	Monoclonal mouse anti-AAV VP [ref.196], supernatant from hybridoma cells	Prof. Dr. Jürgen Kleinschmidt
BA-1000	Polyclonal goat anti-rabbit IgG, biotinylated IgG	Vector Laboratories
sc-2010	Polyclonal goat anti-mouse IgG, FITC-conjugated IgG	Santa Cruz
-	Polyclonal rat anti-Mouse CD31, IgG	BD Pharmingen™
-	Polyclonal rat anti Mouse CD13, igG	AbD serotec
-	Polyclonal donkey anti -rabbit igG, Cy3-conjugated igG	Jackson Immuno Research

2.5 Chemicals & reagents

Chemicals, reagents and cell culture supplements used in this study were obtained from the following companies: Affymetrix, BD Bioscience, Biorad, Carl Roth, Dako, Fermentas, Fluka, GE-Healthcare, Invitrogen, Merck, Serva, Sigma-Aldrich, Roche, Vetequip.

2.6 DNA- and protein ladders

The size of DNA fragments was determined by agarose gel electrophoresis using the Quick Load® 1 kb DNA Ladder (New England Biolabs) or the Quick Load® 100 bp DNA Ladder (New England Biolabs). The size of proteins was determined by SDS PAGE using the PageRuler™ Prestained Protein Ladder 10-170 kDa (Pierce).

2.7 Disposables

Disposables were obtained from the following companies: Beckman Coulter, Biorad, Braun, Corning, Dako, Eppendorf, Greiner, Perkin Elmer, Pierce, Sarstedt, Whatman.

2.8 Standard buffers

The recipes of the most commonly buffers are listed below. Special buffers used for single experiments are specified in chapter **3 Methods**.

PBS (***P**hosphate **B**uffered **S**aline)*

10x stock solution (1 l)	1x working solution
- 80.0 g NaCl	137.0 mM
- 2.0 g KCl	2.7 mM
- 7.6 g Na_2HPO_4 $2H_2O$	4.3 mM
- 2.0 g KH_2PO	1.5 mM
- *ad* 1.0 l $_{dd}H_2O$	

adjusted to pH 7.4, autoclaved 20 min at 121 °C, for 1x PBS diluted 1:10 in sterile $_{dd}H_2O$

PBS-MK (***P**hosphate **B**uffered **S**aline with magnesium [**M**g] / potassium [**K**])*

10x stock solution (1 l)	1x working solution
- 0.95 g Mg_2Cl	137.0 mM
- 1.86 g KCl	2.7 mM
- *ad* 1.00 l 1x PBS	

sterile filtered (0.2 µm filter), for 1x PBS-MK diluted 1:10 in sterile $_{dd}H_2O$

TBS-T (***T**ris **B**uffered **S**aline with **T**ween)*

10x stock solution (1 l)	1x working solution
- 80.0 g NaCl	137.0 mM
- 2.0 g KCl	2.7 mM
- 30.0 g Tris base	4.3 mM
- 2.0 ml Tween 20	1.5 mM
- *ad* 1.0 l $_{dd}H_2O$	

adjusted to pH 8.0, autoclaved 20 min at 121 °C, for 1x TBS-T diluted 1:10 in sterile $_{dd}H_2O$

2.9 Cells

2.9.1 Prokaryotic cells (*Escherichia coli*)

E. coli strains used for amplification of plasmid/bacmid DNA are listed in **Table 6**.

Table 6. Prokaryotic cells

Denotation	Genotype	Reference
DH5α™	F$^-$ ϕ80d*lac*ZΔM15 (*lac*ZYA-argF) U169 *deo*R *rec*A1 *endA*1 hsdR17 (r_K^-, m_K^+), phoA *sup*E44 λ$^-$ *thi*-1 gyrA69 relA1	ref.[197]
DH10BAC™	F$^-$ *mcr*A Δ(*mrr-hsd*RMS-*mcr*BC) ϕ80d*lac*ZΔM15 Δ*lac*X74 *deo*R *rec*A1 *endA*1 *ara*D139 (*ara*, *leu*)7697 *gal*U *gal*K λ$^-$ *rps*L nupG bMON14272 pMON7124	refs.[198, 199]
XL1-Blue	*rec*A1 *endA*1 *gyr*A96 *thi*-1 *hsd*R17 *sup*44 *rel*A1 lac [F'*pro*AB *lac*I^{q}ZΔM15 Tn10 (Tet^r)]	ref.[200]

2.9.2 Eukaryotic cells

Immortalized cell lines used for vector production and analyses of vector mediated transgene expression are listed in **Table 7**.

Table 7. Eukaryotic cell lines

Denotation	Description
HEK-293T	Adenovirus E1A/B and SV40 large T-antigen transformed human embryonic kidney cells[201, 202]
Sf9	*Spodoptera frugiperda* ovarian cells[203]

2.10 Animals

All experiments involving animals were performed with one of the mouse strains (*Mus musculus*) listed in **Table 8**.

Table 8. Mouse strains

Denotation	Source
FVB/N	Immunocompetent inbred albino strain[204], bred in the UKE animal facility
CR57BL/6	"Black Six", Immunocompetent inbred strain, bred in the animal facility of the University of Luebeck
SCID	immunocompromised albino strain, purchased from Janvier

2.11 Viruses

2.11.1 Helper viruses

Ad5	Human wild type Adenovirus 5, kindly provided by the Laboratoire de Thérapie Génique (Nantes France)

2.11.2 Recombinant AAV (vectors)

Recombinant AAVs used in this study are listed in **Table 9.**

Table 9. Recombinant AAVs

Denotation	Description
AAV2-R588$(X)_7$-Shuttle	Random AAV display peptide library transfer shuttles, a pool of particles, each displaying a mixture of wild type AAV2 Cap subunits and AAV2 Cap subunits with random $(X)_7$ peptide insertion at R588, carrying AAV2 *rep* and modified AAV2 *cap* gene from pMT187-0-3 (**2.13**)
AAV2-R588$(X)_7$-Library	Random AAV display peptide library, a pool of particles, each displaying a random $(X)_7$ peptide insertion at R588, carrying AAV2 *rep* and modified AAV2 *cap* gene from pMT187-0-3 (**2.13**)
rAAV2wt-CMV-LUC	Displaying the wild type AAV2 capsid, carrying the pAAV-CMV-LUC expression cassette (**2.13**)
rAAV2-$(X)_7$-CMV-LUC	Displaying the AAV2 capsid with a selected R588 $(X)_7$ peptide insertion, carrying the pAAV-CMV-LUC expression cassette (**2.13**)
rAAV2-$(X)_7$-dsCMV-eGFP	Displaying the AAV2 capsid with a selected R588 $(X)_7$ peptide insertion, carrying the dsAAV-CMV-eGFP expression cassette (**2.13**)
rAAV2-$(X)_7$-CAG-LUC	Displaying the AAV2 capsid with a selected R588 $(X)_7$ peptide insertion, carrying the pAAV-CAG-LUC expression cassette (**2.13**)
rAAV2-$(X)_7$-CAG-eGFP	Displaying the AAV2 capsid with a selected R588 $(X)_7$ peptide insertion, carrying the pAAV-CAG-eGFP expression cassette (**2.13)**

2.12 Synthetic oligonucleotides

All olignucleotides used in this study were synthesized by Metabion and are listed in **Table 10**.

Table 10. Synthetic oligonucleotides

Denotation	Sequence 5' → 3'	GC%	No. Bases	Reference
	Primers for amplification of AAV *cap* gene fragments (with insertion site)			
AAV2_4+	ATG GCA AGC CAC AAG GAC GAT G	50.0	22	ref. [147]
AAV2_4-	CGT GGA GTA CTG TGT GAT GAA G	50.0	22	ref. [147]
AAV2_3+	GGT TCT CAT CTT TGG GAA GCA AG	47.8	23	ref. [147]
AAV2_3-	TGA TGA GAA TCT GTG GAG GAG	47.6	21	ref. [147]
	Oligonucleotide inserts for AAV libraries or peptide displaying single clones			
AAV2_library_insert	CAG TCG GCC AGA GAG GC $(NNK)_7$ GCC CAG GCG GCT GAC GAG	x	56	ref. [141]
AAV2_FHEYGSG	CAG TCG GCC AGA GAG GCT TTC ATG AGT ATG GTT CTG GTG CCC AGG CGG CTG ACG AG	62.5	56	this study
AAV2_ASGHGYF	CAG TCG GCC AGA GAG GCG CGT CTG GTC ATG GTT ATT TTG CCC AGG CGG CTG ACG AG	64.3	56	this study
AAV2_EAGHGYF	CAG TCG GCC AGA GAG GC GAG GCG GGT CAT GGT TAT TTT GCC CAG GCG GCT GAC GAG	62.5	56	this study

Table 10.Synthetic oligonucleotides. ***Part II***

Denotation	Sequence 5' → 3'	GC%	No. Bases	Reference
AAV2_ESAHGYF	CAG TCG GCC AGA GAG GC GAG TCT GCG CAT GGT TAT TTT GCC CAG GCG GCT GAC GAG	62.5	56	this study
AAV2_ESGAGYF	CAG TCG GCC AGA GAG GC GAG TCT GGT GCG GGT TAT TTT GCC CAG GCG GCT GAC GAG	64.3	56	this study
AAV2_ESGHAYF	CAG TCG GCC AGA GAG GC GAG TCT GGT CAT GCG TAT TTT GCC CAG GCG GCT GAC GAG	62.5	56	this study
AAV2_ESGHGAF	CAG TCG GCC AGA GAG GC GAG TCT GGT CAT GGT GCG TTT GCC CAG GCG GCT GAC GAG	66.1	56	this study
AAV2_ESGHGYA	CAG TCG GCC AGA GAG GC GAG TCT GGT CAT GGT TAT GCG GCC CAG GCG GCT GAC GAG	66.1	56	this study
AAV2_WTRDNEG	CAG TCG GCC AGA GAG GCT GGA CTC GGG ATA ATG AGG GGG CCC AGG CGG CTG ACG AG	67.9	56	this study
AAV2_ARGTEWD	CAG TCG GCC AGA GAG GC GCG CGG GGG ACT GAG TGG GAT GCC CAG GCG GCT GAC GAG	73.2	56	this study
AAV2_NAGTEWD	CAG TCG GCC AGA GAG GC AAT GCG GGG ACT GAG TGG GAT GCC CAG GCG GCT GAC GAG	67.9	56	this study
AAV2_NRATEWD	CAG TCG GCC AGA GAG GC AAT CGG GCG ACT GAG TGG GAT GCC CAG GCG GCT GAC GAG	67.9	56	this study
AAV2_NRGAEWD	CAG TCG GCC AGA GAG GC AAT CGG GGG GCG GAG TGG GAT GCC CAG GCG GCT GAC GAG	71.4	56	this study
AAV2_NRGTAWD	CAG TCG GCC AGA GAG GC AAT CGG GGG ACT GCG TGG GAT GCC CAG GCG GCT GAC GAG	69.6	56	this study
AAV2_NRGTEAD	CAG TCG GCC AGA GAG GC AAT CGG GGG ACT GAG GCG GAT GCC CAG GCG GCT GAC GAG	69.6	56	this study
AAV2_NRGTEWA	CAG TCG GCC AGA GAG GC AAT CGG GGG ACT GAG TGG GCG GCC CAG GCG GCT GAC GAG	71.4	56	this study
	AAV library primer for double strand synthesis of olignonucleotide inserts			
AAV library primer	CTC GTC AGC CGC CTG G	75.0	16	ref.[141]
	Primers for virus titration via qPCR			
AAV2_plus	GCA GTA TGG TTC TGT ATC TAC CAA CC	46.2	26	ref.[147]
AAV2_minus	GCC TGG AAG AAC GCC TTG TGT G	59.1	22	ref.[147]
CMV_forw	GGG ACT TTC CTA CTT GGC A	52.6	19	ref.[205]
CMV_rev	GGC GGA GTT GTT ACG ACA T	52.6	19	ref.[205]
scCMV_rev	AAG TCC CGT TGA TTT TGG TG	45.0	20	SM
CAG_fow	GGA CTC TGC ACC ATA ACA CAC	52.4	21	this study
CAG_rev	GTA GGA AAG TCC CAT AAG GTC A	45.5	22	this study
	Primers for insertion of restriction sites			
eGFP_HindIII_fw	GGC GCA AGC TTA CCA TGG TGA GCA AGG GCG AGG AG	62.9	35	this study
eGFP_XbaI_rev	CCG CGT CTA GAT TAC TTG TAC AGC TCG TCC AT	50.0	32	this study
	Primers for sequencing of transgene cassettes			
CAG_end_fw	GTT GGT GTA CAG TAG CTT CCA C	50.0	22	this study
Luc_rev_miR1d	GTG GTT TGT CCA AAC TCA TCA A	40.9	22	SM

SM = Dr. Stefan Michelfelder (Group Receptor Targeting, University Medical Center Hamburg-Eppendorf), unpublished

2.13 Plasmids

Plasmids used in this study are listed in **Table 11.**

Table 11. Plasmids

Denotation	Description	Reference
pMT187-0-3	ITRs, AAV2 *rep*/ AAV2 *cap* R588ins, *Sfi*I sites, used for generation of random AAV2 display peptide libraries	Müller et al.[141]
pXX2-187	AAV2 *rep*/ AAV2 *cap* R588ins, *Sfi*I sites, used for generation of single clone AAV2 R588 mutants	Michelfelder et al.[145]
pXX6	Adenoviral helper plasmid containing E1A, E1B, E2A, E4-orf6, VA, used for production of rAAV vectors	Xiao et al.[79]
pVP3cm	Codon modified AAV2 VP3 under control of the RSV promoter, used for generation of AAV library transfer shuttles	Waterkamp et al.[144]
pAAV-CAG-eGFP	AAV expression cassette, containing the eGFP gene under control of the CAG promoter and the SV40 poly-A signal embedded between AAV2 ITRs (CMV promoter of pAAV-teto2-LUC exchanged with the CAG promoter of pVITRO4-mcs, luciferase exchanged with eGFP of dsAAV-CMV-eGFP)	this study
scAAV-CMV-eGFP	AAV expression cassette containing the eGFP gene under control of the CMV promoter and SV40 poly-A signal embedded between modified AAV2 ITRs which allow the packaging of double stranded DNA	Mc Carty et al.[93]
pAAV-CAG-LUC	AAV expression cassette, containing the luciferase gene under control of the CAG promoter and the SV40 poly-A signal embedded between AAV2 ITRs (CMV promoter of pAAV-teto2-LUC exchanged with the CAG promoter of pVITRO4-mcs)	this study
pAAV-CMV-teto2-LUC	AAV expression cassette, containing the luciferase gene under control of the CMV promoter and the SV40 poly-A signal embedded between AAV2 ITRs	SM
pVITRO4-mcs	Expression vector containing CAG promoter, IRES sequence and two MCS', used for cleavage of the CAG promoter	InvivoGen™
pFASTBAC™ 1	Donor plasmid containing insect cell promoter *polh*, mini-Tn7 target element, used for bacmid transposition in DH10Bac → BEVS	Invitrogen™
pFASTBAC™ Dual	Donor plasmid containing insect promoters *polh* and p10 and mini-Tn7 target element, used for bacmid transposition in DH10Bac → BEVS	Invitrogen™
pFBD-Rep_{in}/Cap_{in}	Donor plasmid based on pFASTBAC™ Dual, containing AAV2 *rep* and *cap* with *polh* containing introns, used for bacmid transposition in DH10Bac → production of AAV2 particles by BEVS	Chen et al.[206]
pFB1-CMV-LUC	Donor plasmid containing insect cell promoter *polh*, mini-Tn7 target element and pAAV-CMV-LUC expression cassette, used for bacmid transposition in DH10Bac → production of rAAV2-CMV-LUC vectors by BEVS	this study
pFB1-CAG-LUC	Donor plasmid containing insect cell promoter *polh*, mini-Tn7 target element and pAAV-CAG-LUC expression cassette, used for bacmid transposition in DH10Bac → production rAAV2-CAG-LUC vectors by BEVS	this study

Table 11. Plasmids. ***Part II***

Denotation	Description	Reference
pFB1-CMV-eGFP	Donor plasmid containing insect cell promoter *polh*, mini-Tn7 target element and pAAV-CMV-eGFP expression cassette, used for bacmid transposition in DH10B$_{ac}$ → production of rAAV2-CMV-eGFP vectors by BEVS	this study
pFB1-CAG-eGFP	Donor plasmid containing insect cell promoter *polh*, mini-Tn7 target element and pAAV-CAG-eGFP expression cassette, used for bacmid transposition in DH10B$_{ac}$ → production of rAAV2-CAG-eGFP vectors by BEVS	this study

SM = Dr. Stefan Michelfelder (Group Receptor Targeting, University Medical Center Hamburg-Eppendorf), unpublished

2.14 Software, online tools and databases

Software, online tools and databases used in this study are listed in **Table 12.**

Table 12. Software, online tools & databases

Denotation	Source	Purpose
Acrobat® 7.0	Adobe®	Generation of PDF files
ApE 2.0 – A plasmid Editor (M. Wayne Davis)	*http://biologylabs.utah.edu/29orgensen/wayned/ape/*	*In silico* DNA analyses
BLAST- Basic Local Alignment Search Tool	*http://blast.ncbi.nlm.nih.gov/Blast.cgi*	Online alignment search for nucleic acid- or protein sequences
Cell^A	Olympus	Documentation and analyses of microphotographs
Clustal Ω	*http://www.ebi.ac.uk/Tools/msa/clustalo/*	Online alignment of multiple nucleic acid- or protein sequences
Endnote X1®	Thomson Reuters/ Adept Scientific	Literature management
Excel 2010	Microsoft	Data editing
Fiji	http://fiji.sc/Fiji	Analyses and graphic editing of fluorescence images
Gene Snap	Syngene	Documentation of agarose gels
ImageJ	Nationale Institutes of Health, USA	Analyses and graphic editing of fluorescence images
Jmol 13.0	*http://jmol.sourceforge.net/*	Protein structure visualization
LAS AF	Leica	Documentation of fluorescence images
Living Image®4.0	Caliper Lifescience	*In vivo* imaging
Magellan 2	Tecan	Measurement of absorbance
MikroWin 2000	Berthold Technologies	Measurement of luminescence
Nanodrop 2000	Thermo Fisher Scientific	Measurement of nucleic acid concentration
PDB – Protein Data Bank	*http://www.rcsb.org/pdb/home/home.do*	Protein structure databank
Photoshop® CS5	Adobe®	Graphic editing
Power Point 2010	Microsoft	Graphic editing
Prism 3.0	GraphPad	Statistics and graphic editing of data
PubMed	*http://www.ncbi.nlm.nih.gov/pubmed*	Online search for literature
SWISS MODEL workspace	*http://swissmodel.expasy.org/workspace/*	*In silico* protein structure modelling
Word 2010	Microsoft	Text editing

2.15 Companies & affiliations

Manufacturers and suppliers of material and software used during this study are listed in **Table 13.**

Table 13. Companies & affiliations

Adobe Systems	Munich, DE	Lonza	Cologne, DE
Abcam	Cambridge, UK	Macherey-Nagel	Dueren, DE
Affymetrix	High Wycombe, UK	Merck	Darmstadt, DE
Axis Shield	Heidelberg, DE	Metabion	Martinsried, DE
BD Bioscience	Heidelberg, DE	Mettler Toledo	Giessen, DE
Beckman Coulter	Krefeld, DE	Microm	Walldorf, DE
Berthold Technologies	Bad Wildbach, DE	Microsoft	Unterschleissheim, DE
Biometra	Goettingen, DE	New England Biolabs (NEB)	Frankfurt a. M., DE
Biorad	Munich, DE	Olympus	Hamburg, DE
Braun	Melsungen, DE	PAA Laboratories	Pasching, DE
Caliper Lifesciences	Mainz, DE	Peqlab	Erlangen, DE
Carl Roth	Karlsruhe, DE	Perkin Elmer	Rodgau, DE
Carl Zeiss	Jena, DE	Pierce/Thermo Scientifc	Schwerte, DE
Corning	Munich, DE	Qiagen	Hilden, DE
Dako	Hamburg, DE	Roche	Mannheim, DE
Eppendorf	Hamburg, DE	Santa Cruz	Heidelberg, DE
Fermentas	St. Leon-Rot, DE	Sanyo Biomedical	Etten Leur, NL
Fluka	Taufkirchen, DE	Sarstedt	Nuembrecht, DE
GE-Healthcare	Munich, DE	Seqlab	Goettingen, DE
Gibco®/ Invitrogen	Darmstadt, DE	Serva	Heidelberg, DE
Gilson	Limburg-Offheim, DE	Sigma-Aldrich	Taufkirchen, DE
GraphPad/Statcon	Witzenhausen, DE	Syngene	Cambridge, UK
Greiner Bio-One	Essen, DE	Tecan Group	Crailsheim, DE
HP Medizintechnik	Oberschleissheim, DE	Thermo Fisher Scientific	Schwerte, DE
Heraeus Instruments	Hanau, DE	Adept Scientific	Frankfurt, DE
Invitrogen	Darmstadt, DE	Vector Laboratories	Eching, DE
Jackson Immuno Research	Suffolk, UK	Vetequip/VWR	Neubiberg, DE
Janvier Labs	St. Berthevin Cedex, FR	Whatman	Dassel, DE
Leica	Wetzlar, DE		

3 Methods

3.1 General molecular biological methods

3.1.1 Plasmid DNA purification

Plasmid DNA was harvested by centrifugation of transformed bacteria (**3.2.3**) at 5,000 x g and 4 °C for 5 min. Plasmids from 5 ml culture were purified using the PeqGold Plasmid Mini Kit (**2.2**), plasmids from 200 ml culture were purified using the NucleoBond® PC 100 Kit (**2.2**) and plasmids from 800 ml culture were purified using the NucleoBond® Xtra Maxi Kit (**2.2**), according to manufacturer's instructions. If not stated otherwise, plasmid DNA was eluted in a volume of 50 µl (5 ml culture), 500 µl (200 ml culture) or 2000 µl (800 ml culture) in the supplied elution buffer or $_{dd}H_2O$.

3.1.2 Digestion of DNA with restriction endonucleases

For analytical and preparative purpose, DNA was digested with appropriate restriction endonucleases according to following scheme:

-	X µl	DNA (0.5-1 µg for analyses, ≈ 5 µg for preparation)
-	1 µl	restriction endonuclease (NEB or Fermentas) per µg DNA
-	1/10 vol.	recommended buffer (NEB or Fermentas, 10 x)
-	1/10 vol.	BSA (NEB, 10 x), if recommended
-	*ad* 1 vol.	$_{dd}H_2O$

The reaction sample was incubated at the recommended working temperature of the used restriction endonuclease(s) for 30 min (Fermentas FastDigest enzymes, **2.3**) or 2-4 h (NEB enzymes, **2.3**) and DNA fragments were analyzed and/or purified by agarose gel electrophoresis (**3.1.6**), if not stated otherwise.

3.1.3 Blunting of DNA fragments with the Klenow Fragment of DNA Polymerase I

If necessary, DNA fragments with incompatible 5' or 3' overhangs (sticky ends) were blunted with the Klenow Fragment of the DNA Polymerase I (**2.3**), by filling-in 5' overhangs and removing 3' overhangs, according to following scheme:

- 1.0 µg	DNA with sticky ends
- 1.0 µl	Klenow Fragment (NEB, 5,000 U/ml)
- 1.0 µl	dNTPs (Fermentas, 10 mM)
- 1/10 vol.	NEB 2 buffer (10 x)
- *ad* 1 vol.	$_{dd}H_2O$

The reaction sample was incubated for 15 min at 25 °C. Afterwards, the Klenow Fragment was inactivated by adding 11/100 vol. EDTA (10 mM) and incubation for 20 min at 75 °C. The blunted DNA fragments were purified with the Qiaquick Nucleotide Removal Kit (**2.2**) according to manufacturer's instrcutions or, in case of blunted plasmid backbones, directly used for dephosphorylation (**3.1.4**).

3.1.4 DNA dephosphorylation with Antarctic Phosphatase

The 5' phosphates of DNA fragments (i.e. blunted plasmid backbones) were removed with the Antarctic Phosphatase (**2.3**) according to following scheme:

- 1.0 µg	blunted DNA
- 1.0 µl	Antarctic Phosphatase (NEB, 5,000 U/ml)
- 1/10 vol.	Antarctic Phosphatase buffer (NEB, 10 x)
- *ad* 1 vol.	$_{dd}H_2O$

The reaction sample had been incubated for 30 min at 37 °C before the Antarctic Phosphatase was inactivated at 65 °C for 5 min. The dephosphorylated DNA fragments were directly used for ligation (**3.1.5**).

3.1.5 Ligation of DNA fragments with T4 DNA Ligase

If not stated otherwise, DNA fragments were ligated with T4 DNA Ligase (**2.3**) in molar ratios of backbone and insert between 1:3 and 1:30, depending on the fragments' size. Reaction samples were prepared on ice according to following scheme:

-	100.00 ng	plasmid backbone DNA
-	X ng	insert fragment DNA ($_{dd}H_2O$ as control)
-	*ad* 17.00 µl	$_{dd}H_2O$

The sample was incubated at 65 °C for 2min and transferred to ice where it was incubated for 5 min. Then, the following reagents were added:

- 2.00 µl	T4 Ligase buffer (NEB, 10 x)
- 1.00 µl	T4 Ligase (NEB, 400,000 U/ml)

The complete reaction sample was incubated for 1-2h at RT or o/n at 16 °C and used for transformation of *E. coli* bacteria (**3.2.3**).

3.1.6 Agarose gel electrophoresis

TAE (***T**ris-**A**cetate-**E**DTA)*

50 x stock solution (1 l)		1 x working solution
- 242.00 g	Tris base dissolved in 500 ml $_{dd}H_2O$	40 mM
- 57.10 ml	EDTA solution (0.5 M, pH 8.0)	1 mM
- 28.55 ml	glacial acetic acid	20 mM
- *ad* 1.00 l	$_{dd}H_2O$	

for 1 x TAE diluted 1:50 in $_{dd}H_2O$

For agarose gels: 0.8 – 2.0 g agarose melted in 100 ml boiling TAE

DNA-containing solution (0.5-1 µg DNA for analytical gels, ≈ 5 µg for preparative gels) was mixed with an appropriate volume of loading dye and transferred to an agarose gel together with one probe (5-10 µl) DNA ladder (**2.6**) to analyze the fragments' sizes. DNA fragments with a size > 1,000 bp were analyzed using gels with 0.8-1% (w/v) agarose/TAE, fragments with a size < 1,000 bp were analyzed using gels with 2% (w/v) agarose/TAE, each adjusted to 1 µg/ml ethidium bromide (Sigma, 10 mg/ml). DNA fragments in the gel were separated in TAE buffer in an agarose gel electrophoresis system (**2.1**) at 100 V for 1 h. The size of the DNA fragments was analyzed and documented under UV-light (254 nm) with a gel documentation system (**2.1**) and the software Gene Snap (**2.14**). For preparative purpose, the DNA fragments of choice were cut out of the gel with a sterile scalpel under UV-light (364 nm) and purified with the PeqGOLD Gel Extraction Kit (**2.2**) following manufacturer's instructions. The DNA was eluted in 30 µl supplied elution buffer or $_{dd}H_2O$.

3.1.7 Polymerase chain reaction (PCR)

3.1.7.1 Standard PCR

To amplify DNA fragments with a low error rate (e.g. for molecular cloning), the Phusion® High Fidelity DNA Polymerase (**2.3**) was used. A mastermix for the desired number of reactions was prepared with appropriate primers on ice and carefully mixed according to following scheme for one reaction:

-	X µl	template DNA (≈ 100 ng)
-	1.00 µl	forward primer (10 µM)
-	1.00 µl	reverse primer (10 µM)
-	0.40 µl	dNTPs (Fermentas, 10 mM)
-	4.00 µl	Phusion® GC/HF reaction buffer (NEB, 5 x)
-	0.20 µl	Phusion® DNA polymerase (NEB, 2 U/µl)
- *ad*	20.00 µl	$_{dd}H_2O$

The PCR was run with following settings:

initial denaturation	98 °C	30 sec		
denaturation	98 °C	10 sec	}	30 x
annealing*	X °C	30 sec		
elongation	72 °C	30 sec/kb		
final elongation	72 °C	5 min		
	4 °C	∞		

**annealing temperature depending on the primers*

The PCR amplified DNA fragments were analyzed and purified by agarose gel electrophoresis (**3.1.6**).

3.1.7.2 Colony PCR

To check bacteria clones for the uptake of the desired plasmid after transformation, single colonies were picked from LB agar plates (**3.2.1.3**) and resuspended in 25 µl $_{dd}H_2O$ each. A mastermix for the desired number of reactions was prepared with appropriate primers on ice and carefully mixed according to following scheme for one reaction:

-	1.00 µl	resuspended bacteria
-	1.00 µl	forward primer (10 µM)
-	1.00 µl	reverse primer (10 µM)
-	0.25 µl	dNTPs (Fermentas, 10 mM)
-	4.00 µl	GoTaq® reaction buffer (Promega, 5 x)
-	0.10 µl	GoTaq® DNA polymerase (Promega, 5 U/µl)
-	10.65 µl	$_{dd}H_2O$

Ideally, primers for colony PCR were allowed to distinguish between:

- bacteria with no plasmid uptake
- bacteria with uptake of plasmid without insert
- bacteria with uptake of plasmid with insert in wrong orientation (blunt ends)
- bacteria with uptake of plasmid with insert in right orientation

The PCR was run with following settings:

initial denaturation	94 °C	2 min		
denaturation	94 °C	30 sec	}	30 x
annealing*	X °C	30 sec		
elongation	72 °C	1 min/kb		
final elongation	72 °C	5 min		
	4 °C	∞		

**annealing temperature depending on the primers*

The PCR amplified DNA fragments were analyzed by agarose gel electrophoresis (**3.1.6**).

3.1.7.3 Viral DNA PCR

Fragments of viral DNA from the random AAV display peptide library encoding the modified *cap* gene with random oligonucleotide insertions was amplified from total DNA from the tissue of interest via PCR. A mastermix for the desired number of reactions was prepared on ice and carefully mixed according to following scheme for one reaction:

-	X µl	total DNA (500 ng)/ if nested PCR 1-3 µl of the 1st PCR product
-	5.00 µl	PCR Buffer (Qiagen, 10x)
-	1.00 µl	dNTPs (Fermentas, 10mM)
-	1.00 µl	forward primer (20 µM)
-	1.00 µl	reverse primer (20 µM)
-	0.50 µl	HotStar Taq DNA Polymerase (Qiagen, 5 U/µl)
- *ad*	50.00 µl	$_{dd}H_2O$

The PCR was run with following settings:

initial denaturation	95 °C	15 min		
denaturation	95 °C	1 min	}	30 x
annealing*	X °C	1 min		
elongation	72 °C	1 min		
final elongation	72 °C	10 min		
	4 °C	∞		

**annealing temperature depending on the primers*

3.1.7.4 Vector titration by quantitative real-time PCR (qPCR)

The genomic titers of viral vector preparations or vector DNA in animal tissues were determined by qPCR, using the LightCycler® Nano system (**2.1**) and the FastStart Essential Green Mastermix (**2.3**) containing SYBR Green I dye.

Primers for different viral vectors were designed to work with the same PCR settings (but varying annealing temperatures) and are listed in chapter **2.12.**

A mastermix for the desired number of reactions was prepared according to following scheme for one reaction:

-	2.00 µl	sample**
-	1.00 µl	forward primer (5 µM)
-	1.00 µl	reverse primer (5 µM)
-	10.00 µl	FastStart Essential Green Mastermix (2x, Roche)
- *ad*	20.00 µl	$_{dd}H_2O$

***vecor titers were determined in different dilutions to omit PCR inhibition:*
1:1,000 and 1:10,000 for iodixanol purified virus samples and 1:10,000 and 1:100,000 for crude cell lysates

The qPCR was run with following settings:

initial denaturation	95 °C		10 min		
denaturation	95 °C	(ramp: 5 °C/sec)	30 sec	}	40 x
annealing*	X °C	(ramp: 5 °C/sec)	30 sec		
elongation	72 °C	(ramp: 5 °C/sec)	30 sec		
Melting curve analyses: 60-95 °C with 1 °C/sec					

**annealing temperature depending on the primers*

To calculate the genomic titers of the viral vectors, standard curves were created by measuring plasmids with corresponding genetic informations and defined length and molecular mass at defined genomic copy numbers (1×10^7; 1×10^6; 1×10^5; 1×10^4; 1×10^3 genomic copies). Purity and concentration of plasmids were determined by multiple photometric measurements (**3.1.9**). The genomic copy number of the PCR standard was determined using the following formulas:

$$m_g = (n_{bp})(1.096 \times 10^{-21}\ g/bp)$$

m_g = mass of genome [ng]; n_{bp} = size of genome (plasmid) in base pairs (bp)

$$n_c = c / m_g$$

n_c = copy number; c = DNA concentration [ng/µl]

Data were analyzed with LightCycler® Nano software 1.0. (**2.14**).

3.1.8 Ethanol precipitation of DNA

To precipitate DNA from DNA containing solutions (e.g., to concentrate or purify it from salts and proteins), the following reagents were thoroughly mixed:

-	1 vol.	DNA sample
-	1/10 vol.	sodium acetate (3 M, pH 5.2)
-	2.5 vol.	> 95% (v/v) ethanol
-	1 µl	glycogen**

*** = not necessary, recommendable for small DNA fragments*

The mixture was incubated for > 2 h at -20°C and centrifuged at 20,000 x g and 4 °C for 30 min. The supernatant was discarded, 500 µl 70% (v/v) ethanol were added to the DNA pellet and the sample was incubated on ice for 5 min. After centrifugation at 20,000 x g and 4 °C for 5 min, the supernatant was carefully removed, the pellet was dried at RT for 10 min and dissolved in the desired volume of $_{dd}H_2O$ or any buffer of choice.

3.1.9 DNA quantification

Purity and concentration of DNA containing solutions were determined by spectrophotometric measurement using the NanoDrop 2000c spectrophotometer (**2.1**). DNA was regarded as pure if the ratio of absorbance at 260 nm/280 nm was > 1.8, indicating low protein contamination (max. absorbance for proteins at 280 nm).

3.1.10 Sodium dodecyl sulfate polyacrylamide gel electrophoresis (SDS-PAGE)

adapted from Laemmli [207]

SDS PAGE running buffer

			10 x stock solution (1l)	1 x working solution
-	30.0 g	Tris base		25 mM
-	144.0 g	glycin		86 mM
-	0.1 l	10% (w/v) SDS solution		0.1% (w/v)
- *ad*	1.0 l	$_{dd}H_2O$		

autoclaved 20 min at 121 °C; for 1x running buffer diluted 1:10 in sterile $_{dd}H_2O$

Protein sample buffer (reducing)

5x working solution (10 ml)		1 x
- 1650 µl	Tris-HCl (1M, pH 6.8)	33 mM
- 3438 µl	10% (w/v) SDS solution	0.69% (w/v)
- 2500 µl	glycerol	5.00% (v/v)
- 500 µl	1% (w/v) bromophenol blue solution	0.01% (w/v)
- 230 µl	ß-mercaptoethanol	0.46% (v/v)
- *ad* 10 ml	$_{dd}H_2O$	

Polyacrylamide protein gels (for one gel)

	6%	**Stacking gel**
$_{dd}H_2O$	2.600 ml	1.690 ml
30% (w/v) Acryl-bisacrylamide mix (Biorad)	1.000 ml	0.4190 ml
Tris (1.5 M, pH 8.8)	1.300 ml	0.3120 ml
10% (w/v) SDS	0.050 ml	0.0250 ml
10% Ammonium persulfate	0.050 ml	0.0250 ml
Tetramethylethylenediamine (TEMED)	0.004 ml	0.0025 ml
Total volume	**5.000 ml**	**2.5000 ml**

To analyze transfected or infected cells for expression of AAV virion proteins, proteins from crude cell lysates or purified viral particles were separated by SDS-PAGE. Proteins were separated in 6% (w/v) acrylamide gels.

The mixture for the separating gel with an appropriate percentage of polyacrylamide was transferred between two glass plates in a gel caster and topped up with 99.5% (v/v) isopropanol until totally polymerized. The isopropanol was replaced by the mixture for the stacking gel and a comb was added to form the sample wells. After complete polymerization, the gel was transferred to the tank of the electrophoresis apparatus (**2.1**), filled with 1x running buffer. After having been denaturated at 95 °C for 10 min in an appropriate volume of reducing probe buffer, the protein samples were transferred into the sample wells of the gel together with one probe of a protein ladder (**2.6**) and the electrophoresis was run at 100 V until the proteins formed a sharp migration front when reaching the separating gel. Electrophoresis was continued at 140 V until the migration front reached the lower end of the gel. The gel was further used for western blotting (**3.1.11**).

3.1.11Western Blot

SDS PAGE transfer buffer

10 x stock solution (1 l)		1 x working solution
- 24.20 g	Tris base	20 mM
- 108.10 g	glycin	65 mM
- *ad* 1.00 l	$_{dd}H_2O$	

autoclaved 20 min at 121 °C

for 1 x transfer buffer:

- 0.10 l	10 x transfer buffer	10% (v/v)
- 0.10 l	methanol	
- *ad* 1.00 l	$_{dd}H_2O$	

3.1.11.1 Protein transfer

A polyvinyl difluoride (PVDF) membrane was cut into the size of the gel containing the separated proteins (**3.1.10**) and incubated 1 min in 99.5% (v/v) methanol, before preparing a "sandwich" in a tank filled with 1 x transfer buffer:

black side of the holder cassette
- foam pad
- filter paper
- gel
- PVDF membrane
- filter paper
- foam pad

white side of the holder cassette

The holder cassette was transferred into the tank of the electrophoresis apparatus (**2.1**), filled with 1x transfer buffer and the tank was placed in a box containing ice water to keep temperature at ≈ 4 °C. Proteins were transferred to the membrane at a voltage of 100 V for 2 h.

3.1.11.2 Protein detection

AP- detection buffer (***A**lkaline **P**hosphatase detection buffer)*

1 x working solution (1 l)

12.11 g	tris base	100 mM
2.03 g	$MgCl_2$ $6H_2O$	10 mM
5.85 g	NaCl	100 mM
ad 1.00 l	$_{dd}H_2O$	

prior to AP-detection, 100 µl of a 100 x BCIP solution (75 mg/ml in DMF) and 100 µl of a 100 x NBT solution (50 mg/ml in DMF) were added to 9.8 ml 1x AP detection buffer

After protein transfer, the PVDF membrane was incubated for 1 min in 99.5% (v/v) methanol and rinsed once in TBS-T (**2.8**). The membrane was blocked in 5 % (w/v) milk powder in TBS-T for 1 h at RT and incubated with the primary antibody (**2.4**) diluted 1:10,000 in 5 % (w/v) milk powder in TBS-T. After incubation for 2 h at RT or o/n at 4 °C , the membrane was washed 3 x 5 min with TBS-T and incubated for 1-2 h at RT with the secondary antibody coupled to alkaline phosphatase (**2.4**) diluted 1:10,000 in 5 % (w/v) milk powder in TBS-T. The membrane was washed 3x 5 min with TBS-T and the antibody was detected by incubating the membrane for < 30 min in detection buffer. Then the membrane was rinsed with $_{dd}H_2O$ and dried at RT.

3.2 Microbiological methods

Media used for culturing and reconstitution of prokaryotic cells and their recipes are listed below:

LB medium (1 l):
Lysogenic broth

-	10.00 g	Bacto™ tryptone
-	5.00 g	Bacto™ yeast extract
-	10.00 g	NaCl
- *ad*	1,000.00 ml	$_{dd}H_2O$

autoclaved for 20 min at 121 °C

LB agar: 15.00 g Bacto™ agar added to 1 l LB medium before autoclaving for 20 min at 121 °C

TB medium (1 l):
Terrific Broth

-	12.00 g	Bacto™ tryptone
-	24.00 g	Bacto™ yeast extract
-	4.00 ml	99.5% (v/v) glycerol
- *ad*	900.00 ml	$_{dd}H_2O$

autoclaved for 20 min at 121 °C before supplemented with 100.00 ml sterile solutions of KH_2PO_4 (0.17 M) and K_2HPO_4 (0.72 M)

SOB medium (1 l):	-	20.00 g	Bacto™ tryptone
Super optimal Broth	-	5.00 g	Bacto™ yeast extract
	-	0.50 g	NaCl
	-	2.50 ml	KCl (1 M)
	- *ad* 1,000.00 ml		$_{dd}H_2O$
autoclaved for 20 min at 121 °C			

SOC medium (1 l):	-	10 ml	$MgCl_2$ (1 M)
Super optimal Broth with	-	20 ml	glucose (1 M)
Catabolite repression	- *ad* 970 ml		SOB medium
autoclaved for 20 min at 121 °C			

Following antibiotics/supplements were added to prokaryotic cell culture media, if necessary:

AMP *Ampicillin*	1.0 ml stock solution (150 mg/ml in $_{dd}H_2O$) for 1 l medium → 150 mg/l
GENT *Gentamycin*	0.7 ml stock solution (10 mg/ml $_{dd}H_2O$) for 1 l medium → 7mg/l
KAN *Kanamycin*	1.0 ml stock solution (50 mg/ml in $_{dd}H_2O$) for 1 l medium → 50 mg/l
TET *Tetracyclin*	2.0 ml stock solution (5 mg/ml in ethanol) for 1 l medium → 10 mg/l
IPTG/X-Gal	1.0 ml stock solution (40 mg/ml IPTG in $_{dd}H_2O$, 40 mg/ml X-Gal in DMF) for 1 l medium → 40 mg/l

Antibiotics and supplements were added after sterilization at a temperature of ≈ 50 °C

3.2.1 Propagation of Escherichia coli

3.2.1.1 Suspension culture

Single clone *E. coli* colonies from agar plates (**3.2.1.3**) or glycerol stocks (**3.2.1.2**) were grown in Erlenmeyer flasks as suspension culture in LB medium to moderate density or in TB medium to high density o/n at 37 °C and 200 rpm. *E. coli* cells carrying AAV ITR-containing plasmids were grown at 30 °C and 175 rpm to preserve the fragile ITRs.

3.2.1.2 Glycerol stocks

To preserve monoclonal bacteria, 5 ml monoclonal suspension culture inoculated from agar plate (**3.2.1.3**) were centrifuged at 5.000 x g for 2 min, the supernatant was discarded, the bacteria-containing pellet was resupsended in a mixture of 0.5 ml 99.5 % (v/v) glycerol and 0.5 ml LB medium, transferred to cryopreservation tubes and frozen at -80 °C

3.2.1.3 Cultivation of E. coli on agar plates

By spreading *E. coli* cells on LB agar plates and incubating them for ≈ 12 h at 37 °C, monoclonal bacteria colonies could be isolated. Bacteria on agar plates were stored at 4 °C for several weeks after sealing the plates with plastic paraffin film.

3.2.1.4 Selection of recombinant E. coli

To select bacteria clones containing a desired plasmid/bacmid with antibiotic resistance and/or lacZ gene for blue-white screening, *E. coli* cells were spread on LB agar plates supplemented with appropriate antibiotic(s) and/or IPTG/X-Gal or grown in supplemented suspension culture.

3.2.2 Preparation of competent *E. coli* bacteria

The protocols described below yielded 3-5 ml competent bacteria. Great care was taken to keep bacteria as cold as possible during the whole procedure, therefore all reagents and material had been pre-cooled in advance.

3.2.2.1 Electrocompetent E. coli bacteria

adapted from Dower et al.[208]

Reagents needed:

-	1,000 ml	SOB medium
-	100 ml	10% (v/v) glycerol
-	1,500 ml	HEPES (1mM, pH 7.0)

A single *E. coli* colony (strain DH5α, **2.9.1**) from an LB agar plate (**3.2.1.3**) was used to inoculate 50 ml SOB medium in a 500 ml Erlenmeyer flask. Bacteria were grown at 37 °C and 200 rpm o/n. The next day, 950 ml SOB medium were evenly distributed to six 1 l Erlenmeyer flasks and each flask was inoculated with 0.5 ml of the overnight culture. Bacteria were grown at 37 °C and 200 rpm to an OD_{600} of 0.6. The Erlenmeyer flasks were put on ice and after 15 min the content of each flask was transferred to a pre-cooled 250 ml centrifugation bottle and centrifuged at 385 x g and 4 °C for 15 min. The supernatant was promptly discarded and bacteria were gently resuspended in 150 ml ice-cold HEPES/bottle by carefully pipetting them up and down while omitting air bubbles. Again bacteria were centrifuged at 385 x g and 4 °C for 15 min, the supernatant was promptly discarded and they were gently resuspended in 60 ml ice-cold HEPES/bottle by carefully pipetting them up and down. Bacteria were pooled in three of the six centrifugation bottles (180 ml each) and centrifuged at

385 x g and 4 °C for 15 min. The supernatant was promptly discarded and bacteria were pooled in one centrifugation bottle after having been suspended in 10 ml ice-cold 10% (v/v) glycerol/bottle by carefully pipetting them up and down (resulting in 30 ml). After a centrifugation step at 867 x g and 4 °C for 10 min, the supernatant was carefully removed with a pipette. Bacteria were gently suspended in 2.5 ml ice-cold 10% (v/v) glycerol (resulting in ≈ 3-5 ml bacteria suspension) and distributed to pre-cooled 1.5 ml reaction tubes (100 µl each) and immediately transferred to dry ice. After 1-2 min, bacteria were transferred to a box which had already been equilibrated in a -80 °C freezer and stored in the back of the freezer to keep temperature as constant as possible.
Test electroporations (**3.2.3.1**) were performed using the same settings as for the experiments the competent bacteria were made for. Bacteria were considered suitable for further use, if 1×10^8 clones from 1 µg transformed DNA could be obtained.

3.2.2.2 Competent E. coli bacteria for heat shock transformation (calcium chloride method)

adapted from Cohen et al.[209]

Reagents needed:

-	1,000 ml	LB medium (with appropriate antibiotics)
-	1,000 ml	$CaCl_2$ (100 mM)
-	5 ml	20% (v/v) glycerol/ $CaCl_2$ (50mM)

E. coli bacteria, strain XL1Blue (**2.9.1**) were streaked out on a LB_{TET} agar plates from a glycerol stock and incubated o/n at 37 °C. One single colony was used to inoculate 50 ml LB_{TET} medium in a 500 ml Erlenmeyer flask. Bacteria were grown at 37 °C and 200 rpm o/n. The next day, 950 ml medium were evenly distributed to six 1 l Erlenmeyer flasks and each flask was inoculated with 0.5 ml of the overnight culture. Bacteria were grown at 37 °C and 200 rpm to an OD_{600} of 0.6. The Erlenmeyer flasks were put on ice for cooling bacteria down and the content of each flask was transferred to a pre-cooled 250 ml centrifugation bottle and centrifuged at 1,950 x g and 4 °C for 5 min. The supernatant was promptly discarded and bacteria were gently resuspended in 150 ml ice-cold 100 mM $CaCl_2$/bottle by carefully pipetting them up and down while omitting air bubbles. The suspension was incubated on ice for 30min and centrifuged at 1,950 x g and 4 °C for 5 min, the supernatant was promptly discarded and they were gently resuspended in 10 ml ice-cold ice-cold 100mM $CaCl_2$/bottle by carefully pipetting them up and down, pooled in one centrifugation bottle and again centrifuged at 1,950 x g and 4 °C for 5 min. The bacteria were gently suspended in 2.5 ml ice-cold 20% (v/v) glycerol/50mM $CaCl_2$ (resulting in 3-4 ml bacteria suspension), distributed to pre-cooled 1.5 ml reaction tubes (100 µl each) and immediately transferred to dry ice. After 1-2 min,

bacteria were transferred to a box which had already been equilibrated in a -80 °C freezer and stored in the back of the freezer to keep temperature as constant as possible.

3.2.3 Transformation of E. coli

3.2.3.1 Transformation by electroporation

adapted from Dower et al. [208]

Electrocompetent *E. coli* (DH5α) bacteria (50 µl) were transferred from the freezer (-80 °C) immediately on ice, where they were thawed for a few minutes. Directly after bacteria had been thawed, they were transferred to a pre-cooled reaction tube containing 1-5 µl of the DNA solution to be transformed (free of salts e.g. ethanol precipitated). Bacteria/DNA suspension was carefully (omitting air bubbles) transferred between the electrodes of a pre-cooled electroporation cuvette (1 mm, Biorad) on ice, the cuvette was transferred to the shocking chamber of the Gene Pulser Xcell™ Electroporation System (**2.1**), the lid was closed and an electro pulse with following settings was induced:

- electrode gap: 1mm
- voltage: 1,800 V
- capacitance: 25 µF
- resitance: 200 Ω

Immediately after finishing the electro pulse, the transformed bacteria were rinsed out of the cuvette with 2 ml pre-warmed SOC medium and incubated at 37°C for 20-60 min. After reconstitution, different dilutions of transformed bacteria were spread on LB agar plates containing appropriate antibiotics and incubated o/n at 37 °C to obtain single clone colonies.

3.2.3.2 Transformation by heat shock

Competent *E. coli* (XL1-Blue, DH10Bac) bacteria (50-100 µl) were transferred from the freezer (-80 °C) immediately on ice, where they were thawed for a few minutes. Directly after bacteria had been thawed, they were transferred to an ice cold reaction tube containing 1-5 µl of the DNA solution to be transformed. After having been incubated on ice for 30 min, the tube containing DNA and bacteria was transferred into a water bath at 42 °C for exact 45 sec and immediately transferred back on ice afterwards. After 2 min incubation on ice, pre-warmed SOC medium (100-1,000 µl) was added to the bacteria and they were incubated at 37 °C for 20-60 min. After reconstitution, different dilutions of

transformed bacteria were spread on LB agar plates containing appropriate antibiotics and incubated o/n at 37 °C to obtain single clone colonies.

3.3 Cytological methods

All experiments with eukaryotic cells described in this thesis have been performed under sterile conditions in a laminar flow sterile work bench approved for biological safety level S2 (**2.1**). All human cells that have been used for experiments are commercially available.

3.3.1 Cultivation of eukaryotic cells

If not stated otherwise, cells for experiments were grown under following conditions:

HEK 293T cells:

DMEM Dulbecco's modified Eagle's Minimal Essential Medium	Purchased as ready-to-use medium (Gibco), supplemented with 10% (v/v) FBS (Gibco) and 1% (v/v) Pen Strep solution (Gibco, 10,000 U/ml penicillin, 10,000 µg/ml streptomycin)

37 °C, humidified atmosphere, 5% (v/v) CO_2

Sf9 cells:

Insect-XPRESS™	Purchased as ready-to-use medium (Lonza), supplemented with 10 mg/l gentamycin (Lonza, 50 mg/ml)

27 °C, without controlled atmosphere, shaking at 110 rpm in case of suspension culture

3.3.2 Seeding of eukaryotic cells

Cryopreserved cells (**3.3.4**) were quickly thawed in a waterbath at 37 °C, cells were resuspended in pre-warmed supplemented medium and centrifuged once for 5 min at 250 x g. The DMSO-containing supernatant was discarded and cells were seeded in fresh pre-warmed supplemented medium in cell culture flasks (1 x 10^7 cells/75 cm^2 flask), followed by a medium change on the next day.

3.3.3 Counting of eukaryotic cells

Adherent cells were detached from the surface of the cell culture dish/bottle by intensively tapping the flask (Sf9) or by removing the medium and incubating them for 3 min at 37 °C in a minimum volume of 1 x Trypsin solution in PBS (HEK 293T). Detached cells were resuspended in supplemented

medium. The cell suspension was diluted 1:10 in 0.2% (w/v) trypan blue solution in PBS and 10 µl were transferred to a Neubauer-improved cell counting chamber. Viable (unstained) cells of four big squares (1 mm^3, each containing 16 small squares) were counted and the concentration of cells in the initial cell suspension was calculated with following formula:

c [cells/ml] = n/4 x d x 10,000 *c = concentration; n = number of counted cells; d = dilution*

3.3.4 Cryopreservation of eukaryotic cells

Cryopreservation medium for HEK 293T cells:

90% (v/v) FBS
10% (v/v) DMSO

Cryopreservation medium for Sf9 cells:

46.25% (v/v) fresh Insect-XPRESS™ without antibiotics
46.25% (v/v) conditioned Insect-XPRESS™ as 2-4 days old supernatant from Sf9 culture
7.50% (v/v) DMSO

After counting (**3.3.3**), cells were centrifuged at 290 x g (HEK 293T) or 150 x g (Sf9) for 5 min, resuspended in the desired volume of cryopreservation medium, distributed to cryopreservation tubes, which were put into a tube holding container filled with isopropanol (Mr. Frosty Freezing Container, Thermo Scientific), ensuring a cooling rate of 1 °C/min and transferred to the freezer (-80 °C). After 24 h cells were transferred to liquid nitrogen.

3.4 Virological methods

3.4.1 Large scale AAV production in HEK 293T cells

adapted from Xiao et al. [79]

3.4.1.1 Transfection of HEK 293T cells

HEK 293T cells were seeded in ≥ 5 cell dishes (15 cm) in supplemented DMEM medium at a density of 1,25 x 10^7 cells/dish and let grown until the next day to 70% confluency. One hour before transfection, the medium was replaced by fresh supplemented DMEM medium (17 ml/dish). For transfection, Polyfect transfection reagent (**2.2**) was used according to manucfacturer's instructions, preparing master mixes for 5 cell dishes at a time. For each 15 cm cell dish following composition was prepared and thoroughly mixed:

12.00 µg	DNA total:
- X µg*	ITR-containing plasmid e.g. reporter plasmids
- X µg*	AAV *rep*/*cap* plasmid without ITRs
- 6.00 µg	Ad-pXX6 (containing E1A, E1B, E2A, E4-orf6, VA)[79]
- *ad* 450.00 µl	serum free DMEM (Gibco)
- 120.00 µl	Polyfect transfection reagent (Qiagen)

** molar ratio 1:1 (6 µg together)*

After incubating the mixture at RT for 10 min to allow complex formation, it was filled up with 1 ml/dish complete DMEM medium. The complete mixture (1.570 ml/dish) was evenly distributed dropwise on the cells and mixed by gentle swirling. Not more than 5 dishes at a time were removed from the incubator to keep stable pH. One day after transfection, the medium was exchanged by fresh supplemented DMEM medium (25 ml/dish) and cells were incubated for another 2-3 days.

3.4.1.2 Harvest of viral particles from HEK 293T cells

Transfected cells (**3.4.1.1**) were carefully washed with 10 ml/dish PBS and detached from the surface of the cell dishes with a cell scraper. The cell dishes were rinsed with 8 ml/dish PBS and the cells of five dishes were transferred to one 50 ml tube. The cell dishes were rinsed again by transferring 10 ml PBS from one dish to another to collect all remaining cells. The cells were centrifuged at 250 x g, the supernatant was discarded and the cell pellet of 5 dishes was resupsended in 5 ml PBS-MK. The viral particles were released from the cells by three repeated freeze/thaw cycles (freezing the tubes in dry ice surrounded by 99.5% $_{(v/v)}$ ethanol for 10 min and thawing them in a water bath at 37 °C for 10 min). Cellular nucleic acids were digested with 50 U/ml Benzonase nuclease (**2.3**) for 30 min at 37 °C and the lysate was clarified by centrifugation at 3,000 x g for 15 min. The supernatant, containing the viral particles, was stored at -80 °C until further purification by iodixanol density gradient centrifugation (**3.4.4**).

3.4.2 Large scale rAAV production in Sf9 insect cells using the Baculovirus Expression Vector System (BEVS)

adapted from Urabe et al.[80]*, Kohlbrenner et al.*[81]*, Chen et al.*[206] *and Wasilko et al.*[210]

3.4.2.1 Generating recombinant baculovirus by site-specific transposition

Cloning of donor plasmids

The production of recombinant AAV vectors with the BVES requires infection of insect cells with two different recombinant baculoviruses, one encoding the AAV Rep and Cap proteins and the other

carrying the transgene cassette of interest embedded between AAV ITRs (e.g. reporter genes like luciferase). Therefore, prior to this work, the two AAV2 genes *rep* and *cap* had been cloned into the donor plasmid pFASTBAC™ Dual containing the polyhedrin (*polh*) promoter and the p10 promoter, according to a protocol by Chen et al.[206] in which an artificial intron containing the *polh* promoter was was additionally cloned into the AAV2 Rep and Cap coding sequences, resulting in expression was additionally cloned into the AAV2 Rep and Cap coding sequences, resulting in expression of large and small AAV Rep and Cap proteins in insect cells (Rep78, Rep52, VP1, VP2 and VP3). The two resulting donor plasmids pFBD-Rep_{in} and pFBD-Cap_{in} had been fused to generate one plasmid designated pFBD-Rep_{in}/Cap_{in} [206].

All AAV2 Rep/Cap donor plasmids used within this work have been generated by cloning the peptide insert encoding region of the *cap* gene of selected AAV clones from the random AAV2 display peptide library into the *cap* gene of pFBD-Rep_{in}/Cap_{in}. The peptide insert encoding region of the *cap* gene and the corresponding region of the wild type AAV2 *rep*/*cap* containing donor plasmid pFBD-Rep_{in}/Cap_{in} were cleaved from pXX2-187 with EcoNI and XbaI. The peptide insert encoding fragment of pXX2-187 (1,929 bp) was separated from the remaining plasmid fragments (4,022/2,408 bp) like the pFBD-Rep_{in}/Cap_{in} backbone (7,921 bp) from the wild type AAV *cap* fragment (1,902 bp) by preparative gel electrophoresis (**3.1.6**). Insert and backbone were purified with the peqGOLD Gel Extraction Kit (**2.2**) according to manufacturer's instructions, purity and concentration of DNA was determined by photometric measurement (**3.1.9**) and the peptide insert encoding region was ligated (**3.1.5**) into the digested pFBD-Rep_{in}/Cap_{in} backbone.

The transgene cassette of interest, containing AAV ITRs, was cleaved from the corresponding AAV vector plasmid (i.e. pAAV-CMV-LUC and pAAV-CAG-eGFP) with SbfI and PvuI.

The donor plasmid pFASTBAC™1 was linearized with PstI. The ITR containing transgene cassettes of the AAV vector plasmids (pAAV-CMV-LUC = 2,995 bp, pAAV-CAG-eGFP = 3,958 bp) were separated from the remaining plasmid fragment (pAAV-CMV-LUC and pAAV-CAG-eGFP = 1,339/1,266 bp) by preparative gel electrophoresis (**3.1.6**). Transgene cassette DNA fragments were purified with the peqGOLD Gel Extraction Kit (**2.2**), while the linearized pFASTBAC™1 (4,776 bp) was purified with the Qiaquick Nucleotide Removal Kit (**2.2**) following manufacturer's instructions. Purity and concentration of DNA was determined by photometric measurement (**3.1.9**). The ITR containing AAV transgene cassette was ligated into the linearized donor plasmid pFASTBAC™.

The ligated plasmids were used to transform XL1blue *E. coli* cells by heat shock (**3.2.3.2**) and single clones from LB_{AMP} agar plates were transferred to 5 ml LB_{AMP} and grown o/n at 37 °C and 200 rpm (30 °C and 175 rpm for ITR containing transgene cassettes). Plasmids were harvested and purified using the peqGOLD Plasmid Mini Kit (**2.2**) according to manufacturer's instructions. Plasmids were

sequenced with the primers "AAV2_4+" (**2.12**) in case of recombinant pFBD-Rep_{in}/Cap_{in} donor plasmid and "LUCrev-miR1" (**2.12**) in case of recombinant pFASTBAC™1 donor plasmids after purity and concentration of DNA had been determined by photometric measurement (**3.1.9**). Sequence verified plasmids were used to transform of DH10BAC™ *E. coli* cells.

Transformation of DH10BAC™ E. coli cells with pFASTBAC™donor plasmids

The recombinant donor plasmids (100 ng) were used to transform 100 µl competent DH10BAC™ *E. coli* cells containing a bacmid carrying the baculovirus genome with a mini-attTn7 target site and a helper plasmid by heat shock (**3.2.3.2**). Within the DH10BAC™ cells, the mini-Tn7 target element on the recombinant pFASTBAC™ donor plasmid was transposed to the target site by the transposition proteins encoded on the helper plasmid. The transformed DH10BAC™ cells were allowed to reconstitute in 1 ml SOC medium for 4 h at 37 °C. After reconstitution, 100 µl of the cells were spread on $LB_{IPTG/X\text{-}Gal/KAN/TET/GENT}$ agar plates and incubated at 37 °C for 24-72 hours until white colonies were clearly distinguishable from blue ones. White colonies were screened by colony-PCR (**3.1.7.2**) with appropriate primers and positive clones were transferred to 5 ml $LB_{KAN/TET/GENT}$ and grown o/n at 37 °C and 200 rpm.

Harvesting recombinant bacmid

Following solutions had been prepared in advance:

Solution A (10 ml):

- 28.21 mg Tris-HCL (pH 8)
- 37.22 mg Na_2 EDTA 2 H_2O
- *ad* 10.00 ml $_{dd}H_2O$

100 µl/ml RNase (Qiagen, 10 mg/ml) were added freshly before use

Solution B (10 ml):

- 80.00 mg NaOH
- 100.00 mg 1% (w/v) SDS
- *ad* 10.00 ml $_{dd}H_2O$

Solution C (10 ml):

- 2.94 g Potassium acetate
- *ad* 10.00 ml $_{dd}H_2O$

Positive recombinant DH10BAC™ cells from 5 ml $LB_{KAN/TET/GENT}$ were centrifuged at 10,000 x g for 1 min. The cell pellet was resuspended in 500 µl Solution I (RNAse A had been added prior to use), then 500 µl Solution II were added, the mixture was inverted five times and incubated for 5 min at RT. Under constant shaking, 500 µl Solution III were added, the tube was inverted five times and incubated on ice for 10 min. The solution was centrifuged at 15,000 x g for 10 min at 4 °C and 900 µl of the supernatant were mixed with 800 µl 99.5% (v/v) isopropanol. After incubation on ice for 10 min, the solution was centrifuged at 15,000 xg for 15 min at RT. The supernatant was discarded and the DNA pellet was washed with 500 µl ice-cold 70% (v/v) ethanol in $_{dd}H_2O$, centrifuged at 15,000 x g for 5 min at 4 °C. After discarding the supernatant, the DNA pellet was dried for 10 min at RT and dissolved in 100 µl TE buffer. Purity and concentration of DNA was determined by photometric measurement (**3.1.9**).

Transfection of Sf9 insect cells

Sf9 insect cells were seeded in 6-well plates (8×10^5 cells in 1 ml complete Insect-XPRESS™ medium/well). While letting the cells attach to the plate, the transfection sample was prepared as follows and mixed thoroughly:

100.00 µl Insect-XPRESS™ without antibiotics + 8.00 µl Cellfectin® Transfection Reagent (**2.2**)
100.00 µl Insect-XPRESS™ without antibiotics + 2.00 µg recombinant bacmid

Both samples were mixed together and incubated at RT. After 30-45 min, 800 µl Insect-XPRESS™ medium without antibiotics were added.

The medium in which the cells were seeded was removed from the cells, they were washed once with Insect-XPRESS™ medium without antibiotics and the transfection medium was carefully added dropwise to the cells. Cells were incubated with the transfection medium for 4-5 h at 27 °C, before replacing it by 3 ml fresh complete Insect-XPRESS™ medium and incubating the cells at 27 °C for further 72 h. Finally, the medium from the transfected cells was harvested and centrifuged for 5 min at 500 x g. The supernatant contained the baculovirus P1 stock and was used for virus amplification by infecting new Sf9 insect cells.

Amplification of baculovirus

The baculovirus P1 stock was used to generate a high titer baculovirus P2 stock contained in Sf9 insect cells. Therefore 7.5×10^7 Sf9 insect cells were resuspended in 50 ml Insect-XPRESS™ medium

(1.5 x10^6 cells/ml) and infected with 1,200 µl of the baculovirus P1 stock in an Erlenmeyer flask. The infected cells were incubated at 27 °C and 110 rpm as suspension culture and after 48 h cells were counted (**3.3.3**) and processed for cryopreservation (**3.3.4**) at a density of 1 x 10^7 cells/ml.

3.4.2.2 Test expression in Sf9 insect cells

Test expression of empty AAV particles

The recombinant baculovirus P2 stocks (contained in P1-infected Sf9 cells) had been produced to infect a new batch of Sf9 insect cells for protein expression (i.e. rAAV vectors). Since baculovirus P2 stocks vary in their viral titers and their strength to mediate recombinant protein expression, it was necessary to find the ideal amount of baculovirus P2 stock to infect new cells for protein expression. Therefore 8 x 10^5 Sf9 insect cells/well were seeded in 6-well plates in 2 ml Insect-XPRESS™ medium supplemented with 10 mg/l gentamycin. After 1 h cells were infected with 1 µl/ 5.0 µl/ 10.0 µl/ 20.0 µl/ 50.0 µl/ 100.0 µl of diluted baculovirus P2 stock for AAV proteins (1 x 10^7 P1-infected cells/ml thawed and diluted 1:50 in Insect-XPRESS™ medium without antibiotics = P2 stock with 2x10^5 cells/ml). Cells were incubated at 27 °C and after 96 h, the medium was removed, cells were rinsed once with 1 ml PBS and detached from the wells by pipetting them up and down with 100 µl PBS-MK and transferred into reaction tubes. The viral particles were released from the cells by three repeated freeze/thaw cycles (freezing the tubes in dry ice surrounded by 99.5% (v/v) ethanol for 10 min and thawing them in a water bath at 37 °C for 10 min) and the crude cell lysate was clarified by centrifugation at 10,000 x g for 5 min.

For SDS-PAGE (**3.1.10**), 20 µl of the supernatant were boiled for 5 min at 95 °C with 5 µl 5 x reducing protein buffer and 20 µl of the sample were used for the gel. The primary antibody (B1, mouse anti VP, **2.4**) for western blot analyses (**3.1.11**) was used as undiluted supernatant from hybridoma cells at 4 °C and the secondary antibody (AP-conjugated anti-mouse IgG, Sigma, **2.4**) was used in an 1:10,000 dilution in 5% milk powder in TBS-T for 1-2 h at RT. The optimal amount of baculovirus P2 stock to infect SF9 cells for AAV protein expression was determined by analyzing the bands of the virion proteins (87, 72, 62 kDa) from the different wells for their strength.

Test expression of rAAV vectors

After the optimal amount of baculovirus P2 stock for the AAV proteins had been determined, 8 x 10^5 Sf9 insect cells/well were seeded in 6-well plates in 2 ml Insect-XPRESS™ medium supplemented with 10 mg/l gentamycin. After 1 h cells were infected with the optimal amount of baculovirus P2 stock

for AAV proteins and additional 0.1 µl/ 1.0 µl/ 5.0 µl/ 20.0 µl/ 50.0 µl/ 100.0 µl of diluted baculovirus P2 stock for the transgene cassette ($1x10^7$ P1-infected cells/ml thawed and diluted 1:50 in Insect-XPRESS™ medium without antibiotic = P2 stock with $2x10^5$ cells/ml). Cells were incubated at 27 °C and after 96 h, the medium was removed, cells were rinsed once with 1 ml PBS and detached from the wells by pipetting them up and down with 100 µl PBS-MK and transferred into reaction tubes. The viral particles were released from the cells by three repeated freeze/thaw cycles (freezing the tubes in dry ice surrounded by 99.5% (v/v) ethanol for 10 min and thawing them in a water bath at 37 °C for 10 min). Cellular nucleic acids were digested with 50 U/ml Benzonase nuclease (**2.3**) for 30 min at 37 °C and the crude cell lysate was clarified by centrifugation at 10,000 x g for 5 min. The supernatant was used for qPCR titration of the contained rAAV vectors (**3.1.7.4**). The optimal ratio of baculovirus P2 stocks for AAV proteins and the transgene expression cassette was chosen for large scale rAAV production in Sf9 insect cells.

3.4.2.3 Large scale rAAV production in Sf9 insect cells

Large scale infection of Sf9 insect cells with baculovirus P2 stocks

Sufficient amounts of Sf9 insect cells were hatched in suspension culture in supplemented Insect-XPRESS™ medium (**3.3.1**) at 27 °C and 110 rpm in advance. Before infection with baculovirus P2 stocks, cell density was adjusted to $1.5x10^6$ cells/ml by spinning cells down in 200 ml centrifugation bottles for 5 min at 150 x g, counting them (**3.3.3**) and suspending them in fresh supplemented Insect-XPRESS™ medium. The optimal amount of baculovirus P2 stocks determined by test expressions was used to infect 6×10^8 Sf9 insect cells in 400 ml supplemented Insect-XPRESS™ medium (= $1.5x10^6$ cells/ml). Cells were incubated at 27 °C and 110 rpm and after 96 h, rAAV vectors were harvested.

Harvest of viral particles from Sf9 cells

Infected cells were transferred to 200 ml centrifugation bottles and spinned down for 5 min at 250 x g. Cell pellet and supernatant were further processed separately:
Viral particles from the cell culture supernatant were precipitated by PEG/NaCl (**3.4.3**), resupended in 4 ml PBS-MK per 400 ml initial supernatant and stored at -80 °C until further purification by iodixanol density gradient centrifugation (**3.4.4**).
The cell pellet of 400 ml culture was resupsended in 8 ml PBS-MK. The viral particles were released from the cells by three repeated freeze/thaw cycles (freezing the tubes in dry ice surrounded by

99.5% (v/v) ethanol for 10 min and thawing them in a water bath at 37 °C for 10 min). Cellular nucleic acids were digested with 50 U/ml Benzonase nuclease (**2.3**) for 30 min at 37 °C and the lysate was clarified by centrifugation at 3,000 x g for 15 min. The supernatant, containing the viral particles, was stored at -80 °C until further purification by iodixanol density gradient centrifugation (**3.4.4**).

3.4.3 AAV precipitation by PEG-8000/NaCl

partially adapted from Guo et al.[211]

3.4.3.1 Precipitation of AAV particles from large volumes

To precipitate AAV particles from large volumes (e.g. from cell culture supernatant), 100 g PEG-8000 and 58.44 g NaCl were added to 1 l of AAV containing suspension (resulting in approx. 10% (w/v) PEG-8000, 1M NaCl), mixed thoroughly and incubated o/n at 4 °C. The next day viral particles were spinned down at 5,000 x g for 30 min and the PEG-containing supernatant was discarded. Remaining traces of PEG-containing solution were removed with a pipette after another round of centrifugation at 5,000 x g for 2 min. The AAV-containing pellet was resuspended in an adequate amount of the desired buffer by carefully pipetting it up and down and slowly shaking it for 15 min at RT. Cellular nucleic acids were digested by adding 50 U/ml Benzonase (**2.3**) and incubation at 37 °C for 30 min. Remaining insoluble material was removed by centrifugation for 10 min at 5,000 x g.

3.4.3.2 Precipitation of AAV particles small volumes

Before starting with the precipitation, a PEG/NaCl (2 x) solution had been prepared as follows:

100 ml 2 x PEG/NaCl solution (20.00% (w/v) PEG-800, 2M NaCl):

- 20.00 g PEG-8000
- 11.69 g NaCl
- *ad* 100.00 ml $_{dd}H_2O$

To each ml AAV-containing suspension, 1 ml of the 2 x PEG/NaCl solution was added, mixed thoroughly and incubated o/n at 4 °C. The next day viral particles were spinned down at 5,000 x g for 30 min and the PEG-containing supernatant was discarded. Remaining traces of PEG-containing solution were removed after another round of centrifugation at 5,000 x g for 2 min. The AAV-containing pellet was resuspended in an adequate amount of the desired buffer by carefully pipetting it up and down and slowly shaking it for 15 min at RT. Cellular nucleic acids were digested by adding 50 U/ml Benzonase (**2.3**) and incubation at 37 °C for 30 min (a step which was skipped if

viral particles were purified by iodixanol density gradient centrifugation prior to PEG/NaCl precipitation). Remaining insoluble material was removed by centrifugation for 10 min at 5,000 x g.

3.4.4 Iodixanol density gradient centrifugation

adapted from Hermens et al.[212]

For discontinuous iodixanol density gradients, following solutions had been prepared in advance (iodixanol was added separately shortly before use):

75.00 ml stock for 15 % iodixanol solution	
- 20.00 ml	NaCl (5M)
- 10.00 ml	PBS-MK (10 x)
- 45.00 ml	$_{dd}H_2O$

60.75 ml stock for 25 % iodixanol solution	
- 0.75 ml	Phenol red solution
- 10.00 ml	PBS-MK (10 x)
- 50.00 ml	$_{dd}H_2O$

33.33 ml stock for 40 % iodixanol solution	
- 10.00 ml	PBS-MK (10 x)
- 23.33 ml	$_{dd}H_2O$

10.75 ml stock for 54 % iodixanol solution	
- 0.75 ml	Phenol red solution
- 10.00 ml	PBS-MK (10 x)

To fill up 13.5 ml Quick-Seal™ Ultra-Clear™ centrifuge tubes (Beckman) for use in the Type 70.1 Ti rotor (**2.1**), master mixes for the desired number of gradients were prepared as follows:

For one gradient:

- 2.500 ml	15% stock;	0.830 ml Optiprep™	= 3.330 ml
- 1.418 ml	25% stock;	0.970 ml Optiprep™	= 2.388 ml
- 0.665 ml	40% stock;	1.330 ml Optiprep™	= 1.995 ml
- 0.215 ml	54% stock;	1.800 ml Optiprep™	= 2.015 ml

For one gradient 4.2 ml virus sample were placed on the bottom of the centrifuge tube with a 5 ml syringe. The sample was carefully underlayed with 3.0 ml of the 15 % iodixanol solution by slowly releasing the solution from the syringe with gentle pressure. Attention was drawn on omitting the release of air bubbles into the centrifugation tube. The procedure was repeated with 2.0 ml of the 25% iodixanol solution, 1.66 ml of the 40% iodixanol solution and 1.66 ml of the 54% iodixanol solution. Integrity of the gradient was indicated by formation of colored bands (due to phenol red in two of the four phases). The gradient was carefully topped up with 1 x PBS-MK to remove all

remaining air and the tube was sealed with a tube topper (Beckman). Before centrifugation, all tubes were balanced and, if necessary, plastic paraffin film (Parafilm) was placed on top of single tubes until difference in weight was below 0.05 g. Gradients were centrifuged for 70 min at 350,000 x g (58,000 rpm in the Type 70.1 Ti Rotor, Beckman, **2.1**) at 18 °C with deceleration brake. After centrifugation, each tube was punctured at its top with a 23 G needle for aspiration of air and purified AAV particles were removed from the 40 % iodixanol phase by puncturing the tube with another 23 G needle attached to a 5 ml syringe from the side just above the lower red band (54% iodixanol) and aspirating the content of the 40% iodixanol phase.
The purified AAV particles were stored at -80 °C until titration (**3.1.7.4**) and further use.

3.4.5 Production of a random AAV display X7 peptide library by a three-step protocol

adopted from Müller et al.[141] *& Waterkamp et al.*[144]

3.4.5.1 Preparation of library backbone plasmid

The library backbone plasmid (pMT187-0-3 [ref.141]) was transformed into DH5α *E. coli* cells by electroporation (**3.2.3.1**). Bacteria were slowly grown to saturation (OD_{600} ≈ 2) in 1 l LB_{AMP} medium (**3.2.1.1**), plasmid was harvested (**3.1.1**) and purity and concentration of plasmid DNA was determined by spectrophotometric measurement (**3.1.9**). The 15 bp "stuffer" fragment was cleaved from 40 µg the plasmid by digestion with SfiI over 4 h at 50 °C (**3.1.2**). The SfiI digested library backbone plasmid was purified with the Qiaquick PCR Purification Kit (**2.2**), using four columns (10 µg each) and following manufacturer's instructions with following exceptions: The DNA was eluted with 50 µl/column of manufacturer's elution buffer (3.3 mM Tris-HCL, pH 8,5) diluted 1:3 in $_{dd}H_2O$. The eluted flow-through was reapplied to the column and centrifuged a second time. Purity and concentration of DNA was determined by spectrophotometric measurement (**3.1.9**).

3.4.5.2 Preparation of random AAV library oligonucleotide inserts

A degenerate oligonucleotide encoding seven random amino acids (encoded by NNK*) at amino acid position R588 of VP1 in AAV2 was commercially synthesized (Metabion) as follows:

5' –CAG TCG GCC AGA GAG GC $(NNK)_7$ GCC CAG GCG GCT GAC GAG- 3'

** N = A, C, G, T; K = G, T*

Due to its superior proofreading activity compared to the Klenow fragment, the Sequenase version 2.0 T7 DNA polymerase was used to generate the corresponding second strand by using the Sequenase 2.0 kit (**2.2**) and the respective library primer 5'-CTC GTC AGC CGC CTG G-3' (**2.12**). Four reactions according to the following scheme were prepared in different tubes:

-	2.00 µg	AAV library insert oligonucleotide
-	4.00 µg	AAV library primer
-	2.00 µl	Sequenase reaction buffer (USB®, 5x)
-	*ad* 10.00 µl	$_{dd}H_2O$

The reactions were incubated in a heating block at 65 °C for 2 min, then slowly cooled down to 40°C by taking the block out of the heating apparatus and placing it on the bench. The samples were transferred to ice for 2 min and briefly spinned to pull down evaporated fluid from the lid. Each 10 µl sample was filled up to 50 µl elongation reaction as follows:

-	10.00 µl	sample
-	2.00 µl	dNTPs (Fermentas, 10mM)
-	5.00 µl	DTT (USB, 0.1 M)
-	31.00 µl	enzyme dilution buffer (USB®)
-	2.00 µl	diluted** Sequenase (USB®)

** *following manufacturer's instructions*

The reaction tubes were incubated at 37 °C for 1 h and the double stranded library insert oligonucleotides were purified with the Qiaquick Nucleotide Removal Kit (**2.2**) following manufacturer's instructions, using three columns. DNA was eluted with 50 µl/column of manufacturer's elution buffer (3.3 mM Tris-HCL, pH 8,5) diluted 1:3 in $_{dd}H_2O$, followed by a second elution with 30 µl/column, yielding 240 µl altogether.

3.4.5.3 Digestion of random AAV display peptide library oligonucleotide inserts

The double stranded library oligonucleotide inserts were digested with BglI according to following scheme:

-	240.00 µl	double stranded oligonucleotide
-	30.00 µl	NEB 3 buffer (10 x)
-	3.00 µl	BSA (NEB, 100 x)
-	30.00 µl	BglI (NEB, 10,000 U/ml)

The digestion reaction was distributed into three reaction tubes and incubated for 4 h at 37 °C. The digested double stranded library oligonucleotide inserts were purified with the Qiaquick Nucleotide

Removal Kit (**2.2**), following manufacturer's instructions, using three columns. DNA was eluted with 50 µl/column of manufacturer's elution buffer (3.3 mM Tris-HCL, pH 8,5) diluted 1:3 in $_{dd}H_2O$. The eluted flow-through was reapplied to the column and centrifuged a second time. Purity and concentration of DNA was determined by spectrophotometric measurement (**3.1.9**).

3.4.5.4 Ligation of library plasmid backbone and random oligonucleotide inserts

Test ligation

To find the optimal ratio of library plasmid backbone and oligonucleotide inserts for large scale ligation, different molar ratios were ligated in small scale (plasmid:insert): 1:10, 1:30 and 1:100 as described in **3.1.5** but with 500 ng plasmid DNA. After ethanol precipitation (**3.1.8**) the ligated DNA samples were dissolved in 25 µl 1 mM Tris-HCl pH 8.5 in $_{dd}H_2O$ (1:10 diluted elution buffer from Qiaquick Kit, **2.2**).
Test electroporations were performed as follows:

- 1.00 µl	ligated plasmid (Tris-HCl as control)
- 25.00 µl	DH5α electrocompetent *E. coli* cells

Electroporated cells were added to pre-warmed SOC medium and allowed to reconstitute at 37 °C at 175 rpm for 1 h. 100 µl of the reconstituted cells were spread on LB_{AMP} plates in 1:10, 1:100 and 1:1000 dilutions and incubated o/n at 37 °C.
By counting the colonies on the plates, the best molar ratio for ligation and the background was calculated. Since a low (< 1.00%) background (number of colonies on a Tris-HCl control ligation divided through the number of colonies on the plate with the best molar ratio of ligation) is crucial for a high diversity of the plasmid library, much focus was set on finding the right molar ratio for ligation. In case ratios of plasmid backbone and insert of 1:10, 1:30 and 1:100 were not sufficient, other molar ratios were tested.

Large scale ligation

The best molar ratio of library plasmid backbone and insert from the test ligation was chosen for large scale ligation.

- X µg	olignucleotide insert
- 10.00 µg	library backbone

The sample was mixed and incubated at 65 °C for 2 min, then transferred to ice. After at least 5 min on ice the sample was filled up with:

-	50.00 µl	T4 ligase buffer (NEB, 10x)
-	30.00 µl	T4 DNA ligase (NEB, 400,000 U/ml)
- *ad*	500.00 µl	$_{dd}H_2O$

The sample was split up in ten 0.5 ml reaction tubes (50.00 µl each) and incubated o/n at 16 °C. After sample precipitation (**3.1.8**) the ligated DNA sample was dissolved in 200 µl 1 mM Tris HCL pH 8.5 in $_{dd}H_2O$ (1:10 diluted elution buffer from Qiaquick Kit, Qiagen)

3.4.5.5 Large scale electroporation

The large scale electroporation was performed in 2 x 50 = 100 single reactions. To ensure rapid processing of the samples, 4 x 50 ml = 200 ml pre-warmed SOC medium (2 ml per electroporation), 4 x 950 ml = 3,8 l pre-warmed LB_{AMP} medium in 2 l Erlenmeyer flasks (38 ml per electroporation) and 4 x 16 LB_{AMP} plates were prepared in advance.

50 electroporations were performed at a time with the same settings of the electroporation apparatus as described in (**3.2.3.1**). Electroporation cuvettes (1 mm, Biorad) for 50 electroporations were placed in ice buckets to cool them to 0-4 °C by the time of use and the tubes with the SOC medium were placed in a water bath at 37 °C.
For each electroporation twice the amount of DNA and cells than for the test ligation was used:

2.00 µl	ligated plasmid
50.00 µl	DH5α electrocompetent *E. coli* cells

A mastermix for 50 electroporations (100 µl plasmid and 2,500 µl bacteria), split into five tubes, was prepared on ice very carefully. Pipetting bacteria up and down was restricted to minimum and the sample was kept as cool as possible. The actual electroporations were performed with three persons to keep the speed and thereby the quality of the bacteria at maximum. The first person transferred 52 µl of the plasmid bacteria solution between the electrodes of the electroporation cuvettes. The second person placed the cuvettes into the electroporation apparatus, pressed the button and removed the cuvettes after electroporation (**3.2.3.1**). The third person transferred the electroporated cells into a tube by adding 1 ml pre-warmed SOC to the cuvette, removing the entire content and rinsing the cuvette with another 1 ml of pre-warmed SOC. After having performed 25

electroporations, the electroporated cells (in 50 ml SOC) were placed into an incubator and let shake at 200 rpm for 1 h while the remaining electroporations were performed.
After reconstitution in SOC for 1 h, bacteria of each 50 ml tube were added to 950 ml LB_{AMP} medium. 100 µl of each 1000 ml LB_{AMP} bacteria culture were spread on LB_{AMP} plates in different dilutions (undiluted, 1:10, 1:100, 1:1000) and incubated o/n at 37 °C to calculate the diversity of the plasmid library. Bacteria in the 1000 ml cultures were let grown at 30 °C and 175 rpm to saturation (OD_{600} approx. 2), the plasmid was harvested (**3.1.1**) and purity and concentration of plasmid DNA was determined by spectrophotometric measurement (**3.1.9**).

3.4.5.6 AAV transfer shuttle particle production

AAV transfer shuttles were produced according to the protocol described in **3.4.1** in ≥ 10 cell dishes (1×10^7 cells in each 15cm dish) with following plasmids (amount of DNA per 15 cm dish):

3.00 µg*	library plasmid (including ITRs)[141, 143]
3.00 µg*	pVP3cm (containing codon modified AAV2 wild type c*ap*, without ITRs)[144]
6.00 µg	Ad-pXX6 (containing E1A, E1B, E2A, E4-orf6, VA)[79]

** ≈ molar ratio 1:1 (similar molecular weight of plasmids), other ratios have also been tested*

The transfer shuttles were harvested and purified using iodixanol density gradients (**3.4.4**) and the replicative titer was determined by rep assay (**3.4.6**).

3.4.5.7 AAV peptide library particle production

HEK 293T cells were seeded in ≥ 10 cell dishes (15 cm dish) at a density of $1{,}25 \times 10^7$ cells/dish. The next day, at 70% confluency, cells were infected with AAV transfer shuttles at an MOI of 1 replicative unit per cell in 7 ml serum free DMEM medium (Gibco). Cells were co-infected with Ad5 at an MOI of 5 plaque forming units per cell. After 30 min cells were topped up to 20 ml per dish with supplemented DMEM medium. Three days later, when 50% cytopathic effect was observed, AAV peptide library particles were harvested from the cells according to the protocol in chapter **3.4.1.2**. Additionally, the supernatant was concentrated to a workable volume (1 ml per dish) by Vivaspin® centrifugal concentrator tubes, added to the harvested AAV peptide library particles from the cells and remaining Ad5 was heat inactivated at 55 °C for 1 h. The pooled AAV peptide library particles were purified by iodixanol density gradient centrifugation (**3.4.4**).
The genomic titer of the AAV display peptide library was determined by qPCR (**3.1.7.4**).

3.4.6 Replicative titer assay

HEK-293T cells were seeded (**3.3.2**) in poly-L-lysine coated 96-well plates in 100 µl supplemented DMEM medium ($2{,}5x10^4$/well). The next day, when cells reached 70-80% confluency, 100 µl AAV transfer shuttles in a 1:5 dilution in complete DMEM medium were added to the first well (resulting in a 1:10 dilution in the first well "A1"). A dilution series in the first line of the 96-well plate (A1-A12) was prepared by transferring 100 µl from each well to the next well on the right and mixing carefully. The dilution series was continued downwards in 1:11 dilution steps by transferring 10 µl from the wells in the upper line to the wells in the line below until all wells (A1-E12) having received AAV transfer shuttles in different dilutions.

After having incubated the cells for 1 h with the AAV transfer shuttles, they were superinfected with Ad5 at an MOI of 5 pfu/cell in 50 µl DMEM medium without supplements (the first well A1 was left uninfected as first negative control). Cells were washed with 200 µl PBS/well and fixed with 3.5% (w/v) paraformaldehyde in PBS (50 µl/well) for 10 min at RT 24 h after superinfection. After fixation, cells were permeabilized with 0.2% (v/v) Triton X-100 in PBS (50 µl/well) for 10 min at RT and blocked with 3% (w/v) BSA; 0.5% (v/v) Tween 20 in PBS for 1h. After blocking, cells were incubated with murine antibody "AK76.3" against AAV Rep protein (**2.4**) diluted 1:2 in 3% (w/v) BSA; 0.5% (v/v) Tween 20 in PBS for 1 h at RT (the second well A2 was left untreated as second negative control). Incubation with the primary antibody against AAV Rep protein was followed by washing the cells twice with 200 µl PBS/well and incubating them with FITC-labeled rabbit anti mouse antibody (**2.4**) diluted 1:200 in 1:2 in 3% (w/v) BSA; 0.5% (v/v) Tween 20 for 1 h in the dark at RT. After incubation with the second antibody, cells were washed twice with 200 µl PBS/well and positive stained cells were counted under a fluorescence microscope (Zeiss, Axiovert 40 CFL, **2.1**). The numbers of cells in wells ranging from one to approx. 200 positive events were taken to calculate the replicative titer of the undiluted AAV transfer shuttles.

3.4.7 Preparation of plasmids with X_7 peptide inserts for rAAV2 vector production

To produce rAAV transgene vectors (**2.11.2**) displaying selected peptide variants, the oligonucleotides encoding the corresponding peptides needed to be transferred into an ITR-less plasmid backbone with *cap* insertion site.

3.4.7.1 Transfer of peptide-encoding oligonucleotides from AAV2 library plasmids into AAV2 rep/cap plasmids without ITRs

The insert-encoding fragment of the viral *cap* gene from selected clones of the random AAV display peptide library was amplified by PCR using single clone library plasmids (pMT187-0-3 [ref.141] with inserts) as template similar to the amplification of viral *cap* gene fragments from total DNA (**3.1.7.3**) but at smaller scale (< 5 PCR reactions). The oligonucleotides were digested with BglI, purified as described in **3.4.5.3** and ligated into the corresponding SfiI digested ITR-less backbone plasmids (pXX2-187 [ref.145]).

3.4.7.2 Preparation of synthetic oligonucleotide inserts for transfer into AAV2 rep/cap plasmids without ITRs

To test vectors displaying modified peptides (e.g. alanine scan) or to transfer pre-selected peptides from one AAV serotype to another, oligonucleotides encoding the seven amino acids of choice at amino acid position R588 of VP1 in AAV2 were commercially synthesized (Metabion) as follows:

5' –CAG TCG GCC AGA GAG GC $(X)_{21}$ GCC CAG GCG GCT GAC GAG- 3'

$(X)_{21}$ = specific nucleotide sequence of peptide chosen for analyses

The oligonucleotides were further prepared in ¼ scale as described under **3.4.5.2** and ligated into the corresponding SfiI-digested ITR-less backbone plasmid (pXX2-187 [ref.145])

XL1-Blue *E. coli* cells were transformed by heat shock (**3.2.3.2**), single colonies from LB_{AMP} agar plates were incubated o/n at 37 °C and 200 rpm in 200 ml LB_{AMP} medium, plasmids were harvested (**3.1.1**), purity and concentration of the plasmid DNA was determined by spectrophotometric measurement and plasmids were used for rAAV vector production (**3.1.9**).

3.4.8 *In* vivo selection of random AAV display peptide libraries

adapted from Michelfelder et al.[19]

3.4.8.1 Circulation of library particles

FVB mice were injected intravenously with a random AAV display peptide library at $1x10^{11}$ gp/mouse (**2.11.2**). After two days (brain) or eight days (lung) of particle circulation, the tissue of interest as well as control organs (brain, heart, lung, liver, spleen, kidney, skeletal muscle) were used for isolation of total DNA (**3.5.3**).

3.4.8.2 PCR amplification of AAV display peptide library inserts enriched in the tissue of interest

The fragments of the viral DNA from the random AAV display peptide library encoding the modified *cap* gene with the random oligonucleotide insertions was amplified from total DNA from the tissue of interest via PCR (**3.1.7.3**) with the primers AAV2_4+ and AAV2_4+ (**2.12**). To retain library diversit y, ≥ 15 PCR reactions were performed from each tissue of interest with 500 ng template/reaction. If no bands or only weak bands were detectable, a second (nested-) PCR was performed with the primers AAV2_3+ and AAV2_3+ (**2.12**) in ≥ 15 reactions using 3 µl samples from each first PCR reaction as template.

The PCR-products were precipitated (**3.1.8**) and dissolved in a total volume of 50 µl elution buffer (Qiagen, 3.3 mM Tris-HCL, pH 8,5) diluted 1:3 in $_{dd}H_2O$.

3.4.8.3 Digestion of PCR-amplified random AAV display peptide library inserts

The PCR-amplified random AAV display peptide library oligonucleotide inserts (10-40 µg) were digested with BglI (**3.1.2**). The digested oligonucleotide inserts were purified with the Qiaquick PCR Purification Kit (**2.2**), using the flow-through of two columns after the first centrifugation step (the longer cleaved ends remained in the column while the smaller inserts were contained in the flow-through!). The digested library inserts were precipitated from the flow-through (**3.1.8**) and dissolved in a total volume of 50 µl elution buffer (Qiagen, 3.3 mM Tris-HCL, pH 8,5) diluted 1:3 in $_{dd}H_2O$. Purity and concentration of DNA was determined by spectrophotometric measurement (**3.1.9**).

3.4.8.4 Producing secondary libraries for subsequent rounds of selection

The digested PCR amplified random oligonucleotide inserts (**3.4.8.3**) enriched in the tissue of interest were used to generate pre-selected secondary AAV display peptide libraries for subsequent rounds of selection. In case of the brain selection, the secondary libraries were produced following the steps **3.4.5.4** with following exception: Due to the limited diversity of pre-selected secondary AAV display peptide libraries, it was sufficient to perform 10-12 electroporation reactions with the remaining sample of the test ligation (500 ng library plasmid backbone + X ng insert) after finding the best molar ratio of insert and library plasmid backbone, instead of performing large scale ligation and electroporation as for the primary random AAV display peptide library. In case of the lung selection, the secondary libraries were produced similar but without the extra step of library transfer shuttles, by directly transfecting HEK 293T cells with the plasmid library (1 plasmid/cell) and the adenoviral helper plasmid pXX6 without the codon-modified AAV2 *cap* plasmid pVP3cm.

3.4.8.5 Enrichment of library particles with desired tropism

Secondary libraries were intravenously injected into FVB/N mice at a dose of 1 x 10^{11} gp/mouse with two days circulation time (brain) or at a dose of 1 x 10^{9} gp/mouse with eight days circulation time (lung). To enrich library particles with the desired tropism, at least four subsequent rounds of *in vivo* selection were performed. After each round of selection, single library clones were picked from LB_{AMP} plates after transformation of the ligated library plasmids (**3.4.5.4**), transferred to 5 ml LB_{AMP} medium and grown o/n at 30 °C and 175 rpm. Plasmids were harvested and purified (**3.1.1**) and the modified *cap* genes carrying the oligonucleotide inserts were sequenced (Seqlab) and analyzed for enrichment of single clones or sequence motifs.

3.5 Assessment of rAAV vectors

3.5.1 Animals and vector administration

All experiments at the University Medical Center Hamburg-Eppendorf (UKE) involving animals were conducted in accordance with the German animal protection code (Tierschutzgesetz). Approval („Selektion gewebsspezifischer Gentherapievektoren mit auf adeno-assozierten Viren exprimierten randomisierten Peptidbanken“, G42/09) was granted by the local authority and the ethics review board (Behörde für Soziales, Familie, Gesundheit und Verbraucherschutz – Lebensmittelsicherheit und Veterinärwesen, Hamburg, DE). Animals were housed in individual ventilated cages (IVCs) with a 12 h light cycle at the UKE animal facility.

Animal experiments at the Institute of Experimental and Clinical Pharmacology and Toxicology, University of Lübeck were approved (AZ V 312-72241.122-22) by the authority and the ethics review board of the state Schleswig-Holstein (Minesterium für Energiewende, Landwirtschaft, Umwelt und ländliche Räume).

Purified AAV library particles and recombinant AAV vectors were injected into the tail vein or the retro-orbital venous sinus of 8-10 weeks old mice (strain FVB/N, C57BL/6 or SCID) under gas anesthesia (2% (v/v) isoflurane, 98% (v/v) oxygen) in a total volume of 200 µl (diluted in PBS). For determination of luciferase activity (**3.5.4**) and DNA isolation (**3.5.3**), animals were killed by cervical dislocation under gas anesthesia, the tissue of interest and control organs were carefully removed, rinsed in PBS, snap frozen in liquid nitrogen and stored at -80 °C until further processing.

3.5.2 Animal tissue homogenization

The tissue of interest and possibly several control organs were cut on ice into small pieces, each organ (depending on its size) distributed to 6-12 pre-cooled tissue homogenizing tubes filled with ceramic beads (CK28, Precellys®, Peqlab) and topped up with an appropriate volume of the desired buffer (depending on further processing of the homogenized tissues).

Tissues were homogenized using Precellys®24 tissue homogenizer (**2.1**) with following settings:

Brain:	1x	20 sec	5,500 rpm	
Heart, liver, spleen, kidney:	2x	20 sec	5,500 rpm	10 sec pause
Skeletal muscle:	2x	30 sec	6,000 rpm	20 sec pause

3.5.3 Isolation of total DNA from animal tissues

The tissue of interest and control organs were homogenized (**3.5.2**) in 180 µl ATL buffer/tube from the DNeasy Blood & Tissue Kit (**2.2**). Total DNA was isolated with the DNeasy Blood & Tissue Kit (**2.2**) according to manufacturer's instructions with an initial lyses time of ≈ 1 h. After elution, total DNA from each organ was pooled in one tube/organ and thoroughly mixed. Purity and concentration of DNA was determined by spectrophotometric measurement (**3.1.9**)

3.5.4 Analyses of luciferase activity in animal tissues

Tissues were homogenized (**3.5.2**) in 180 µl/tube 1 x Reporter Lysis Buffer (Promega). After homogenization, the samples were centrifuged at 10.000 x g and 4 °C for 10 min and the clarified supernatant was (20 µl of each tissue) transferred to an intransparent 96 well microtiter plate and analyzed for luciferase expression after automatic addition of Luciferase Assay Reagent (Promega) in a luminometer (Mithras LB 940, Berthold Technologies, **2.1**) with following settings:

- Measurement
    - Dispense
        - Volume: 100 µl/well Luciferase Assay Reagent (Promega)
        - Speed: low
    - Delay: 2 sec
    - Counting Time: 10 sec

Luminescence values were normalized to total protein levels (**3.5.5**).

3.5.5 Quantification of protein levels in animal tissues

Protein levels in animal tissues were determined by the Roti® Nanoquant Protein assay (Roth, Karlsruhe, Germany), according to the manufacturer's instructions. The Roti® Nanoquant Protein assay is a modified version of Bradford's protein assay[213]. The homogenized tissue samples (**3.5.2**) were diluted 1:500 and 1:1000 in $_{dd}H_2O$ in 96 well microtiter plates on ice and 50 µl of each diluted sample and a BSA (Albumin Fraction V) standard dilution series (0-200 µg/ml) were filled up with 200 µl 1 x Roti® Nanoquant solution. The optical density of the samples was measured at 590 nm and 470 nm in an ELISA-reader (**2.1**) and the protein content was determined by plotting the ratio OD_{590}/OD_{470}, analyzing all probes within the linear range.

3.5.6 Analyses of vector genome distribution (homing) in mice

To analyze the vector distribution independently of transgene expression, total DNA from relevant organs was isolated (**3.5.3**) and the copy numbers of vector DNA were determined by qPCR (**3.1.7.4**) with appropriate primers (**2.12**). Vector copy numbers were normalized to total DNA levels, quantified by spectrophotometric measurement (**3.1.9**).

3.5.7 Bioluminescence imaging (BLI)

For analyses of luciferase transgene expression, BLI was performed at different time points after intravenous vector administration (**3.5.1**) using the Xenogen IVIS 200 imaging system (**2.1**). After intraperitoneally injecting 200 µl/mouse firefly D-luciferin potassium salt (30 mg/ml in PBS) under gas anesthesia (2% (v/v) isoflurane, 98% (v/v) oxygen), representative images were taken when luminescence (photons/sec/cm^2) reached the highest intensity (normally around 15 min after i.p. administration of D-luciferin). Luminescence was measured over a period of 3 min/measurement, with a binning = 1. Data were analyzed with the software Living Image 4.0 (**2.14**).

3.5.8 Immunohistochemistry on paraffin embedded tissues

Immunohistochemistry and histological analyses were performed at the Division of Asthma Mouse Models of the Leibniz-Center for Medicine and Biosciences, Borstel, Germany with kind help of Lars Lunding.

Two weeks after vector administration (**3.5.1**), animals were killed by i.p. administration of 240 mg/kg ketamine and 16 mg/kg xylazine in 0.9% (w/v) NaCl solution. Lungs were carefully removed *en block* with trachea and heart and fixed *ex situ* with 4% (w/v) paraformaldehyde via the trachea under hydrostatic pressure of a 20 cm water column for 20 min, followed by 24 h immersion in the same fixative at 4 °C. Brains were directly immersed in 4% (w/v) paraformaldehyde at 4 °C. Lung and brain tissues were rinsed, dehydrated and embedded in paraffin wax in an automatic tissue processor (**2.1**). Paraffined tissues were sectioned (2 µm) in a microtome (HM 355 S, Microm, **2.1**) and sections were dewaxed, rehydrated and used for immunohistochemistry. Endogenous peroxidase activity was inactivated with 1% H_2O_2 in methanol for 30 min. Prior to CD31 staining, sections were heated to 100°C in citrate buffer, pH 6 for 20 min for antigen retrieval. After washing in PBS, the sections were incubated for 30 min with PBS, 10% (v/v) goat serum (Vector Lab), 2% (w/v) dry milk. Immunohistochemistry was performed with polyclonal antibodies against GFP (A-11122; Invitrogen, **2.4**) or CD31 (ab28364; Abcam, **2.4**) each diluted 1:100 in 2% (w/v) dry milk in PBS. Primary antibodies were allowed to bind for 1 h at 37 °C. After washing in PBS, the sections were incubated for 30 min with a secondary biotinylated goat anti-rabbit antibody (Vector Lab, **2.4**), diluted 1:100 in 2% (w/v) day milk in PBS. Bound antibodies were visualized using the VECTASTAIN Elite ABC Kit (Vector Lab) and 3,3'-diaminobenzidine (DAB; Sigma-Aldrich). Selected sections were counterstained with hemalum. Sections were analyzed under a microscope (BX-51, Olympus, **2.1** at 10-fold to 100-fold magnification using the software cell^A (**2.14**).

3.5.9 Immunofluorescence on agarose embedded tissues

Immunofluorescence and histological analyses were kindly performed by Dr. Godwin Dogbevia at the Institute of Experimental and Clinical Pharmacology and Toxicology, University of Lübeck, Germany.

Two weeks after vector administration (**3.5.1**), animals were killed by transcardial perfusion with warm 4% (w/v) PFA in PBS under isoflurane aesthesia (2% (v/v) isoflurane, 98% (v/v) oxygen). Tissues were postfixed o/n at 4 °C in 4% (w/v) PFA in PBS, followed by embedding in 2.5% (w/v) agarose in PBS. Coronal sections (60-100 µm) were prepared with a vibratome (VT1200S, Leica, **2.1**) and stored in PBS at 4 °C. Prior to staining, sections were rinsed three times in TBS-T and blocked in 5% (w/v) BSA in TBS-T for 2 h. For staining, sections were incubated o/n at 4 °C with primary antibodies against CD31 (rat anti-mouse CD31, BD Pharmingen™,**2.4**), CD13 (rat anti-mouse CD13, AbD serotec, **2.4**) or collagen IV (ab6586, Abcam, **2.4**), diluted 1:500 (CD31, CD13) or 1:1,000 (collagen IV) in 5% (w/v) BSA in TBS-T. The next day, sections were rinsed three times in TBS-T and incubated in the dark for 2 h at RT with the secondary Cy3-labelded donkey anti-rat antibody (AP189C, Merck Millipore, **2.4**) or donkey anti-rabbit antibody (Jackson Immuno Research, **2.4**) diluted 1:400 in 5% (w/v) BSA in TBS-T.

After antibody incubation, sections were rinsed three times in TBS-T and mounted on slides. Sections were analyzed under a microscope (DMI6000 B, Leica, **2.1**) at 10-fold and 20-fold magnification using the software LAS AF, ImageJ and Fiji[214] (**2.14**).

3.5.10 In silico modeling of the protein structure of selected AAV2 capsid variants

The published structure of the wild-type AAV2 capsid with the protein data bank number pdb:1LP3 [ref.43] was used as template for homology modeling of modified AAV2 capsid with peptide insertion by the SWISS-MODEL Workspace [215-218] (**2.14**) and visualized with the software jmol version 13.0 (**2.14**).

3.5.11 Statistics

Statistics for luciferase activity (**3.5.4**) and vector distribution data (**3.5.3**) were performed with the program Prism 3.0 (**2.14**) as one-way ANOVA, followed by Bonferroni's multiple comparison test. Values are shown as mean + standard deviation (SD). Levels of significance: $p < 0.05$ = *; $p < 0.01$ = **; $p < 0.001$ = ***

4 Results

4.1 Generation of a random AAV2 display X_7 peptide library

The BglI-digested heptapeptide-encoding oligonucleotides were ligated with the SfiI-digested AAV2 library plasmid backbone pMT187-0-3 in different molar ratios to obtain the best ligation conditions. With a background of 0.52%, a molar ratio of 1:30 gave the best result and was chosen for large scale ligation of the plasmid library (**3.4.5.4**). The theoretical maximum diversity of a random AAV display peptide library is limited by the diversity of the respective plasmid library which can be calculated from the number of transformed *E. coli* clones. With 10 µg ligated plasmid, 3.4 x 10^8 *E. coli* clones could be transformed, representing the theoretical maximum diversity of the plasmid library.
By transfection of 2 x 10^8 HEK 293T cells in twenty 15 cm cell culture dishes, a total 1 x 10^{12} gp (2.5 ml with 4.85 x 10^{11} gp/ml) AAV2 library transfer shuttles could be generated (**3.4.5.6**), as quantified by qPCR (**3.1.7.4**). A fragment of the viral *cap* gene, encapsidated in the library transfer shuttles was amplified by PCR (**3.1.7.3**) to check for unwanted homologous recombination between the plasmid library and the AAV2 wild type *cap* gene from the plasmid pVP3cm which was used for transfection. DNA fragments with a size of 113 bp could be amplified, corresponding to the library insert-encoding *cap* region. Fragments of the *cap* gene without library inserts (88 bp) could not be amplified from the library transfer shuttles (**Figure 7**), indicating that the AAV2 library transfer shuttles were free of wild type AAV2 contamination.

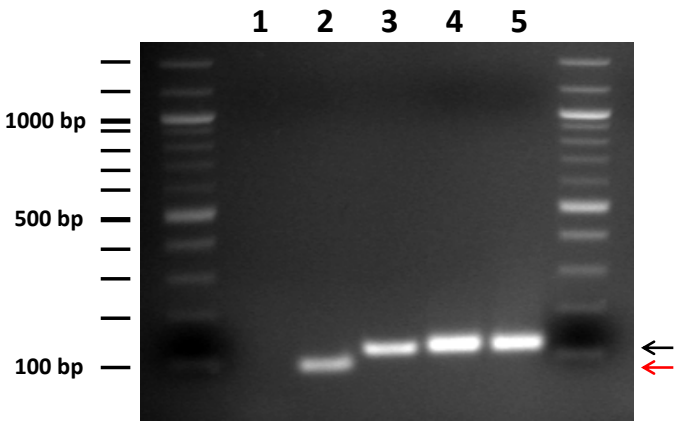

Figure 7. Library transfer shuttles & random AAV library carrying oligonucleotide inserts
Fragments of the *cap* gene carrying heptapaptide-encoding oligonucleotide inserts were amplified with the primer pair AAV2_1+/AAV2_1-. Samples were separated in 2% (w/v) agarose in TAE at 80 V for 1 h and stained with ethidium bromide. DNA ladder: Quick-Load® 100 bp DNA Ladder (New England Biolabs). **Lane 1**: No template. **Lane 2**: Insert-less wild type AAV2 control (pXX2) **Lane 3**: Plasmid library incl. oligonucleotide insert (pMT187-0-3). **Lane 4**: Library transfer shuttles. **Lane 5**: Random AAV display peptide library. Red arrow: 88 bp fragment (no insert). Black arrow: 113 bp fragments (with insert)

The replicative titer of the library transfer shuttles was determined at 1 x 10^8/ml by replicative titer assay (**3.4.6**). To produce the final random AAV2 display peptide library, transfer shuttles were used at an MOI = 1 to infect 2 x 10^8 HEK 293T cells (**3.4.5.7**). The genomic titer of the resulting random AAV2 display peptide library was 1.13 x 10^{12} gp/ml, as determined by qPCR (**3.1.7.4**). Since the library transfer shuttles and the final random AAV2 display peptide library were produced in 2 x 10^8 cells

each, the final library's theoretical maximum diversity was limited to 2 x 10^8 which is less than the diversity calculated at plasmid level (3.4 x 10^8). Like the library transfer shuttles, the final random AAV display peptide library was checked for wild type AAV2 contamination by PCR (**3.1.7.3**). Only DNA fragments with a size of 113 bp could be amplified, corresponding to the library insert-encoding *cap* region (**Figure 7**). To verify integrity of the encapsidated genomes harboring the heptapeptide-encoding inserts, three random clones from the AAV2 display peptide library were used for sequencing analyses. Heptapeptide-encoding inserts were present in frame at nucleotide position 3967 in the AAV genome (R588, VP1) in all sequenced clones (**Figure 8**).

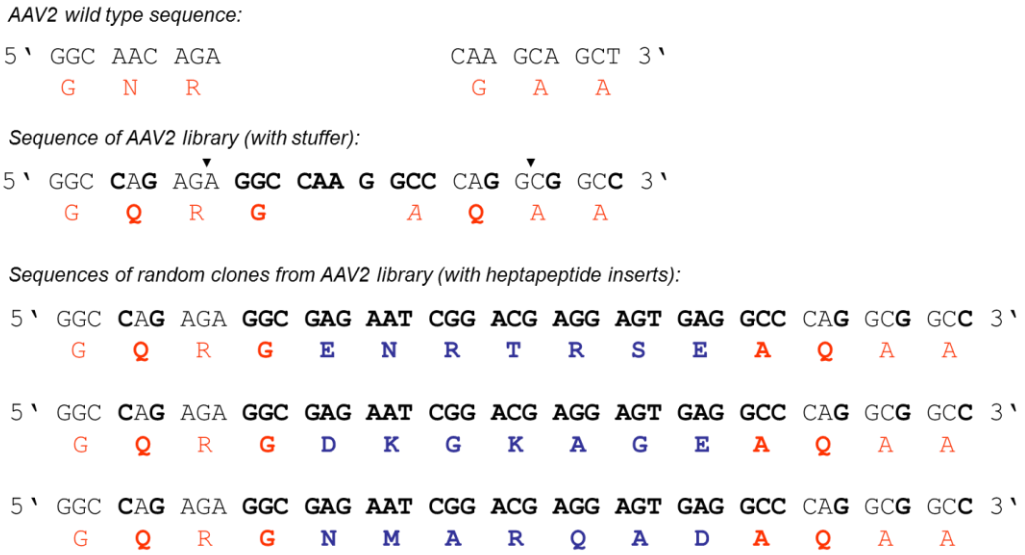

Figure 8. Random oligonucleotide inserts of the AAV display peptide library in frame at R588 (VP1)
Nucleotide sequences are indicated in black characters, amino acid sequences are indicated as one letter code in red (virus plasmid backbone) or blue (heptapeptide inserts). Nucleotides and amino acids that differ from the wild type sequence are indicated in bold characters. **1st row:** Nucleotide and amino acid sequence of the wild type AAV2 cap gene around amino acid position R588 (VP1). **2nd row**: Modified nucleotide and amino acid sequence of library plasmid (pMT187-0-3) with "stuffer". The SfiI cleavage sites are indicated with black arrows. **Row 3-5**: Sequenced heptapeptide-encoding oligonucleotide inserts from three random clones of the AAV display peptide library.

After having confirmed the genomic integrity of the random AAV2 display peptide library, the library was further used for an *in vivo* screening (**3.4.8**) in mice to select vector capsids specifically homing to and mediating transduction of the brain after systemic administration.

4.2 *In vivo* screening of the AAV2 display X_7 peptide library in mice

4.2.1 Rescue of library genomes from murine brains

After having injected 5 x 10^{10} gp of the original AAV2 display X_7 peptide library or, in subsequent rounds of selection, pre-selected AAV2 display X_7 peptide libraries systemically into the tail vein of mice (**3.5.1**), the viral particles were given 48 h time to circulate and transduce their target tissues. After each round of *in vivo* selection, approximately 500 µg total DNA could be extracted from the brain (**3.5.3**). The peptide insert-encoding fragment of the modified viral *cap* gene was amplified from total DNA by PCR (**3.1.7.3**).

After the first round of *in vivo* selection, only a barely visible band with a size of 486 bp could be detected after a first PCR . Thus, a second (nested) PCR was performed, resulting in a strong band with 359 bp and a smaller, less distinct band with approx. 400 bp (**Figure 9**). Both rounds of PCR yielded bands in the expected range (486/359 bp) indicating the presence of peptide insert-encoding oligonucleotides and the absence of wild type *cap* genes which would have resulted in bands with a size of 459 bp (1^{st} PCR) and 332 bp (2^{nd} PCR).

PCR amplification of the insert-encoding fragments of the modified viral *cap* gene after the second round of *in vivo* selection yielded a faint band with a size of 486 bp, which still was slightly stronger than the band obtained after the first round. A second (nested) PCR was performed, resulting in a strong band with 359 bp and a smaller, less distinct band with approx. 400 bp. Only DNA fragments containing insert-encoding oligonucleotides were amplified whereas no wild type *cap* genes were detectable (**Figure 9**).

In the third and subsequent rounds of *in vivo* selection, PCR amplification of the insert-encoding fragments of the modified viral *cap* gene yielded strong bands with sizes of 486 bp, making second (nested) PCRs obsolete. Like in prior rounds, only DNA fragments containing insert-encoding oligonucleotides were amplified whereas no wild type *cap* genes (without library inserts) were detectable (**Figure 9**).

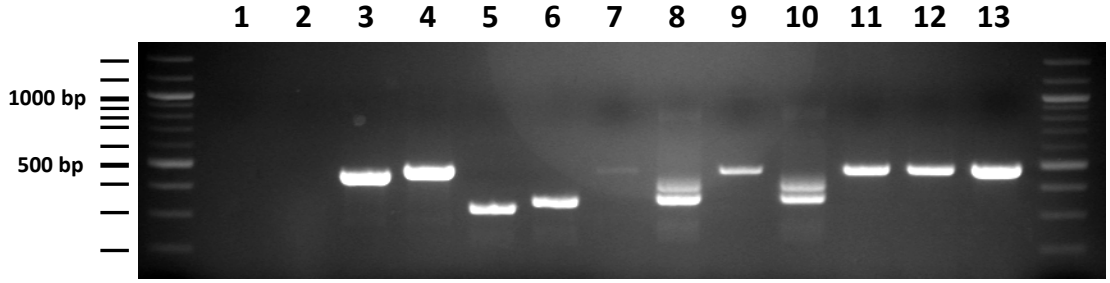

Figure 9. Amplification of viral cap fragments carrying oligonucleotide inserts from total mouse DNA
Fragments of the *cap* gene carrying heptapaptide-encoding oligonucleotide inserts were amplified by (nested-) PCR from 500 ng total tissue DNA with the primer pairs AAV2_4+/AAV2_4- (1st PCR) and AAV2_3+/AAV2_3- (2nd PCR). Samples were separated in 2% (w/v) agarose in TAE at 80 V for 45 min and stained with ethidium bromide. DNA ladder: Quick-Load® 100 bp DNA Ladder (New England Biolabs). **Lane 1**: 1st PCR without template. **Lane 2**: 2nd PCR with without template. **Lane 3**: 1st PCR with wild type AAV2 plasmid (pXX2). **Lane 4**: 1st PCR with plasmid library incl. oligonucleotide insert (pMT187-0-3). **Lane 5**: 2nd PCR with wild type AAV2 (pXX2). **Lane 6**: 2nd PCR with plasmid library incl. oligonucleotide insert (pMT187-0-3) **Lane 7**: 1st PCR from total DNA after 1st selection round. **Lane 8**: 2nd PCR after 1st selection round. **Lane 9**: 1st PCR from total DNA after 2nd selection round. **Lane 10**: 2nd PCR after 2nd selection round. **Lane 11**: 1st PCR from total DNA after 3rd selection round. **Lane 12**: 1st PCR from total DNA after 4th selection round. **Lane 13**: 1st PCR from total DNA after 5th selection round.

4.2.2 Generation of subsequent (preselected) AAV libraries during *in vivo* selection in murine brain

After PCR-amplification (**3.4.8.2**), the enriched insert-encoding fragments of the modified viral *cap* gene were ligated into the AAV2 library plasmid backbone at different molar ratios to test the best conditions. A molar ratio of 1:10 (backbone:insert) gave the best result at test ligation after each round of selection. After the first round, test ligation yielded 2.8×10^7 transformed clones/500 ng DNA with a background of 0.02%. Large-scale electroporation for the secondary plasmid library resulted in 6.6×10^6 transformed clones/500 ng DNA (**Table 14**) and was used for transfection of 5×10^7 HEK 293T cells (**3.4.8.4**) yielding a total of 1.2×10^{12} gp library transfer shuttles (1.5 ml with 8.05×10^{11} gp/ml) with a replicative titer of 8×10^8 rep U/ml (**Table 14**). The library transfer shuttles were used for infection of 5×10^7 HEK 293T cells at an MOI of 1 rep U/cell and yielded a secondary AAV2 display library (**Table 14**) with a total of 1.7×10^{12} gp (1.5 ml with 1.13×10^{12} gp/ml).
After the second round of *in vivo* selection, test ligation yielded 3.7×10^7 transformed clones/500 ng DNA with a background of 0.03%. The large-scale electroporation for the tertiary plasmid library resulted in 1×10^7 transformed clones/500 ng DNA. Transfection of 5×10^7 HEK 293T cells yielded a total of 3×10^{12} gp library transfer shuttles (1.5 ml with 2.03×10^{11} gp/ml) with a replicative titer of 3×10^7 rep U/ml (**Table 14**). The library transfer shuttles were used for infection of 5×10^7 HEK 293T cells at an MOI of 1 rep U/cell and yielded a tertiary AAV2 display library (**Table 14**) with a total of 5.4×10^{11} gp (1.5 ml with 3.61×10^{11} gp/ml).

The test ligation yielded 1.2 x 10^7 transformed clones/500 ng DNA with a background of 0% after the third round of *in vivo* selection. The large-scale electroporation for the quaternary plasmid library resulted in 7 x 10^7 transformed clones/500 ng DNA. The plasmid library was used for transfection of 5 x 10^7 HEK 293T cells, yielding a total of 1.7 x 10^{12} gp library transfer shuttles (1.5 ml with 1.11 x 10^{12} gp/ml) with a replicative titer of 3 x 10^8 rep U/ml (**Table 14**). The library transfer shuttles were used for infection of 5 x 10^7 HEK 293T cells at an MOI of 1 rep U/cell and yielded a quaternary AAV2 display library (**Table 14**) with a total of 1.7 x 10^{12} gp (1.5 ml with 1.1 x 10^{12} gp/ml).

After the fourth round of *in vivo* selection, test ligation yielded 3.5 x 10^7 transformed clones/500 ng DNA with a background of 1.5%. The large-scale electroporation for the quinary plasmid library resulted in 3 x 10^7 transformed clones/500 ng DNA (**Table 14**). The plasmid library was used for transfection of 5 x 10^7 HEK 293T cells, yielding a total of 6.8 x 10^{12} gp library transfer shuttles (1.5 ml with 4.56 x 10^{12} gp/ml) with a replicative titer of 1.5 x 10^8 rep U/ml (**Table 14**). The library transfer shuttles were used for infection of 5 x 10^7 HEK 293T cells at an MOI of 1 rep U/cell and yielded a quinary AAV2 display library (**Table 14**) with a total of 2 x 10^{12} gp (1.5 ml with 1.3 x 10^{12} gp/ml).

The insert-encoding fragments of the modified viral *cap* gene, PCR-amplified after the fifth round of selection, were ligated into the AAV2 library plasmid backbone, yielding 1.8 x 10^8 transformed clones/500 ng DNA. No background was determined.

Table 14. Titers of pre-selected plasmid libraries, library transfer shuttles and AAV display peptide libraries during *in vivo* selection in murine brains

	Plasmid library [transformed clones]*	Background [%]	Genomic titer of library transfer shuttles [gp/ml]	Rep titer of library transfer shuttles [rep U/ml]	Genomic titer of AAV display library [gp/ml]
1st round	6.6 x 10^6	0.02	8.05 x 10^{11}	8 x 10^8	9.28 x 10^{11}
2nd round	1.0 x 10^7	0.03	2.03 x 10^{11}	3 x 10^7	3.61 x 10^{11}
3rd round	7.0 x 10^7	0.00	1.11 x 10^{12}	3 x 10^8	1.10 x 10^{12}
4th round	3.0 x 10^7	1.50	4.56 x 10^{11}	1.5 x 10^8	1.30 x 10^{12}

** The theoretical maximum diversity of subsequent libraries is limited by the highest number of possibly different clones during prior rounds of selection, i.e. 6.6 x 10^6 transformed clones after the first round of selection*

After each round of selection, the library transfer shuttles and the pre-selected AAV display peptide library were analyzed for wild type AAV2 contaminations by PCR (**3.1.7.3**). Only DNA fragments with a size of 113 bp could be amplified, corresponding to the library insert-encoding *cap* region. Fragments of the *cap* gene without library inserts (88 bp) could not be amplified from library transfer shuttles or pre-selected secondary AAV library, indicating the absence of wild type AAV2 contamination (**Figure 10**).

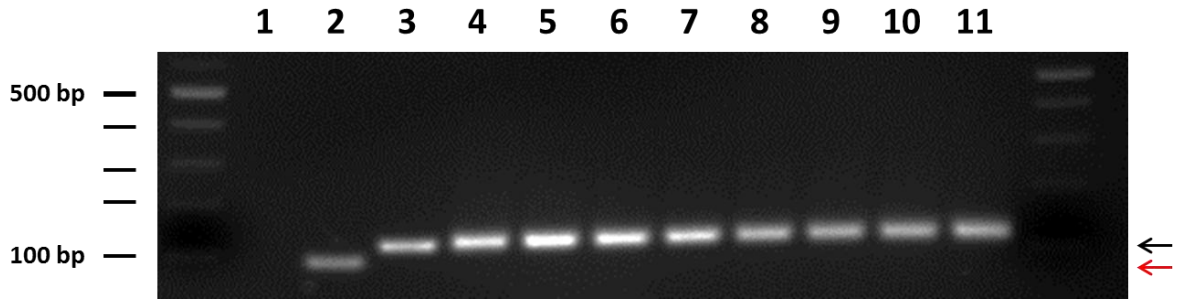

Figure 10. Library transfer shuttles and pre-selected AAV libraries carrying oligonucleotide inserts
Fragments of the *cap* gene carrying heptapaptide-encoding oligonucleotide inserts were amplified with the primer pair AAV2_plus/AAV2_minus. Samples were separated in 2% (w/v) agarose in TAE at 80 V for 1 h and stained with ethidium bromide. DNA ladder: Quick-Load® 100 bp DNA Ladder (New England Biolabs). **Lane 1**: No template. **Lane 2**: Insert-less wild type AAV2 (pXX2). **Lane 3**: Plasmid library incl. oligonucleotide insert (pMT187-0-3). **Lane 4**: Secondary transfer shuttle library. **Lane 5**: Secondary AAV display peptide library. **Lane 6**: Tertiary transfer shuttle library. **Lane 7**: Tertiary AAV display peptide library. **Lane 8**: Quaternary transfer shuttle library **Lane 9**: Quaternary AAV display peptide library. **Lane 10**: Quinary transfer shuttle library. **Lane 11**: Quinary AAV display peptide library.

4.2.3 Enrichment of library particles displaying potential brain-targeting peptides

After each round of *in vivo* selection, ten of the enriched library clones were picked randomly from the corresponding pre-selected plasmid library and used for sequencing of the insert-encoding fragment of the *cap* gene. Although each of the ten sequenced clones displayed a distinct heptapeptide after the first round of selection, four out of ten clones displayed a peptide beginning with asparagine (N), five out of ten clones displayed alanine (A) at peptide position two or three, four out of ten clones displayed arginine (R) at position four or five and six out of ten clones displayed glutamic acid (E) at position six or seven, resulting in the consensus sequence $\mathbf{N}^{X\ X\ X\ X\ X\ X}_{A\ A\ R\ R\ E\ E}$ (**Table 15**)
After the second round of selection, six out of ten clones displayed distinct heptapeptides, whereas one clone, **N**NV**R**TS**E**, was represented four times. Prior to this study, the peptide **N**NV**R**TS**E** had already been identified in our laboratory by *in vitro* screenings on the different human cancer cell lines DU4475, DU145, PC3, LNCaP and MCF7 as well as by *in vivo* screening for lung-targeting vectors in mice. Four out of the seven different clones from the second round of *in vivo* selection in brains displayed a peptide beginning with asparagine (N), five out of seven different clones displayed arginine (R) at peptide position four or five and three out of seven different clones displayed glutamic acid (E) at position seven, resulting in a consensus sequence **N**XX$^{X\ X}_{R\ R}$X**E**, similar to the one after the first round (**Table 15**). None of the clones sequenced after the second round had already been identified after the first round of selection.
After the third round of selection, only four out of ten clones differed in the sequence of their displayed heptapeptides. The clone **N**NV**R**TS**E** which had already been identified after the second round of selection was still represented twice. None of the other clones revealed any similarity to the

clones sequenced during the first two rounds of selection. A new and clearly distinguishable sequence motif became apparent which comprised all clones except **N**NV**R**TS**E**. Two out of four different clones displayed aspartic acid (D) at peptide position two, three out four different clones displayed glycine (G) at peptide position three and three out of four different clones displayed tryptophan (W) at position six resulting in the consensus sequence X**DG**XX**W**X (**Table 15**). The most dominant peptide S**DG**LT**W**S was displayed by six out of ten sequenced clones. The clone NR**G**TE**W**D matched the motif X**DG**XX**W**X only partially, displaying arginine (R) instead of at aspartic acid (D) at peptide position two.

Five out of ten sequenced clones differed within the sequence of their displayed heptapeptides after the fourth round of selection (**Table 15**). Three out of the five different clones matched the motif X**DG**XX**W**X completely whereas the clone NR**G**TE**W**D, which had already been identified after the third round of selection, matched the motif only partially. The peptide S**DG**LT**W**S which also had already been identified after the third round of selection still was most dominant, displayed by six out of ten sequenced clones. One clone displayed the peptide **N**M**AR**QAD which did not match the new motif X**DG**XX**W**X but the motif from the first round of selection $\mathbf{N}^{X\ X\ X\ X\ X\ X}_{A\ A\ R\ R\ E\ E}$.

After the fifth round of selection, the diversity of the brain-targeting particle library was further reduced and only three out of ten sequenced clones displayed distinct heptapeptides (**Table 15**). The peptide **N**M**AR**QAD which had already been identified after the fourth round of selection was still presented once. The remaining two distinct peptides displayed by the rest of the ten sequenced clones both matched the motif X**DG**XX**W**X. The dominant peptide S**DG**LT**W**S which had already been identified during prior rounds of selection was displayed by eight out of ten sequenced clones, whereas the peptide D**DG**VS**W**K was displayed once. Since almost all clones sequenced after the third round of selection matched the motif X**DG**XX**W**X and no further change of this motif was expected after round five, the *in vivo* screening was stopped after the fifth round of selection.

Table 15. Peptides enriched during *in vivo* selection in murine brains

1st round	2nd round	3rd round	4th round	5th round
AHGAEQA	NRTADTG	NNVRTSE	NMARQAD	NMARQAD
GWQPQVQ	NSGYGYT	NNVRTSE	NRGTEWD	DDGVSWK
GSDKGES	NNVRTSE	NRGTEWD	ADGVQWT	SDGLTWS
GTDGGEN	NNVRTSE	DDGVSWK	SDGLAWV	SDGLTWS
NAERGEG	NNVRTSE	SDGLTWS	SDGLTWS	SDGLTWS
NNATRDW	NNVRTSE	SDGLTWS	SDGLTWS	SDGLTWS
NSAARIE	NESRRLE	SDGLTWS	SDGLTWS	SDGLTWS
NSAARWE	GGGKRRE	SDGLTWS	SDGLTWS	SDGLTWS
KDAWERE	EGDIRWV	SDGLTWS	SDGLTWS	SDGLTWS
KKQQWDQ	SNYSRVM	SDGLTWS	SDGLTWS	SDGLTWS
NXXXXXX	NXXXXXE	XDGXXWX	XDGXXWX	XDGXXWX

*Ten random clones from the AAV plasmid library were sequenced after each round of *in vivo* selection. The amino acid sequences of the enriched peptide inserts are displayed as one letter code. Amino acids that are characteristic for the emerging consensus motifs are highlighted in different colors. The consensus motif of each selection round is indicated at the bottom of each column. Sequences were considered to show a consensus if a particular amino acids was displayed at the same position or at two neighboring positions in at least three individual clones.

4.2.4 Side chain classification of brain enriched peptides

The enriched peptides were analyzed by amino acid side chain classification to identify regularities potentially underlying the sequence motifs revealed before (**4.2.3**). Focus was set on charge pattern and polarity as well as the abundance of bulky aromatic residues. After the first round of selection the properties of the enriched peptides' amino acid side chains did not seem to exhibit any regularity. Half of the peptides showed neutral net charge, one peptide showed positive (+1) charge, while four peptides showed negative net charge (three times -1, one time -2). Five out of ten peptides displayed the bulky aromatic residue tryptophan (W) (**Table 16**). After the second round of selection four out of seven different peptides showed neutral net charge, two peptides showed positive net charge (+1 and +2), while one peptide showed negative net charge (-1). The aromatic residues tryptophan (W) and tyrosine (Y) were displayed by three out of seven different peptides, again showing no clear pattern (**Table 16**). With the emergence of the sequence motif X**DG**XX**W**X in round three of selection, the peptide's amino acid side chains seemed to exhibit regularities for the first time. Five out of seven different peptides enriched during selection rounds three, four and five showed negative net charge (-1) and displayed the bulky amino acid tryptophan (W), whereas only two peptides from round three, four and five showed neutral net charge and none of the them was positively charged (**Table 16**). All enriched peptides from selection round three, four and five

matching the sequence motif X**DG**XX**W**X were chosen for further analyses of their potential brain-targeting properties.

Table 16. Side chain classification of brain-enriched peptides

	Amino acid sequences	Side chain classification	Net charge
1st round	KKQQWDQ	+ + x x y − x	+
	NNATRDW	x x y x + − y	n
	NSAARIE	x x y y + y −	n
	NSAARWE	x x y y + y −	n
	GWQPQVQ	y y x y x y x	n
	AHGAEQA	y + y y − x y	n
	KDAWERE	+ − y y − + −	−
	GSDKGES	y x − + y − x	−
	NAERGEG	x y − + y − y	−
	GTDGGEN	y x − y y − x	−−
2nd round	SNYSRVM	x x x x + y y	+
	GGGKRRE	y y y + + + −	++
	NRTADTG	x + x y − x y	n
	NSGYGYT	x x y x y x x	n
	NNVRTSE	x x y + x x −	n
	NESRRLE	x − x + + y −	n
3rd round	NNVRTSE	x x y + x x −	n
	NRGTEWD	x + y x − y −	−
	SDGLTWS	x − y y x y x	−
	DDGVSWK	− − y y x y +	−
4th round	NMARQAD	x y y + x y −	n
	NRGTEWD	x + y x − y −	−
	SDGLTWS	x − y y x y x	−
	SDGLAWV	x − y y y y y	−
	ADGVQWT	y − y y x y x	−
5th round	NMARQAD	x y y + x y −	n
	SDGLTWS	x − y y x y x	−
	DDGVSWK	− − y y x y +	−

*Different clones from the AAV2 library enriched during an *in vivo* screening in murine brains. Amino acid sequences are displayed as one letter code. Clones were sorted according to amino acid side chain classification, x representing uncharged polar, y representing nonpolar, + representing positively charged and - representing negatively charged side chains. Aromatic residues are highlighted in red.

4.3 Enrichment of library particles displaying potential lung-targeting peptides

After each round of in vivo selection in murine lungs, which had been performed prior to this work by Dr. Stefan Michelfelder, four to ten enriched library particles had been sequenced. Sequenced library particles were analyzed as part of this work.

Only four clones had been sequenced after the first round of selection, two of which shared the same amino acid sequence GQIGGSA. Due to the limited number of sequenced clones after the first round, no sequence motif could be identified (**Table 17**). Three out of five different sequenced clones after the second round of selection displayed asparagine (N) at first position and valine (V) at third position, representing a minimal consensus motif **N**X**V**XXXX. Two of these clones, **N**D**V**RAVS and **N**S**V**AATA, were each represented twice (**Table 17**).

Seven out of ten sequenced clones from the third round of selection showed distinct amino acid sequences whereas one clone, EGRLGAG, was represented three times (**Table 17**). No sequence motif could be identified but one of the clones displayed the peptide A**DG**AM**W**L which clearly matches the sequence motif X**DG**XX**W**X enriched during the *in vivo* screening in mice brains (**Table 15**). After the fourth round of selection four out of nine sequenced clones displayed distinct amino acid sequences. The peptide **N**N**V**TRS**E**, which had already been identified in our group prior to this study during *in vitro* screenings on the different human cancer cell lines DU4475, DU145, PC3, LNCaP and MCF7 (unpublished data) as well as during the *in vivo* screening in mice brains described above, was displayed by one of the four different clones. The peptide ESGHGYF, which had already been sequenced once after the third round of selection, was enriched most strongly and displayed by five out of nine sequenced clones, although it shows no explicit similarity to any other sequenced peptide. The peptide A**DG**VM**W**L which, like the peptide A**DG**AM**W**L, matches the motif X**DG**XX**W**X, found during the *in vivo* screening in mice brains (**Table 15**), was displayed by two out of nine sequenced clones (**Table 17**).

Table 17. Peptides enriched during *in vivo* selection in murine lungs

1st round	2nd round	3rd round	4th round
GQIGGSA	PRTLAEL	PRSVDLS	NNVRTSE
GQIGGSA	TLREQSP	EGRLGAG	ESGHGYF
LTRAAGV	NDVRAVS	EGRLGAG	ESGHGYF
VPWSPSV	NDVRAVS	EGRLGAG	ESGHGYF
	NSVAATA	NSVNDRS	ESGHGYF
	NSVAATA	QGDLGLS	ESGHGYF
	NQVGSWS	RGDVTKE	GEVYVSF
		GGRPMHE	ADGVMWL
		ESGHGYF	ADGVMWL
		ADGAMWL	
	NXVXXXX		

*Several random clones from the AAV plasmid library were sequenced after each round of *in vivo* selection. The amino acid sequences of the enriched peptide inserts are displayed as one letter code. Amino acids that are characteristic for the enriched consensus motif in round two of selection or for consensus motifs known from the *in vivo* selection in the brains of mice are highlighted in different colors. The consensus motif of the second selection round is indicated at the bottom of the column. Sequences were considered to show a consensus if a particular amino acids was displayed at the same position or at two neighboring positions in at least three individual clones.

Regarding the classification of their side chains, many of the lung-enriched peptides displayed a relative excess of hydrophobic residues (**Table 18**). One out of three different peptides enriched in the first round of selection was positively charged (+1) while the other two peptides showed a neutral net charge. After the second round of selection four out of five different peptides showed neutral net charge, while one was negatively charged (-1). One out of eight different peptides enriched in round three of selection was positively charged (+1) while five peptides showed neutral net charge and two peptides were negatively (-1) charged. After the fourth round of selection two out of four different peptides showed neutral net charge, while two were negatively charged (-1). The most dominant clone from the fourth round of selection, ESGHGYF, which had already been identified after the third round of selection, displayed the two bulky aromatic residues tyrosine (Y) and phenylalanine (F). Another peptide enriched in the fourth round of selection, GEFYVSF, even displayed three bulky aromatic residues, phenylalanine (F) twice and tyrosine (Y) once.

Table 18. Side chain classification of lung-enriched peptides

	Amino acid sequences	Side chain classification	Net charge
1st round	LTRAAGV	y x + y y y y	+
	GQIGGSA	y x y y y x y	n
	VPWSPSV	y y y x y x y	n
2nd round	PRTLAEL	y + x y y - y	n
	NDVRAVS	x - y + y y x	n
	NSVAATA	x x y y y x y	n
	NQVGSGS	x x y y x y x	n
	TLREQSP	x y + - x x y	-
3rd round	GGRPMHE	y y + y y + -	+
	PRSVDLS	y + x y - y x	n
	ERGLGAG	- + y y y y y	n
	NSVNDRS	x x y x - + x	n
	RGDVTKE	+ y - y x + -	n
	ESGHGYF	- x y + y x y	n
	ADGAMWL	y - y y x y y	-
	GQDLGLS	y x - y y y x	-
4th round	NNVRTSE	x x y + x x -	n
	ESGHGYF	- x y + y x y	n
	ADGVMVL	y - y y x y y	-
	GEFYVSF	y - y x y x y	-

*Different clones from the AAV2 library enriched during an *in vivo* screening in murine lungs. Amino acid sequences are displayed as one letter code. Clones were sorted according to amino acid side chain classification, x representing uncharged polar, y representing nonpolar, + representing positively charged and - representing negatively charged side chains. Aromatic residues are highlighted in red.

4.4 Production of recombinant AAV2 vectors displaying potential targeting peptides

4.4.1 Vector production in HEK 293T cells

Brain-enriched AAV particles displaying the peptides ADGVQWT, DDGVSWK, SDGLAWV, SDGLTWS and NRGTEWD as well as the most dominant lung-enriched peptide ESGHGYF were produced as rAAV2 vectors carrying the luciferase gene under control of the strong constitutive CMV promoter by triple-transfection of HEK 293T cells (**4.4.1**). An unmodified wild type AAV2 capsid, a randomly picked clone from the AAV display peptide library (CVGSPCG) as well as the clone NNVRTSE enriched during *in vivo* screenings in brain and lung as well as *in vitro* screenings in diverse cell lines were produced as controls. For further analyses, the peptides NRGTEWD and ESGHGYF were also used to produce vectors carrying the eGFP gene and/or the chicken ß-actin promoter combined with the CMV

enhancer (= CAG promoter). Production of rAAV2 vectors displaying brain- or lung-enriched peptides yielded between 1.5×10^{11} gp and 1.4×10^{12} gp after iodixanol purification from 5×10^{7} HEK 293T cells in five 15 cm cell culture dishes (2.8×10^{3} to 2.8×10^{4} gp/cell), comparable to the yield of rAAV2 wild type vectors (3.4×10^{3} to 1.1×10^{4} gp/cell). These numbers indicate that the enriched peptides do not negatively influence capsid assembly or gene packaging. Yields and titers of all HEK 293T-produced vector stocks are listed in **Table 19**.

Table 19. Recombinant AAV2 vectors produced in HEK 293T cells

	Capsid	Expression cassette	Vector titer [gp/ml]	Vector yield [gp/cell]	Total vector yield [gp]
Brain-enriched peptides	ADGVQWT	CMV luciferase	4.06×10^{11}	1.2×10^{4}	6.1×10^{11}
	DDGVSWK	CMV luciferase	5.35×10^{11}	1.6×10^{4}	8.0×10^{11}
	NRGTEWD	CMV luciferase	1.38×10^{11}	4.2×10^{3}	2.1×10^{11}
	NRGTEWD	CAG luciferase	3.03×10^{11}	9.0×10^{3}	4.5×10^{11}
	SDGLTWS	CMV luciferase	6.34×10^{11}	1.9×10^{4}	9.5×10^{11}
	SDGLTWS	CMV luciferase	2.93×10^{11}	8.8×10^{3}	4.4×10^{11}
	SDGLAWV	CMV luciferase	1.01×10^{11}	3.0×10^{3}	1.5×10^{11}
Lung-enriched peptides	ADGVMWL	CMV luciferase	8.81×10^{11}	2.6×10^{3}	1.3×10^{12}
	ESGHGYF	CMV luciferase	3.30×10^{11}	1.0×10^{4}	5.0×10^{11}
	ESGHGYF	CMV luciferase	3.41×10^{11}	1.0×10^{4}	5.1×10^{11}
	ESGHGYF	CMV luciferase	9.13×10^{11}	2.8×10^{3}	1.4×10^{12}
	ESGHGYF	CMV luciferase	2.34×10^{11}	7.0×10^{3}	3.5×10^{11}
	ESGHGYF	scCMV eGFP	2.69×10^{11}	8.0×10^{3}	4.0×10^{11}
	ESGHGYF	scCMV eGFP	2.30×10^{11}	7.0×10^{3}	3.5×10^{11}
Control peptides	wild type	CMV luciferase	3.49×10^{11}	1.0×10^{4}	5.2×10^{11}
	wild type	CMV luciferase	2.47×10^{11}	7.4×10^{3}	3.7×10^{11}
	CVGSPCG	CMV luciferase	3.61×10^{11}	1.1×10^{4}	5.4×10^{11}
	NNVRTSE	CMV luciferase	1.74×10^{11}	5.2×10^{3}	2.6×10^{11}

4.4.2 Vector production in Sf9 cells by BEVS

For more detailed *in vivo* analyses requiring larger amounts of vector, the brain-enriched capsid with the peptide NRGTEWD and the lung-enriched capsid with the peptide ESGHGYF were produced as rAAV2 vectors in Sf9 insect cells using the baculovirus vector expression system. Therefore, empty AAV2 virions displaying the peptides ESGHGYF and NRGTEWD were produced by infecting Sf9 cells with pre-infected cells (P2 stock) at different MOIs (**4.4.2**). In case of the NRGTEWD-displaying capsid, an MOI of 2×10^{-4} (2×10^{2} pre-infected P2 cells on 1×10^{6} fresh Sf9 cells) was sufficient to result in strong expression of all three virion proteins (87 kDa; 72 kDa; 62 kDa), VP1 (87 kDa) displaying the most dominant band, analyzed by western blot (**3.1.11, Figure 11 a**). In case of the ESGHGYF-displaying capsid, an MOI of 2×10^{-2} (2×10^{4} pre-infected P2 cells on 1×10^{6} fresh Sf9 cells) was needed to produce equally strong protein bands (**Figure 11 b**).

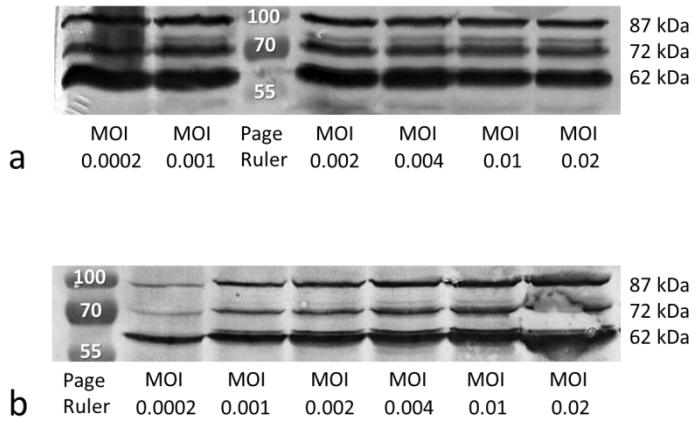

Figure 11. Test expression of modified AAV virion proteins in Sf9 cells
Fresh Sf9 cells were infected in small scale with different amounts of pre-infected Sf9 cells containing baculovirus with the genetic information for peptide-displaying AAV capsids (P2 stock) to find the ideal MOI for large scale production. AAV particles were harvested 4 days after infection. Proteins were separated in 6% SDS PAGE in reducing probe buffer. Protein ladder: PageRuler™ (Pierce). (**a**) Test expression of AAV virion proteins displaying the peptide NRGTEWD. (**b**) Test expression of AAV virion proteins displaying the peptide ESGHGYF

In a next step, rAAV vectors were produced by co-infecting Sf9 cells with pre-infected cells carrying baculoviruses for the modified AAV capsid at MOIs determined by western blot (see above) and pre-infected cells carrying baculoviruses with the desired expression cassettes at different MOIs. Large scale production of the vector rAAV2-NRGTEWD-CAG-eGFP yielded a total of 9.46×10^{13} gp after iodixanol purification (**3.4.4, Table 20**) of the cell lysate and the PEG/NaCl- precipitated particles from cell culture medium (**3.4.2.3**), harvested four days after infection of 1.2×10^{9} cells (7.88×10^{4} gp/cell) with the CAG-eGFP-carrying P2 stock at an MOI of 2×10^{-2} (2×10^{4} pre-infected P2 cells on 1×10^{6} fresh Sf9 cells). Large scale production of the vector rAAV2-ESGHGYF-CMV-LUC yielded 2.39×10^{12} gp (**Table 20**), after iodixanol purification of the cell lysate harvested four days after infection of 3×10^{8} cells (7.97×10^{3} gp/cell) with CMV-LUC-carrying P2 stock at an MOI of 1×10^{-2} (2×10^{4} pre-infected P2 cells on 1×10^{6} fresh Sf9 cells). Thereby the total vector yields of BEVS-produced rAAV2 vectors clearly exceeded the total vector yields obtained by production of rAAV2 vectors in HEK 293T cells.

Table 20. Recombinant AAV2 vectors produced in Sf9 cells

Capsid	Expression cassette	Vector titer [gp/ml]	Vector yield [gp/cells]	Total vector yield [gp]
NRGTEWD	CAG eGFP	9.5×10^{12}	7.88×10^{4}	9.46×10^{13}
ESGHGYF	CMV LUC	2.39×10^{12}	7.97×10^{3}	2.39×10^{12}

4.5 Analyses of rAAV luciferase vectors displaying potential targeting peptides

4.5.1 Luminescence imaging of vector-treated mice

Recombinant AAV vectors displaying potential targeting peptides enriched during several rounds of *in vivo* selection in brains and lungs of mice (**4.2.3** & **4.3**) were analyzed for their expression profile *in vivo*. Therefore, mice at the age of eight to twelve weeks each received 5 x 10^{10} gp of the respective rAAV vector by tail vein injection (**3.5.1**). Peptide-mediated tissue targeting of the rAAV vectors was visualized by imaging the CMV-driven luciferase expression as luminescence at different time points (**3.5.7**). All vector-treated mice started to exhibit weak to moderate luminescence signals (≥ 10^4 p/sec/cm^2/r) as early as seven days post injection. Depending on the displayed peptide, the signal strength increased until day 14 or, in case of peptides matching the motif X**DG**XX**W**X, until day 28. Luminescence images were taken at the time point of highest signal strength, either 14 days (**Figure 12 a, b, i**) or 28 days (**Figure 12 c, d, e, f, g, h)** post injection. After *in vivo* imaging, animals were sacrificed, single organs (brain, heart, lung, liver, spleen, kidney, skeletal muscle) were explanted immediately and measured *ex vivo*. Only minor individual differences could be observed between different mice treated with the same vector (n = 3). Thus, only one representative animal is shown for each vector (**Figure 12**). Since the tested vectors differed considerably in their expression strength, luminescence images of vector-treated mice are displayed with different scales indicating different sensitivity.

Mice treated with vectors based on the unmodified wild type AAV2 capsid displayed weak luminescence (≤ 10^4 p/sec/cm^2/r) in an area corresponding to the liver, if imaged ventrally. No luminescence signal from the lung or the brain could be detected. *Ex vivo* imaging of freshly explanted organs confirmed weak luminescence in the liver, whereas no luminescence could be detected in various control organs (**Figure 12 a**).

Vector displaying the randomly picked control peptide CVGSPCG seemed to mediate weak gene expression (≤ 10^4 p/sec/cm^2/r) in the heart and in few apparently randomly distributed spots in the abdomen, best seen ventrally. As with the wild type rAAV2-treated mice, no luminescence signal from the lung or the brain could be detected. These findings were confirmed by imaging the single explanted organs (**Figure 12 b**).

The peptide NNVRTSE which had already been enriched during *in vitro* screenings on different cells lines, before it was found again during the *in vivo* screenings in brain and lung of mice, seemed to mediate moderate gene expression (≥ 10^4 p/sec/cm^2/r) in an area corresponding to the liver. No

luminescence signal from the lung or the brain could be detected. The luminescence in the liver, measured *in vivo*, could barely be detected when measured *ex vivo* (**Figure 12 c**).

Mice treated with the brain-enriched peptide ADGVQWT showed comparably strong gene expression ($\geq 10^5$ p/sec/cm^2/r) mainly in the skeletal musculature, best seen dorsally mainly at the hind legs and the shoulders. *Ex vivo* imaging confirmed the skeletal muscles as main source of luminescence (**Figure 12 d**). The peptide DDGVSWK mediated transgene expression most prominently ($\geq 10^4$ p/sec/cm^2/r) in the lung (seen dorsally and ventrally), the brain (seen dorsally) and to a lesser extend in the skeletal musculature of the hind legs (seen dorsally and ventrally). The luminescence in the lung could be confirmed by *ex vivo* measuring of the explanted organ, whereas the luminescence in brain and musculature detected *in vivo* could not be measured *ex vivo* after explanting the organs (**Figure 12 e**).

The peptide SDGLAWV seemed to mediate weak gene expression ($\leq 10^4$ p/sec/cm^2/r) in the lung (seen ventrally) and even weaker gene expression in the brain (seen dorsally). Only the luminescence in the lung could be confirmed by measuring the explanted organ *ex vivo* (**Figure 12 f**). Luminescence mediated by the peptide SDGLTWS was localized in the same areas as the luminescence mediated by the peptide SDGLAWV (lung and brain) but the signal was slightly stronger. Again, only the luminescence in the lung could also be detected *ex vivo* (**Figure 12 g**).

The peptide NRGTEWD, the only brain-enriched peptide which was chosen for further analyses without completely matching the sequence motif X**DG**XX**W**X, mediated weak gene expression ($\leq 10^4$ p/sec/cm^2/r) predominantly in brain (seen dorsally) and lung (seen ventrally). *Ex vivo* imaging confirmed weak luminescence in the whole lung and just a very small spot of weak luminescence could be detected in the brain (**Figure 12 h**).

The peptide most strongly enriched during the *in vivo* screening in the lung of mice, ESGHGYF, mediated strong ($\geq 10^5$ p/sec/cm^2/r) and lung-specific gene expression, seen dorsally and ventrally, which also could be confirmed by *ex vivo* measurement (**Figure 12 i**).

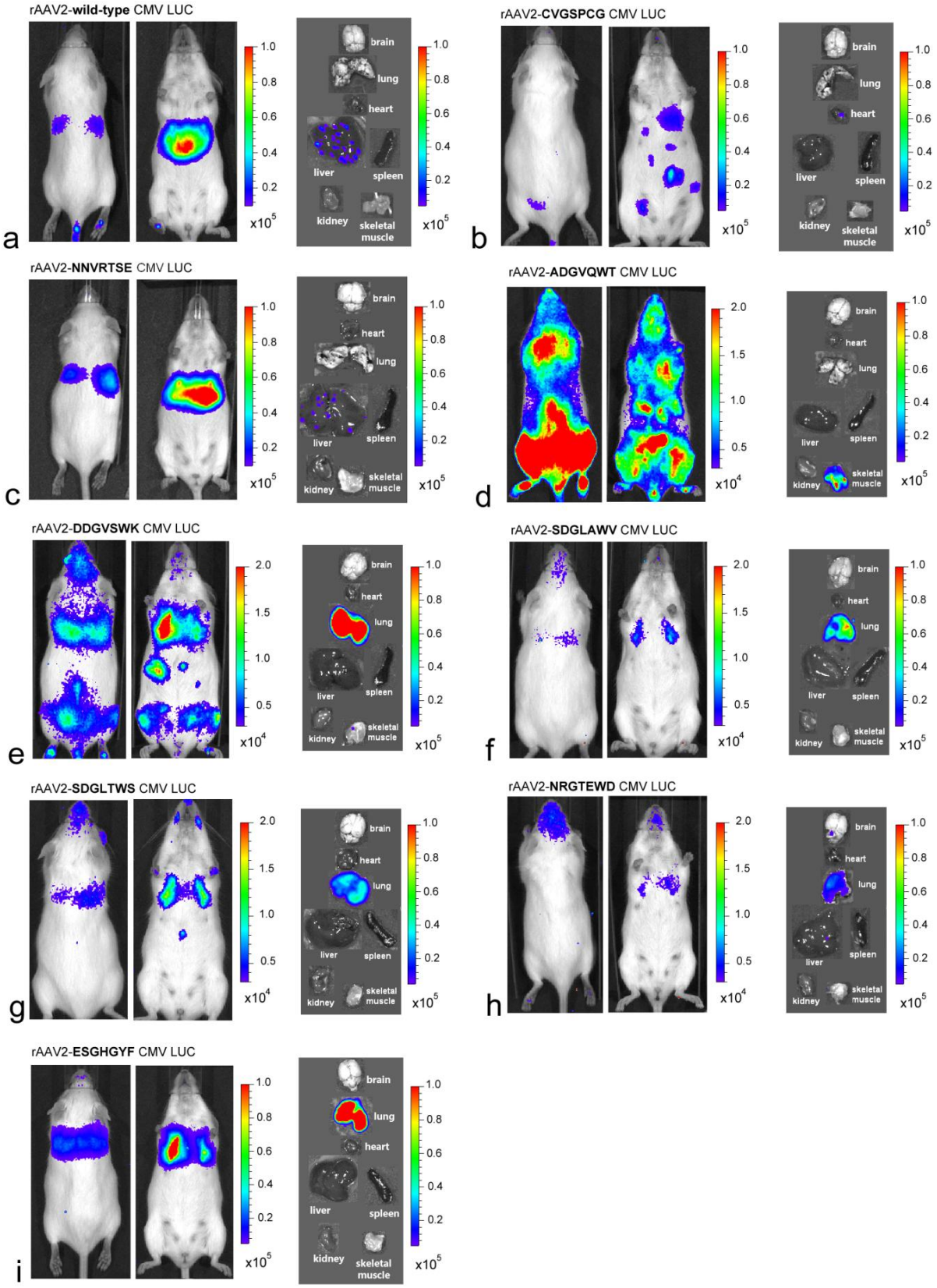

Figure 12. Luminescence mediated by selected rAAV2 vectors

Recombinant AAV2 vectors carrying the luciferase gene under control of the CMV promoter were administered into the tail vein of mice at a dose of 5×10^{10} gp/mouse. Mice were imaged 14 d.p.i. (a, b, i) or 28 d.p.i. (c, d, e, f, g, h), when luminescence reached peak values after i.p. administration of luciferin potassium salt. *Left two panels of each set*: Mouse imaged *in vivo*; dorsally (left) and ventrally (second from left). *Right panel of each set*: Single organs, measured directly after explantation, *ex vivo*. *Note the differences in scale!* Three mice were treated per vector of which one representative example is shown. (**a**) rAAV2-wild type. (**b**) rAAV2-CVGSPCG. (**c**) rAAV2-NNVRTSE. (**d**) rAAV2-ADGVQWT. (**e**) rAAV2-DDGVSWK. (**f**) rAAV2-SDGLAWV. (**g**) rAAV2-SDGLTWS. (**h**) rAAV2-NRGTEWD. (**i**) rAAV2-ESGHGYF

Although the tested vectors differed considerably in their expression strengths and the onset of maximum expression, it was thought to be informative to compare all vectors directly in the same setting. A direct comparison of all tested vectors is shown in **Figure 13** in which mice were imaged at the same time point after vector administration (14 d.p.i.). The images in **Figure 13** are displayed at the same very sensitive scale, allowing the detection of even extremely weak luminescence signals. Luminescence could mainly be detected in the liver (wild type, NNVRTSE), skeletal muscles (SDGVQWT), lung (DDGVSWK, SDGLAWV, SDGLTWS, ESGHGYF), brain (DDGVSWK, NRGTEWD), and some apparently random spots, most likely representing gene expression in muscles (wild type, VGSPCG, DDGVSWK).

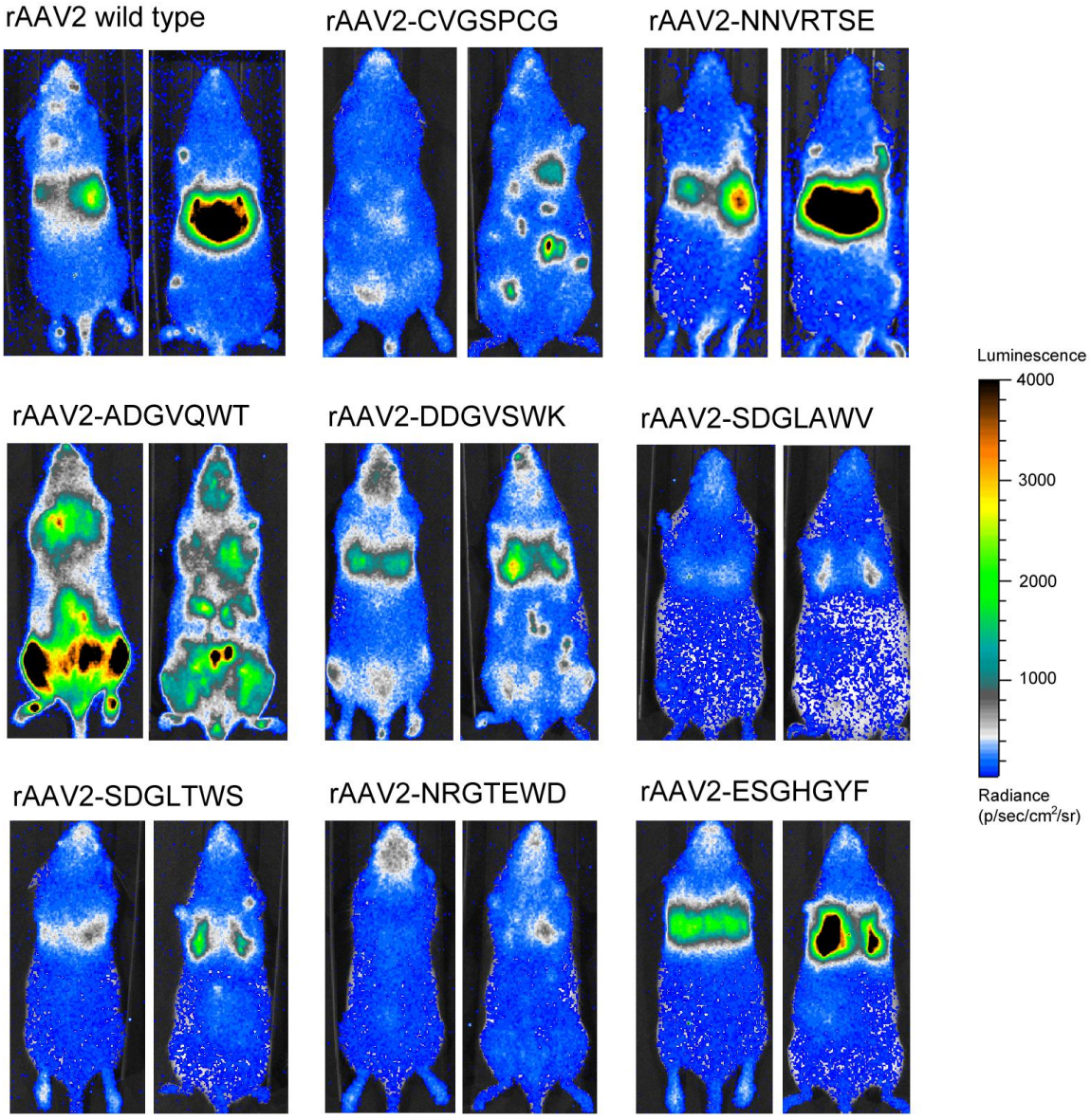

Figure 13. Direct comparison of CMV-driven luminescence mediated by recombinant rAAV2 vectors
Recombinant AAV2 vectors carrying the luciferase gene under control of the CMV promoter were administered into the tail vein of mice at a dose of 5×10^{10} gp/mouse. Mice were imaged *in vivo*,14 d.p.i., when luminescence reached peak values after i.p. administration of luciferin potassium salt. The left side of each panel displays the vector-treated mouse dorsally, the right side of each panel displays the mouse ventrally.

4.5.2 Measurement of luciferase activity from tissue lysates of vector-treated mice

After having analyzed vector-mediated transgene expression in living mice, luciferase activity from tissue lysates was determined for greater quantitative accuracy (**3.5.4**).

Fourteen days post injection of 5 x 10^{10} gp/mouse, wild type rAAV2 mediated weak gene expression (1.2 x 10^4 ± 1.8 x 10^3 RLU/mg protein) in the kidney which was still considerably higher ($p < 0.01$) than in all other tested organs (**Figure 14 a**). Liver and brain were the organs with the second most strong luminescence (both organs 4.7 x 10^3 ± 2.2 x 10^3 RLU/mg protein). Here, the luminescence data from tissue lysates seem to differ slightly from the *in vivo/ex vivo* data, in which luminescence could only be detected in the liver. Transgene expression in the lung was not measureable, in this regard confirming the *in vivo/ex vivo* data (**Figure 12 a** & **Figure 13)**. The random insert control peptide CVGSPCG mediated moderate gene expression (8.7 x 10^4 ± 3.6 x 10^4 RLU/mg protein) specifically in the heart ($p < 0.001$), no luminescence was detected in the brain or in the lung (**Figure 14 b**). As already shown in the luminescence images (**Figure 12 c, Figure 13**), the peptide NNVRTSE which had already been enriched during *in vitro* screenings on different cells lines, before it was found again during the *in vivo* screenings in brain and lung of mice, mediated transgene expression predominantly ($p < 0.01$) in the liver (4.5 x 10^4 ± 8.2 x 10^3 RLU/mg protein) which can be seen in **Figure 14 c**.

Vector displaying the brain-enriched peptide ADGVQWT mediated transgene expression at similar strength in brain (6.9 x 10^4 ± 1.9 x 10^4 RLU/mg protein) and heart (7.1 x 10^4 ± 9.4 x 10^3 RLU/mg protein) and approx. one third of the strength in skeletal muscle (2.4 x 10^4 ± 1.4 x 10^4 RLU/mg protein), 28 days after vector administration (**Figure 14 d**). Thus, luminescence mediated by the peptide ADGVQWT was 15-fold higher in the brain and 15-fold lower in the liver than luminescence mediated by wild type rAAV2 (**Figure 14 a, c**).

The peptide DDGVSWK mediated transgene expression of similar strength (**Figure 14 e**) in brain (6.3 x 10^4 ± 1.3 x 10^4 RLU/mg protein), heart (4.5 x 10^4 ± 2.5 x 10^3 RLU/mg protein), and lung (9.7 x 10^4 ± 6.3 x 10^4 RLU/mg protein), thereby showing 13-fold increased transgene expression in the brain compared to wild type AAV2 and an almost 600-fold decrease in the liver (**Figure 15 a, c**). Luciferase expression mediated by the peptide SDGLAWV was less than for the other brain-enriched peptides, brain (1.1 x 10^4 ± 1.1 x 10^4 RLU/mg protein) and lung (1.1 x 10^4 ± 1.1 x 10^4 RLU/mg protein) being the organs with the relatively strongest transgene expression (**Figure 14 f**). Still, transgene expression in the brain was more than two times higher than with wild type rAAV2 (**Figure 15 a**).

Transgene expression mediated by the peptide SDGLTWS was predominantly ($p < 0.001$) detectable in the lung (**Figure 14 g**), where it was of similar strength (1.5 x 10^5 ± 4.0 x 10^4 RLU/mg protein) compared to the transgene expression mediated by the peptide DDGVSWK (**Figure 14 e**). Transgene expression in the brain was within the same range (4.6 x 10^4 ± 8.1 x 10^3 RLU/mg protein) as with the

other brain-enriched peptides and approx. ten times higher than the wild type rAAV2-mediated transgene expression (**Figure 15 a**). The peptide NRGTEWD mediated strongest ($p < 0.001$) luciferase expression in the brain ($9.6 \times 10^4 \pm 1.8 \times 10^4$ RLU/mg protein), which can be seen in **Figure 14**. NRGTEWD-mediated transgene expression in the brain was over 20 times stronger than expression mediated by wild type rAAV2 (**Figure 15 a**), whereas no transgene expression could be detected in the liver or the kidneys, the organs of highest wild type rAAV2-mediated transgene expression.

Fourteen days post injection, vectors displaying the lung-targeted ESGHGYF capsid mediated strong ($4.1 \times 10^5 \pm 2.0 \times 10^5$ RLU/mg) and specific ($p < 0.001$) gene expression in the lung (**Figure 14 i**), confirming the *in vivo* luminescence images (**Figure 12 i and Figure 13**). Yet, luminescence in the brain ($2.1 \times 10^4 \pm 3.0 \times 10^3$ RLU/mg) was stronger as with wild type rAAV2 (**Figure 15 a**). In the liver (**Figure 15 c**) and the kidney (**Figure 15 d**), i.e. the two organs of strongest transgene expression mediated by wild-type rAAV2, the lung-targeted ESGHGYF vectors only mediated gene expression around background level ($\approx 1 \times 10^2$ RLU/mg protein). In the lung, in contrast, transgene expression mediated by AAV2-ESGHGYF was more than 200-fold higher than the expression mediated by wild-type AAV2 or the control CVGSPCG vectors (**Figure 15 b**).

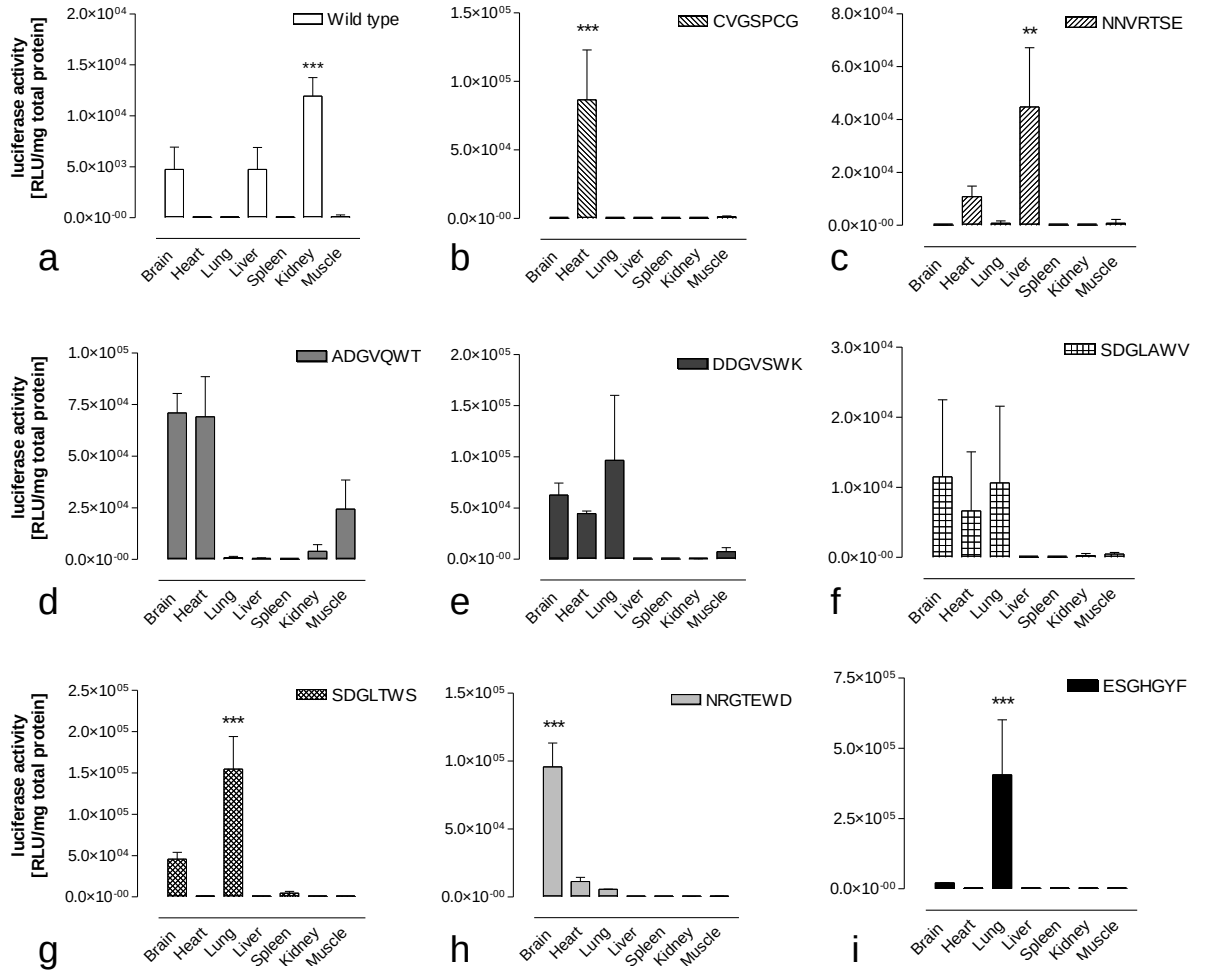

Figure 14. Luciferase expression pattern mediated by rAAV2 vectors displaying selected peptides
Recombinant AAV2 vectors carrying the luciferase gene under control of the CMV promoter were administered into the tail vein of mice at a dose of 5 x 10^{10} gp/mouse. Luminescence in homogenized tissues was measured and normalized to total protein contained in the probes. Organs were explanted when luminescence determined by *in vivo* imaging reached peak values, 14 d.p.i (a, b, i) or 28 d.p.i (c, d, e, f, g, h). Data are shown as mean +SD. Statistics were performed as one way ANOVA followed by Bonferroni's multiple comparison test. Levels of significance: $p < 0.05$ = *; $p < 0.01$ = **; $p < 0.001$ = *** (n=3). *Note the differences in scale!* (**a**) Unmodified wild type rAAV2. (**b**) Vector displaying the randomly picked control peptide CVGSPCG. (**c**) Vector displaying the peptide NNVRTSE, which had been found in multiple AAV library screenings (*in vitro* and *in vivo*). (**d**) Vector displaying the brain-selected peptide ADGVQWT. (**e**) Vector displaying the brain-selected peptide DDGVSWK. (**f**) Vector displaying the brain-selected peptide SDGLAWV. (**g**) Vector displaying the brain-selected peptide SDGLTWS. (**h**) Vector displaying the brain-selected peptide NRGTEWD. (**i**) Vector displaying the lung-selected peptide ESGHGYF.

In summary, all of the brain-enriched peptides were able to mediate stronger transgene expression in the brain than wild type rAAV2 (**Figure 15 a**), whereas expression in the liver (**Figure 15 c**) and in the kidney (**Figure 15 d**) was significantly decreased. Although selected in the brain, all peptides except one (ADGVQWT) mediated elevated transgene expression in the lung compared to wild type rAAV2 (**Figure 15 b**).

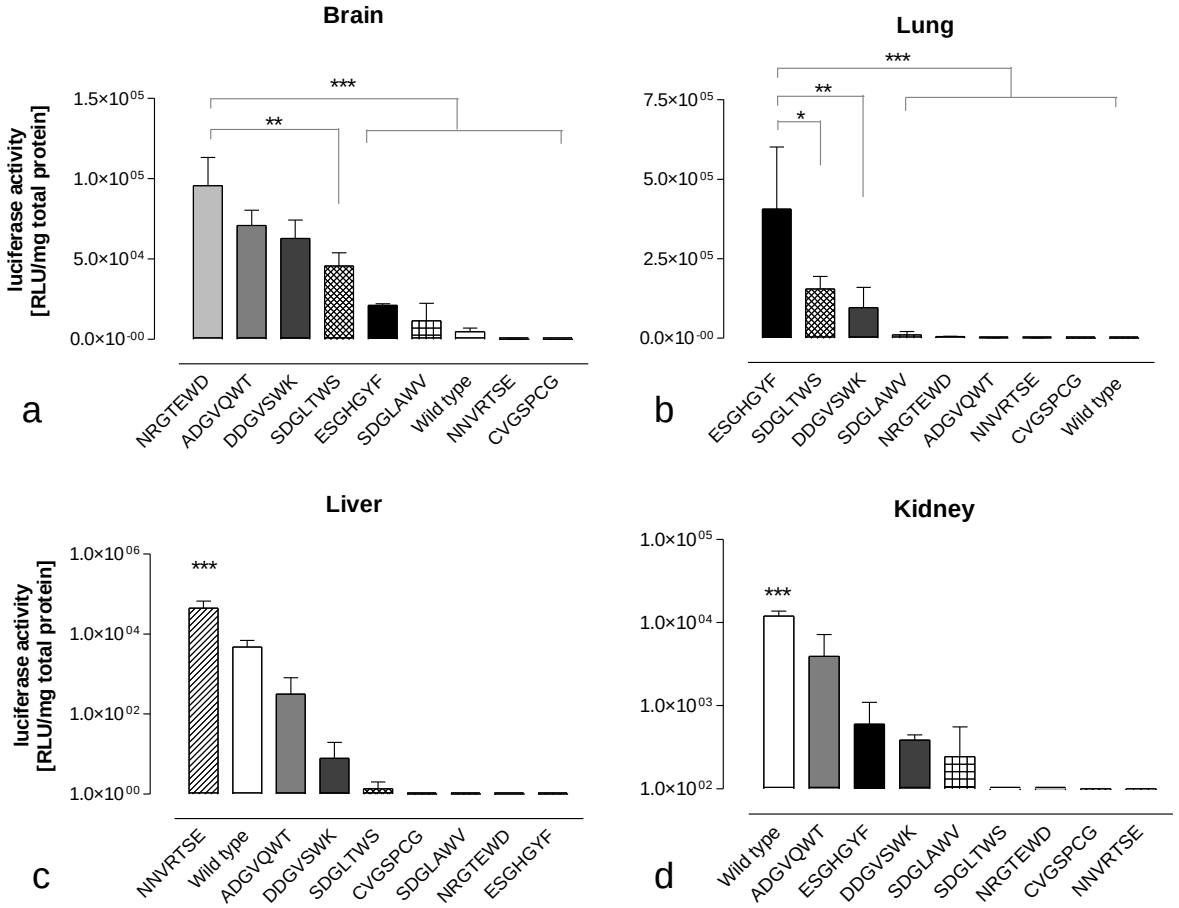

Figure 15. Comparison of vector-mediated luciferase expression in selected tissues
Recombinant AAV2 vectors carrying the luciferase gene under control of the CMV promoter were administered into the tail vein of mice at a dose of 5 x 10^{10} gp/mouse. Luminescence in homogenized tissues was measured and normalized to total protein contained in the probes. Organs were explanted when luminescence determined by *in vivo* imaging reached peak values, 14 d.p.i or 28 d.p.i. Data are shown as mean +SD. Statistics were performed as one way ANOVA followed by Bonferroni's multiple comparison test. Levels of significance: $p < 0.05$ = *; $p < 0.01$ = **; $p < 0.001$ = *** (n=3). *Note the differences in scale!* (**a**) Luminescence mediated by different peptide-displaying rAAV2 vectors in the brain. (**b**) Luminescence mediated by different peptide-displaying rAAV2 vector in the lung. (**c**) Luminescence mediated by different peptide-displaying rAAV2 vector in the liver. (**d**) Luminescence mediated by different peptide-displaying rAAV2 vectors in the heart.

Of all tested vectors, those displaying the peptide NRGTEWD proved to mediate strongest and most specific ($p < 0.001$) transgene expression within the brain, whereas vectors displaying the peptide ESGHGYF proved to mediate strongest and most specific ($p < 0.001$) transgene expression within the lung. Therefore all further analyses were focussed on vectors displaying one of those two peptides.

4.5.3 Comparison of different promoters for peptide-displaying rAAV2 luciferase vectors

After having tested the transduction patterns of peptide-displaying rAAV vectors with the constitutive and relatively unbiased CMV promoter (**4.5.1** & **4.5.2**), another promoter was tested to further enhance gene expression. Since the CAG promoter has been reported to drive even higher gene expression than the CMV promoter, at least in several cell lines and tissues, the peptides NRGTEWD and ESGHGYF were tested as vectors carrying the luciferase gene under control of the CAG promoter. By *in vivo* luminescence imaging (**3.5.7**) and by measurement of luciferase activity from tissue lysates (**3.5.4**), the expression patterns of vectors carrying the CAG promoter were compared to the respective CMV vectors. Vector-mediated luminescence was analyzed 14 days after administration of 5 x 10^{10} gp/mouse. *In vivo* bioluminescence images of mice treated with NRGTEWD-displaying vectors showed approx. 40-fold stronger luminescence in the brain when transgene expression was driven by the CAG promoter (≈2x10^5 p/sec/cm^2/r, **Figure 16**) compared to the CMV promoter (≈ 5x10^3 p/sec/cm^2/r, **Figure 12**), if imaged dorsally. If imaged ventrally, no luminescence could be detected. *In vivo* bioluminescence images of mice treated with ESGHGYF-displaying vectors showed approx. 20-fold stronger luminescence in the lung when transgene expression was driven by the CAG promoter (≈ 4x10^6 p/sec/cm^2/r) compared to the CMV promoter (≈ 2x10^5 p/sec/cm^2/r, **Figure 12**), if imaged ventrally. If imaged dorsally, strong luminescence (≈ 5x10^5 p/sec/cm^2/r) could also be detected in the brain as non-target organ upon using the CAG promoter (**Figure 16**).

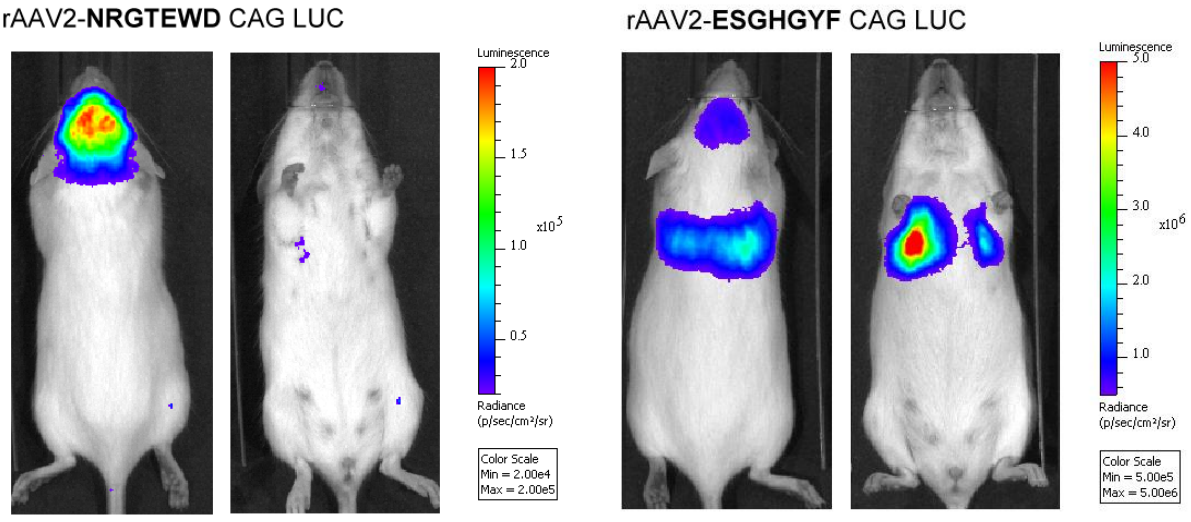

Figure 16. Luminescence of peptide-displaying rAAV2 vectors driven by the CAG promoter
Recombinant AAV2 vectors carrying the luciferase gene under control of the CAG promoter were administered into the tail vein of mice at a dose of 5 x 10^{10} gp/mouse. Mice were imaged 14 d.p.i., when luminescence reached peak values after i.p. administration of luciferin potassium salt. *Left panel*: rAAV2-NRGTEWD-treated mouse, imaged dorsally. *Second from left panel*: rAAV2-NRGTEWD-treated mouse, imaged ventrally. *Second from right panel*: rAAV2-ESGHGYF-treated mouse, imaged dorsally. *Right panel*: rAAV2-ESGHGYF-treated mouse, imaged ventrally. Three mice were treated per vector of which one representative example is shown. *Note the differences in scale!*

A direct comparison of CAG-driven luciferase vectors displaying the brain-enriched peptide NRGTEWD and the lung-enriched peptide ESGHGYF is shown in **Figure 17** in which luminescence images are displayed with the same sensitive scale to detect even very weak luminescence signals. A strong bias of the CAG promoter towards brain tissue was detected in rAAV2-ESGHGYF-treated mice.

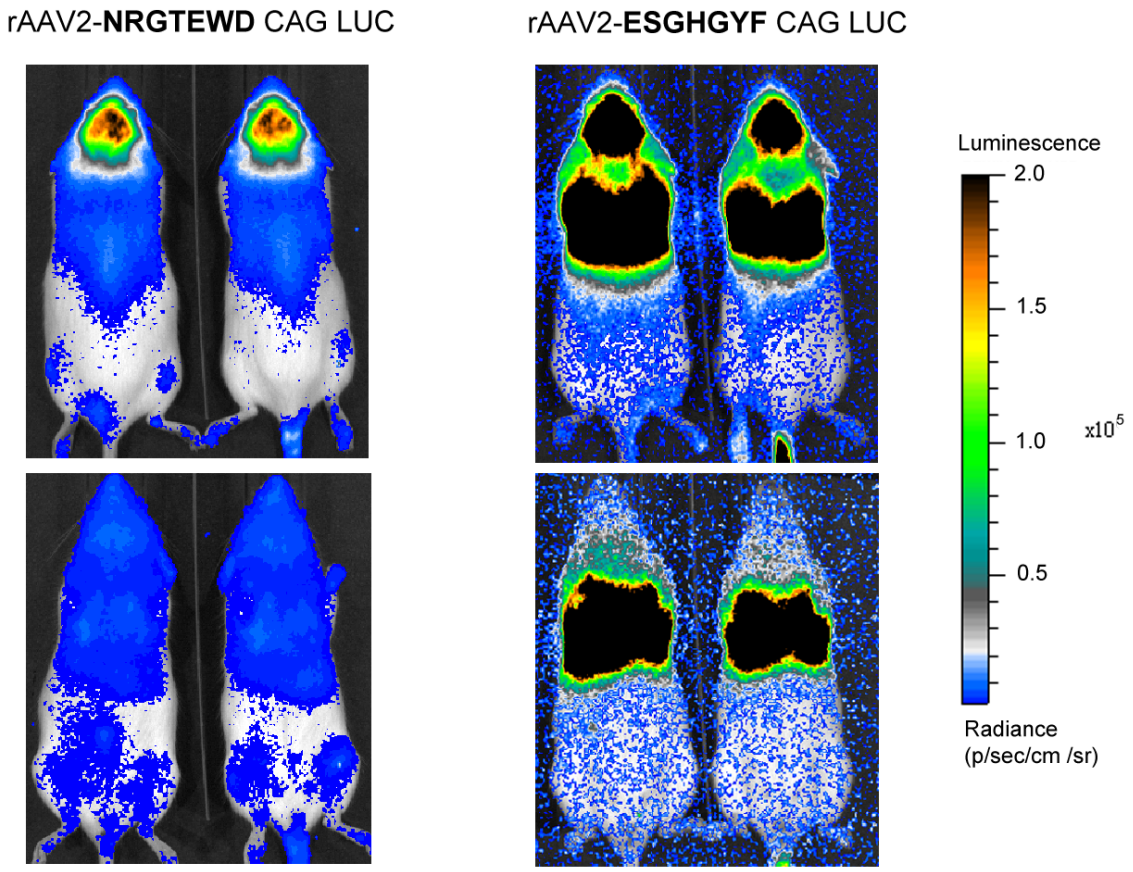

Figure 17. Direct comparison of CAG-driven luminescence mediated by recombinant rAAV2 vectors
Recombinant AAV2 vectors carrying the luciferase gene under control of the CAG promoter were administered into the tail vein of mice at a dose of 5 x 10^{10} gp/mouse. Mice were imaged 14 d.p.i., when luminescence reached peak values after i.p. administration of luciferin potassium salt. *Left panel*: Mice treated with rAAV2-NRGTEWD CAG LUC. *Right panel*: Mice treated with rAAV2-ESGHGYF CAG LUC. *Upper row*: Mice imaged dorsally. *Lower row*: Mice imaged ventrally.

Measurement of luciferase activity from tissue lysates (**3.5.4**) of mice treated with NRGTEWD-displaying vectors revealed a very strong ($1.1 \times 10^7 \pm 1.1 \times 10^6$ RLU/mg protein) and specific ($p < 0.001$) signal in the brain, which was over 60 times stronger than the signal in the lung ($1.8 \times 10^5 \pm 7.9 \times 10^4$ RLU/mg protein), being the organ with the second strongest luminescence and almost 100 times stronger than in the heart ($1.1 \times 10^5 \pm 6.0 \times 10^3$ RLU/mg protein) being the organ with the third strongest luminescence (**Figure 18**). The liver, which has shown no luminescence whatsoever in mice treated with NRGTWED-displaying CMV-driven luciferase rAAV2 vectors (**4.5.1** & **4.5.2**), revealed moderate luminescence ($1.65x\ 10^4 \pm 7.2 \times 10^3$ RLU/mg protein) when using the CAG promoter confirming the luminescence images of mice treated with rAAV2-NRGTEWD-CAG-LUC (**Figure 16** & **Figure 17**)

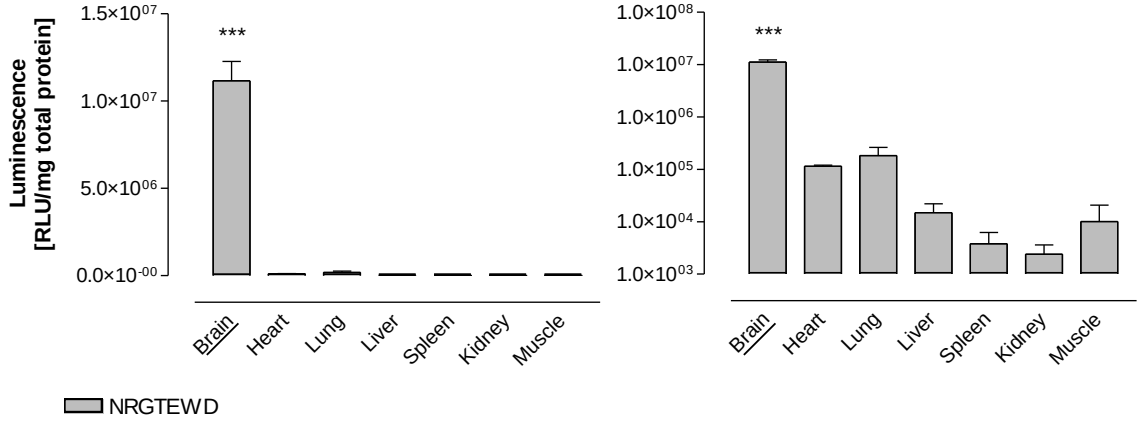

Figure 18. CAG-driven luminescence mediated by rAAV2-NRGTEWD
Recombinant AAV2 vectors displaying the brain-enriched peptide NRGTEWD, carrying the luciferase gene under control of the CAG promoter were administered into the tail vein of mice at a dose of 5×10^{10} gp/mouse. Luminescence in homogenized tissues was measured and normalized to total protein contained in the probes. Organs were explanted 14 d.p.i. Data are shown as mean +SD. Statistics were performed as one way ANOVA followed by Bonferroni's multiple comparison test. Levels of significance: $p < 0.05$ = *; $p < 0.01$ = **; $p < 0.001$ = *** (n=3). *Note the difference in scale! Left panel*: Linear scale. *Right panel*: Logarithmic scale.

A direct comparison of CAG- and CMV-driven transgene expression of NRGTEWD-displaying luciferase vectors revealed approx. 120-fold stronger transgene expression in the brain driven by the CAG promoter compared to the CMV promoter. All other tested organs also revealed increased strength of luminescence. Of all tested tissues that revealed detectable luminescence with the CMV promoter, skeletal musculature showed the highest (almost 7500-fold) and the heart the lowest increase (10-fold) in transgene expression if driven by the CAG promoter compared to the CMV promoter (**Figure 19**). Since the CAG promoter enhanced the NRGTEWD-mediated transgene expression in the brain relatively strong without enhancing transgene expression in the non-target organs too much, the CAG promoter was chosen for all further experiments with the NRGTEWD vector.

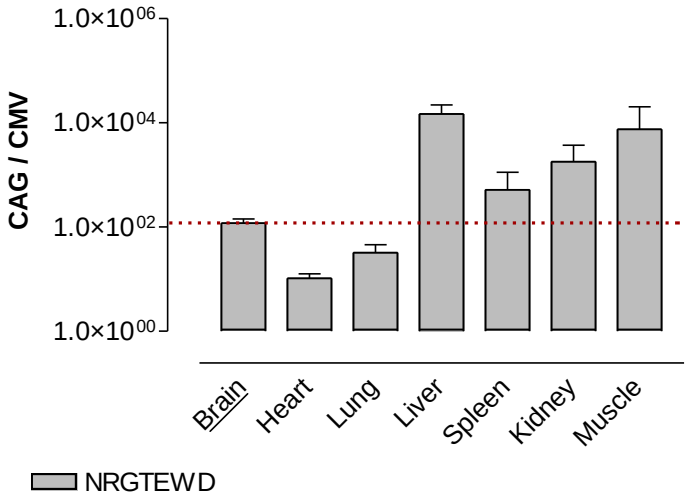

Figure 19. Ratio of NRGTEWD-mediated luminesce driven by CAG and CMV promoter
Recombinant AAV2 vectors displaying the brain-enriched peptide NRGTEWD, carrying the luciferase gene under control of the CAG promoter or the CMV promoter were administered into the tail vein of mice at a dose of 5 x 10^{10} gp/mouse. Luminescence in homogenized tissues was measured and normalized to total protein contained in the probes. Values of luminescence [RLU / mg total protein] driven by the CAG promoter were divided through values of luminescence driven by the CMV promoter. Organs were explanted when luminescence determined by *in vivo* imaging reached peak values, 14 d.p.i. in case of vectors carrying the CAG promoter and 28 d.p.i. in case of vectors carrying the CMV promoter. The increase in luminescence driven by the CAG promoter compared to the CMV promoter in the brain as tissue of interest is pointed out as red line.

Measurement of luciferase activity from tissue lysates (**3.5.4**) of mice treated with ESGHYGF-displaying vectors revealed a very strong signal in the lung ($1.4 \times 10^7 \pm 4.6 \times 10^6$ RLU/mg). Yet, luminescence in the lung was exceeded by the signal in the brain ($2.6 \times 10^7 \pm 1.0 \times 10^7$ RLU/mg protein). In contrast to ESGHGYF-mediated transgene expression driven by the CMV promoter, transgene expression driven by the CAG promoter (**Figure 20**) did not seem to be lung-specific.

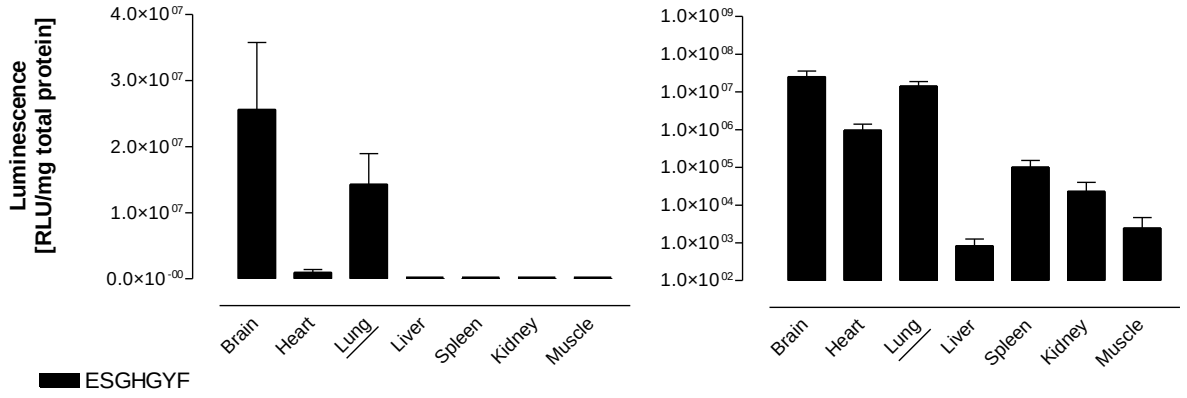

Figure 20. CAG-driven luminescence mediated by rAAV2-ESGHGYF
Recombinant AAV2 vectors displaying the lung-enriched peptide ESGHGYF, carrying the luciferase gene under control of the CAG promoter were administered into the tail vein of mice at a dose of 5×10^{10} gp/mouse. Luminescence in homogenized tissues was measured and normalized to total protein contained in the probes. Organs were explanted 14 d.p.i. Data are shown as mean +SD. Statistics were performed as one way ANOVA followed by Bonferroni's multiple comparison test. No single organ showed significant stronger luminescence than all other organs (n=3). *Note the difference in scale! Left panel*: Linear scale. *Right panel*: Logarithmic scale.

A direct comparison of CAG- and CMV-driven transgene expression of ESGHGYF-displaying luciferase vectors confirmed 42-fold stronger transgene expression in the lung when driven by the CAG promoter compared to the CMV promoter, thereby being the organ with the lowest increase in expression strength (**Figure 21**). On the other hand, CAG-driven luminescence in the brain increased as much as 1200-fold compared to the CMV promoter. All tested tissues that had previously revealed detectable luminescence with the CMV promoter, showed increased strength of luminescence if treated with CAG-driven vectors (**Figure 21**). Since the CAG promoter enhanced the ESGHYGF-mediated transgene expression in the lung relatively little (42-fold) compared to strongly enhanced transgene expression in the brain as non-target tissue, the CMV promoter but not the CAG promoter was chosen for all further experiments with the ESGHGYF vector.

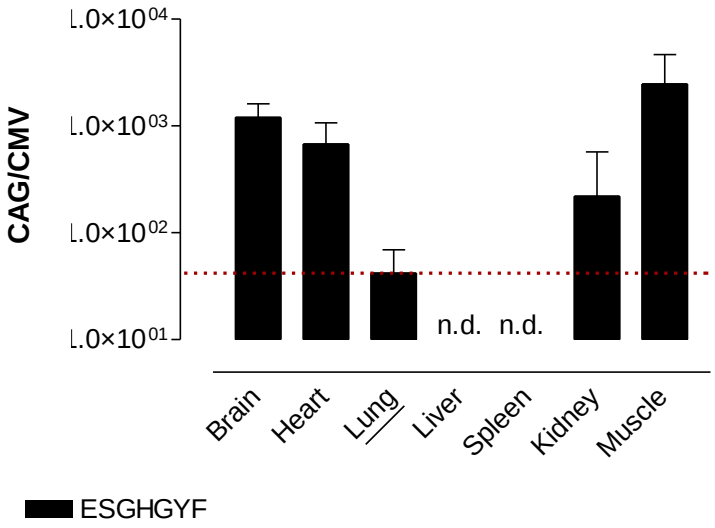

Figure 21. Ratio of ESGHGYF-mediated luminescence driven by CAG and CMV promoter
Recombinant AAV2 vectors displaying the lung-enriched peptide ESGHGYF, carrying the luciferase gene under control of the CAG promoter or the CMV promoter were administered into the tail vein of mice at a dose of 5 x 10^{10} gp/mouse. Luminescence in homogenized tissues was measured and normalized to total protein contained in the probes. Luminescence [RLU / mg total protein] driven by the CAG promoter was divided through the luminescence driven by the CMV promoter. Organs were explanted 14 d.p.i. The increase in luminescence driven by the CAG promoter compared to the CMV promoter in the lung as tissue of interest is pointed out as red line. In liver, spleen and muscle no luminescence had been detected with the CMV promoter (n.d. = no data).

4.6 Vector distribution

To analyze whether the observed brain- and lung-targeted transgene expression is caused by specific vector homing mediated by the selected peptides or if it is merely based on preferential expression in those tissues mediated the chosen promoters or by intracellular post-entry processing of viral DNA, the vector distribution was analyzed by qPCR (**3.5.6**) independently from the transgene expression.

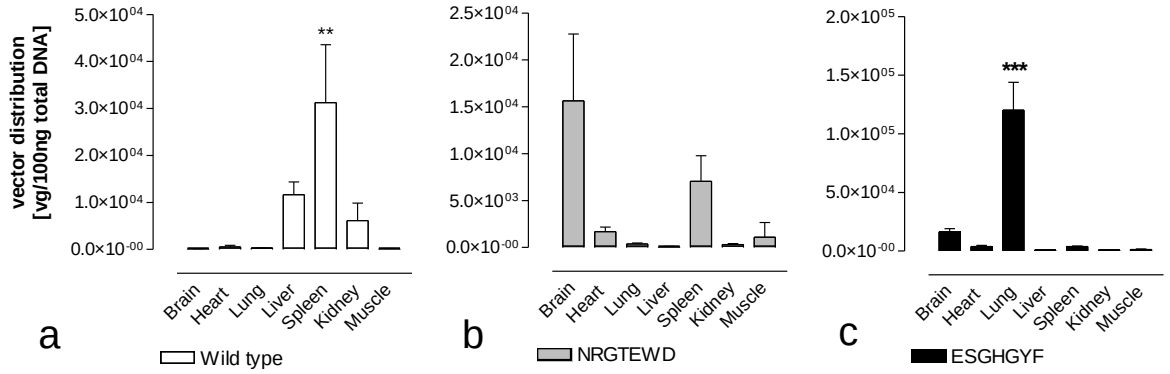

Figure 22. Genome distribution of rAAV2 vectors displaying selected peptides
Recombinant AAV2 vectors displaying selected peptides were administered into the tail vein of mice at a dose of 5 x 10^{10} gp/mouse. 14 d.p.i. vector distribution was analyzed by qPCR and normalized to total genomic DNA. Data are shown as mean +SD. Statistics were performed as one way ANOVA followed by Bonferroni's multiple comparison test. Levels of significance: $p < 0.05$ = *; $p < 0.01$ = **; $p < 0.001$ = *** (n=3). *Note the differences in scale!* (**a**) Unmodified wild type rAAV2. (**b**) Vector displaying the brain-selected peptide NRGTEWD. (**c**) Vector displaying the lung-selected peptide ESGHGYF.

At the time point of luminescence imaging, 14 days after administration of 5 x 10^{10} gp/mouse, wild type rAAV2 vector (**Figure 22 a**) could mostly be recovered from spleen (3.1 x 10^4 ± 1.2 x 10^4 vg/100 ng total DNA), liver (1.2 x 10^4 ± 2.7 x 10^3 vg/100 ng total DNA) and kidney (6.1 x 10^3 ± 3.7 x 10^3 vg/100 ng total DNA). Compared to the luminescence data, the amount of vector genomes recovered from spleen was unexpected high. Vector displaying the brain-selected peptide NRGTEWD on the other hand, could indeed mostly be recovered from the brain (1.6 x 10^4± 7.1 x 10^3 vg/100 ng total DNA), still followed by the spleen (7.1 x 10^3± 2.7 x 10^3 vg/100 ng total DNA) which can be seen in **Figure 22 b**. The amount of DNA of the NRGTEWD-displaying vector which could be recovered from the heart (1.7 x 10^3± 4.7 x 10^2 vg/100 ng total DNA), being the organ with the third-biggest quantity of vector DNA, was approx. ten-fold lower than the amount of vector DNA recovered from the brain (**Figure 22 b**). The amount of detected vectors displaying the peptide NRGTEWD in the brain was 168-fold higher than in brains of mice injected with wild-type rAAV2 (9.3 x 10^1± 4.8 x 10^1 vg/100 ng total DNA) which can be seen in **Figure 23 a**. Distribution data of genomes delivered by vectors displaying the lung-targeted peptide ESGHGYF strongly resembled the transgene expression data with specific ($p<0.001$) enrichment in the lung (**Figure 22 c**). The amount of detected vectors displaying the peptide ESGHGYF in the lung (1.2 x 10^5± 2.4 x 10^4 vg/100 ng total DNA) was seven times higher than in the brain (1.6 x 10^4± 2.8 x 10^3 vg/100 ng total DNA) and 263-fold higher than in the liver (4.6 x 10^2± 2.6 x 10^2 vg/100 ng total DNA). Up to 460-times more ESGHGYF-displaying vector than wild-type rAAV2 (2.6 x 10^2± 3.8 x 10^1 vg/100 ng total DNA) and 315-times more than NRGTEWD-displaying vector (3.8 x 10^2± 2.2 x 10^2 vg/100 ng total DNA) could be recovered from the lung (**Figure 23 b**). From the

liver, mostly wild type rAAV2 delivered genomes could be rescued (**Figure 23 c**). The amount of vector genomes which could be detected in the spleen was highest with wild type rAAV2, followed by NRGTEWD and ESGHGYF (**Figure 23 d**).

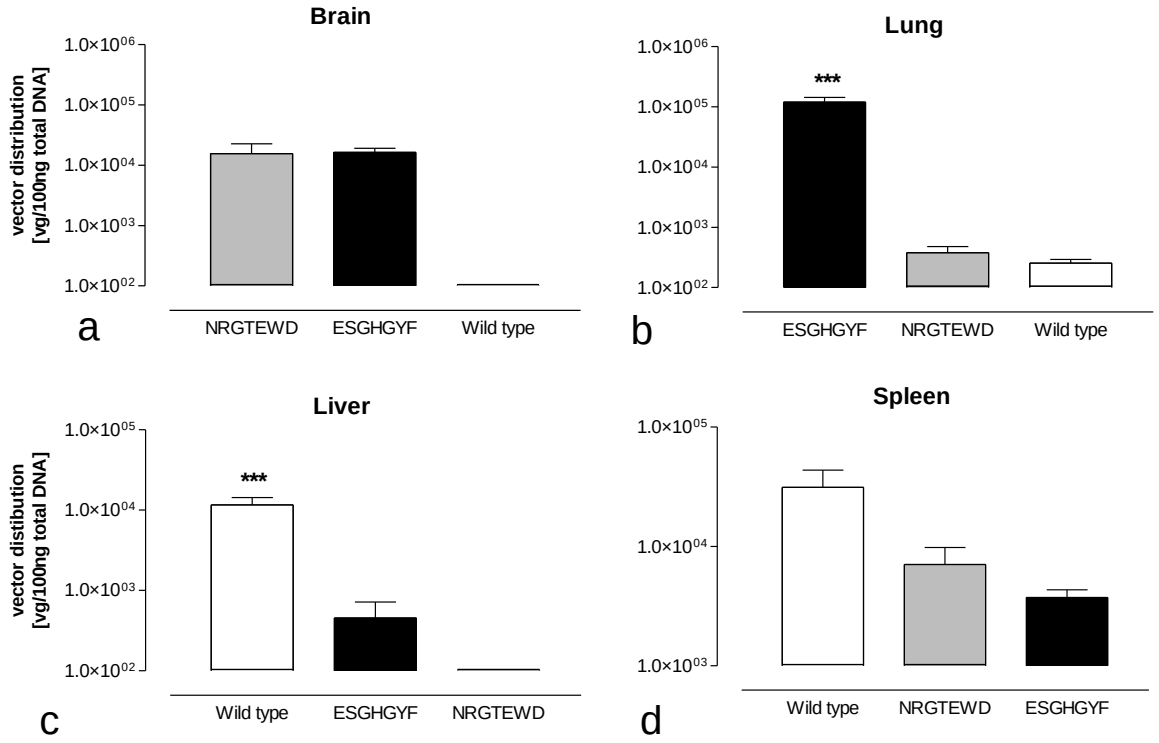

Figure 23. Genome distribution of rAAV2 vectors displaying selected peptides
Recombinant AAV2 vectors displaying selected peptides were administered into the tail vein of mice at a dose of 5 x 10^{10} gp/mouse. 14 d.p.i. vector distribution was analyzed by qPCR and normalized to total genomic DNA. Data are shown as mean +SD. Statistics were performed as one way ANOVA followed by Bonferroni's multiple comparison test. Levels of significance: $p < 0.05$ = *; $p < 0.01$ = **; $p < 0.001$ = *** (n=3). *Note differences in scale!* (**a**) Unmodified wild type rAAV2. (**b**) Vector displaying the randomly picked control peptide CVGSPCG. (**c**) Vector displaying the brain-selected peptide NRGTEWD. (**d**) Vector displaying the lung-selected peptide ESGHGYF.

4.7 Histological analyses of the peptide-mediated transduction profile of rAAV vectors

Having analyzed the tissue-specific homing, transgene delivery and transgene expression mediated by the brain- or lung-targeted vectors, it remained open which were the target cells of the selected vector capsids. Therefore immunohistochemistry was performed to visualize transgene expression at cellular level in brain, lung and liver, 14 days after i.v. administration of rAAV GFP-vectors displaying the brain- or lung-targeted peptide.

In brains of mice injected with rAAV2-NRGTEWD (1×10^{11} gp/mouse), microscopy of paraffin embedded tissue slides (**3.5.8**) revealed intense staining throughout the entire microvasculature of the brain and, to lesser extent, in slightly larger vessels (**Figure 24**).

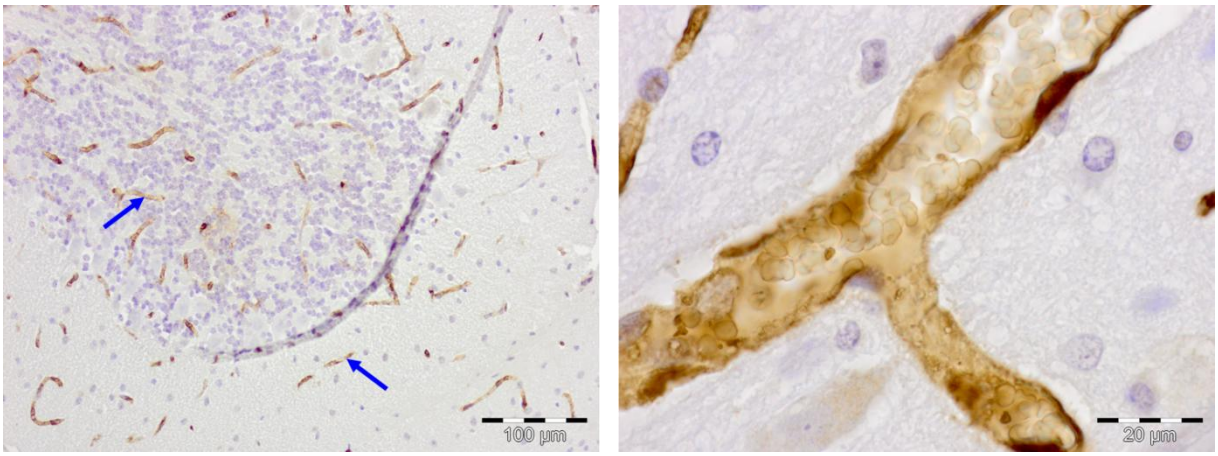

Figure 24. Histological analyses of the NRGTEWD-mediated rAAV transduction profile in murine brain tissue
Immunohistochemistry performed on paraffin embedded tissue, sectioned sagittal (2 µm), 14 days after tail vein injection of 1 x 10^{11} gp of rAAV2-NRGTEWD-CAG-eGFP vector. A representative area of the brain with part of the cerebellum is shown in different magnifications. *Left panel*: 20-fold magnification. *Right panel*: 100-fold magnification. Size of scale bars: 100 µm at 20x magnification and 20 µm at 100x magnification. Vector mediated eGFP staining (brown) is visible in microvasculature throughout the whole brain (blue arrows). *Images kindly provided by Lars Lunding (Division of Asthma Mouse Models, Leibniz-Center for Medicine and Biosciences Borstel, DE).*

In fluorescence microphotographs of agarose embedded tissue sections (**3.5.9**), brains of mice treated with rAAV2-NRGTEWD (6.0 x 10^{10} – 1.8 x 10^{11} gp/mouse) showed intense green eGFP signal in the microvasculature throughout the whole brain. To confirm tissue specificity, the liver (a tissue known to frequently show high transgene expression after wild-type rAAV vector injection) was analyzed as a control organ. Liver tissue of mice treated with rAAV2-NRGTEWD showed no vector-mediated eGFP signal. Representative areas of brain and liver of vector-treated mice are shown in **Figure 25**.

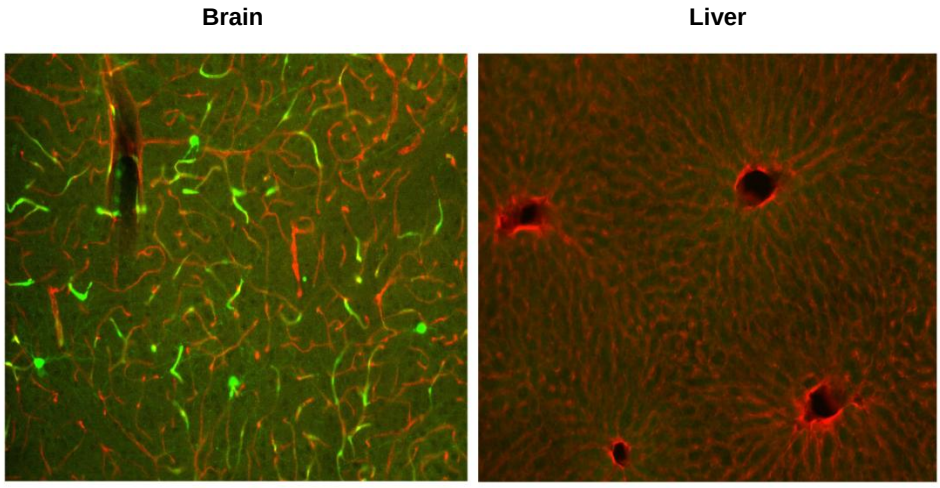

Figure 25. Immunofluorescence analyses of NRGTEWD-mediated rAAV transduction in murine tissue
14 days after injection of 6 x 10^{10} gp of rAAV2-NRGTEWD-CAG-eGFP. Representative areas are shown in 20-fold magnification *Left panel*: vector mediated fluorescence (green) is detectable throughout the microvasculature of the brain. The endothelium is co-stained with antibody against CD31 (red). *Right panel*: No vector-mediated fluorescence is detectable in the liver. Basement membranes are stained with antibody against collagen IV (red). *Images kindly provided by Dr. Godwin Dogbevia (Inst. of Experimental and Clinical Pharmacology and Toxicology, University of Luebeck, DE)*

Co-stainings (**3.5.9)** with antibodies against CD31 and CD13 were performed to distinguish between endothelial cells (CD31) and pericytes (CD13). Although the staining patterns of endothelial cells and pericytes resembled each other to some degree, the vector-mediated eGFP signal showed more congruency with the CD31 staining of the vascular endothelium (**Figure 26**).

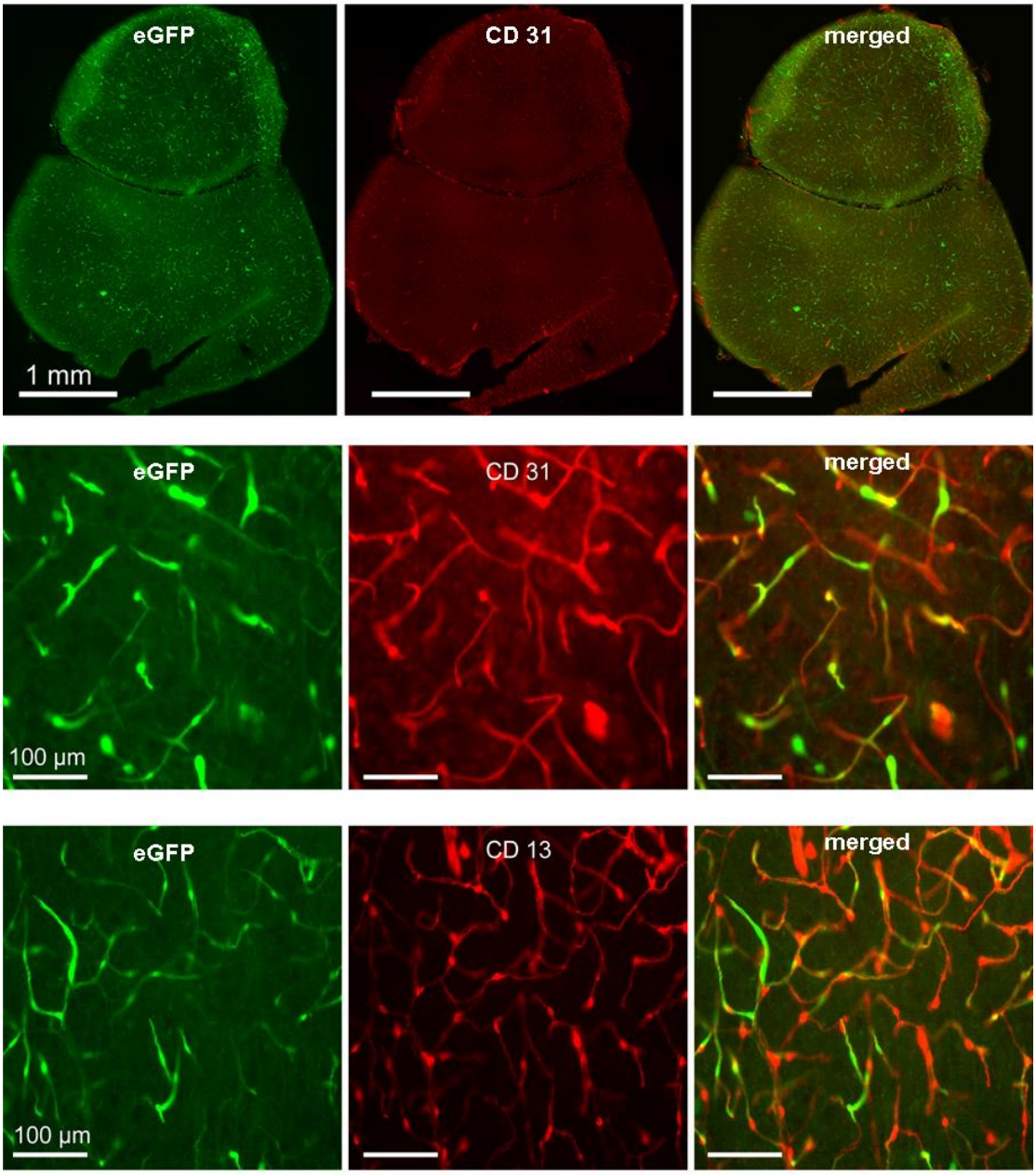

Figure 26. Immunofluorescence analyses of NRGTEWD-mediated rAAV transduction in murine brain
14 days after injection of 1.6 x 10^{10} gp of rAAV2-NRGTEWD-CAG-eGFP. *Upper row*: Coronal section through the whole brain, stained with antibody against the endothelium marker CD31 (red). Scale bars: 1 mm. *Middle row:* Representative part of a coronal brain section, stained with antibody against CD31 (red) in higher magnification. Scale bars: 100 µm. *Lower row*: Representative part of a coronal brain section, stained with antibody against the pericyte marker CD13 (red) in high magnification. Scale bars: 100 µm. *Images kindly provided by Dr. Godwin Dogbevia*

Analyses of the spinal cord of mice treated with rAAV2-NRGTEWD revealed that not only the endothelial cells of the brain, but rather the endothelial cells of the entire central nervous system are transducible by the brain-selected vector rAAV2-NRGTEWD. The endothelial nature of the transduced cells was again reconfirmed by co-staining with CD31 antibody (**Figure 27**).

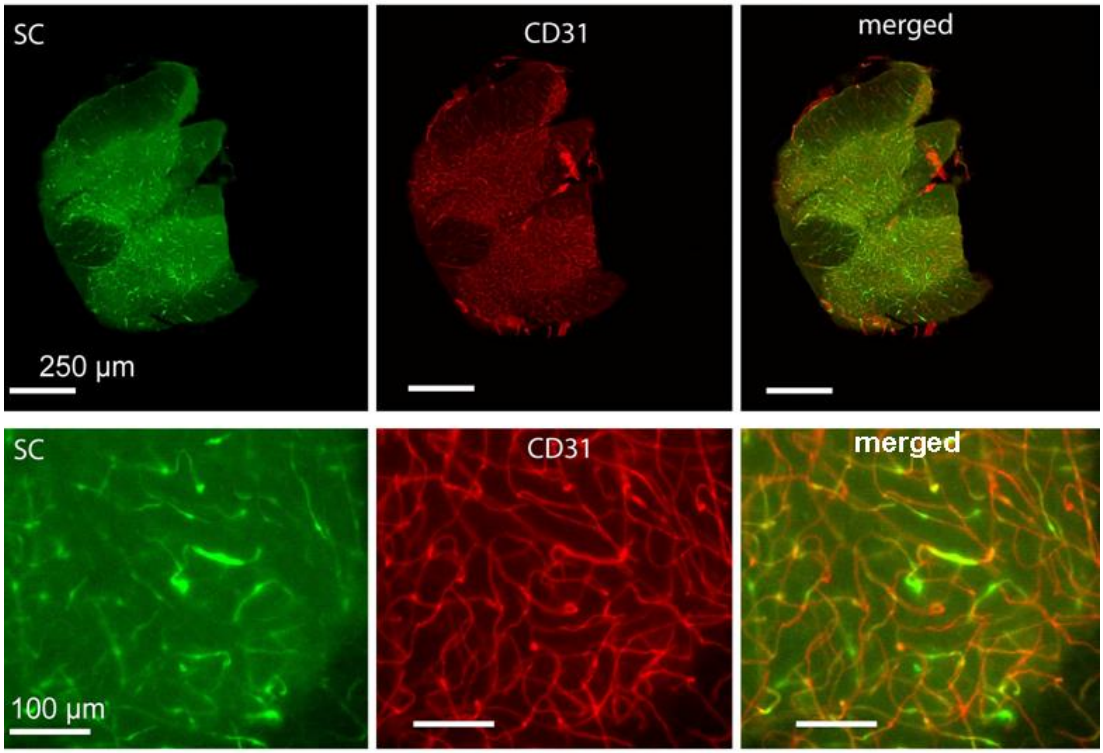

Figure 27. Immunofluorescence analyses of NRGTEWD-mediated transduction in murine spinal cord
14 days after injection of 1.6 x 10^{10} gp of rAAV2-NRGTEWD-CAG-eGFP. *Upper row*: Transverse section of the spinal cord, stained with antibody against the endothelium marker CD31 (red). Scale bar: 250 µm. *Lower row:* Representative part of a transverse section of the spinal cord, stained with antibody against CD31 (red) in higher magnification. Scale bar: 100 µm. Images *kindly provided by Dr. Godwin Dogbevia*

In lungs of mice injected with rAAV2-ESGHGYF-dsCMV-eGFP, microscopy of paraffin embedded tissue slides (**3.5.8**) revealed intense staining throughout the entire pulmonary microvasculature and, to slightly lesser extent, in larger pulmonary vessels (**Figure 28 a** & **b**). In contrast, pulmonary tissue of mice injected with the respective wild type rAAV2 vector showed no staining at all (**Figure 28 b**). In the liver, staining of hepatocytes was observed after administration of wild-type rAAV2 vector but no staining could be detected after administration of rAAV2-ESGHGYF vector (**Figure 28 b**).

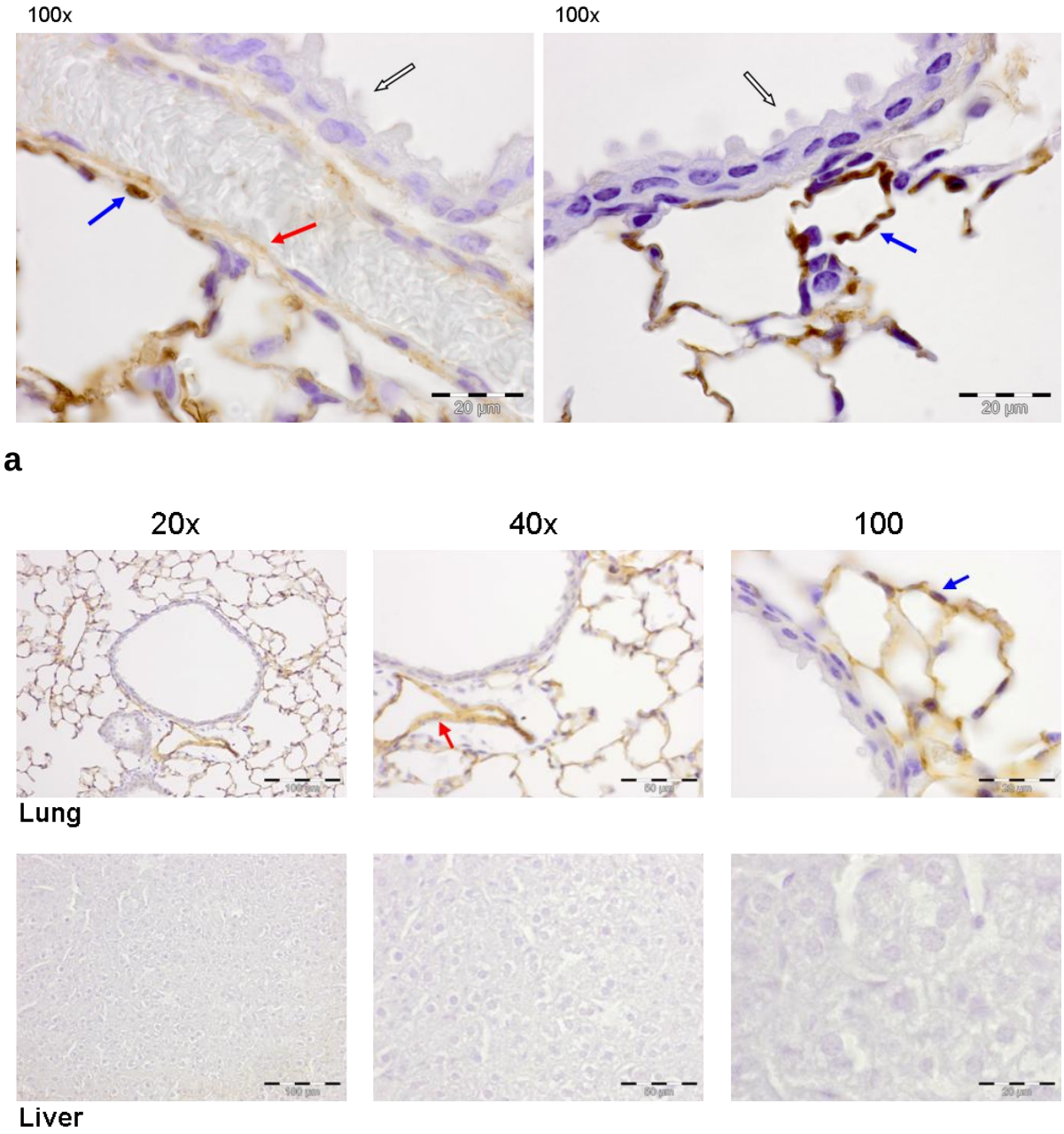

Figure 28. Histological analyses of ESGHGYF-mediated rAAV transduction in murine tissues
Immunohistochemistry performed on paraffin embedded tissue sections (2 µm), 14 days after tail vein injection of $1x10^{11}$ gp of rAAV2 eGFP vectors. Representative areas of the tissue of interest are shown in different magnifications. Size of scale bars: 100 µm at 20x magnification; 50 µm at 40x magnification and 20 µm at 100x magnification. (**a**) Lung tissue with staining of the vasculature (brown) mediated by rAAV2-ESGHGYF. Red arrows: Larger pulmonary vessel. Blue arrow: Pulmonary microvasculature. White arrows: No vector-mediated staining whatsoever in one of the diverse pulmonary airway cells. (**b**) *Upper row*: Overview of lung tissue with endothelial staining (brown) mediated by rAAV2-ESGHGYF, distributed throughout the whole lung. Red arrow: Larger pulmonary vessels. Blue arrow: Pulmonary microvasculature. *Lower row*: Liver sections of vector-treated mice. No staining in the liver of mice treated with rAAV2-ESGHGYF. *Images kindly provided by Lars Lunding.*

Since inflated lungs are best preserved as paraffin embedded tissues, which in turn are not well suited for immunofluorescence stainings, the nature of the vector-transduced cells within the lung was analyzed by standard immunohistochemistry (**3.5.8)**. A CD31 staining exactly reproduced the GFP staining pattern in serial sections of lungs of mice injected with rAAV2-ESGHGYF, thereby confirming the endothelial nature of the vector-transduced cells (**Figure 29**).

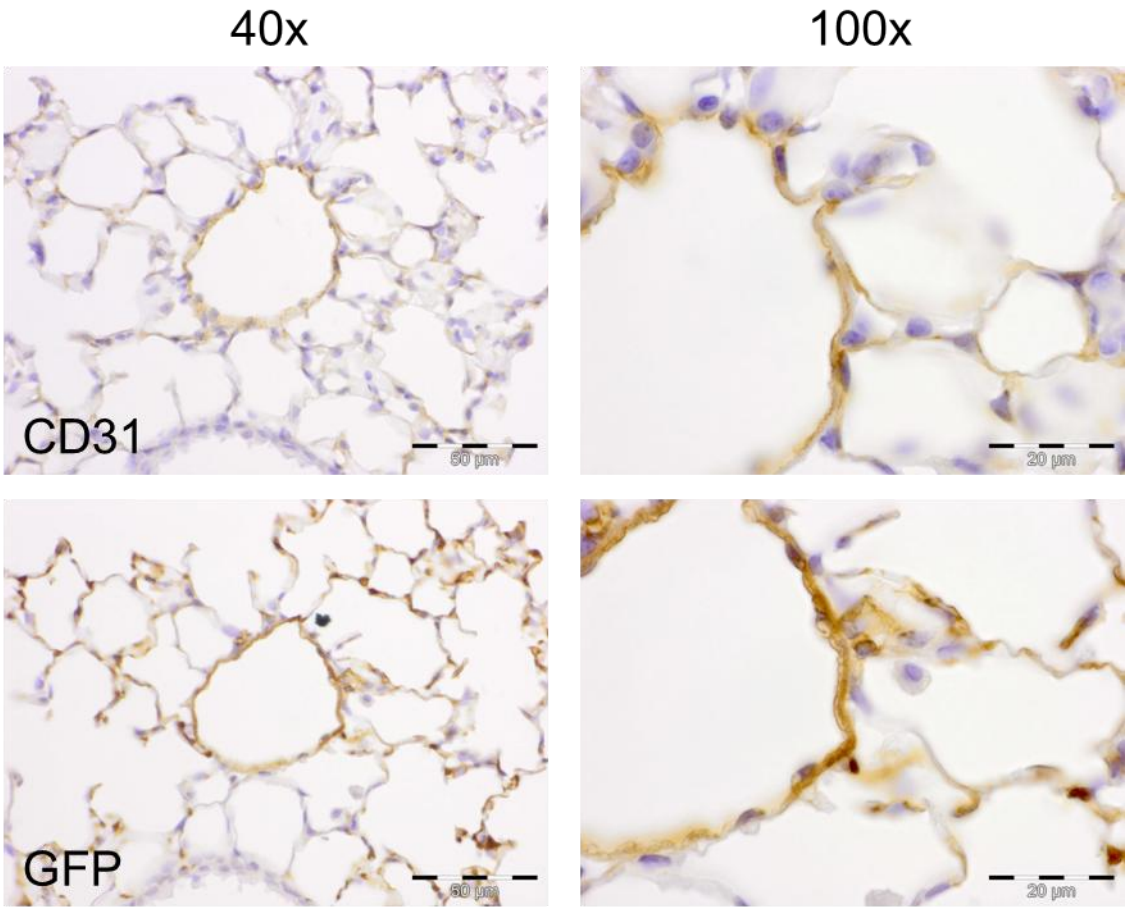

Figure 29. Endothelial staining of the pulmonary vasculature
Serial sections (2 µm) of a mouse lung, 14 days after tail vein injection of $1x10^{11}$ gp of rAAV2-ESGHGYF-dsCMV-eGFP. *Upper row*: CD 31 staining (endothelial marker). *Lower row*: eGFP staining (vector). *Images kindly provided by Lars Lunding.*

4.8 Characterization of the targeting peptides

4.8.1 Alanine scanning mutagenesis of brain- and lung enriched peptides

To gain more information about the enriched peptides' specific nature and the importance of single amino acids within the peptides, including the identification of potentially interfering amino acids, alanine scanning mutagenesis was performed. Thus, every single amino acid of the peptides was replaced by alanine (**3.4.7**) and the peptide mutants were produced as luciferase vectors (**3.4.1**) and tested for their transgene expression profile by luminescence imaging (**3.5.7**). Additionally, one scrambled version of each selected peptide was tested in this way.

The vector rAAV2-**A**RGTEWD, being the first tested mutant of the brain-selected peptide NRGTEWD, seemed to be almost transduction-deficient, showing almost no luminescence signal *in vivo* end *ex vivo* after organ explantation (**Figure 30 a**). The vector displaying the peptide N**A**GTEWD mediated strong gene expression in the heart (> 10^5 p/sec/cm^2/r) and a little bit less in the skeletal musculature. No luminescence signal could be detected in the brain. Luminescence imaging of the explanted organs confirmed this finding (**Figure 30 b**). The peptide NR**A**TEWD mediated strong gene expression (> 10^5 p/sec/cm^2/r) predominantly in heart and liver, without displaying transgene expression in the brain, seen in the living animal and in the explanted organs *ex vivo* (**Figure 30 c**). The expression profile mediated by the peptide NRG**A**EWD (**Figure 30 d**) resembled the pattern mediated by the peptide N**A**GTEWD with strong expression in heart and skeletal musculature, whereas the expression profile of rAAV2- NRGT**A**WD (**Figure 30 e**) with predominant luminescence in heart and liver resembled the pattern of rAAV2-NR**A**TEWD. The peptide NRGTE**A**D mediated strong transgene expression (> 10^5 p/sec/cm^2/r) mostly in heart and skeletal muscle (**Figure 30 f**), whereas the peptide NRGTEW**A** seemed to be more or less specific for the liver, seen *in vivo* and confirmed by the explanted organs imaged *ex vivo* (**Figure 30 g**). The scrambled version of the brain-selected peptide, WTRDNEG, mediated expression with a profile very similar to the expression mediated by N**A**GTEWD and NRG**A**EWD (strong expression of heart and skeletal muscle, **Figure 30 h**). Taken together, none of the tested variants of the peptide NRGTEWD mediated enhanced transgene expression in the brain, whereas most of them mediated enhanced expression in heart and skeletal muscle, compared the unmodified peptide NRGTEWD.

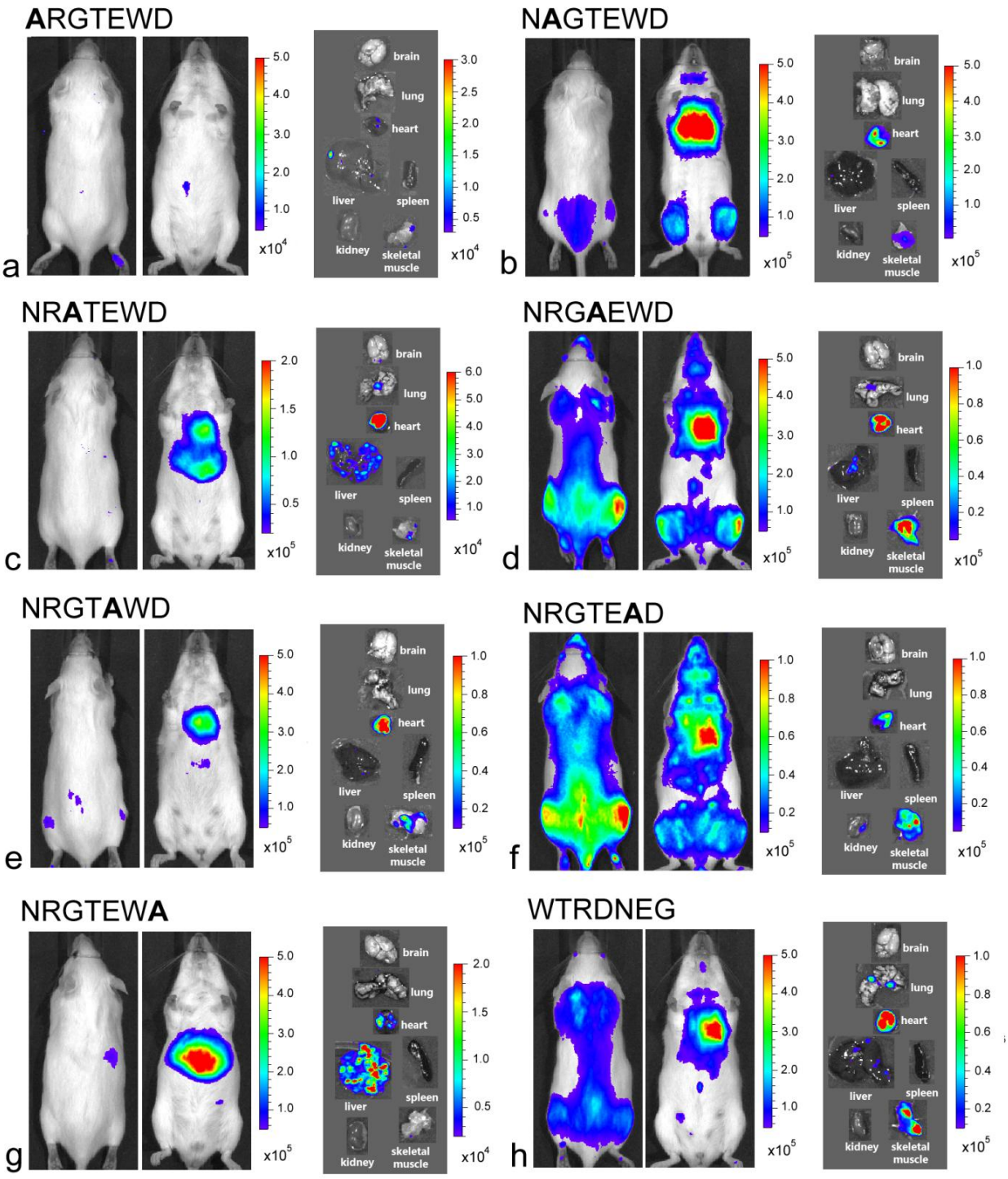

Figure 30. Alanine scanning mutagenesis of the brain-selected peptide NRGTEWD
Recombinant AAV2 vectors carrying the luciferase gene under control of the CAG promoter were administered into the tail vein of mice at a dose of 5 x 10^{10} gp/mouse. Mice were imaged 14 d.p.i, when luminescence reached peak values after i.p. administration of luciferin potassium salt. *Left two panels of each vector*: Mouse imaged *in vivo*; dorsally (*left*) and ventrally (*second from left*). *Right panel of each vector*: Single organs, measured directly after explantation, *ex vivo*. *Note the differences in scale!* Three mice were treated per vector of which one representative example is shown. (**a**) rAAV2-ARGTEWD. (**b**) rAAV2-NAGTEWD. (**c**) rAAV2-NRATEWD. (**d**) rAAV2-NRGAEWD. (**e**) rAAV2-NRGTAWD. (**f**) rAAV2-NRGTEAD. (**g**) rAAV2-NRGTEWA. (**h**) rAAV2-WTRDNEG.

A very different pattern was observed when imaging vectors displaying mutants of the lung-enriched peptide ESGHGYF. Mice treated with rAAV2 vector displaying the peptide **A**SGHGYF exhibited luminescence (> 10^6 p/sec/cm^2/r) restricted to the lung (**Figure 31 a**), which was approx. 10-fold stronger than luminescence mediated by the unmodified peptide ESGHGYF (**Figure 12**). The peptide E**A**GHGYF also mediated strong transgene expression in the lung (> 10^5 p/sec/cm^2/r), approx. at the same level as the peptide ESGHYGF. In addition, comparably strong transgene expression (> 10^4 p/sec/cm^2/r) in the brain could be detected when imaging the living mouse and the explanted organs *ex vivo* (**Figure 31 b**). The peptide ES**A**HGYF mediated moderate transgene expression in the skeletal musculature (≈ 10^4 p/sec/cm^2/r). No luminescence in the lung could be detected. If imaged dorsally, some minor gene expression (< 10^4 p/sec/cm^2/r) in the brain could be detected as well. Luminescence images of the explanted organs only confirmed the transgene expression in the skeletal musculature (**Figure 31 c)**. Mice treated with rAAV2 vector displaying the peptide ESG**A**GYF showed weak to moderate transgene expression (≈ 10^4 p/sec/cm^2/r) in heart and skeletal musculature. Some minor transgene expression (< 10^4 p/sec/cm^2/r) in the brain could also be detected, whereas no luminescence was detectable within the lung. The explanted organs showed no luminescence at all (**Figure 31 d)**. The peptides ESGH**A**YF (**Figure 31 e**), ESGHG**A**F (**Figure 31 f**) and ESGHGY**A** (**Figure 31 g**) as well as the scrambled version FHEYGSG (**Figure 31 h**) mediated strong transgene expression (10^5 p/sec/cm^2/r to 10^6 p/sec/cm^2/r) in heart and skeletal musculature, without mediating any transgene expression in the lung. Luminescence in heart and skeletal muscles could be confirmed by *ex vivo* imaging of the explanted organs.

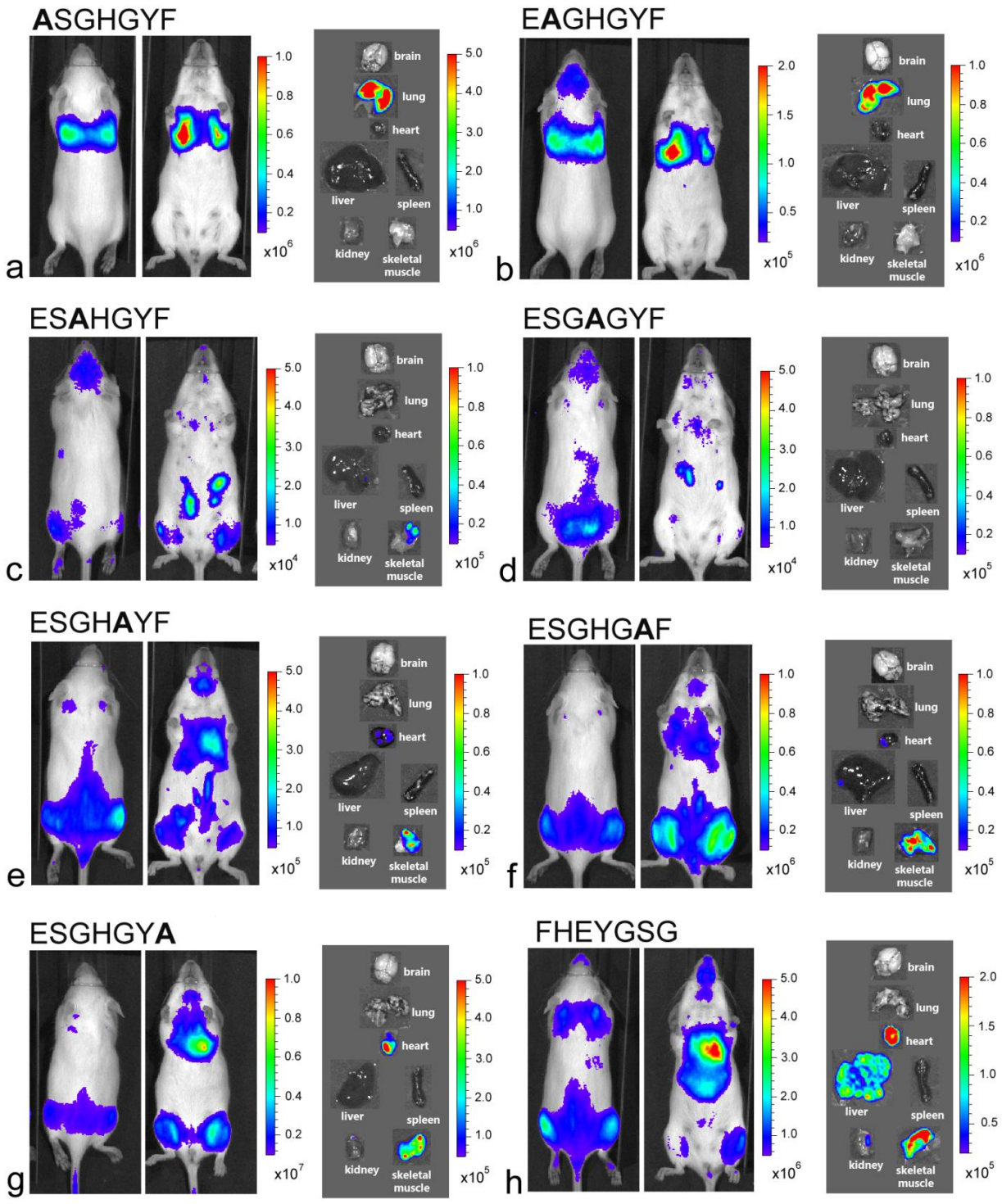

Figure 31. Alanine scanning mutagenesis of the lung-selected peptide ESGHGYF
Recombinant AAV2 vectors carrying the luciferase gene under control of the CAG promoter were administered into the tail vein of mice at a dose of 5 x 10^{10} gp/mouse. Mice were imaged 14 d.p.i, when luminescence reached peak values after i.p. administration of luciferin potassium salt. *Left two panels of each vector*: Mouse imaged *in vivo*; dorsally (l*eft*) and ventrally (*second from left*). *Right panel of each vector*: Single organs, measured directly after explantation, *ex vivo*. *Note the differences in scale!* Three mice were treated per vector of which one representative example is shown. (**a**) rAAV2-ASGHGYF. (**b**) rAAV2-EAGHGYF. (**c**) rAAV2-ESAHGYF. (**d**) rAAV2-ESGAGYF. (**e**) rAAV2-ESGHAYF. (**f**) rAAV2-ESGHGAF. (**g**) rAAV2-ESGHGYA. (**h**) rAAV2-FHEYGSG.

4.8.2 Prediction of the structure of AAV virions displaying selected peptides

A comparison between the published[43] structure of the AAV2 wild type VP1 monomer (**Figure 32 a**) and the predicted structure of the AAV2-NRGTEWD VP1 monomer, obtained by homology modelling (**4.8.2**, **Figure 32 b**), suggests the existence of an exposed loop at the peptide insertion site at amino acid R588.

In contrast, the predicted structure of the AAV2-ESGHGYF VP1 monomer (**Figure 32 c**) suggests the existence of additional antiparallel ß-sheets at the peptide insertion site compared to the wild type AAV2 VP1 monomer (**Figure 32 a**).

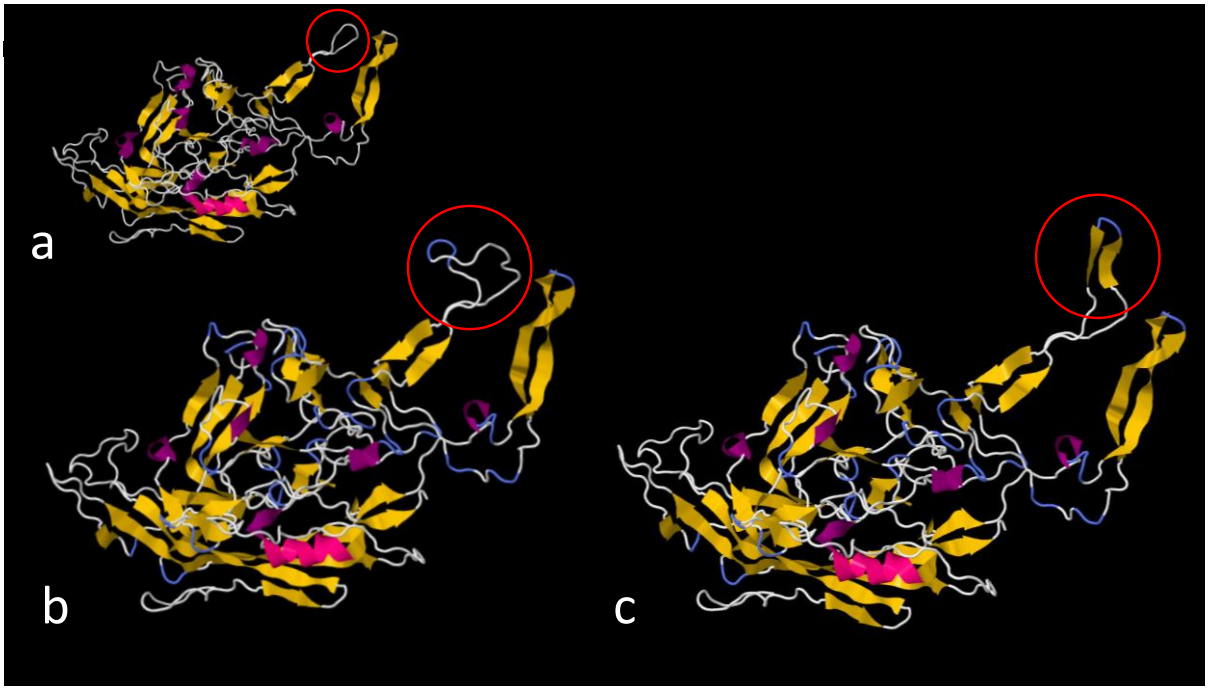

Figure 32. Prediction of the structure of AAV virion proteins displaying selected peptides
The structure of the wild-type AAV2 VP1 with the data bank number pdb:1LP3 [ref.43] was used as a template for homology modeling of modified AAV2 capsid with peptide insertion at R588 by the SWISS-MODEL Workspace[215-218] and visualized with the software jmol version 13.0. Alpha-helices are shown in magenta, ß-sheets are displayed as yellow arrows and random coils are indicated in white. The region around R588 is highlighted (red circle). (**a**) VP1 wildtype AAV2. (**b**) VP1 AAV2-NRGTEWD. (**c**) VP1 AAV2-ESGHGYF.

4.9 Further characterization of the lung-targeted vector rAAV2-ESGHGYF

4.9.1 Analyses of rAAV2-ESGHGYF mediated homing

The ESGHGYF-displaying vector was chosen to analyze the vector distribution(**3.5.6**) as early as 4 hours after intravenous administration of 5 x 10^{10} gp/mouse, to gain information about the kinetics of vector homing. Overall, the data after four hours strongly resembled the vector distribution after 14 days (**Figure 22 c)** but the total amount of recovered vector DNA was much higher (**Figure 33**). The amount of vector genomes which could be detected in the lung ($3.8x10^5$ ± $1.9x10^5$ vg/100ng total DNA) was approx. 6- to 100-fold higher than the amount of vector genomes detected in the other tested organs, indicating a fast and specific vector homing ($p<0.01$).

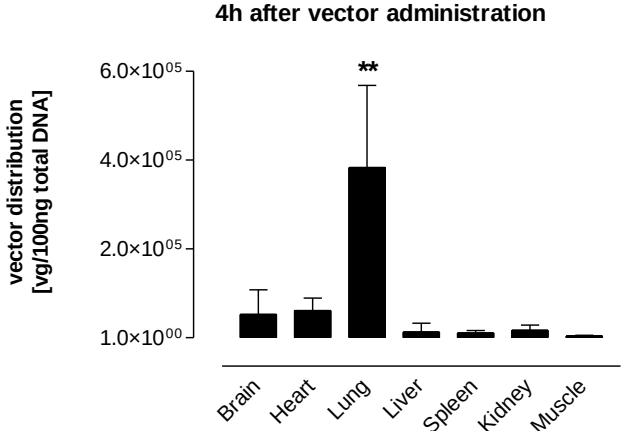

Figure 33. Homing of rAAV2-ESGHGYF
Recombinant AAV2 vector displaying the lung-selected peptide ESGHGYF was administered into the tail vein of mice at a dose of 5 x 10^{10} gp/mouse. 4 h after injection, vector distribution was analyzed by qPCR and normalized to total genomic DNA. Data are shown as mean +SD. Statistics were performed as one way ANOVA followed by Bonferroni's multiple comparison test. Levels of significance: $p < 0.05$ = *; $p < 0.01$ = **; $p < 0.001$ = *** (n=3). peptide ESGHGYF.

4.9.2 Virtual cross sectioning of mice treated with rAAV2-ESGHGYF vector by *in vivo* bioluminescence imaging

In vivo bioluminescence images of a mouse treated with rAAV2-ESGHGYF vector were reconstructed three-dimensionally, by measuring different wavelengths of the emitted light (**3.5.7**). Virtual cross sections confirmed the lung-specific transgene expression, which had already been shown by *in vivo* bioluminescence imaging of the mouse's surface (**4.5.1**) and measurement of luciferase activity from tissue lysates (**4.5.2**). Like on the previous images, the luminescence signal from the left lung seemed to be lower than the signal from the right lung. No other source of luminescence than the lung could be identified (**Figure 34**).

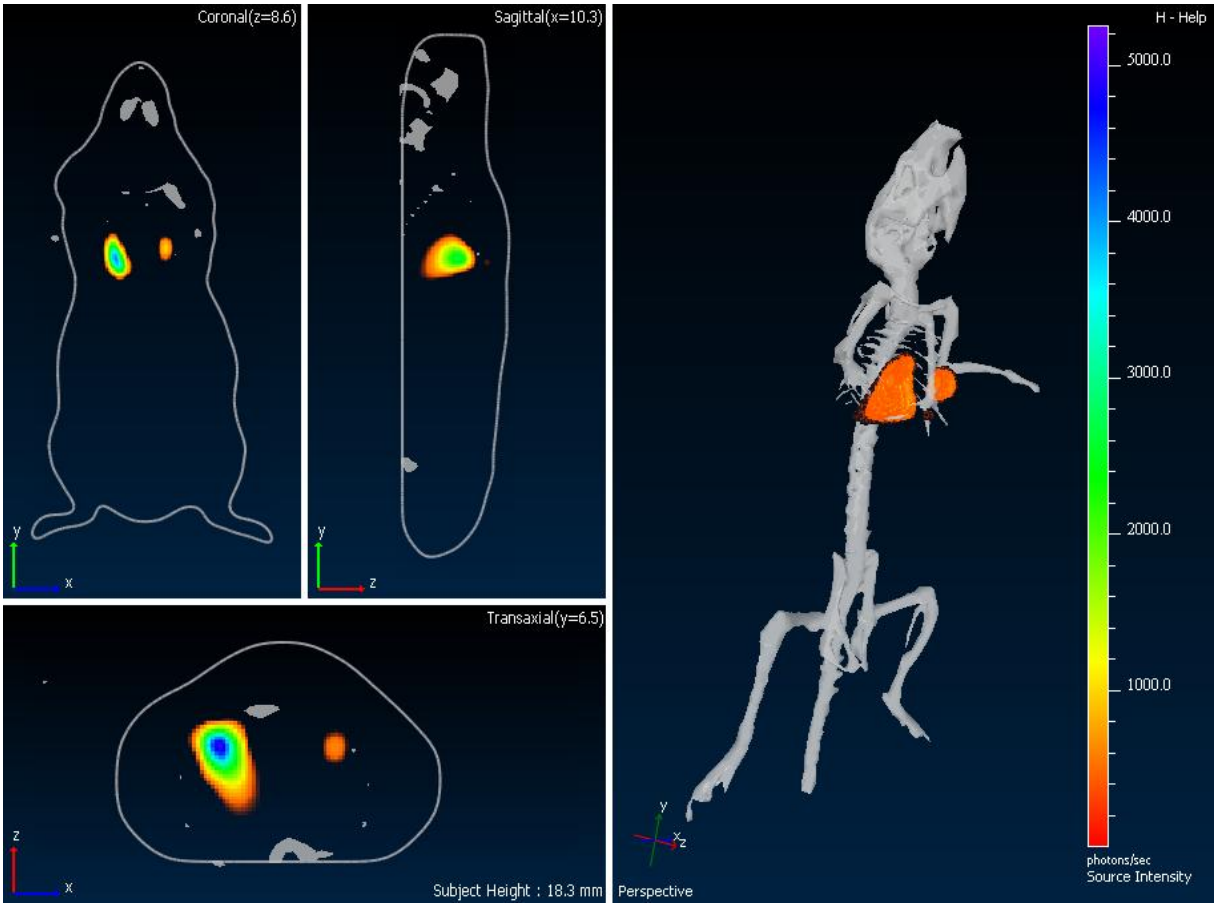

Figure 34. Virtual cross sectioning of mice treated with rAAV2-ESGHYGF vector by *in vivo* bioluminescence imaging
Coronal, sagittal and transaxial sections (*left*) and three-dimensional reconstruction (*right*) of the luminescence images of a mouse, 14 d.p.i. after tail vein injection of 5×10^{10} gp of rAAV2-ESGHGYF vector. Images were obtained by measuring different wavelengths of the emitted light.

4.9.3 Analyses of rAAV2-ESGHGYF mediated transgene expression over prolonged periods of time

After intravenous administration of the lung-targeted rAAV2-ESGHGYF luciferase vector (5×10^{10} gp/mouse), transgene expression was analyzed (**3.5.7**) at six time points over a period of 164 days in an immunocompromised SCID mouse (**3.5.1**). Thus, the transgene-expression could be analyzed independently from potential immunogenicity of the viral vector (ESGHGYF-displaying AAV2 capsid), the viral promoter (CMV) or the transgene itself (luciferase). The emitted radiance of the lung as the region of interest (ROI) was counted to quantify transgene expression. Throughout the whole period, transgene expression was stable at high levels and continued to be restricted to the lung. The relatively lowest expression in the lung was measured at the first time point at day seven (2.5×10^6 p/sec/cm2/sr), reached a peak at day 42 (6.8×10^6 p/sec/cm2/sr) and decreased until day 86 to approx. half (3.9×10^6 p/sec/cm2/sr) of the maximum luminescence from which day on it stayed relatively stable until the last measurement at day 164 (**Figure 35**). In a next step, transgene expression was analyzed (**3.5.7**) in immunocompetent wild type FVB/N mice (**3.5.1**). Here, albeit being lower, transgene expression was also relatively stable at high levels and continued to be restricted to the lung throughout the whole period of measurements (187 days). In FVB/N mice the peak of transgene expression was measured at day 14 (3.5×10^6 p/sec/cm2/sr) and decreased until day 84 to approx. half (1.5×10^6 p/sec/cm2/sr) of the maximum luminescence from which day on it stayed stable until the last measurement at day 187 like in the SCID mouse (**Figure 35**). Although all animals have grown substantially during the experiment (the SCID mouse started with ≈ 20 g and ended with ≈ 40 g, FVB/N mice started with ≈ 20 g and ended with ≈ 50 g), the shift in luminescence was relatively little. After the last measurement, the SCID mouse died from anesthesia. The experiment with the FVB/N mice is still ongoing.

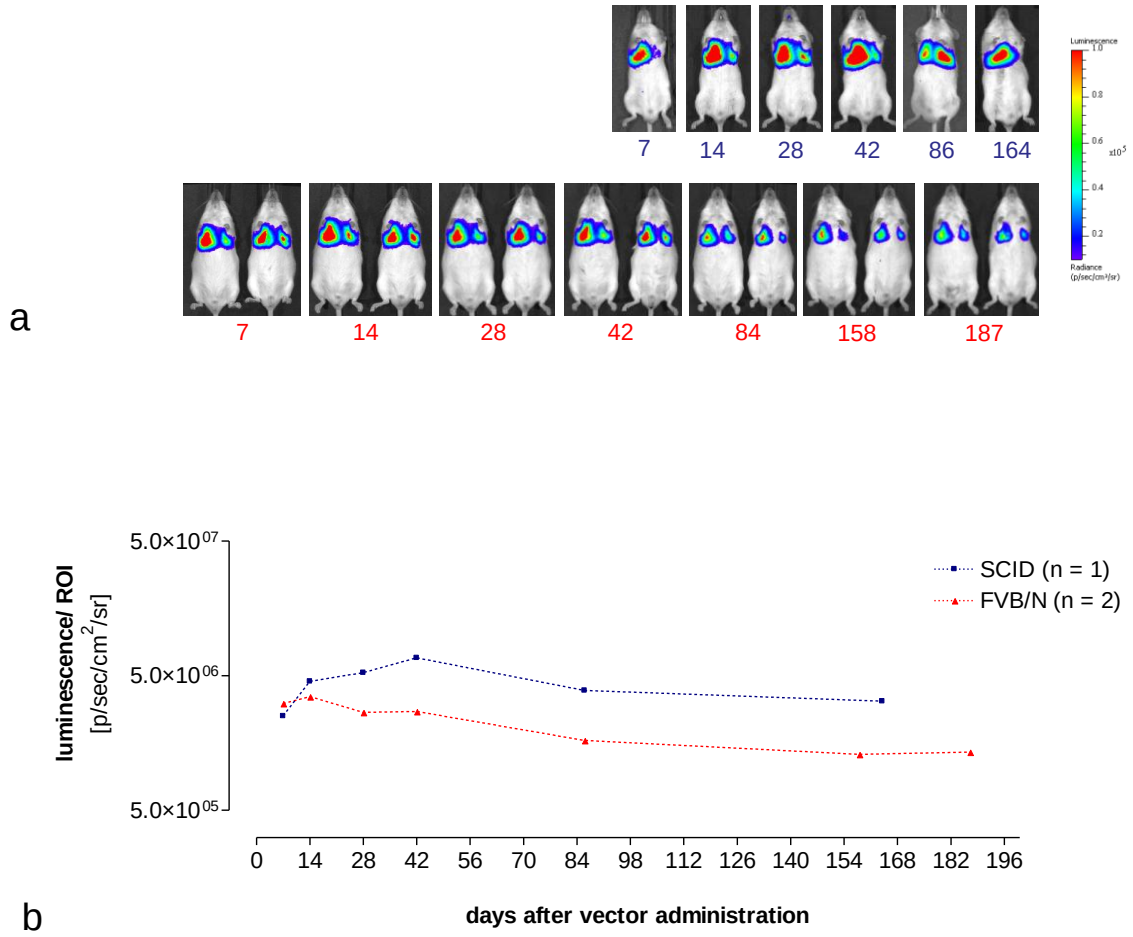

Figure 35. Long-term observation of rAAV2-ESGHGYF mediated transgene expression
Mice were imaged at several time points after tail vein injection of 5 x 10^{10} gp of rAAV2-ESGHGYF vector over a period of 164 days (SCID mouse) or 187 days (FVB/N mice). (**a**) Luminescence images of vector treated mice. *Upper row*: SCID mouse. *Lower row*: FVB/N mice (**b**) Luminescence in the lung was counted as region of interest (ROI). Blue squares: SCID mouse. Red triangles: FVB/N mice.

5 Discussion

5.1 Overview

The future of gene therapy is strongly dependent of the development of safe, efficient and target-specific vectors. Over the last two decades, different strategies have been developed to direct potential gene therapy vectors towards therapeutically relevant tissues. Among the viral vectors, AAV has emerged as one of the most promising and most widely used candidates for clinical gene transfer[82, 219]. In particular the central nervous system[13, 118, 150, 151, 162, 166-173, 175-177, 220-226], the eyes[152, 227-229] or the lung[62, 115, 179, 180, 187, 190, 230-234] have been subject to numerous pre-clinical and clinical studies utilizing rAAV vectors, due to their high transduction efficiency and their superior safety profile compared to other viruses. Still, the variety of natural AAV serotypes is limited and most of them are far from being convincing in terms of specificity and efficacy. Vectors with impressive improvements of transduction efficiency have been generated by combining structural proteins of different AAV serotypes[108, 113-118], sometimes coupled with random mutagenesis of structural relevant sites[119, 120], and one of them even found its way into a clinical trial[121]. Still, most of these vectors lack the high degree of specificity needed for sensitive gene therapy approaches. The observed inability to generate sufficient tissue specificity may be explained by the limited availability of different natural serotypes to be combined, and at least in some of these approaches, the absence of a systematic disruption of endogenous receptor binding sites. Conjugation of specific antibodies or high affinity ligands to the AAV capsid seemed to be another promising approach and yielded specific vectors *in vitro*[122, 123] and *in vivo*[130]. However, conjugated vectors often are very large and fragile, they potentially increase immunogenicity, they do not necessarily mediate target cell infection, their large-scale production is expensive and time-consuming and in particular, their production is completely dependent on the existence of highly specific ligands or antibodies which unfortunately are only available for a limited number of different targets.

After the receptor binding site within the capsid of AAV2 had been identified[43-47], many attempts aimed at disrupting its endogenous tropism by incorporating small, previously selected targeting peptides directly into this region[78]. These approaches have proven to yield vectors with enhanced transduction capability *in vitro*[136] and *in vivo*[137-140]. Nonetheless, the targeting capacity of peptides seem to change when transferring them into the structural context of AAV, thus only leading to limited increase in efficacy and specificity compared to the unmodified virus. The random AAV display peptide library which was developed ten years ago independently by two groups[141, 142], was the first systematic report of a system enabling the selection of peptides directly within the constraints of the assembled AAV capsid. Although screening of such libraries has yielded numerous

well suited vectors for *in vitro* experiments[141-147], the yield of efficient and tissue-specific vectors for *in vivo* applications has been very poor so far. Four years ago[147] our group first reported on particles enriched *in vivo* from random AAV display peptide libraries. Although these particles have clearly shown enhanced transduction of target tissues, they still also transduced non-target organs. The first – and until now - only report of a specific vector, selected *in vivo* from a random AAV display peptide library was published in 2010, presenting a heart-targeted AAV[148].

Despite the limited success of previous *in vivo* screenings[112, 147], we assumed that the high potential of random AAV display peptide libraries has simply not been fully exploited yet. Many variables in the fragile process of *in vivo* screening are prone to influence its outcome. Three parameters were considered to be of major importance: a) the quality of the utilized random AAV display peptide library, b) the prevention of contaminations (e.g. wild type AAV contamination, cross-contamination between parallel library screenings or different selection rounds) and c) the choice of the right clone from the pool of enriched particles after the completed screening.

5.2 The random AAV display peptide library employed in this study

A good quality peptide library is the prerequisite for successful *in vivo* screenings. A high diversity (= high number of different peptides contained in the library) and a low background (= low abundance of clones without peptide insert) are certainly two of the key factors defining a good quality library. Although it is very difficult to calculate the actual diversity of a final peptide library[235, 236], its maximum theoretical diversity can be calculated at the plasmid level[141]. The calculated maximum theoretical diversity of the random AAV display peptide library used in this study, with 3.4×10^8 clones determined at plasmid level, was further reduced during production by the number of producer cells (2×10^8) for practical reasons. Thus, the library's diversity was within the same range as the library initially described by Müller et al.[141] In contrast to the initially described library, contamination with wild type AAV2 could completely be avoided due to a protocol by Waterkamp et al.[144] Another important parameter of a peptide library is its coverage (= percentage of theoretically possible different peptides covered by the library). Due to the degenerated code, each amino acid is encoded by one to six nucleotide triplets. Thus, in a library containing heptapeptide inserts encoded by completely randomized oligonucleotides, theoretically there are peptides encoded by just one nucleotide sequence (1^7) and others encoded by 279,936 different nucleotide sequences (6^7). In addition, shorter non-functional peptides would not be excluded due to the presence of stop codons within the randomized oligonucleotides. These factors dramatically reduce the library's diversity. Therefore, the library which was developed by Müller et al.[141] and used in this study was produced

with random oligonucleotides following the $(NNK)_7$ scheme (N = all nucleotides; K = G or T) to reduce the maximum number of different oligonucleotides encoding one single peptide to 2,187 (3^7) and to exclude two of three stop codons (UAA, UGA), thus increasing the library's diversity by avoiding redundancies. A library containing peptide inserts that are encoded by defined trimer-based oligonucleotides - with each peptide corresponding to just one nucleotide sequence - would outperform a $(NNK)_7$-based library in terms of coverage and diversity[237]. Still, the benefits of a trimer-based library compared to a $(NNK)_7$-based library were thought to be too small to legitimate the considerably higher costs for its synthesis and the $(NNK)_7$-based library has already proven its general functionality in screenings *in vitro* and *in vivo*. Thus, the *in vivo* screenings described in this study were performed with the $(NNK)_7$-based library.

5.3 The process of *in vivo* screening

In general, there are different ways of amplifying pre-selected particles for subsequent rounds of selection during *in vivo* screenings with random AAV display peptide libraries. Particles can either be amplified by adenovirus or by PCR-based approaches[147]. During the screenings described in this study, library particles were amplified by PCR, since not all cells within the murine target tissues are susceptible to infection with human adenovirus and even if they were, it has not been shown that AAV can replicate in murine cells superinfected with human adenovirus. One of the two *in vivo* screenings described in this study (target tissue: lung) had been performed prior to the *in vivo* screening which was performed as part of this study (target tissue: brain). The pre-selected secondary AAV libraries of the selection in murine lungs were generated by directly transfecting HEK 293-T cells with the plasmid library in a limited dilution. The plasmid library in turn was produced with PCR-amplified viral DNA fragments, like described in Ref.[147]. During the *in vivo* screening which was performed as part of this study (brain) on the other hand, library transfer shuttles were generated after each round of selection as additional step, like for the production of the primary random AAV display peptide library[141], to ensure that each encapsidated genome corresponds to the modified virion proteins display on the viral surface.

The necessity to perform nested-PCRs to rescue enough insert-encoding viral DNA from murine brains during the first two rounds of selection, while single PCRs were sufficient from the third round on, indicates enrichment of brain-targeting particles during selection. Unfortunately no such data were available for the *in vivo* screening in murine lungs. The actual diversity of pre-selected AAV libraries is supposed to decrease dramatically during subsequent rounds of selection, since only particles which specifically target the tissue of interest should get enriched. Thus, it was thought to

be sufficient to use less DNA to generate pre-selected plasmid libraries during the *in vivo* screenings in brain and lung than for the initial primary random AAV display peptide library, although leading to a decrease in their theoretical maximum diversity. The genomic titers of the pre-selected libraries on the other hand seemed to stay more or less stable during subsequent rounds of selection, indicating that the pre-selected peptide inserts do not negatively influence particle assembly and stability.

5.4 Evaluation of the enriched peptides and their consensus sequences

It can be hypothesized that successful *in vivo* screenings comprise different levels of selection. Theoretically, generally non-functional and unstable virions would be dismissed from the pool of particles during the first round of selection, followed by particles which are somehow stable and infectious *in vitro* but non-infectious *in vivo*. In subsequent rounds of selection, generally well-infectious but nonspecific particles would be replaced by target-specific particles, since the non-target organs passed during circulation provide a "substrate" for negative selection. The initial minimum consensus motifs described in this work, **N**XX$^{X}_{R}$$^{X}_{R}$X**E** (brain) and **N**X**V**XXXX (lung), enriched during the first two rounds of selection are good examples for particles which potentially show high stability and infectivity but low specificity *in vivo*. Sequence motifs enriched by others *in vitro* on primary coronary artery cells[141] (**NSVRDL**$^{G}_{S}$), primary human venous endothelial cells[144] (**N**X**VR**XXX) or Kasumi-1 acute myeloid leukemia cells[145] (**N**X**V**XXXX) clearly display high similarity. Clones matching these motifs have also been enriched by our group i*n vitro* in diverse other cell lines (unpublished data). Some single clones enriched in brain and/or lung seem to have a particularly broad tropism like NNVRTSE which has also been enriched by our group in the human cancer cell lines DU4475, DU145, PC3, LNCaP and MCF7 (unpublished data). The lung-enriched peptide NDVRAVS which has already been enriched in the lung previously upon screening of a combinatorial multispecies AAV display peptide library[112], could also be find in primary human venous endothelial cells[144] and primary coronary artery cells[141].

Interestingly, during selection for brain-targeted vectors the potentially unspecific sequence motif switched after the third round of *in vivo* selection, revealing the totally distinct but very dominant motif X**DG**XXW**X** which does not show similarity to any enriched sequence motif ever noticed before. In the selection for lung-targeted vectors, on the other hand, no consenus motif but a strong enrichment of a single distinct clone could be observed. The reason for the observed differences between the *in vivo* screenings in brain and lung, especially regarding the absence of a clear sequence motif in the lung, are unclear. However, it can be assumed that the differences in the preparation of the pre-selected secondary libraries may not have played a major role, since the extra step of library transfer shuttles (performed during the screening in murine brain) has been omitted in

prior *in vivo* screenings[147] which still led to the enrichment of sequence motifs. The only difference between the screening in the lung presented here and previously published screenings[147] is the prolonged circulation time of eight days. It is conceivable that a prolonged waiting period until organ harvest might increase specificity by directing the selection away from accidently trapped particles towards successfully internalized particles.

Perabo et al.[134] analyzed peptides in a random AAV2 X_7 library according to side chain classification and abundance of single amino acids. Initial non-selected libraries were compared with fractions of the library that still bind HSPG, the primary attachment receptor of wild type AAV2, and with non-binding fractions. In summary, an excess of the small amino acids proline (P), glycine (G), alanine (A) and a defect of the biggest and aromatic amino acids phenylalanine (F), tryptophan (W) and tyrosine (Y) was found in the initial non-selected library, suggesting a negative selection against substantial structural rearrangements during the library production itself[134]. The HSPG-binding pool, which hypothetically comprises particles that reconstitute the capsid properties of the natural wild type AAV2, showed an excess of the positively charge amino acid arginine (R), resulting in an unexpected high rate of peptides with positive net charge. The non-binding pool, on the other hand, showed an excess of the negatively charged amino acids aspartic acid (D) and glutamic acid (E), resulting in unexpected high rate of negatively charged peptides[134]. These findings can be used to interpret the outcome of the library screenings analyzed in this study. Interestingly, the peptides presented in this study, enriched *in vivo* in murine brain and lung, changed during subsequent rounds of selection from a more wild type like and HSPG-binding pattern according to Perabo et al.[134] with an excess of small (A) or positively charged (R) amino acids to a more non-binding pattern with an excess of bulky aromatic residues (F, W, Y) or negatively charged amino acids (D, E). Since the goal of this study was the selection of particles with new binding properties that differ from wild type AAV2 (i.e. particles that do not bind to HSPG), the observed change in the amino acid sequences of enriched particles was interpreted as an indicator for a successfully accomplished screening.

5.5 Bioluminescence analyses of selected library particles

All clones matching the brain-enriched sequence motif X^{X}_{D}**G**XX**W**X as well as the most dominant lung-enriched clone ESGHGYF were thought to be worth further analyses. Wild type AAV2, the randomly picked clone CVGSPCG and the non-specific and widespread clone NNVRTSE were used as controls a) to analyze the differences between hypothetically tissue-specific *in vivo* selected clones and the unmodified natural variant, b) to gain information about the influence of random heptapeptide inserts in general and c) to test the hypothesis that widespread clones like NNVRTSE potentially

resemble the wild type AAV2 phenotype. Luciferase-mediated bioluminescence is commonly used to analyze gene expression in transgenic mouse models[238, 239] or rAAV vector studies[107, 112, 148, 240] since it is detectable even in very low quantities and it can be monitored *in vivo* in real time with little effort[241]. Thus, the library clones enriched *in vivo* and controls were produced as vectors carrying the luciferase gene under control of the strong and constitutive CMV promoter, which has been proven to drive strong gene expression in murine tissue *in* vivo[242], while only showing minor discrepancies between vector genome distribution and gene expression and therefore has been used in numerous comparable studies[107, 112, 147, 240]. The fact that all vectors, irrespective of the displayed peptide, were producible equally well with titers comparable to wild type rAAV2 vectors, clearly reconfirms that the selected peptides do not negatively influence capsid assembly and genome packaging, like already shown for pre-selected libraries during *in vivo* selection.

Bioluminescence imaging of living vector-treated mice and freshly explanted organs as well as bioluminescence analyses from homogenized tissues allowed characterizing the transduction profiles of selected library clones. Of note, data obtained by *in vivo* bioluminescence imaging and determination of luminescence from homogenized tissues showed a high degree of consistency. Still, it attracted our attention that luminescence in the brain could barely be detected *in vivo*, even if it was of moderate strength and clearly detectable in homogenized tissue. The reason for this phenomenon remains unclear, since the cranium is supposed to be well permeable for light emitted by firefly luciferase[243, 244]. Imaging of freshly explanted organs on the other hand seemed to show an unexpected high bias. Here, luminescence in brain and liver seemed to be clearly underestimated compared to *in vivo* imaging and measurement of luminescence from tissue lysates. This finding in turn could possibly be explained by the need of ATP and oxygen during conversion of the substrate luciferin which is needed for emission of light. It could be speculated that the levels of ATP and oxygen in brain and liver are subject to a fast decrease after explantation due to the high energy consumption of these organs. Nonetheless, no more than three minutes passed from the killing of mice to luminescence measurement of explanted organs *ex vivo* to keep this phenomenon to a minimum.

Overall the transgene expression pattern mediated by the wild type rAAV2 control vector seemed to be coherent with the findings published previously by our group and others[107, 112, 147, 240]. Generally wild type AAV2 is known to show transduction of the liver and to lesser extend of the heart. Luminescence measurement of homogenized tissues from wild type rAAV2-treated mice also revealed significant transgene expression in the brain and in the kidney, which could neither be observed *in vivo* nor in freshly explanted organs *ex vivo*. This does not necessarily contradict the previous findings, as liver, heart, kidney and spleen are referred to as “typical AAV targets”[112] and individual differences between different wild type rAAV2 preparations are well known among

scientist working with this vector (Dr. Stefan Michelfelder & Dr. Karl Varadi: personal communication).

Abrogation of the wild type AAV2 tropism and its re-direction from the liver towards heart and skeletal muscle as observed in this study with the randomly picked control clone CVGSPCG, one of the brain-selected clones (ADGVQWT) and the majority of the alanine mutants (which are discussed in more detail in chapter **5.11**) has already been reported for several HSPG-defective AAV2 mutants[45]. AAV2 library clones previously screened by our group in murine lung tissue or breast tumors[147] have also shown transduction of heart, in addition to the tissue they had been selected for. This observed phenomenon in HSPG-defective AAV2 mutants may have several reasons. Kern et al.[45] proposed that the lack of a receptor binding site for HSPG within the viral capsid most likely simply increases the particles' probability to act with one of its alternative secondary receptors like FGFR-1 or integrin αVß5 which are strongly expressed in heart tissue. Binding of HSPG-defective AAV2 mutants to integrin could be proven at least for several defined peptide inserts[132, 245]. Taken together, these findings could also be an explanation for the fact that until now there has not been any report of vectors selected from random AAV2 display peptide libraries with real tissue specificity for any other targets than the heart[148].

As already speculated, luminescence analyses indeed revealed that the non-specific clone NNVRTSE clearly resembles the wild type AAV2 tropism with predominant transduction of the liver and to lesser extent of the heart. This finding raises the question, how a predominantly liver-directed particle could have been enriched in diverse cell lines and tissues *in vitro* and *in vivo*. It can be speculated that particles which potentially have high similarity to the wild type AAV2 structure show superior stability and infectivity compared to structurally very different particles. This could be beneficial during particle production in HEK 293T producer cells. Still, the procedure of *in vivo* screening applied in this study seemed to have proven its functionality in terms of negative selection, since the non-specific clone NNVRTSE was no longer apparent after the fourth round of selection in the brain and at least was far from being dominant in the fourth round of selection in the lung.

All tested brain-enriched clones matching the motif X^{D}_{X}**G**XX**W**X indeed showed increased transgene expression in the brain while luminescence in the liver decreased compared to wild type AAV2 and the other control vectors. Thus, the concept of *in vivo* screening of random AAV2 display peptide libraries applied in this study has been proven to work.

5.6 Brain- and lung-enriched particles and their potential receptors

Surprisingly, most brain-enriched particles also mediated increased transgene expression in the lung, which for some clones (DDGVSWK, SDGLTWS) was even stronger than in the brain. These findings become even more interesting when also taking into account the lung-selected clone ESGHGYF. Although ESGHGYF has been shown to predominantly mediate transgene expression in its target organ, the lung, minor luminescence could also be detected in the brain. Since both *in vivo* screenings presented here have been performed independently from each other with a time lag of > 2 years, cross-contamination during selection can be excluded as an explanation for the apparently "connected" tropism for lung and brain tissue. Interestingly, Work at al.[138] reported of a phage display *in vivo* screening in brains and lungs of rats during which several clones could be enriched in both tissues. Although cross-contamination may not completely be excluded in case of the reported phage display screening[138], its results seem to support the authenticity of the findings presented here. Presumably, the targeted cells (i.e. microvascular endothelial cells, discussed in chapter **5.10**) within brain and lung share a common cell surface molecule which in turn distinguishes them from endothelial cells in other organs. The large diversity of the vascular endothelium is a well-known phenomenon which has been subject to numerous studies, analyzing differences in its phenotype (reviewed in ref.[246]), its transcriptome[247, 248], and its microRNA profile[249] or simply mapping its differences by phage display screenings[138, 250-254] ("vascular ZIP codes"). Since the endothelial diversity might also, at least partially, be caused by differences in glycosylation, like it has already been observed for inflammatory sites[255, 256] and AAV in general is well known to differentiate between diverse glycans[44, 62, 64, 257, 258], it is not an easy task to reveal the nature of the postulated structural similarity between vascular endothelium of brain and lung. However, the identification of the structure potentially serving as receptor for brain- and lung-homing particles is of high importance and subject of ongoing investigations in our laboratory, following three different routes:

1) immunoprecipitation of potential receptors from membrane protein-enriched tissue lysates (brain, lung and controls) with brain- and/or lung-enriched AAV library particles coupled to columns or magnetic beads
2) identification of proteins that are predominantly expressed in murine brain and/or lung by data mining followed by overexpression and/or knockdown of these proteins to alter the susceptibility of cell lines to brain- and/or lung-enriched AAV library particles
3) differential digestion of sugar structures on the surface of cells that are known to be susceptible to infection with brain- and/or lung-enriched AAV library particles (e.g. primary murine brain and/or lung microvasculature endothelial cells) and subsequent analyses of remaining susceptibility

5.7 Target specificity of the brain- and lung-enriched library particles

Despite the fact that all brain-enriched library clones seemed to mediate varying degrees of gene expression in the lung, and the lung-enriched clone ESGHGYF in turn mediated minor gene expression in the brain, at least when utilizing the CMV promoter, the clones NRGTEWD (brain) and ESGHGYF (lung) were still considered to be target specific, i.e. both of them mediated significant, at least ten-fold higher transgene expression in their respective target tissue compared to all other tested tissues. Targeted viral[140, 259, 260] and non-viral vectors[261-268] for brain and lung previously published by others, have either not been analyzed for their specificity after intravenous injection *in vivo*[261, 263, 264, 268], or their degree of specificity was far below the one observed for the AAV clones presented in this study, as far as comparable. Kumar at al.[262] achieved a three-fold stronger gene silencing in brain compared to liver and spleen by peptide-mediated siRNA transfer. Utilization of a monoclonal antibody against human insulin receptor, coupled to vector plasmid DNA in pegylated liposomes by Zhang et al.[265] achieved transgene expression in the brain half as strong as in the liver but three times stronger than in the spleen in rhesus monkeys and half as strong as in liver and spleen in rats. A peptide selected by phage display was used by Chen et al.[140] to direct modified AAV2 to the brain vasculature endothelium in equal amounts as to the liver. Wilson et al.[267] packaged oligodeoxynucleotides in lipid vectors coupled to endothelium specific antibody and could detect approx. 25% uptake in the lungs but over 30% uptake in the spleen, 45 min after application. An adenoviral vector coupled to an antibody against angiotensin-converting enzyme developed by Reynolds et al.[259] mediated a 20-fold increase in transgene expression in the lungs and a decrease of 80% in the liver compared to the unmodified control. Even an improved version of this adenoviral vector (which was described as being 300,000 times more specific) only showed two times stronger transgene expression in lung compared to the liver[260], indicating how unspecific the prior version of this vector must have been.

Thus, the brain- and lung-selected AAV library clones of this study appeared to be very promising and were therefore chosen for further analyses. Since the observed target specific transgene expression did not necessarily need to be caused by tissue-specific vector homing mediated by the selected targeting peptides but could have also been caused by transcriptional effects or by intracellular post-entry processing of the viral vectors[269, 270], the vector distribution was analyzed independently of transgene expression. Here, the distribution profiles of the brain- (NRGTEWD) and lung- (ESGHGYF) selected vectors roughly resembled their transgene expression profiles. Indeed, most vector genomes could be recovered from brain (NRGTEWD) and lung (ESGHYGF). Interestingly, a big fraction of each vector could be recovered from the spleen, although the amount of brain- and lung-selected vectors recovered from spleen was smaller than the amount of wild type rAAV2 vector. However, no transgene expression had been observed in this tissue. This finding can presumably be explained by

unspecific trapping of viral particles in the fenestrated spleen, independently of transduction. The lung-specific homing of ESGHGYF could also be reconfirmed by measuring vector genomes in individual organs as early as 4 h after injection.

5.8 Effect of the CAG promoter on transgene expression

After having confirmed that tissue specific transgene expression really is caused by peptide-mediated vector homing, a strategy was tested to further enhance expression strength. The hybrid CAG promoter[271] (a combination of the CMV early enhancer and the chicken ß–actin promoter, sometimes also referred to as CBA promoter) has been reported to outperform other constitutive promoters *in vivo* in brain, kidney, heart[272], the airway epithelium[190], in vascular progenitor cells[273], neurons[274, 275] and has been widely used to drive transgene expression in the brain. Therefore, the brain-and lung enriched peptides were tested as luciferase vectors utilizing the CAG promoter, after having already tested them with the CMV promoter. The observed overall increase in expression strength was surprisingly high with both tested vectors since it led to detectable luminescence in all organs, also in those that did not show any luminescence when utilizing the CMV promoter. Regarding the vector distribution quantified by qPCR, even extremely low copy numbers of vector genomes seemed to be sufficient to drive measurable gene expression when utilizing the CAG promoter. The observed high bias of the CAG promoter towards several organs was not completely unexpected but the inconsistency between the two tested vectors rAAV2-NRGTEWD and rAAV2-ESGHGYF was surprising. The differences in the CAG-mediated increase of transgene expression in single organs like the brain, observed for rAAV2-NRGTEWD (brain: 120-fold) and rAAV2-ESGHGYF (brain: 1,200-fold) can unlikely be explained by transduction of different cell types within these organs since an endothelial tropism has been shown for both vectors in later experiments. However, as the brain-selected vector rAAV2-NRGTEWD did not only show increased overall expression strength but also a higher specificity for the brain when equipped with the CAG- instead of the CMV promoter, the former was chosen for further experiments with this vector. The lung-selected vector rAAV2-ESGHYGYF on the other hand, did not benefit from the CAG promoter. The lung seemed to be one of the organs with the lowest increase in transgene expression compared to the brain as one of the organs with the highest increase. The specificity of rAAV2-ESGHGYF for the lung, determined by qPCR and CMV-driven luminescence could not be confirmed at expression level when using the CAG promoter since CAG-mediated expression in the brain outperformed expression in the lung. Therefore, all further experiments with rAAV2-ESGHGYF were performed with the CMV promoter. Admittedly, this phenomenon could not have been observed if the peptide ESGHGYF would provide

absolute specificity instead of just “a high degree” of specificity. Nevertheless, the presumption to achieve absolute specificity with any biological targeting system seems to be somewhat unrealistic.

5.9 Longterm transgene expression mediated by the lung-enriched peptide ESGHGYF

The lung-selected vector ESGHGYF was identified prior to the brain-selected vector NRGTEWD, leaving enough time to analyze its gene expression over a prolonged period of time. Within the last years AAV has occasionally been reported to elicit a T-cell response leading to elimination of transduced cells followed by a rapid decline of transgene expression in clinical trials[102-104]. Also transgenes like GFP[276] have been reported to provoke immune responses and viral promoters like the CMV promoter are suspected to be recognizable as viral elements by the host cell, potentially leading to down regulation of expression[277]. Still, most AAV serotypes have already proven to mediate luciferase expression driven by the CMV promoter in mice for at least 100 days[107]. Thus, the ESGHGYF-mediated transgene expression was analyzed in two different mouse strains, one immunocompetent (FVB/N) and one immunocompromised (SCID). Although transgene expression in the SCID mouse was approx. two times higher than transgene expression in FVB/N mice, it was surprisingly high and durable in both mouse strains. Stabilization of transgene expression could be observed in both mouse strains (after it had fallen to approx. the half of its initial strength around day 80), indicating the absence of major immunogenic effects. In contrast, the observed decrease in expression strength seems to be extremely small when taking into account that a) each cell has a certain turnover rate, b) rAAV vectors are believed to integrate into the host genome only at negligible rates, c) episomal vector DNA should only be passed to one daughter cell and d) treated mice had grown considerably during the experiment (they had more than doubled their weight between first and last evaluation of transgene expression!), leading to a “dilution” of vector-containing cells. The observed time range of 164/187 days might appear to be far from impressive from the human perspective but certainly is quite a long time in the life of a mouse. Unfortunately the SCID mouse died from anesthesia and could not be observed longer but the experiment with the FVB/N mice is still ongoing. A longterm experiment involving mice treated with the brain targeting vector NRGTEWD has been started very recently.

5.10 Endothelial transduction of brain- and lung-enriched library particles

For further potential therapeutic applications of the selected vectors, the identification of the actual target cells within the organs of interest was of high priority. Since vector DNA from whole homogenized organs has been used for the *in vivo* screening, selection was not directed towards defined cell types. Theoretically the selected particles could have been enriched in any of the different cell types in brain or lung. Certainly, there also would have been the possibility to screen the AAV library directly on defined cell types during the *in vivo* selection procedure. However, the isolation of single cells after each selection round would have been time- and labor- intensive and the amount of recovered viral DNA from those single cells could have been too little to generate subsequent libraries. Thus, it had initially been decided to perform the screening on whole organs and to identify the target cells after successful *in vivo* selection.

Immunohistochemistry clearly revealed the vasculature of brain and lung being the target structures for the selected peptides. In case of the brain-selected peptide NRGTEWD, the immunofluorescence co-stainings of brain tissue with antibodies against CD31 (endothelial cells) and CD13 (pericytes) were not easily distinguishable since both cell layers are tightly connected to form the blood brain barrier. However, the vector-mediated fluorescence showed much higher congruency to the CD31 staining pattern than to the CD13 staining. The endothelial tropism of NRGTEWD could also be reconfirmed *in vitro* on murine primary brain microvasculature endothelial cells (data not shown). Interestingly, injection of rAAV2-NRGTEWD at a dose of 1.6×10^{11} gp/mouse yielded as much as ≈ 50% transduced endothelial cells throughout the entire brain but fluorescence was not completely restricted to this organ and also included the spinal cord. This finding indicates the existence of a structural similarity of the vasculature endothelium of the entire CNS (brain and spinal cord), i.e. the existence of a particular cell curface molecule which could be used as attachment receptor by the brain-targeted AAV and which might be connected with the function of the endothelium as part of the BBB (e.g. a protein associated with tight junctions).

In the lung, the identity of endothelial cells as targets of the lung-targeted ESGHGYF vectors could not be proven by direct immunofluorescent double staining within a single tissue section. Immunofluorescence in the lung is difficult to perform when the integrity of anatomic structure is needed. In contrast to the brain, the fragile natural macroscopic structure of the lung is not easily preservable after removal of the organ for post mortem analyses. Structural integrity of the lung is best preserved in inflated paraffin embedded tissue. Paraffin embedded tissues, on the other hand, are not well suited for immunofluorescence stainings. Thus, the endothelial nature of the ESGHGYF-mediated eGFP staining of lung vasculature was confirmed by serial sections revealing exactly the same staining pattern when treated with CD31 antibody.

5.11 Alanine scanning mutagenesis of brain- and lung-enriched library particles

After having analyzed the tissue-specific tropism of the brain- and lung-enriched capsid variants, it was tried to gain insights into their structural characteristics. To test the importance of each single amino acid for the selected peptide's functional integrity, alanine scanning mutagenesis[278] was performed. The fact that none of the amino acids contained in the peptide NRGTEWD could be replaced without abrogating its brain tropism clearly demonstrates the difference between peptide libraries either displayed on phages or on AAV. Peptides presented on phages usually act as "autonomous", structurally more or less independent entities. Often they have a free N-terminus and are C-terminally fused to a linker which minimizes the interactions between structural phage proteins and the presented peptides[279]. Therefore it is less likely that the replacement of single amino acids within phage-presented peptides leads to major structural rearrangements unless they involve amino acids directly contributing to the physical interaction with the binding partner (here: the receptor). In AAV display peptide libraries on the other hand, like the one utilized in this study, the peptides are embedded within the tight protein context of the AAV capsid and forced into its structural constraints[141]. It seems to be a realistic assumption that the replacement of single amino acids in AAV virion-embedded peptides leads to bigger structural rearrangements than in the comparably flexible phage-displayed peptides. Nevertheless, the peptide ESGHGYF allowed the replacement of each of the two first amino acids without being altered substantially in its tropism. The unexpected increase in vector transduction after replacement of glutamic acid (E) by alanine (A) may be explained by the low theoretical probability of any given peptide to be included in a peptide library at all, due to the library's limited diversity. This could lead to the enrichment of particles which may not present the theoretically best peptide for a given purpose but possibly the second or third best. Such peptides could display single amino acids interfering with their intended purpose, solely because no superior peptide versions would be selected during the screening procedure. If ESGHGYF was such a peptide, the observed improved lung transduction after replacement of the hypothetically interfering glutamic acid would be reasonable. Still, this finding contradicts the proposed importance of negatively charged amino acids on the peptides functionality discussed before (page 116). The enhanced transduction of brain tissue by three of the seven alanine mutants (EAGHGYF, ESAHGYF, ESGAGYF) was another remarkable finding, which supports the idea of the proposed similarity between the vascular endothelium of brain and lung. As mentioned above, ongoing efforts in our laboratory aim to identify these hypothetical similarities.

The functional prediction of virion-embedded peptides seems not to be easy and the choice of the right peptides after a successful *in vivo* screening remains one of the major challenges. Although the *in vivo* screenings described in this study both yielded well suited, efficient and highly specific

vectors, it remains unclear why prior *in vivo* sceenings[112, 147] have been less successful in terms of specificity. Since conventional sequencing of few library clones after each selection round only provides extremely limited information about the real composition of the enriched pool of capsid variants, an improved and yet unpublished approach of *in vivo* screening has recently been developed in our laboratory, utilizing the advantages of next generation sequencing (NGS). By sequencing extremely large numbers of library particles enriched in the tissue of interest and control organs, scores for the particles' efficacy and specificity can be calculated, allowing the precise prediction of candidates meeting all demands. Applied to the lung, the NGS-guided *in vivo* screening approach indeed reconfirmed ESGHGYF as being the library's best suited peptides for target-specific redirection of AAV2.

5.12 Outlook

Taken together, this is the first report of rAAV vectors selected from random AAV display peptide libraries that enable specific transduction of target organs other than the heart[148] after simple intravenous injection. Transgene expression mediated by these vectors has been proven to be restricted to the vascular endothelium of their respective target organs.

Since preclinical studies with modified AAV vectors in mice have previously identified the brain endothelium as clinically highly relevant tissue and target site for gene-based interventions in the CNS[140], the findings presented in this study appear to be very promising. In terms of specificity and efficacy, the selected library clone NRGTEWD seems to outperform all previously published vectors[138, 140, 262, 265], at least after intravenous injection. Therefore, a preclinical study utilizing the brain-targeting vector rAAV2-NRGTEWD is about to begin with two different settings aiming at the treatment of experimental autoimmune encephalomyelitis (EAE), a mouse model for brain inflammatory diseases like multiple sclerosis (reviewed in ref.[280]). The chemokine CCL2 (also referred to as monocyte chemoattractant protein 1 = MCP1) plays a crucial role in inflammation by disrupting the tight junctions of the BBB and stimulating immune cell infiltration into the CNS[281-287] . It is planned to abrogate the immunostimulative functions of CCL2 by rAAV2-NRGTEWD-mediated overexpression of a dominant negative mutant (CCL2-7ND) which forms heterodimers with CCL2 that still bind to CCR2 but inhibit downstream signalling, thereby abrogating monocyte chemotaxis[288]. In another setting with the same mouse model it is planned to overexpress claudin-1 to seal the BBB which is leaky in EAE mice due to a disease-correlated loss of claudin-3. Proof-of-principle for this approach has been provided in a study on claudin-1 transgenic EAE mice[289].

Important lung diseases involving the airways and the pulmonary epithelium like CF[179] and AAT-deficiency[180] have been subject to numerous preclinical and clinical gene therapy trials, mostly

utilizing vectors based on adenovirus[181, 290] or AAV[62, 115, 187-190, 234] by inhalative application. Other severe pulmonary diseases like PH have also been addressed in gene therapy studies based on vector inhalation[193, 194], irrespective of the fact that the target structure (i.e. the endothelium of the pulmonary vasculature) is barely transducible via the airways. Thus, it is planned to use the lung-targeted vector rAAV2-ESGHGYF to treat PH in a mouse model by two different approaches. By overexpression of the inducible nitric oxide synthase (iNOS = NOS2), it is planned to utilize the vasodilatory effect of NO to lower the elevated blood pressure in the right heart of PH mice, a concept which has already been proven to work with less specific and less efficient adenoviral vectors[291, 292], even with less efficient NOS species[293] like the endothelial NOS (eNOS =NOS3). In another approach, it will be tried to overexpress the bone morphogenetic protein receptor type II (BMPR2) in lung endothelia using an ESGHGYF vector, since this protein is described to positively influence the course of disease[294, 295], potentially due to its pro-apoptotic effect on the remodeld and thickened vasculature in PH patients[296]. An endothelium-targeted adenoviral vector, coupled to bi-specific antibodies against angiotensin-converting enzyme (ACE) and equipped with the BMPR2 gene, has recently proven the positive influence of BMPR2 on PH in a preclinical model[192]. Since the lung-targeted rAAV vector presented in this study seems to be of much higher efficacy and specificity than the ACE-directed adenovirus[192, 259, 260], it is very likely to achieve even more impressive therapeutic effects.

Besides the potential therapeutic utility of our lung- and brain-targeted vectors, the work presented here could have even much broader implications in the field of gene therapy and translational research since the functionality of random AAV display peptide libraries *in vivo* is not necessarily restricted to the brain and the lung but very likely might also be applicable to any given tissue of interest. The question wether sucessfully enriched library particles are restricted to the species in which the library was screened needs to be addressed in larger animal models. The applicability of vectors - such as the ones presented in this study – also for human gene therapy might be possible and will be better assessable after identification of their receptors.

6 References

1. Tatum, E.L. Molecular biology, nucleic acids, and the future of medicine. *Perspect Biol Med* **10**, 19-32 (1966).

2. Friedmann, T. & Roblin, R. Gene therapy for human genetic disease? *Science* **175**, 949-955 (1972).

3. Blaese, R.M., Culver, K.W., Miller, A.D., Carter, C.S., Fleisher, T. et al. T lymphocyte-directed gene therapy for ADA- SCID: initial trial results after 4 years. *Science* **270**, 475-480 (1995).

4. Eibel, B., Rodrigues, C.G., Giusti, II, Nesralla, I.A., Prates, P.R. et al. Gene therapy for ischemic heart disease: review of clinical trials. *Rev Bras Cir Cardiovasc* **26**, 635-646 (2012).

5. Griesenbach, U. & Alton, E.W. Gene transfer to the lung: lessons learned from more than 2 decades of CF gene therapy. *Adv Drug Deliv Rev* **61**, 128-139 (2009).

6. Coune, P.G., Schneider, B.L. & Aebischer, P. Parkinson's disease: gene therapies. *Cold Spring Harb Perspect Med* **2**, a009431 (2012).

7. Cross, D. & Burmester, J.K. Gene therapy for cancer treatment: past, present and future. *Clin Med Res* **4**, 218-227 (2006).

8. Gene Therapy Clinical Trials Worldwide (2013), Web Page: http://www.wiley.com/legacy/wileychi/genmed/clinical/ Date cited: 2013/03/13

9. Herzog, R.W., Cao, O. & Srivastava, A. Two decades of clinical gene therapy--success is finally mounting. *Discov Med* **9**, 105-111 (2010).

10. Grossman, M., Raper, S.E., Kozarsky, K., Stein, E.A., Engelhardt, J.F. et al. Successful ex vivo gene therapy directed to liver in a patient with familial hypercholesterolaemia. *Nat Genet* **6**, 335-341 (1994).

11. Aiuti, A., Slavin, S., Aker, M., Ficara, F., Deola, S. et al. Correction of ADA-SCID by stem cell gene therapy combined with nonmyeloablative conditioning. *Science* **296**, 2410-2413 (2002).

12. Follistatin Gene Transfer to Patients With Becker Muscular Dystrophy and Sporadic Inclusion Body Myositis (2012), Web Page: http://clinicaltrials.gov/show/NCT01519349 Date cited: 2013/03/11

13. Kaplitt, M.G., Feigin, A., Tang, C., Fitzsimons, H.L., Mattis, P. et al. Safety and tolerability of gene therapy with an adeno-associated virus (AAV) borne GAD gene for Parkinson's disease: an open label, phase I trial. *Lancet* **369**, 2097-2105 (2007).

14. Kay, M.A., Glorioso, J.C. & Naldini, L. Viral vectors for gene therapy: the art of turning infectious agents into vehicles of therapeutics. *Nat Med* **7**, 33-40 (2001).

15. Thomas, C.E., Ehrhardt, A. & Kay, M.A. Progress and problems with the use of viral vectors for gene therapy. *Nat Rev Genet* **4**, 346-358 (2003).

16. Jafari, M., Soltani, M., Naahidi, S., Karunaratne, D.N. & Chen, P. Nonviral approach for targeted nucleic acid delivery. *Curr Med Chem* **19**, 197-208 (2012).

17. Gao, X., Kim, K.S. & Liu, D. Nonviral gene delivery: what we know and what is next. *AAPS J* **9**, E92-104 (2007).

18. Waehler, R., Russell, S.J. & Curiel, D.T. Engineering targeted viral vectors for gene therapy. *Nat Rev Genet* **8**, 573-587 (2007).

19. Michelfelder, S. & Trepel, M. Adeno-associated viral vectors and their redirection to cell-type specific receptors. *Adv Genet* **67**, 29-60 (2009).

20. Goncalves, M.A. Adeno-associated virus: from defective virus to effective vector. *Virol J* **2**, 43 (2005).

21. Boutin, S., Monteilhet, V., Veron, P., Leborgne, C., Benveniste, O. et al. Prevalence of serum IgG and neutralizing factors against adeno-associated virus (AAV) types 1, 2, 5, 6, 8, and 9 in the healthy population: implications for gene therapy using AAV vectors. *Hum Gene Ther* **21**, 704-712 (2010).

22. Gao, G., Vandenberghe, L.H., Alvira, M.R., Lu, Y., Calcedo, R. et al. Clades of Adeno-associated viruses are widely disseminated in human tissues. *J Virol* **78**, 6381-6388 (2004).

23. McCarty, D.M., Young, S.M., Jr. & Samulski, R.J. Integration of adeno-associated virus (AAV) and recombinant AAV vectors. *Annu Rev Genet* **38**, 819-845 (2004).

24. Kotin, R.M., Linden, R.M. & Berns, K.I. Characterization of a preferred site on human chromosome 19q for integration of adeno-associated virus DNA by non-homologous recombination. *Embo J* **11**, 5071-5078 (1992).

25. Samulski, R.J., Zhu, X., Xiao, X., Brook, J.D., Housman, D.E. et al. Targeted integration of adeno-associated virus (AAV) into human chromosome 19. *Embo J* **10**, 3941-3950 (1991).

26. Hamilton, H., Gomos, J., Berns, K.I. & Falck-Pedersen, E. Adeno-associated virus site-specific integration and AAVS1 disruption. *J Virol* **78**, 7874-7882 (2004).

27. Atchison, R.W., Casto, B.C. & Hammon, W.M. Adenovirus-Associated Defective Virus Particles. *Science* **149**, 754-756 (1965).

28. Srivastava, A., Lusby, E.W. & Berns, K.I. Nucleotide sequence and organization of the adeno-associated virus 2 genome. *J Virol* **45**, 555-564 (1983).

29. Koczot, F.J., Carter, B.J., Garon, C.F. & Rose, J.A. Self-complementarity of terminal sequences within plus or minus strands of adenovirus-associated virus DNA. *Proc Natl Acad Sci U S A* **70**, 215-219 (1973).

30. Berns, K.I. Parvovirus replication. *Microbiol Rev* **54**, 316-329 (1990).

31. Ryan, J.H., Zolotukhin, S. & Muzyczka, N. Sequence requirements for binding of Rep68 to the adeno-associated virus terminal repeats. *J Virol* **70**, 1542-1553 (1996).

32. Im, D.S. & Muzyczka, N. The AAV origin binding protein Rep68 is an ATP-dependent site-specific endonuclease with DNA helicase activity. *Cell* **61**, 447-457 (1990).

33. Snyder, R.O., Im, D.S., Ni, T., Xiao, X., Samulski, R.J. et al. Features of the adeno-associated virus origin involved in substrate recognition by the viral Rep protein. *J Virol* **67**, 6096-6104 (1993).

34. Brister, J.R. & Muzyczka, N. Mechanism of Rep-mediated adeno-associated virus origin nicking. *J Virol* **74**, 7762-7771 (2000).

35. Smith, R.H. & Kotin, R.M. The Rep52 gene product of adeno-associated virus is a DNA helicase with 3'-to-5' polarity. *J Virol* **72**, 4874-4881 (1998).

36. Bleker, S., Sonntag, F. & Kleinschmidt, J.A. Mutational analysis of narrow pores at the fivefold symmetry axes of adeno-associated virus type 2 capsids reveals a dual role in genome packaging and activation of phospholipase A2 activity. *J Virol* **79**, 2528-2540 (2005).

37. King, J.A., Dubielzig, R., Grimm, D. & Kleinschmidt, J.A. DNA helicase-mediated packaging of adeno-associated virus type 2 genomes into preformed capsids. *Embo J* **20**, 3282-3291 (2001).

38. Trempe, J.P. & Carter, B.J. Alternate mRNA splicing is required for synthesis of adeno-associated virus VP1 capsid protein. *J Virol* **62**, 3356-3363 (1988).

39. Sonntag, F., Schmidt, K. & Kleinschmidt, J.A. A viral assembly factor promotes AAV2 capsid formation in the nucleolus. *Proc Natl Acad Sci U S A* **107**, 10220-10225 (2010).

40. Grieger, J.C., Snowdy, S. & Samulski, R.J. Separate basic region motifs within the adeno-associated virus capsid proteins are essential for infectivity and assembly. *J Virol* **80**, 5199-5210 (2006).

41. Grieger, J.C., Johnson, J.S., Gurda-Whitaker, B., Agbandje-McKenna, M. & Samulski, R.J. Surface-exposed adeno-associated virus Vp1-NLS capsid fusion protein rescues infectivity of noninfectious wild-type Vp2/Vp3 and Vp3-only capsids but not that of fivefold pore mutant virions. *J Virol* **81**, 7833-7843 (2007).

42. Girod, A., Wobus, C.E., Zadori, Z., Ried, M., Leike, K. et al. The VP1 capsid protein of adeno-associated virus type 2 is carrying a phospholipase A2 domain required for virus infectivity. *J Gen Virol* **83**, 973-978 (2002).

43. Xie, Q., Bu, W., Bhatia, S., Hare, J., Somasundaram, T. et al. The atomic structure of adeno-associated virus (AAV-2), a vector for human gene therapy. *Proc Natl Acad Sci U S A* **99**, 10405-10410 (2002).

44. Summerford, C. & Samulski, R.J. Membrane-associated heparan sulfate proteoglycan is a receptor for adeno-associated virus type 2 virions. *Journal of Virology* **72**, 1438-1445 (1998).

45. Kern, A., Schmidt, K., Leder, C., Muller, O.J., Wobus, C.E. et al. Identification of a heparin-binding motif on adeno-associated virus type 2 capsids. *Journal of Virology* **77**, 11072-11081 (2003).

46. Opie, S.R., Warrington, K.H., Agbandje-McKenna, M., Zolotukhin, S. & Muzyczka, N. Identification of amino acid residues in the capsid proteins of adeno-associated virus type 2 that contribute to heparan sulfate proteoglycan binding. *Journal of Virology* **77**, 6995-7006 (2003).

47. Summerford, C., Bartlett, J.S. & Samulski, R.J. alpha V beta 5 integrin: a co-receptor for adeno-associated virus type 2 infection. *Nature Medicine* **5**, 78-82 (1999).

48. Asokan, A., Hamra, J.B., Govindasamy, L., Agbandje-McKenna, M. & Samulski, R.J. Adeno-associated virus type 2 contains an integrin alpha5beta1 binding domain essential for viral cell entry. *J Virol* **80**, 8961-8969 (2006).

49. Qing, K., Mah, C., Hansen, J., Zhou, S.Z., Dwarki, V. et al. Human fibroblast growth factor receptor 1 is a co-receptor for infection by adeno-associated virus 2. *Nature Medicine* **5**, 71-77 (1999).

50. Kashiwakura, Y., Tamayose, K., Iwabuchi, K., Hirai, Y., Shimada, T. et al. Hepatocyte growth factor receptor is a coreceptor for adeno-associated virus type 2 infection. *J Virol* **79**, 609-614 (2005).

51. Akache, B., Grimm, D., Pandey, K., Yant, S.R., Xu, H. et al. The 37/67-kilodalton laminin receptor is a receptor for adeno-associated virus serotypes 8, 2, 3, and 9. *J Virol* **80**, 9831-9836 (2006).

52. Lerch, T.F., Xie, Q. & Chapman, M.S. The structure of adeno-associated virus serotype 3B (AAV-3B): insights into receptor binding and immune evasion. *Virology* **403**, 26-36 (2010).

53. Padron, E., Bowman, V., Kaludov, N., Govindasamy, L., Levy, H. et al. Structure of adeno-associated virus type 4. *J Virol* **79**, 5047-5058 (2005).

54. Walters, R.W., Agbandje-McKenna, M., Bowman, V.D., Moninger, T.O., Olson, N.H. et al. Structure of adeno-associated virus serotype 5. *J Virol* **78**, 3361-3371 (2004).

55. Xie, Q., Lerch, T.F., Meyer, N.L. & Chapman, M.S. Structure-function analysis of receptor-binding in adeno-associated virus serotype 6 (AAV-6). *Virology* **420**, 10-19 (2011).

56. Nam, H.J., Lane, M.D., Padron, E., Gurda, B., McKenna, R. et al. Structure of adeno-associated virus serotype 8, a gene therapy vector. *J Virol* **81**, 12260-12271 (2007).

57. DiMattia, M.A., Nam, H.J., Van Vliet, K., Mitchell, M., Bennett, A. et al. Structural insight into the unique properties of adeno-associated virus serotype 9. *J Virol* **86**, 6947-6958 (2012).

58. Blackburn, S.D., Steadman, R.A. & Johnson, F.B. Attachment of adeno-associated virus type 3H to fibroblast growth factor receptor 1. *Arch Virol* **151**, 617-623 (2006).

59. Kaludov, N., Brown, K.E., Walters, R.W., Zabner, J. & Chiorini, J.A. Adeno-associated virus serotype 4 (AAV4) and AAV5 both require sialic acid binding for hemagglutination and efficient transduction but differ in sialic acid linkage specificity. *J Virol* **75**, 6884-6893 (2001).

60. Di Pasquale, G., Davidson, B.L., Stein, C.S., Martins, I., Scudiero, D. et al. Identification of PDGFR as a receptor for AAV-5 transduction. *Nat Med* **9**, 1306-1312 (2003).

61. Seiler, M.P., Miller, A.D., Zabner, J. & Halbert, C.L. Adeno-associated virus types 5 and 6 use distinct receptors for cell entry. *Hum Gene Ther* **17**, 10-19 (2006).

62. Halbert, C.L., Allen, J.M. & Miller, A.D. Adeno-associated virus type 6 (AAV6) vectors mediate efficient transduction of airway epithelial cells in mouse lungs compared to that of AAV2 vectors. *J Virol* **75**, 6615-6624 (2001).

63. Weller, M.L., Amornphimoltham, P., Schmidt, M., Wilson, P.A., Gutkind, J.S. et al. Epidermal growth factor receptor is a co-receptor for adeno-associated virus serotype 6. *Nat Med* **16**, 662-664 (2010).

64. Shen, S., Bryant, K.D., Brown, S.M., Randell, S.H. & Asokan, A. Terminal N-linked galactose is the primary receptor for adeno-associated virus 9. *J Biol Chem* **286**, 13532-13540 (2011).

65. Duan, D., Li, Q., Kao, A.W., Yue, Y., Pessin, J.E. et al. Dynamin is required for recombinant adeno-associated virus type 2 infection. *J Virol* **73**, 10371-10376 (1999).

66. Bartlett, J.S., Wilcher, R. & Samulski, R.J. Infectious entry pathway of adeno-associated virus and adeno-associated virus vectors. *J Virol* **74**, 2777-2785 (2000).

67. Ding, W., Zhang, L., Yan, Z. & Engelhardt, J.F. Intracellular trafficking of adeno-associated viral vectors. *Gene Ther* **12**, 873-880 (2005).

68. Sanlioglu, S., Benson, P.K., Yang, J., Atkinson, E.M., Reynolds, T. et al. Endocytosis and nuclear trafficking of adeno-associated virus type 2 are controlled by rac1 and phosphatidylinositol-3 kinase activation. *J Virol* **74**, 9184-9196 (2000).

69. Xiao, P.J. & Samulski, R.J. Cytoplasmic trafficking, endosomal escape, and perinuclear accumulation of adeno-associated virus type 2 particles are facilitated by microtubule network. *J Virol* **86**, 10462-10473 (2012).

70. Linden, R.M., Winocour, E. & Berns, K.I. The recombination signals for adeno-associated virus site-specific integration. *Proc Natl Acad Sci U S A* **93**, 7966-7972 (1996).

71. Wonderling, R.S. & Owens, R.A. Binding sites for adeno-associated virus Rep proteins within the human genome. *J Virol* **71**, 2528-2534 (1997).

72. Young, S.M., Jr. & Samulski, R.J. Adeno-associated virus (AAV) site-specific recombination does not require a Rep-dependent origin of replication within the AAV terminal repeat. *Proc Natl Acad Sci U S A* **98**, 13525-13530 (2001).

73. Samulski, R.J. & Shenk, T. Adenovirus E1B 55-Mr polypeptide facilitates timely cytoplasmic accumulation of adeno-associated virus mRNAs. *J Virol* **62**, 206-210 (1988).

74. Yalkinoglu, A.O., Heilbronn, R., Burkle, A., Schlehofer, J.R. & zur Hausen, H. DNA amplification of adeno-associated virus as a response to cellular genotoxic stress. *Cancer Res* **48**, 3123-3129 (1988).

75. Bantel-Schaal, U. Carcinogen-induced accumulation of adeno-associated parvovirus DNA is transient as a result of two antagonistic activities that both require de novo protein synthesis. *Int J Cancer* **53**, 334-339 (1993).

76. Hunter, L.A. & Samulski, R.J. Colocalization of adeno-associated virus Rep and capsid proteins in the nuclei of infected cells. *J Virol* **66**, 317-324 (1992).

77. Wistuba, A., Kern, A., Weger, S., Grimm, D. & Kleinschmidt, J.A. Subcellular compartmentalization of adeno-associated virus type 2 assembly. *J Virol* **71**, 1341-1352 (1997).

78. Buning, H., Perabo, L., Coutelle, O., Quadt-Humme, S. & Hallek, M. Recent developments in adeno-associated virus vector technology. *J Gene Med* **10**, 717-733 (2008).

79. Xiao, X., Li, J. & Samulski, R.J. Production of high-titer recombinant adeno-associated virus vectors in the absence of helper adenovirus. *Journal of Virology* **72**, 2224-2232 (1998).

80. Urabe, M., Ding, C. & Kotin, R.M. Insect cells as a factory to produce adeno-associated virus type 2 vectors. *Hum Gene Ther* **13**, 1935-1943 (2002).

81. Kohlbrenner, E., Aslanidi, G., Nash, K., Shklyaev, S., Campbell-Thompson, M. et al. Successful production of pseudotyped rAAV vectors using a modified baculovirus expression system. *Mol Ther* **12**, 1217-1225 (2005).

82. Carter, B.J. Adeno-associated virus vectors in clinical trials. *Hum Gene Ther* **16**, 541--550 (2005).

83. Donsante, A., Vogler, C., Muzyczka, N., Crawford, J.M., Barker, J. et al. Observed incidence of tumorigenesis in long-term rodent studies of rAAV vectors. *Gene Ther* **8**, 1343-1346 (2001).

84. Bell, P., Moscioni, A.D., McCarter, R.J., Wu, D., Gao, G. et al. Analysis of tumors arising in male B6C3F1 mice with and without AAV vector delivery to liver. *Mol Ther* **14**, 34-44 (2006).

85. Nathwani, A.C., Cochrane, M., McIntosh, J., Ng, C.Y., Zhou, J. et al. Enhancing transduction of the liver by adeno-associated viral vectors. *Gene Ther* **16**, 60-69 (2009).

86. Snyder, R.O., Miao, C., Meuse, L., Tubb, J., Donahue, B.A. et al. Correction of hemophilia B in canine and murine models using recombinant adeno-associated viral vectors. *Nat Med* **5**, 64-70 (1999).

87. Mount, J.D., Herzog, R.W., Tillson, D.M., Goodman, S.A., Robinson, N. et al. Sustained phenotypic correction of hemophilia B dogs with a factor IX null mutation by liver-directed gene therapy. *Blood* **99**, 2670-2676 (2002).

88. Dong, J.Y., Fan, P.D. & Frizzell, R.A. Quantitative analysis of the packaging capacity of recombinant adeno-associated virus. *Hum Gene Ther* **7**, 2101-2112 (1996).

89. Hermonat, P.L., Quirk, J.G., Bishop, B.M. & Han, L. The packaging capacity of adeno-associated virus (AAV) and the potential for wild-type-plus AAV gene therapy vectors. *FEBS Lett* **407**, 78-84 (1997).

90. Wu, Z., Yang, H. & Colosi, P. Effect of genome size on AAV vector packaging. *Mol Ther* **18**, 80-86 (2010).

91. Duan, D., Yue, Y. & Engelhardt, J.F. Expanding AAV packaging capacity with trans-splicing or overlapping vectors: a quantitative comparison. *Mol Ther* **4**, 383-391 (2001).

92. Ferrari, F.K., Samulski, T., Shenk, T. & Samulski, R.J. Second-strand synthesis is a rate-limiting step for efficient transduction by recombinant adeno-associated virus vectors. *J Virol* **70**, 3227-3234 (1996).

93. McCarty, D.M., Monahan, P.E. & Samulski, R.J. Self-complementary recombinant adeno-associated virus (scAAV) vectors promote efficient transduction independently of DNA synthesis. *Gene Ther* **8**, 1248-1254 (2001).

94. Wang, Z., Ma, H.I., Li, J., Sun, L., Zhang, J. et al. Rapid and highly efficient transduction by double-stranded adeno-associated virus vectors in vitro and in vivo. *Gene Ther* **10**, 2105-2111 (2003).

95. Ren, C., Kumar, S., Shaw, D.R. & Ponnazhagan, S. Genomic stability of self-complementary adeno-associated virus 2 during early stages of transduction in mouse muscle in vivo. *Hum Gene Ther* **16**, 1047-1057 (2005).

96. Hernandez, Y.J., Wang, J., Kearns, W.G., Loiler, S., Poirier, A. et al. Latent adeno-associated virus infection elicits humoral but not cell-mediated immune responses in a nonhuman primate model. *J Virol* **73**, 8549-8558 (1999).

97. Zaiss, A.K. & Muruve, D.A. Immune responses to adeno-associated virus vectors. *Curr Gene Ther* **5**, 323-331 (2005).

98. Rapti, K., Louis-Jeune, V., Kohlbrenner, E., Ishikawa, K., Ladage, D. et al. Neutralizing antibodies against AAV serotypes 1, 2, 6, and 9 in sera of commonly used animal models. *Mol Ther* **20**, 73-83 (2012).

99. Mingozzi, F. & High, K.A. Therapeutic in vivo gene transfer for genetic disease using AAV: progress and challenges. *Nat Rev Genet* **12**, 341-355 (2011).

100. Chen, J., Wu, Q., Yang, P., Hsu, H.C. & Mountz, J.D. Determination of specific CD4 and CD8 T cell epitopes after AAV2- and AAV8-hF.IX gene therapy. *Mol Ther* **13**, 260-269 (2006).

101. Wang, L., Figueredo, J., Calcedo, R., Lin, J. & Wilson, J.M. Cross-presentation of adeno-associated virus serotype 2 capsids activates cytotoxic T cells but does not render hepatocytes effective cytolytic targets. *Hum Gene Ther* **18**, 185-194 (2007).

102. Manno, C.S., Pierce, G.F., Arruda, V.R., Glader, B., Ragni, M. et al. Successful transduction of liver in hemophilia by AAV-Factor IX and limitations imposed by the host immune response. *Nat Med* **12**, 342-347 (2006).

103. Nathwani, A.C., Tuddenham, E.G., Rangarajan, S., Rosales, C., McIntosh, J. et al. Adenovirus-associated virus vector-mediated gene transfer in hemophilia B. *N Engl J Med* **365**, 2357-2365 (2011).

104. Li, H., Lasaro, M.O., Jia, B., Lin, S.W., Haut, L.H. et al. Capsid-specific T-cell responses to natural infections with adeno-associated viruses in humans differ from those of nonhuman primates. *Mol Ther* **19**, 2021-2030 (2011).

105. Vandenberghe, L.H., Wang, L., Somanathan, S., Zhi, Y., Figueredo, J. et al. Heparin binding directs activation of T cells against adeno-associated virus serotype 2 capsid. *Nat Med* **12**, 967-971 (2006).

106. Moskalenko, M., Chen, L., van Roey, M., Donahue, B.A., Snyder, R.O. et al. Epitope mapping of human anti-adeno-associated virus type 2 neutralizing antibodies: implications for gene therapy and virus structure. *J Virol* **74**, 1761-1766 (2000).

107. Zincarelli, C., Soltys, S., Rengo, G. & Rabinowitz, J.E. Analysis of AAV Serotypes 1-9 Mediated Gene Expression and Tropism in Mice After Systemic Injection. *Mol Ther* (2008).

108. Bowles, D.E., Rabinowitz, J.E. & Samulski, R.J. Marker rescue of adeno-associated virus (AAV) capsid mutants: a novel approach for chimeric AAV production. *J Virol* **77**, 423-432 (2003).

109. Hauck, B., Chen, L. & Xiao, W. Generation and characterization of chimeric recombinant AAV vectors. *Mol Ther* **7**, 419-425 (2003).

110. Rabinowitz, J.E., Bowles, D.E., Faust, S.M., Ledford, J.G., Cunningham, S.E. et al. Cross-dressing the virion: the transcapsidation of adeno-associated virus serotypes functionally defines subgroups. *J Virol* **78**, 4421-4432 (2004).

111. Wu, Z., Asokan, A. & Samulski, R.J. Adeno-associated virus serotypes: vector toolkit for human gene therapy. *Mol Ther* **14**, 316-327 (2006).

112. Grimm, D., Lee, J.S., Wang, L., Desai, T., Akache, B. et al. In vitro and in vivo gene therapy vector evolution via multispecies interbreeding and re-targeting of adeno-associated viruses. *J Virol* (2008).

113. Koerber, J.T., Jang, J.H. & Schaffer, D.V. DNA shuffling of adeno-associated virus yields functionally diverse viral progeny. *Mol Ther* **16**, 1703-1709 (2008).

114. Excoffon, K.J., Koerber, J.T., Dickey, D.D., Murtha, M., Keshavjee, S. et al. Directed evolution of adeno-associated virus to an infectious respiratory virus. *Proc Natl Acad Sci U S A* **106**, 3865-3870 (2009).

115. Li, W., Zhang, L., Johnson, J.S., Zhijian, W., Grieger, J.C. et al. Generation of novel AAV variants by directed evolution for improved CFTR delivery to human ciliated airway epithelium. *Mol Ther* **17**, 2067-2077 (2009).

116. Romero, P.A. & Arnold, F.H. Exploring protein fitness landscapes by directed evolution. *Nat Rev Mol Cell Biol* **10**, 866-876 (2009).

117. Yang, L., Jiang, J., Drouin, L.M., Agbandje-McKenna, M., Chen, C. et al. A myocardium tropic adeno-associated virus (AAV) evolved by DNA shuffling and in vivo selection. *Proc Natl Acad Sci U S A* **106**, 3946-3951 (2009).

118. Gray, S.J., Blake, B.L., Criswell, H.E., Nicolson, S.C., Samulski, R.J. et al. Directed evolution of a novel adeno-associated virus (AAV) vector that crosses the seizure-compromised blood-brain barrier (BBB). *Mol Ther* **18**, 570-578 (2010).

119. Maheshri, N., Koerber, J.T., Kaspar, B.K. & Schaffer, D.V. Directed evolution of adeno-associated virus yields enhanced gene delivery vectors. *Nat Biotechnol* **24**, 198-204 (2006).

120. Perabo, L., Endell, J., King, S., Lux, K., Goldnau, D. et al. Combinatorial engineering of a gene therapy vector: directed evolution of adeno-associated virus. *J Gene Med* **8**, 155-162 (2006).

121. Bowles, D.E., McPhee, S.W., Li, C., Gray, S.J., Samulski, J.J. et al. Phase 1 gene therapy for Duchenne muscular dystrophy using a translational optimized AAV vector. *Mol Ther* **20**, 443-455 (2012).

122. Bartlett, J.S., Kleinschmidt, J., Boucher, R.C. & Samulski, R.J. Targeted adeno-associated virus vector transduction of nonpermissive cells mediated by a bispecific F(ab 'gamma)(2) antibody. *Nature Biotechnology* **17**, 181-186 (1999).

123. Ponnazhagan, S., Mahendra, G., Kumar, S., Thompson, J.A. & Castillas, M., Jr. Conjugate-based targeting of recombinant adeno-associated virus type 2 vectors by using avidin-linked ligands. *J Virol* **76**, 12900-12907 (2002).

124. Ried, M.U., Girod, A., Leike, K., Buning, H. & Hallek, M. Adeno-associated virus capsids displaying immunoglobulin- binding domains permit antibody-mediated vector retargeting to specific cell surface receptors. *Journal of Virology* **76**, 4559-4566 (2002).

125. Michelfelder, S. Selection and characterization of targeted vector capsids from random adeno-associated virus type 2 (AAV-2) display peptide libraries. Ph.D Thesis: Fachbereich Biologie, Universitaet Konstanz, 19 (2008)

126. Loiler, S.A., Conlon, T.J., Song, S., Tang, Q., Warrington, K.H. et al. Targeting recombinant adeno-associated virus vectors to enhance gene transfer to pancreatic islets and liver. *Gene Therapy* **10**, 1551-1558 (2003).

127. Lux, K., Goerlitz, N., Schlemminger, S., Perabo, L., Goldnau, D. et al. Green fluorescent protein-tagged adeno-associated virus particles allow the study of cytosolic and nuclear trafficking. *J Virol* **79**, 11776-11787 (2005).

128. Wu, P., Xiao, W., Conlon, T., Hughes, J., Agbandje-McKenna, M. et al. Mutational analysis of the adeno-associated virus type 2 (AAV2) capsid gene and construction of AAV2 vectors with altered tropism. *Journal of Virology* **74**, 8635-8647 (2000).

129. Warrington, K.H., Gorbatyuk, O.S., Harrison, J.K., Opie, S.R., Zolotukhin, S. et al. Adeno-associated virus type 2 VP2 capsid protein is nonessential and can tolerate large peptide insertions at its N terminus. *Journal of Virology* **78**, 6595-6609 (2004).

130. Munch, R.C., Janicki, H., Volker, I., Rasbach, A., Hallek, M. et al. Displaying High-affinity Ligands on Adeno-associated Viral Vectors Enables Tumor Cell-specific and Safe Gene Transfer. *Mol Ther* **21**, 109-118 (2013).

131. Girod, A., Ried, M., Wobus, C., Lahm, H., Leike, K. et al. Genetic capsid modifications allow efficient re-targeting of adeno-associated virus type 2. *Nature Medicine* **5**, 1052-1056 (1999).

132. Shi, W. & Bartlett, J.S. RGD inclusion in VP3 provides adeno-associated virus type 2 (AAV2)-based vectors with a heparan sulfate-independent cell entry mechanism. *Mol Ther* **7**, 515-525 (2003).

133. Shi, X., Fang, G., Shi, W. & Bartlett, J.S. Insertional mutagenesis at positions 520 and 584 of adeno-associated virus type 2 (AAV2) capsid gene and generation of AAV2 vectors with eliminated heparin- binding ability and introduced novel tropism. *Hum Gene Ther* **17**, 353-361 (2006).

134. Perabo, L., Goldnau, D., White, K., Endell, J., Boucas, J. et al. Heparan sulfate proteoglycan binding properties of adeno-associated virus retargeting mutants and consequences for their in vivo tropism. *J Virol* **80**, 7265-7269 (2006).

135. Huttner, N.A., Girod, A., Perabo, L., Edbauer, D., Kleinschmidt, J.A. et al. Genetic modifications of the adeno-associated virus type 2 capsid reduce the affinity and the neutralizing effects of human serum antibodies. *Gene Therapy* **10**, 2139-2147 (2003).

136. Work, L.M., Nicklin, S.A., Brain, N.J.R., Dishart, K.L., Von Seggern, D.J. et al. Development of efficient viral vectors selective for vascular smooth muscle cells. *Molecular Therapy* **9**, 198-208 (2004).

137. White, S.J., Nicklin, S.A., Buning, H., Brosnan, M.J., Leike, K. et al. Targeted gene delivery to vascular tissue in vivo by tropism-modified adeno-associated virus vectors. *Circulation* **109**, 513-519 (2004).

138. Work, L.M., Buning, H., Hunt, E., Nicklin, S.A., Denby, L. et al. Vascular bed-targeted in vivo gene delivery using tropism-modified adeno-associated viruses. *Mol Ther* **13**, 683-693 (2006).

139. Yu, C.Y., Yuan, Z., Cao, Z., Wang, B., Qiao, C. et al. A muscle-targeting peptide displayed on AAV2 improves muscle tropism on systemic delivery. *Gene Ther* (2009).

140. Chen, Y.H., Chang, M. & Davidson, B.L. Molecular signatures of disease brain endothelia provide new sites for CNS-directed enzyme therapy. *Nat Med* **15**, 1215-1218 (2009).

141. Müller, O.J., Kaul, F., Weitzman, M.D., Pasqualini, R., Arap, W. et al. Random peptide libraries displayed on adeno-associated virus to select for targeted gene therapy vectors. *Nat Biotechnol* **21**, 1040-1046 (2003).

142. Perabo, L., Buning, H., Kofler, D.M., Ried, M.U., Girod, A. et al. In vitro selection of viral vectors with modified tropism: The adeno-associated virus display. *Molecular Therapy* **8**, 151-157 (2003).

143. Varadi, K., Michelfelder, S., Korff, T., Hecker, M., Trepel, M. et al. Novel random peptide libraries displayed on AAV serotype 9 for selection of endothelial cell-directed gene transfer vectors. *Gene Ther* (2011).

144. Waterkamp, D.A., Muller, O.J., Ying, Y., Trepel, M. & Kleinschmidt, J.A. Isolation of targeted AAV2 vectors from novel virus display libraries. *J Gene Med* **8**, 1307-1319 (2006).

145. Michelfelder, S., Lee, M.K., Delima-Hahn, E., Wilmes, T., Kaul, F. et al. Vectors selected from adeno-associated viral display peptide libraries for leukemia cell-targeted cytotoxic gene therapy. *Exp Hematol* **35**, 1766-1776 (2007).

146. Stiefelhagen, M., Sellner, L., Kleinschmidt, J.A., Jauch, A., Laufs, S. et al. Application of a haematopoetic progenitor cell-targeted adeno-associated viral (AAV) vector established by selection of an AAV random peptide library on a leukaemia cell line. *Genet Vaccines Ther* **6**, 12 (2008).

147. Michelfelder, S., Kohlschutter, J., Skorupa, A., Pfennings, S., Muller, O. et al. Successful expansion but not complete restriction of tropism of adeno-associated virus by in vivo biopanning of random virus display Peptide libraries. *PLoS One* **4**, e5122 (2009).

148. Ying, Y., Muller, O.J., Goehringer, C., Leuchs, B., Trepel, M. et al. Heart-targeted adeno-associated viral vectors selected by in vivo biopanning of a random viral display peptide library. *Gene Ther* **17**, 980-990 (2010).

149. Fitzsimons, H.L., Bland, R.J. & During, M.J. Promoters and regulatory elements that improve adeno-associated virus transgene expression in the brain. *Methods* **28**, 227-236 (2002).

150. Shevtsova, Z., Malik, J.M., Michel, U., Bahr, M. & Kugler, S. Promoters and serotypes: targeting of adeno-associated virus vectors for gene transfer in the rat central nervous system in vitro and in vivo. *Exp Physiol* **90**, 53-59 (2005).

151. Gray, S.J., Foti, S.B., Schwartz, J.W., Bachaboina, L., Taylor-Blake, B. et al. Optimizing promoters for recombinant adeno-associated virus-mediated gene expression in the peripheral and central nervous system using self-complementary vectors. *Hum Gene Ther* **22**, 1143-1153 (2011).

152. Bainbridge, J.W., Smith, A.J., Barker, S.S., Robbie, S., Henderson, R. et al. Effect of gene therapy on visual function in Leber's congenital amaurosis. *N Engl J Med* **358**, 2231-2239 (2008).

153. Wang, B., Li, J., Fu, F.H., Chen, C., Zhu, X. et al. Construction and analysis of compact muscle-specific promoters for AAV vectors. *Gene Ther* **15**, 1489-1499 (2008).

154. Phillips, M.I., Tang, Y., Schmidt-Ott, K., Qian, K. & Kagiyama, S. Vigilant vector: heart-specific promoter in an adeno-associated virus vector for cardioprotection. *Hypertension* **39**, 651-655 (2002).

155. Sands, M.S. AAV-mediated liver-directed gene therapy. *Methods Mol Biol* **807**, 141-157 (2011).

156. Qiao, C., Yuan, Z., Li, J., He, B., Zheng, H. et al. Liver-specific microRNA-122 target sequences incorporated in AAV vectors efficiently inhibits transgene expression in the liver. *Gene Ther* **18**, 403-410 (2010).

157. Geisler, A., Jungmann, A., Kurreck, J., Poller, W., Katus, H.A. et al. microRNA122-regulated transgene expression increases specificity of cardiac gene transfer upon intravenous delivery of AAV9 vectors. *Gene Ther* **18**, 199-209 (2010).

158. Brown, B.D., Cantore, A., Annoni, A., Sergi, L.S., Lombardo, A. et al. A microRNA-regulated lentiviral vector mediates stable correction of hemophilia B mice. *Blood* **110**, 4144-4152 (2007).

159. Cawood, R., Chen, H.H., Carroll, F., Bazan-Peregrino, M., van Rooijen, N. et al. Use of tissue-specific microRNA to control pathology of wild-type adenovirus without attenuation of its ability to kill cancer cells. *PLoS Pathog* **5**, e1000440 (2009).

160. Kelly, E.J., Hadac, E.M., Greiner, S. & Russell, S.J. Engineering microRNA responsiveness to decrease virus pathogenicity. *Nat Med* **14**, 1278-1283 (2008).

161. Suzuki, T., Sakurai, F., Nakamura, S., Kouyama, E., Kawabata, K. et al. miR-122a-regulated expression of a suicide gene prevents hepatotoxicity without altering antitumor effects in suicide gene therapy. *Mol Ther* **16**, 1719-1726 (2008).

162. Aebischer, P., Schluep, M., Deglon, N., Joseph, J.M., Hirt, L. et al. Intrathecal delivery of CNTF using encapsulated genetically modified xenogeneic cells in amyotrophic lateral sclerosis patients. *Nat Med* **2**, 696-699 (1996).

163. Feigin, A., Kaplitt, M.G., Tang, C., Lin, T., Mattis, P. et al. Modulation of metabolic brain networks after subthalamic gene therapy for Parkinson's disease. *Proc Natl Acad Sci U S A* **104**, 19559-19564 (2007).

164. Nagabhushan Kalburgi, S., Khan, N.N. & Gray, S.J. Recent gene therapy advancements for neurological diseases. *Discov Med* **15**, 111-119 (2013).

165. Armulik, A., Genove, G., Mae, M., Nisancioglu, M.H., Wallgard, E. et al. Pericytes regulate the blood-brain barrier. *Nature* **468**, 557-561 (2010).

166. McCown, T.J., Xiao, X., Li, J., Breese, G.R. & Samulski, R.J. Differential and persistent expression patterns of CNS gene transfer by an adeno-associated virus (AAV) vector. *Brain Res* **713**, 99-107 (1996).

167. During, M.J., Samulski, R.J., Elsworth, J.D., Kaplitt, M.G., Leone, P. et al. In vivo expression of therapeutic human genes for dopamine production in the caudates of MPTP-treated monkeys using an AAV vector. *Gene Ther* **5**, 820-827 (1998).

168. Mandel, R.J., Rendahl, K.G., Spratt, S.K., Snyder, R.O., Cohen, L.K. et al. Characterization of intrastriatal recombinant adeno-associated virus-mediated gene transfer of human tyrosine hydroxylase and human GTP-cyclohydrolase I in a rat model of Parkinson's disease. *J Neurosci* **18**, 4271-4284 (1998).

169. Davidson, B.L., Stein, C.S., Heth, J.A., Martins, I., Kotin, R.M. et al. Recombinant adeno-associated virus type 2, 4, and 5 vectors: transduction of variant cell types and regions in the mammalian central nervous system. *Proc Natl Acad Sci U S A* **97**, 3428-3432 (2000).

170. Markakis, E.A., Vives, K.P., Bober, J., Leichtle, S., Leranth, C. et al. Comparative transduction efficiency of AAV vector serotypes 1-6 in the substantia nigra and striatum of the primate brain. *Mol Ther* **18**, 588-593 (2010).

171. Cearley, C.N. & Wolfe, J.H. Transduction characteristics of adeno-associated virus vectors expressing cap serotypes 7, 8, 9, and Rh10 in the mouse brain. *Mol Ther* **13**, 528-537 (2006).

172. de Backer, M.W., Brans, M.A., Luijendijk, M.C., Garner, K.M. & Adan, R.A. Optimization of adeno-associated viral vector-mediated gene delivery to the hypothalamus. *Hum Gene Ther* **21**, 673-682 (2010).

173. Alonso, A., Reinz, E., Leuchs, B., Kleinschmidt, J., Fatar, M. et al. Focal Delivery of AAV2/1-transgenes Into the Rat Brain by Localized Ultrasound-induced BBB Opening. *Mol Ther Nucleic Acids* **2**, e73 (2013).

174. Shen, F., Kuo, R., Milon-Camus, M., Han, Z., Jiang, L. et al. Intravenous delivery of adeno-associated viral vector serotype 9 mediates effective gene expression in ischemic stroke lesion and brain angiogenic foci. *Stroke* **44**, 252-254 (2013).

175. Dayton, R.D., Wang, D.B. & Klein, R.L. The advent of AAV9 expands applications for brain and spinal cord gene delivery. *Expert Opin Biol Ther* **12**, 757-766 (2012).

176. Foust, K.D., Nurre, E., Montgomery, C.L., Hernandez, A., Chan, C.M. et al. Intravascular AAV9 preferentially targets neonatal neurons and adult astrocytes. *Nat Biotechnol* **27**, 59-65 (2009).

177. Duque, S., Joussemet, B., Riviere, C., Marais, T., Dubreil, L. et al. Intravenous administration of self-complementary AAV9 enables transgene delivery to adult motor neurons. *Mol Ther* **17**, 1187-1196 (2009).

178. Driskell, R.A. & Engelhardt, J.F. Current status of gene therapy for inherited lung diseases. *Annu Rev Physiol* **65**, 585-612 (2003).

179. Martini, S.V., Rocco, P.R. & Morales, M.M. Adeno-associated virus for cystic fibrosis gene therapy. *Braz J Med Biol Res* **44**, 1097-1104 (2011).

180. Flotte, T.R. & Mueller, C. Gene therapy for alpha-1 antitrypsin deficiency. *Hum Mol Genet* **20**, R87-92 (2011).

181. Rosenfeld, M.A., Yoshimura, K., Trapnell, B.C., Yoneyama, K., Rosenthal, E.R. et al. In vivo transfer of the human cystic fibrosis transmembrane conductance regulator gene to the airway epithelium. *Cell* **68**, 143-155 (1992).

182. Yang, Y., Nunes, F.A., Berencsi, K., Gonczol, E., Engelhardt, J.F. et al. Inactivation of E2a in recombinant adenoviruses improves the prospect for gene therapy in cystic fibrosis. *Nat Genet* **7**, 362-369 (1994).

183. Brantly, M.L., Chulay, J.D., Wang, L., Mueller, C., Humphries, M. et al. Sustained transgene expression despite T lymphocyte responses in a clinical trial of rAAV1-AAT gene therapy. *Proc Natl Acad Sci U S A* **106**, 16363-16368 (2009).

184. Song, S., Morgan, M., Ellis, T., Poirier, A., Chesnut, K. et al. Sustained secretion of human alpha-1-antitrypsin from murine muscle transduced with adeno-associated virus vectors. *Proc Natl Acad Sci U S A* **95**, 14384-14388 (1998).

185. Brantly, M.L., Spencer, L.T., Humphries, M., Conlon, T.J., Spencer, C.T. et al. Phase I trial of intramuscular injection of a recombinant adeno-associated virus serotype 2 alphal-antitrypsin (AAT) vector in AAT-deficient adults. *Hum Gene Ther* **17**, 1177-1186 (2006).

186. Chulay, J.D., Ye, G.J., Thomas, D.L., Knop, D.R., Benson, J.M. et al. Preclinical evaluation of a recombinant adeno-associated virus vector expressing human alpha-1 antitrypsin made using a recombinant herpes simplex virus production method. *Hum Gene Ther* **22**, 155-165 (2011).

187. Limberis, M.P. & Wilson, J.M. Adeno-associated virus serotype 9 vectors transduce murine alveolar and nasal epithelia and can be readministered. *Proc Natl Acad Sci U S A* **103**, 12993-12998 (2006).

188. Auricchio, A., O'Connor, E., Weiner, D., Gao, G.P., Hildinger, M. et al. Noninvasive gene transfer to the lung for systemic delivery of therapeutic proteins. *J Clin Invest* **110**, 499-504 (2002).

189. Zabner, J., Seiler, M., Walters, R., Kotin, R.M., Fulgeras, W. et al. Adeno-associated virus type 5 (AAV5) but not AAV2 binds to the apical surfaces of airway epithelia and facilitates gene transfer. *J Virol* **74**, 3852-3858 (2000).

190. Halbert, C.L., Lam, S.L. & Miller, A.D. High-efficiency promoter-dependent transduction by adeno-associated virus type 6 vectors in mouse lung. *Hum Gene Ther* **18**, 344-354 (2007).

191. Meng, L.K. & Liu, C.G. Gene therapies for pulmonary hypertension-from experimental trials to bedside aspects. *Eur J Cardiothorac Surg* **37**, 407-419 (2009).

192. Reynolds, A.M., Holmes, M.D., Danilov, S.M. & Reynolds, P.N. Targeted gene delivery of BMPR2 attenuates pulmonary hypertension. *Eur Respir J* **39**, 329-343 (2012).

193. Umar, S., Steendijk, P., Ypey, D.L., Atsma, D.E., van der Wall, E.E. et al. Novel approaches to treat experimental pulmonary arterial hypertension: a review. *J Biomed Biotechnol* **2010**, 702836 (2010).

194. Machado, R.D. Seeking the right targets: gene therapy advances in pulmonary arterial hypertension. *Eur Respir J* **39**, 235-237 (2012).

195. Wistuba, A., Weger, S., Kern, A. & Kleinschmidt, J.A. Intermediates of adeno-associated virus type 2 assembly: identification of soluble complexes containing Rep and Cap proteins. *J Virol* **69**, 5311-5319 (1995).

196. Wobus, C.E., Hugle-Dorr, B., Girod, A., Petersen, G., Hallek, M. et al. Monoclonal antibodies against the adeno-associated virus type 2 (AAV-2) capsid: epitope mapping and identification

of capsid domains involved in AAV-2-cell interaction and neutralization of AAV-2 infection. *J Virol* **74**, 9281-9293 (2000).

197. Hanahan, D. Studies on transformation of Escherichia coli with plasmids. *J Mol Biol* **166**, 557-580 (1983).

198. Bac-to-Bac Baculovirus expression system An efficient site-specific transposition system to generate baculovirus for high-level expression of recombinant proteins (2010), Web Page: *http://tools.invitrogen.com/content/sfs/manuals/bactobac_man.pdf* Date cited: 2013/04/18

199. Barry, G.F. A broad-host-range shuttle system for gene insertion into the chromosomes of gram-negative bacteria. *Gene* **71**, 75-84 (1988).

200. Bullock, W.O., Fernandez, J M, Short, J M XL1-Blue: A high efficiency plasmid transforming recA Escherichia coli strain with beta-galactosidase selection *Biotechniques* **5**, 376-378 (1987).

201. Graham, F.L., Smiley, J., Russell, W.C. & Nairn, R. Characteristics of a human cell line transformed by DNA from human adenovirus type 5. *J Gen Virol* **36**, 59-74 (1977).

202. DuBridge, R.B., Tang, P., Hsia, H.C., Leong, P.M., Miller, J.H. et al. Analysis of mutation in human cells by using an Epstein-Barr virus shuttle system. *Mol Cell Biol* **7**, 379-387 (1987).

203. Vaughn, J.L., Goodwin, R.H., Tompkins, G.J. & McCawley, P. The establishment of two cell lines from the insect Spodoptera frugiperda (Lepidoptera; Noctuidae). *In Vitro* **13**, 213-217 (1977).

204. Taketo, M., Schroeder, A.C., Mobraaten, L.E., Gunning, K.B., Hanten, G. et al. FVB/N: an inbred mouse strain preferable for transgenic analyses. *Proc Natl Acad Sci U S A* **88**, 2065-2069 (1991).

205. Rohr, U.P., Wulf, M.A., Stahn, S., Steidl, U., Haas, R. et al. Fast and reliable titration of recombinant adeno-associated virus type-2 using quantitative real-time PCR. *J Virol Methods* **106**, 81-88 (2002).

206. Chen, H. Intron splicing-mediated expression of AAV Rep and Cap genes and production of AAV vectors in insect cells. *Mol Ther* **16**, 924-930 (2008).

207. Laemmli, U.K. Cleavage of structural proteins during the assembly of the head of bacteriophage T4. *Nature* **227**, 680-685 (1970).

208. Dower, W.J., Miller, J.F. & Ragsdale, C.W. High efficiency transformation of E. coli by high voltage electroporation. *Nucleic Acids Res* **16**, 6127-6145 (1988).

209. Cohen, S.N., Chang, A.C. & Hsu, L. Nonchromosomal antibiotic resistance in bacteria: genetic transformation of Escherichia coli by R-factor DNA. *Proc Natl Acad Sci U S A* **69**, 2110-2114 (1972).

210. Wasilko, D.J., Lee, S.E., Stutzman-Engwall, K.J., Reitz, B.A., Emmons, T.L. et al. The titerless infected-cells preservation and scale-up (TIPS) method for large-scale production of NO-sensitive human soluble guanylate cyclase (sGC) from insect cells infected with recombinant baculovirus. *Protein Expr Purif* **65**, 122-132 (2009).

211. Guo, P., El-Gohary, Y., Prasadan, K., Shiota, C., Xiao, X. et al. Rapid and simplified purification of recombinant adeno-associated virus. *J Virol Methods* **183**, 139-146 (2012).

212. Hermens, W.T., ter Brake, O., Dijkhuizen, P.A., Sonnemans, M.A., Grimm, D. et al. Purification of recombinant adeno-associated virus by iodixanol gradient ultracentrifugation allows rapid and reproducible preparation of vector stocks for gene transfer in the nervous system. *Hum Gene Ther* **10**, 1885--1891 (1999).

213. Bradford, M.M. A rapid and sensitive method for the quantitation of microgram quantities of protein utilizing the principle of protein-dye binding. *Anal Biochem* **72**, 248-254 (1976).

214. Schindelin, J., Arganda-Carreras, I., Frise, E., Kaynig, V., Longair, M. et al. Fiji: an open-source platform for biological-image analysis. *Nat Methods* **9**, 676-682 (2012).

215. Arnold, K., Bordoli, L., Kopp, J. & Schwede, T. The SWISS-MODEL workspace: a web-based environment for protein structure homology modelling. *Bioinformatics* **22**, 195-201 (2006).

216. Kiefer, F., Arnold, K., Kunzli, M., Bordoli, L. & Schwede, T. The SWISS-MODEL Repository and associated resources. *Nucleic Acids Res* **37**, D387-392 (2009).

217. Guex, N. & Peitsch, M.C. SWISS-MODEL and the Swiss-PdbViewer: an environment for comparative protein modeling. *Electrophoresis* **18**, 2714-2723 (1997).

218. Schwede, T., Kopp, J., Guex, N. & Peitsch, M.C. SWISS-MODEL: An automated protein homology-modeling server. *Nucleic Acids Res* **31**, 3381-3385 (2003).

219. Mueller, C. & Flotte, T.R. Clinical gene therapy using recombinant adeno-associated virus vectors. *Gene Ther* **15**, 858-863 (2008).

220. LeWitt, P.A., Rezai, A.R., Leehey, M.A., Ojemann, S.G., Flaherty, A.W. et al. AAV2-GAD gene therapy for advanced Parkinson's disease: a double-blind, sham-surgery controlled, randomised trial. *Lancet Neurol* **10**, 309-319.

221. Bartlett, J.S., Samulski, R.J. & McCown, T.J. Selective and rapid uptake of adeno-associated virus type 2 in brain. *Hum Gene Ther* **9**, 1181-1186 (1998).

222. Burger, C., Gorbatyuk, O.S., Velardo, M.J., Peden, C.S., Williams, P. et al. Recombinant AAV viral vectors pseudotyped with viral capsids from serotypes 1, 2, and 5 display differential efficiency and cell tropism after delivery to different regions of the central nervous system. *Mol Ther* **10**, 302-317 (2004).

223. Fu, H., Muenzer, J., Samulski, R.J., Breese, G., Sifford, J. et al. Self-complementary adeno-associated virus serotype 2 vector: global distribution and broad dispersion of AAV-mediated transgene expression in mouse brain. *Mol Ther* **8**, 911-917 (2003).

224. Kaplitt, M.G., Leone, P., Samulski, R.J., Xiao, X., Pfaff, D.W. et al. Long-term gene expression and phenotypic correction using adeno-associated virus vectors in the mammalian brain. *Nat Genet* **8**, 148-154 (1994).

225. Kordower, J.H., Emborg, M.E., Bloch, J., Ma, S.Y., Chu, Y. et al. Neurodegeneration prevented by lentiviral vector delivery of GDNF in primate models of Parkinson's disease. *Science* **290**, 767-773 (2000).

226. Taymans, J.M., Vandenberghe, L.H., Haute, C.V., Thiry, I., Deroose, C.M. et al. Comparative analysis of adeno-associated viral vector serotypes 1, 2, 5, 7, and 8 in mouse brain. *Hum Gene Ther* **18**, 195-206 (2007).

227. Maguire, A.M., Simonelli, F., Pierce, E.A., Pugh, E.N., Jr., Mingozzi, F. et al. Safety and efficacy of gene transfer for Leber's congenital amaurosis. *N Engl J Med* **358**, 2240-2248 (2008).

228. Hauswirth, W.W., Aleman, T.S., Kaushal, S., Cideciyan, A.V., Schwartz, S.B. et al. Treatment of leber congenital amaurosis due to RPE65 mutations by ocular subretinal injection of adeno-associated virus gene vector: short-term results of a phase I trial. *Hum Gene Ther* **19**, 979-990 (2008).

229. Surace, E.M. & Auricchio, A. Versatility of AAV vectors for retinal gene transfer. *Vision Res* **48**, 353-359 (2008).

230. Wagner, J.A., Messner, A.H., Moran, M.L., Daifuku, R., Kouyama, K. et al. Safety and biological efficacy of an adeno-associated virus vector-cystic fibrosis transmembrane regulator (AAV-CFTR) in the cystic fibrosis maxillary sinus. *Laryngoscope* **109**, 266-274 (1999).

231. Flotte, T.R., Solow, R., Owens, R.A., Afione, S., Zeitlin, P.L. et al. Gene expression from adeno-associated virus vectors in airway epithelial cells. *Am J Respir Cell Mol Biol* **7**, 349-356 (1992).

232. Flotte, T.R., Zeitlin, P.L., Reynolds, T.C., Heald, A.E., Pedersen, P. et al. Phase I trial of intranasal and endobronchial administration of a recombinant adeno-associated virus serotype 2 (rAAV2)-CFTR vector in adult cystic fibrosis patients: a two-part clinical study. *Hum Gene Ther* **14**, 1079-1088 (2003).

233. Halbert, C.L. & Miller, A.D. AAV-mediated gene transfer to mouse lungs. *Methods Mol Biol* **246**, 201-212 (2004).

234. Limberis, M.P., Vandenberghe, L.H., Zhang, L., Pickles, R.J. & Wilson, J.M. Transduction efficiencies of novel AAV vectors in mouse airway epithelium in vivo and human ciliated airway epithelium in vitro. *Mol Ther* **17**, 294-301 (2009).

235. Rodi, D.J., Soares, A.S. & Makowski, L. Quantitative assessment of peptide sequence diversity in M13 combinatorial peptide phage display libraries. *J Mol Biol* **322**, 1039-1052 (2002).

236. Firth, A.E. & Patrick, W.M. GLUE-IT and PEDEL-AA: new programmes for analyzing protein diversity in randomized libraries. *Nucleic Acids Res* **36**, W281-285 (2008).

237. Hare, E., Sieber, T., Hoffmann, H. & Trepel, M. Pelica - The Peptide Library Calculator (2013), Web Page: http://glimmer.rstudio.com/erichare/pelica/ Date cited: 2013/07/01

238. Hsieh, C.L., Xie, Z., Liu, Z.Y., Green, J.E., Martin, W.D. et al. A luciferase transgenic mouse model: visualization of prostate development and its androgen responsiveness in live animals. *J Mol Endocrinol* **35**, 293-304 (2005).

239. Zhang, W., Purchio, A.F., Chen, K., Wu, J., Lu, L. et al. A transgenic mouse model with a luciferase reporter for studying in vivo transcriptional regulation of the human CYP3A4 gene. *Drug Metab Dispos* **31**, 1054-1064 (2003).

240. Michelfelder, S., Varadi, K., Raupp, C., Hunger, A., Korbelin, J. et al. Peptide ligands incorporated into the threefold spike capsid domain to re-direct gene transduction of AAV8 and AAV9 in vivo. *PLoS One* **6**, e23101 (2011).

241. Sato, A., Klaunberg, B. & Tolwani, R. In vivo bioluminescence imaging. *Comp Med* **54**, 631-634 (2004).

242. Al-Dosari, M., Zhang, G., Knapp, J.E. & Liu, D. Evaluation of viral and mammalian promoters for driving transgene expression in mouse liver. *Biochem Biophys Res Commun* **339**, 673-678 (2006).

243. Szentirmai, O., Baker, C.H., Lin, N., Szucs, S., Takahashi, M. et al. Noninvasive bioluminescence imaging of luciferase expressing intracranial U87 xenografts: correlation with magnetic resonance imaging determined tumor volume and longitudinal use in assessing tumor growth and antiangiogenic treatment effect. *Neurosurgery* **58**, 365-372; discussion 365-372 (2006).

244. Phillips, A.T., Stauft, C.B., Aboellail, T.A., Toth, A.M., Jarvis, D.L. et al. Bioluminescent imaging and histopathologic characterization of WEEV neuroinvasion in outbred CD-1 mice. *PLoS One* **8**, e53462 (2013).

245. Shi, W.F., Arnold, G.S. & Bartlett, J.S. Insertional mutagenesis of the adeno-associated virus type 2 (AAV2) capsid gene and generation of AAV2 vectors targeted to alternative cell-surface receptors. *Human Gene Therapy* **12**, 1697-1711 (2001).

246. Aird, W.C. Endothelial cell heterogeneity. *Cold Spring Harb Perspect Med* **2**, a006429 (2012).

247. Richardson, M.R., Lai, X., Witzmann, F.A. & Yoder, M.C. Venous and arterial endothelial proteomics: mining for markers and mechanisms of endothelial diversity. *Expert Rev Proteomics* **7**, 823-831 (2010).

248. Daneman, R., Zhou, L., Agalliu, D., Cahoy, J.D., Kaushal, A. et al. The mouse blood-brain barrier transcriptome: a new resource for understanding the development and function of brain endothelial cells. *PLoS One* **5**, e13741 (2010).

249. McCall, M.N., Kent, O.A., Yu, J., Fox-Talbot, K., Zaiman, A.L. et al. MicroRNA profiling of diverse endothelial cell types. *BMC Med Genomics* **4**, 78 (2011).

250. Pasqualini, R. & Ruoslahti, E. Organ targeting in vivo using phage display peptide libraries. *Nature* **380**, 364-366 (1996).

251. Rajotte, D., Arap, W., Hagedorn, M., Koivunen, E., Pasqualini, R. et al. Molecular heterogeneity of the vascular endothelium revealed by in vivo phage display. *J Clin Invest* **102**, 430-437 (1998).

252. Teesalu, T., Sugahara, K.N. & Ruoslahti, E. Mapping of vascular ZIP codes by phage display. *Methods Enzymol* **503**, 35-56 (2012).

253. Arap, W., Kolonin, M.G., Trepel, M., Lahdenranta, J., Cardo-Vila, M. et al. Steps toward mapping the human vasculature by phage display. *Nat Med* **8**, 121-127 (2002).

254. Aird, W.C. Phenotypic heterogeneity of the endothelium: II. Representative vascular beds. *Circ Res* **100**, 174-190 (2007).

255. Renkonen, J., Tynninen, O., Hayry, P., Paavonen, T. & Renkonen, R. Glycosylation might provide endothelial zip codes for organ-specific leukocyte traffic into inflammatory sites. *Am J Pathol* **161**, 543-550 (2002).

256. Scott, D.W. & Patel, R.P. Endothelial heterogeneity and adhesion molecules N-glycosylation: implications in leukocyte trafficking in inflammation. *Glycobiology* **23**, 622-633 (2013).

257. Shen, S., Bryant, K.D., Sun, J., Brown, S.M., Troupes, A. et al. Glycan binding avidity determines the systemic fate of adeno-associated virus type 9. *J Virol* **86**, 10408-10417 (2012).

258. Ng, R., Govindasamy, L., Gurda, B.L., McKenna, R., Kozyreva, O.G. et al. Structural characterization of the dual glycan binding adeno-associated virus serotype 6. *J Virol* **84**, 12945-12957 (2010).

259. Reynolds, P.N., Zinn, K.R., Gavrilyuk, V.D., Balyasnikova, I.V., Rogers, B.E. et al. A targetable, injectable adenoviral vector for selective gene delivery to pulmonary endothelium in vivo. *Mol Ther* **2**, 562-578 (2000).

260. Reynolds, P.N., Nicklin, S.A., Kaliberova, L., Boatman, B.G., Grizzle, W.E. et al. Combined transductional and transcriptional targeting improves the specificity of transgene expression in vivo. *Nat Biotechnol* **19**, 838-842 (2001).

261. Paris-Robidas, S., Emond, V., Tremblay, C., Soulet, D. & Calon, F. In vivo labeling of brain capillary endothelial cells after intravenous injection of monoclonal antibodies targeting the transferrin receptor. *Mol Pharmacol* **80**, 32-39 (2011).

262. Kumar, P., Wu, H., McBride, J.L., Jung, K.E., Kim, M.H. et al. Transvascular delivery of small interfering RNA to the central nervous system. *Nature* **448**, 39-43 (2007).

263. Karkan, D., Pfeifer, C., Vitalis, T.Z., Arthur, G., Ujiie, M. et al. A unique carrier for delivery of therapeutic compounds beyond the blood-brain barrier. *PLoS One* **3**, e2469 (2008).

264. Coloma, M.J., Lee, H.J., Kurihara, A., Landaw, E.M., Boado, R.J. et al. Transport across the primate blood-brain barrier of a genetically engineered chimeric monoclonal antibody to the human insulin receptor. *Pharm Res* **17**, 266-274 (2000).

265. Zhang, Y., Schlachetzki, F. & Pardridge, W.M. Global non-viral gene transfer to the primate brain following intravenous administration. *Mol Ther* **7**, 11-18 (2003).

266. Li, S., Tan, Y., Viroonchatapan, E., Pitt, B.R. & Huang, L. Targeted gene delivery to pulmonary endothelium by anti-PECAM antibody. *Am J Physiol Lung Cell Mol Physiol* **278**, L504-511 (2000).

267. Wilson, A., Zhou, W., Champion, H.C., Alber, S., Tang, Z.L. et al. Targeted delivery of oligodeoxynucleotides to mouse lung endothelial cells in vitro and in vivo. *Mol Ther* **12**, 510-518 (2005).

268. Ma, Z., Zhang, J., Alber, S., Dileo, J., Negishi, Y. et al. Lipid-mediated delivery of oligonucleotide to pulmonary endothelium. *Am J Respir Cell Mol Biol* **27**, 151-159 (2002).

269. Naumer, M., Popa-Wagner, R. & Kleinschmidt, J.A. Impact of capsid modifications by selected peptide ligands on recombinant adeno-associated virus serotype 2-mediated gene transduction. *J Gen Virol* **93**, 2131-2141 (2012).

270. Popa-Wagner, R., Porwal, M., Kann, M., Reuss, M., Weimer, M. et al. Impact of VP1-specific protein sequence motifs on adeno-associated virus type 2 intracellular trafficking and nuclear entry. *J Virol* **86**, 9163-9174 (2012).

271. Niwa, H., Yamamura, K. & Miyazaki, J. Efficient selection for high-expression transfectants with a novel eukaryotic vector. *Gene* **108**, 193-199 (1991).

272. Michalkiewicz, M., Michalkiewicz, T., Geurts, A.M., Roman, R.J., Slocum, G.R. et al. Efficient transgenic rat production by a lentiviral vector. *Am J Physiol Heart Circ Physiol* **293**, H881-894 (2007).

273. Alexopoulou, A.N., Couchman, J.R. & Whiteford, J.R. The CMV early enhancer/chicken beta actin (CAG) promoter can be used to drive transgene expression during the differentiation of murine embryonic stem cells into vascular progenitors. *BMC Cell Biol* **9**, 2 (2008).

274. Lawlor, P.A., Bland, R.J., Mouravlev, A., Young, D. & During, M.J. Efficient gene delivery and selective transduction of glial cells in the mammalian brain by AAV serotypes isolated from nonhuman primates. *Mol Ther* **17**, 1692-1702 (2009).

275. Klein, R.L., Dayton, R.D., Tatom, J.B., Henderson, K.M. & Henning, P.P. AAV8, 9, Rh10, Rh43 vector gene transfer in the rat brain: effects of serotype, promoter and purification method. *Mol Ther* **16**, 89-96 (2008).

276. Stripecke, R., Carmen Villacres, M., Skelton, D., Satake, N., Halene, S. et al. Immune response to green fluorescent protein: implications for gene therapy. *Gene Ther* **6**, 1305-1312 (1999).

277. Papadakis, E.D., Nicklin, S.A., Baker, A.H. & White, S.J. Promoters and control elements: designing expression cassettes for gene therapy. *Curr Gene Ther* **4**, 89-113 (2004).

278. Cunningham, B.C. & Wells, J.A. High-resolution epitope mapping of hGH-receptor interactions by alanine-scanning mutagenesis. *Science* **244**, 1081-1085 (1989).

279. Pande, J., Szewczyk, M.M. & Grover, A.K. Phage display: concept, innovations, applications and future. *Biotechnol Adv* **28**, 849-858 (2010).

280. Constantinescu, C.S., Farooqi, N., O'Brien, K. & Gran, B. Experimental autoimmune encephalomyelitis (EAE) as a model for multiple sclerosis (MS). *Br J Pharmacol* **164**, 1079-1106 (2011).

281. Babcock, A.A., Kuziel, W.A., Rivest, S. & Owens, T. Chemokine expression by glial cells directs leukocytes to sites of axonal injury in the CNS. *J Neurosci* **23**, 7922-7930 (2003).

282. dos Santos, A.C., Barsante, M.M., Arantes, R.M., Bernard, C.C., Teixeira, M.M. et al. CCL2 and CCL5 mediate leukocyte adhesion in experimental autoimmune encephalomyelitis--an intravital microscopy study. *J Neuroimmunol* **162**, 122-129 (2005).

283. Dzenko, K.A., Song, L., Ge, S., Kuziel, W.A. & Pachter, J.S. CCR2 expression by brain microvascular endothelial cells is critical for macrophage transendothelial migration in response to CCL2. *Microvasc Res* **70**, 53-64 (2005).

284. Fuentes, M.E., Durham, S.K., Swerdel, M.R., Lewin, A.C., Barton, D.S. et al. Controlled recruitment of monocytes and macrophages to specific organs through transgenic expression of monocyte chemoattractant protein-1. *J Immunol* **155**, 5769-5776 (1995).

285. Song, L. & Pachter, J.S. Monocyte chemoattractant protein-1 alters expression of tight junction-associated proteins in brain microvascular endothelial cells. *Microvasc Res* **67**, 78-89 (2004).

286. Stamatovic, S.M., Keep, R.F., Kunkel, S.L. & Andjelkovic, A.V. Potential role of MCP-1 in endothelial cell tight junction 'opening': signaling via Rho and Rho kinase. *J Cell Sci* **116**, 4615-4628 (2003).

287. Teixeira, M.M., Vilela, M.C., Soriani, F.M., Rodrigues, D.H. & Teixeira, A.L. Using intravital microscopy to study the role of chemokines during infection and inflammation in the central nervous system. *J Neuroimmunol* **224**, 62-65 (2010).

288. Zhang, Y. & Rollins, B.J. A dominant negative inhibitor indicates that monocyte chemoattractant protein 1 functions as a dimer. *Mol Cell Biol* **15**, 4851-4855 (1995).

289. Pfeiffer, F., Schafer, J., Lyck, R., Makrides, V., Brunner, S. et al. Claudin-1 induced sealing of blood-brain barrier tight junctions ameliorates chronic experimental autoimmune encephalomyelitis. *Acta Neuropathol* **122**, 601-614 (2011).

290. Rosenfeld, M.A., Siegfried, W., Yoshimura, K., Yoneyama, K., Fukayama, M. et al. Adenovirus-mediated transfer of a recombinant alpha 1-antitrypsin gene to the lung epithelium in vivo. *Science* **252**, 431-434 (1991).

291. Janssens, S.P., Bloch, K.D., Nong, Z., Gerard, R.D., Zoldhelyi, P. et al. Adenoviral-mediated transfer of the human endothelial nitric oxide synthase gene reduces acute hypoxic pulmonary vasoconstriction in rats. *J Clin Invest* **98**, 317-324 (1996).

292. Budts, W., Pokreisz, P., Nong, Z., Van Pelt, N., Gillijns, H. et al. Aerosol gene transfer with inducible nitric oxide synthase reduces hypoxic pulmonary hypertension and pulmonary vascular remodeling in rats. *Circulation* **102**, 2880-2885 (2000).

293. McCarthy, H.O., Coulter, J.A., Robson, T. & Hirst, D.G. Gene therapy via inducible nitric oxide synthase: a tool for the treatment of a diverse range of pathological conditions. *J Pharm Pharmacol* **60**, 999-1017 (2008).

294. Atkinson, C., Stewart, S., Upton, P.D., Machado, R., Thomson, J.R. et al. Primary pulmonary hypertension is associated with reduced pulmonary vascular expression of type II bone morphogenetic protein receptor. *Circulation* **105**, 1672-1678 (2002).

295. Morrell, N.W. Pulmonary hypertension due to BMPR2 mutation: a new paradigm for tissue remodeling? *Proc Am Thorac Soc* **3**, 680-686 (2006).

296. Takahashi, H., Goto, N., Kojima, Y., Tsuda, Y., Morio, Y. et al. Downregulation of type II bone morphogenetic protein receptor in hypoxic pulmonary hypertension. *Am J Physiol Lung Cell Mol Physiol* **290**, L450-458 (2006).

List of Publications

Manuscripts under editorial consideration

Körbelin J., Sieber, T., Michelfelder, S., Lunding, L., Hunger, A., Alawi, M., Indenbirken, D., Müller, O. J., Pasqualini, R., Arap, W., Kleinschmidt, J. A., Trepel, M. Targeting genes to the pulmonary endothelium by a highly specific lung-homing vector. *Submitted to Nature Medicine* (2013)

Contributions to scientific conferences

Körbelin, J., Michelfelder, S., Müller, O. J., Trepel, M. Screening of random AAV display peptide libraries in vivo yields tissue specific AAV vectors with enhanced transduction capability. *Selected abstract for oral presentation at the XIX. Annual Meeting German Society for Gentherapy [DG-GT]* (2013).

Awards

Winner of the UCCH Hubertus Wald Young Investigator Award 2013.

Körbelin, J. Michelfelder, S. Hunger, A., Trepel, M. Screening of random AAV peptide display libraries in vivo yields tissue-specific AAV vectors with enhanced transduction capability. *Oral presentation at the V. Research Retreat of the University Cancer Center Hamburg [UCCH]* (2013).

Patents

Trepel, M., **Körbelin, J**., Michelfelder, S. Neue Peptide mit Spezifität für die Lunge (DE 10 2013 215 817.3). *Patent application submitted to Deutsches Patent- und Markenamt (German Patent and Trademark Office)*

Publications with content not directly related to this study

Körbelin, J., Adam, G., Willingmann, P., Heinze, C. The complete sequence of tobacco mosaic virus isolate Ohio V reveals a high accumulation of silent mutations in all open reading frames. *Arch Virol* **157**, 387-389 (2012).

Michelfelder, S., Varadi, C., Raupp, C., Hunger, A., **Körbelin, J**., Pahrmann, C., Schrepfer, S., Müller, O. J., Kleinschmidt, J. A., Trepel, M. Peptide ligands incorporated into the threefold spike capsid domain to re-direct gene transduction of AAV8 and AAV9 in vivo. *PLoS One* **6**, e23101 (2011)

Acknowledgments

This work carried out between April 2010 and July 2013 in the University Medical Center Hamburg-Eppendorf (Universitätsklinikum Hamburg-Eppendorf, UKE) under supervision of Prof. Dr. Martin Trepel, Scientific Director of the University Cancer Center Hamburg (UCCH), and Prof. Dr. Thorsten Burmester, Director of the the Zoologial Institute, University of Hamburg.

I am particularly grateful to Prof. Dr. Martin Trepel for giving me the opportunity to work with him in the fascinating field of viral vectorology and for always encouraging and supporting me. I also want to thank him for his confidence in this project, our fruitful scientific discussions and for his critical supervision of my work.

I want to thank Prof. Dr. Thorsten Burmester for supporting me by taking the time to review this study and I am grateful to Prof. Dr. Susanne Dobler for her readiness to chair the disputation.

Dr. Stefan Michelfelder, still our undisputed AAV expert, earns my gratitude for introducing me into the field of AAV-based vectors. I want to thank him for all his support and for sharing his promising projects with me. Not less important, he taught me that beer and sparkling wine can indeed be mixed together and enjoyed as refreshing longdrink, so thanks for that, Stefan… ;-)

I am also very grateful to Agnes Hunger for her endless assistance in the lab. Within the 3.5 years we have spent working together, I have never heard her saying “no” if I needed a helping hand at one of the numerous experiments. Agnes, without you I wouldn’t have made it! Thank you so much!

Dr. Henning Seismann did not only establish the Baculovirus Expression Vector System in our lab which has been an extremely useful tool ever since, he is also never getting tired of supporting us with new ideas. Thanks, Henning!

Of course I do not only want to thank the persons mentioned above. I am very grateful to every single colleague of mine for their support and all their help. All of you help fighting the daily routine in the lab…

I thank Oliver Müller from the Medical Center of the University of Heidelberg for supporting us with material and for our successful collaboration.

I also want to thank my friend Lars Lunding from the Leibniz-Center for Medicine and Biosciences Borstel for everything he has done for me so far and especially for his assistance at preserving and staining the murine lungs. I am very glad that we managed to work together at this project.

I am very grateful to Dr. Godwin Dogbevia from the Institute of Experimental and Clinical Pharmacology and Toxicology of the University of Luebeck for his help regarding the brain-targeted AAV vector. I would not have been able to perform so many immunofluorescence analyses of murine brains in such a short time without him. I also want to thank him and Prof. Dr. Markus Schwaninger, Director of the Institute of Experimental and Clinical Pharmacology and Toxicology of the University of Luebeck, for our enlightening discussions and I am looking forward to a fruitful collaboration.

Last but not least, I wish to thank my whole family, especially my sisters Clara and Hannah, and all my friends for their support. I would not have made it without you! Thank you, Toby, for always encouraging me.

Isis, you are the love of my life! Sorry for all the lost time that I have spent in the lab. Thank you so much for everything!